High vs Low Thrust Station Keeping Maneuver Planning for Geostationary Satellites

Damiana Losa

High vs Low Thrust Station Keeping Maneuver Planning for Geostationary Satellites

by

Damiana LOSA

Dottore in Ingegneria Elettronica
Politecnico di Milano (2002)

Under the supervision of
Prof. Marco LOVERA and Prof. Jean-Paul MARMORAT

A thesis submitted for the degree of
Doctor of Philosophy
in Real-Time Computer Science, Robotics, Control Engineering
at the École Nationale Supérieure des Mines de Paris

February 9, 2007

High vs Low Thrust Station Keeping Maneuver Planning for Geostationary Satellites

by

Damiana LOSA

Doctorate

School	École Nationale Supérieure des Mines de Paris
Department	Centre de Mathématiques Appliquées
Subject	Real-Time Computer Science, Robotics, Control Engineering
Founded by	⋆ École Nationale Supérieure des Mines de Paris (ENSMP)
	⋆ Alcatel Alenia Space (AAS)
Hosts	⋆ Centre de Mathématiques Appliquées (CMA)
	École Nationale Supérieure des Mines de Paris — France (main host)
	⋆ Dipartimento di Elettronica e Informazione (DEI)
	Politecnico di Milano — Italy

Defence

Date	February 9, 2007
Place	École Nationale Supérieure des Mines de Paris — Sophia Antipolis
Committee	⋆ Pierre BERNHARD (referee)
	Polytech'Nice Sophia, Nice-Sophia Antipolis University high school — France
	⋆ Jacques BERNUSSOU (referee)
	LAAS, CNRS laboratory — Toulouse, France
	⋆ Thierry DARGENT (examiner)
	AAS Research and Development department — Cannes, France
	⋆ Paul LEGENDRE (examiner)
	CNES — Toulouse, France
	⋆ Marco LOVERA (examiner and supervisor)
	DEI, Politecnico di Milano departement — Milan, Italy
	⋆ Jean-Paul MARMORAT (examiner and supervisor)
	CMA, ENSMP departement — Sophia Antipolis, France
	⋆ Joël AMALRIC (guest)
	AAS Mission Engineering department — Cannes, France
	⋆ Rémi DRAI (guest)
	ESA ESTEC — Noordwijk, The Netherlands
	⋆ Catherine LEGRAND (guest)
	AAS Mission Engineering department — Cannes, France

Titre de la thèse	Planification de manoeuvres à poussée forte vs à poussée faible pour le maintien à poste de satellites géostationnaires
Auteur	Damiana LOSA
Mots clés	Dynamique orbitale et théorie des perturbations Systèmes de propulsion chimique et électrique Maintien à poste de satellites géostationnaires Contrôle d'orbite Contraintes de saturation sur le contrôle Optimisation de trajectoire par méthodes directes Contrôle optimal sous contraintes à horizon fixe Contrôle optimal sous contraintes à horizon glissant Platitude différentielle
Résumé	Page 9
Introduction	Page 11
Conclusion	Page 277

High vs low thrust station keeping maneuver planning for geostationary satellites	**Thesis title**
Damiana LOSA	**Author**
Orbital dynamics and perturbation theory Chemical and electrical propulsion systems Geostationary satellite station keeping Orbit control Control saturation constraints Trajectory optimization via direct methods Fixed horizon optimal control with constraints Receding horizon optimal control with constraints Differential flatness	**Key words**
See page 17	**Abstract**
See page 47	**Introduction**
See page 273	**Conclusion**

Dedicated to
Mirella and Paolo, my parents,
Cristina and Mariachiara, my sisters,
Valentina and Claudio, my parents-in-law,
Marcello, my brother-in-law.

Achieved for
Alberto, my husband,
me,
our future.

Résumé

Ce mémoire de thèse traite du problème de la planification de manoeuvres pour le maintien à poste de satellites géostationnaires équipés de tuyères électriques (à poussée faible). Nous évaluons l'opportunité de substituer une telle planification à celle traditionnellement utilisée pour les satellites géostationnaires équipés de tuyères chimiques (à poussée forte).

Dès son apparition, la technologie des systèmes de propulsion à poussée faible a rencontré un vif intérêt auprès des agences et des sociétés spatiales. Grâce à sa haute impulsion spécifique (qui implique une basse consommation de carburant), cette technologie est devenue très compétitive par rapport à la technologie traditionnelle des propulseurs chimiques à poussée forte, surtout dans les phases de transfert et rendez-vous des missions spatiales.

Pendant la définition des missions à poussée faible, les analyses de faisabilité des phases de transfert et rendez-vous (via la solution de problèmes d'optimisation de trajectoire) ont été réalisées avec des solutions d'optimisation alternatives. En effet, pendant ces phases, il est nécessaire d'activer les systèmes de propulsion à poussée faible sur des longues portions du temps de transfert. Par conséquent, les problèmes d'optimisation de trajectoire à poussée forte (typiquement formulés en temps discret) ont été remplacés par des problèmes d'optimisation de trajectoire à poussée faible formulés en temps continu et résolus par des techniques de contrôle en temps continu.

Le premier objectif de cette thèse est de comprendre quel est l'impact de la technologie à poussée faible lors de l'analyse de faisabilité de la phase de maintien à poste de satellites géostationnaires. Nous étudions en particulier l'impact de l'utilisation des systèmes de propulsion à poussée faible sur la planification de manoeuvres et sur la boucle entière de maintien à poste géostationnaire. L'étude consiste à déduire si la planification de manoeuvres à poussée faible est compétitive au regard des stratégies classiques de planification couramment employées pour des manoeuvres à poussée forte.

Généralement, les stratégies classiques à long terme pour le maintien à poste sont déduites de modèles de propagation d'orbite simplifiés (en fonctions des paramètres orbitaux moyennés) par la conjonction des trois facteurs suivants : la forte poussée des propulseurs, la dimension de la fenêtre de maintien à poste pas très contraignante ainsi que la possibilité d'exécuter des manoeuvres à basse fréquence. Dans le cadre de cette thèse, compte tenu du faible niveau des poussées et des contraintes strictes en position (fenêtres de maintien à poste petites), nous considérons comme plus appropriés l'hypothèse d'une plus haute fréquence de manoeuvres et l'utilisation d'un modèle de propagation d'orbite en fonction de paramètres osculateurs.

Pour la planification de manoeuvres, nous proposons une solution par approche directe : le problème de maintien à poste en tant que problème de contrôle optimal est discrétisé et traduit en un problème d'optimisation paramétrique. Deux techniques différentes d'optimisation sont proposées : l'optimisation sous contraintes à horizon fixe et celle à horizon glissant. Cette deuxième technique est appliquée aux équations linéarisées du mouvement préalablement transformées via un changement de variable à la Lyapunov sur l'état des déviations des paramètres équinoxiaux osculateurs. Cette transformation de Lyapunov définit des nouveaux paramètres orbitaux. Elle rend le processus de planification plus compréhensible du point de vue du contrôle et plus facile à implémenter d'un point de vue numérique, grâce aux concepts de platitude et inclusion différentielles.

Les résultats de la planification de manoeuvres à poussée faible sont obtenus dans un premier temps en fonction des changements de vitesse, dans un deuxième temps en fonction des forces engendrées par les tuyères des systèmes de propulsion classiques. Le but est de déterminer la solution la plus efficace en conditions nominales et en cas de panne d'un des propulseurs.

Le problème du positionnement simultané de plusieurs satellites dans une même grande fenêtre de maintien à poste n'est pas adressé explicitement. Il est implicitement résolu en proposant une technique fine de contrôle pour maintenir chaque satellite à poste dans une fenêtre de dimension très petite.

Mots clés

Dynamique orbitale et théorie des perturbations. Systèmes de propulsion chimique et électrique. Maintien à poste de satellites géostationnaires. Contrôle d'orbite. Contraintes de saturation sur le contrôle. Optimisation de trajectoire par méthodes directes. Contrôle optimal sous contraintes à horizon fixe. Contrôle optimal sous contraintes à horizon glissant. Platitude différentielle.

Introduction (*en français*)

Motivations et objectifs

Le bon fonctionnement des satellites géostationnaires nécessite que leur latitude et longitude soient confinées durant toute leur durée de vie. Dans ce but, une stratégie de maintien à poste adéquate est implémentée, dont les objectifs sont l'ensemble des manoeuvres à exécuter pour contrecarrer les effets des forces des perturbations naturelles qui modifient la position d'un satellite. La stratégie est décidée en prédisant les changements des paramètres orbitaux sur la base de modèles simplifiés de la dynamique des satellites en tenant compte uniquement des forces des principales perturbations naturelles: la force d'attraction de la Lune et du Soleil, la pression des radiations solaires et la force gravitationnelle terrestre non homogène.

De nos jours, pour atteindre les objectifs d'une stratégie de maintien à poste, la plus grande partie des satellites géostationnaires sont équipés avec des systèmes de propulsion chimique : pour contrecarrer les changements des paramètres orbitaux, les tuyères chimiques sont généralement allumées une fois toutes les deux semaines pour un intervalle temporel T_m de quelques dizaines de minutes, en fournissant ainsi des forces de quelques dizaines de Newton. Compte tenu du petit rapport entre T_m et la période orbitale, on peut considérer les poussées chimiques comme impulsives. Cette dernière hypothèse donne un sens au fait qu'on définit la stratégie de maintien à poste sans considérer les forces non conservatives (les poussées entraînées par les tuyères) dans les équations de la dynamique.

Cependant, depuis peu, l'emploi de systèmes de propulsion électrique est pris en considération comme alternative viable aux classiques actionneurs chimiques. Cette solution devient rapidement le choix de base sur les nouvelles plate-formes des satellites de télécommunication. L'utilisation de systèmes de propulsion à poussée faible est obligatoire quand la dimension de la fenêtre de maintien à poste est très petite. Dans ce cas, les accélérations entraînées par les tuyères doivent avoir le même ordre de grandeur que les accélérations entraînées par les forces des perturbations environnementales.

Comparée à la technologie de propulsion chimique, celle électrique permet d'améliorer significativement les performances d'une plate-forme, en terme de masse et/ou en terme de durée de vie. Cette amélioration est due à une augmentation de l'impulsion spécifique d'un facteur entre 5 et 10 à laquelle correspond une réduction du même facteur de la masse de carburant nécessaire pour

exécuter les manoeuvres de maintien à poste durant tout le temps de vie du satellite.

Le remplacement des tuyères chimiques par des tuyères électriques a toutefois des implications du point de vue du contrôle. Puisque les tuyères électriques ne peuvent fournir qu'un niveau de poussée très faible (de l'ordre des milliNewtons) il est nécessaire, pour atteindre les mêmes objectifs que la stratégie de maintien à poste à poussée forte, que les tuyères électriques soient allumées quelques heures tous les jours. Il est important de re-concevoir la stratégie de contrôle comme un processus continu à optimiser. L'objectif principal de cette thèse est celui d'évaluer quel est l'impact de la substitution d'un système de propulsion à poussée forte avec un système à poussée faible en terme de synthèse du contrôle pour le maintien à poste géostationnaire.

Approche proposée

La dynamique d'un satellite GEO sera étudiée dans le détail afin d'obtenir un modèle dynamique le plus précis possible. Ce modèle sera obtenu en utilisant les équations de Gauss des variations des paramètres osculateurs qui contiennent les accélérations entraînées par les perturbations environnementales, plutôt que les fonctions potentielles de perturbation des équations de Lagrange. Ces dernières sont les équations traditionnellement utilisées dans la planification des manoeuvres de maintien à poste. L'idée est d'implémenter un contrôleur pour le maintien à poste de satellite géostationnaires qui s'appuie sur un modèle écrit en terme de paramètres orbitaux équinoxiaux plutôt qu'en terme de paramètres moyennés. Un tel contrôleur permet de planifier de manière automatique les manoeuvres de maintien à poste et il pourrait être intégré à bord en vue d'une boucle de maintien à poste géostationnaire entièrement autonome.

Nous allons prêter attention aux performances réelles d'un système de propulsion électrique. En particulier, les propulseurs électriques actuels sont en mesure de fournir seulement des poussées on-off. Cette spécification technologique comporte une formulation du problème de maintien à poste en terme de problème de contrôle optimal sous contraintes mixtes : de nature continue sur les variables d'état et de nature discrète sur les variables de contrôle.

L'approche que nous avons l'intention d'adopter est un approche directe. Le problème de maintien à poste formulé comme problème de contrôle optimal sera traduit en un problème d'optimisation paramétrique. Nous allons, en suite, résoudre ce dernier problème via des programmes d'optimisation linéaire et non linéaire.

Une approche d'optimisation à horizon glissant sera utilisée pour déterminer la trajectoire optimale qui satisfait les besoins orbitaux qui caractérisent la mission géostationnaire. En suite, nous allons chercher une transformation de l'espace d'état du satellite telle que le système linéaire géostationnaire (initialement non stationnaire) une fois transformé soit plat au sens différentiel et avec coefficients constants. Cela signifie que trois sorties du système (les sorties plates) et leurs dérivées suffiront pour décrire la dynamique entière d'un satellite géostationnaire. De plus, les variables de contrôle pourront s'exprimer explicitement en fonction des sorties plates et de leurs dérivées.

Organisation du rapport

Le Chapitre 1 du manuscrit est une introduction (voir page 47 pour la version anglaise et page 11 pour la version française). Les autres chapitres sont organisés comme suit.

Chapitre 2. C'est un chapitre de base où l'on donne des définitions fondamentales pour être en mesure de comprendre ce qui sera expliqué dans la suite du manuscrit. Nous présentons les repères du temps, les repère de l'espace et les systèmes de coordonnées associées. C'est dans ces repères de l'espace et en fonction de ces coordonnées que les équations du mouvement d'un satellite géostationnaire seront définies. Nous définissons les représentations d'état d'un satellite en terme de position et vitesse, de paramètres orbitaux classiques et de paramètres équinoxiaux, ainsi que les formules de conversion d'un jeu de paramètres et d'un repère à l'autre. Ces formules seront utilisées dans le simulateur de la dynamique d'un satellite géostationnaire. Le concept de paramètres orbitaux moyens et osculateurs est introduit et les différentes techniques pour examiner les effets des perturbations sur la propagation d'orbite sont brièvement passées en revue.

Chapitre 3. Dans ce chapitre, nous décrivons (soit en terme d'accélérations, soit en terme des fonctions potentielles correspondantes) les trois principales perturbations environnementales qui affectent la position d'un satellite géostationnaire. Nous prenons en considération aussi les accélérations entraînées par les tuyères du système de propulsion. Ces accélérations doivent être en mesure de contrecarrer l'effet perturbant des accélérations environnementales. En ce qui concerne les systèmes de propulsion, nous définissons leurs principaux paramètres de performance et nous expliquons la différence entre la propulsion chimique et électrique. Les accélérations générées par les tuyères sont exprimées en fonction de la disposition des tuyères sur le satellite et des forces de propulsion générées par chaque tuyère, pour donner un modèle des accélérations du système de propulsion. Dans ce chapitre, nous dépeignons aussi les configurations des systèmes de propulsion à poussée forte habituellement employées et celles à poussée faible proposées plus récemment pour le propos du maintien à poste géostationnaire.

Chapitre 4. Dans ce chapitre, nous présentons différents modèles de la dynamiques de translation d'un satellite géostationnaire: des modèles non linéaires en conditions képlériennes non perturbées et des modèles non linéaire en conditions képlériennes perturbées (les équations des variations des paramètres osculateurs dans les formes proposées par Gauss et Lagrange). Nous décrivons aussi une procédure analytique pour résoudre l'équation de Kepler en présence de paramètres près de zéro Les composantes du vecteur position géographique sont présentées comme fonctions non linéaires des éléments orbitaux équinoxiaux. Enfin, un modèle orbital géostationnaire linéarisé est déduit en développant les accélérations des perturbations naturelles en série de Taylor jusqu'à l'ordre zéro. Ce dernier modèle est décrit par les équations classiques de Clohessy-Wiltshire du mouvement relatif d'un satellite géostationnaire par rapport à une orbite géostationnaire idéale, connues aussi comme équations de Hill. Des résultats

de simulations sont présentés le long de tous ce chapitre avec le but de montrer l'évolution dans le temps des composantes du vecteur d'état et du vecteur position du satellite en coordonnées géographiques sphériques.

Chapitre 5. Dans ce chapitre, nous traitons plus dans le détail du problème de maintien à poste. Nous définissons les besoins orbitaux d'un satellite géostationnaire. Nous expliquons la différence entre les manoeuvres à poussée forte et à poussée faible. Nous définissons le problème du maintien à poste comme un problème de planification de manoeuvres dans son acception la plus générale, en excluant dans un premier temps des importantes spécifications qui se rattachent à des considérations opérationnelles et à la technologie des systèmes de propulsion. En fait, la planification de manoeuvres de maintien à poste s'insère dans la boucle de contrôle de maintien à poste géostationnaire. C'est une des trois principales opérations qui doivent être exécutées pour assurer le bon fonctionnement de de la boucle entière de maintien à poste géostationnaire. Les deux autre opérations sont la détermination d'orbite et l'exécution des manoeuvres. Dans ce chapitre, ces deux dernières opérations sont brièvement décrites en fournissant des références bibliographiques concertantes. Un passage en revue des travaux de l'état de l'art sur la planification de manoeuvres de maintien à poste géostationnaire conclut ce chapitre. Les travaux qui se rattachent à la planification de manoeuvres à poussée faible sont passés en revue séparément de ceux concernant la planification de manoeuvres à poussée forte. Sur la base de cette distinction, trois travaux (concernant le maintien à poste autonome) se distinguent par le fait que ils traitent le problème de maintien à poste comme un problème de maintien de configuration d'une formation, c'est à dire comme un problème de régulation.

Chapitre 6. Dans ce chapitre, nous abordons la planification de manoeuvres de maintien à poste en résolvant une séquence de problèmes de contrôle optimal sur des horizons de temps finis avec contraintes sur les variables d'état et de contrôle. L'ensemble des contraintes sur les variables d'état est la traduction en termes mathématiques des besoins orbitaux de la mission. Une fois choisi le système de propulsion, l'ensemble des contraintes sur les variables de contrôle représente la traduction en termes mathématiques des besoins technologiques du système de propulsion. Dans un premier temps, nous allons formuler le problème de planification de manoeuvres sous des conditions technologiques virtuelles : un système de propulsion composé de six tuyères chacune avec impulsion spécifique infinie, montées le long des trois axes du repère orbital RTN et capables de générer à chaque instant un vecteur accélération avec direction et module quelconques. Nous proposons une solution qui se base sur la transcription directe du problème en termes de problèmes d'optimisation paramétrique. Afin d'implémenter la solution avec des codes de programmation linéaire, nous nous adressons au développement de Taylor au premier ordre des équations variationnelles de Gauss autour de la trajectoire de maintien à poste nominale. Toutefois, la solution du problème d'optimisation sera validée avec des modèles non linéaires. Ce chapitre contient aussi un bref passage en revue des

méthodes de solution des problèmes d'optimisation de trajectoire. Nous allons présenter et commenter quelques résultats de simulation du problème ainsi simplifié, obtenus avec une approche d'optimisation à horizon fixe et une autre à horizon glissant. En suite, nous allons progressivement prendre en compte les spécifications technologiques du système de propulsion et nous allons accomplir des études de faisabilité en présence de nouvelles contraintes sur les variables de contrôle. On s'occupera de deux modèles idéalisés pour décrire le comportement des tuyères électriques. Le premier modèle est celui de propulseurs qui sont capables de fournir des poussées modulables. Le deuxième est celui de propulseurs qui sont capables de fournir un seul niveau de poussée. Nous allons finalement relaxer l'hypothèse de configuration des six tuyères fonctionnant indépendamment et montées orthogonalement sur le corps du satellite, pour répondre aux questions suivantes : y a-t-il des directions privilégiées de poussée dans le système de coordonnées RTN, telles que, avec des tuyères montées le long de ces directions, on puisse réduire le nombre de propulseurs grâce à une synchronisation des manoeuvres le long des trois directions du repère orbital RTN?

Chapitre 7. Dans ce chapitre, nous expliquons comment transformer le système linéaire avec coefficients non stationnaires qui décrit la dynamique d'un satellite GEO, en un système linéaire stationnaire. Un changement de variable est réalisé via une transformation de Lyapunov qui ne modifie pas les propriétés de stabilité du système original. De plus, cette transformation permet de reconnaître la platitude différentielle dans la dynamique d'un satellite géostationnaire.

Le Chapitre 8 est le chapitre de conclusion (voir page 273 pour la version anglaise et page 277 pour la version française).

Abstract

This dissertation focuses on the problem of station keeping maneuver planning for geostationary satellites equipped with thrusters at low thrust level. We evaluate the opportunity of substituting such a planning to the more traditional one used for geostationary satellites equipped with thrusters at high thrust.

Since the birth of low thrust technology, its use has always met with the spacecraft companies approval. The well-known advantage of low fuel consumption due to the high specific impulse achieved by the high values of specific impulsion makes this technology highly competitive with respect to the high trust level one, especially during transfer and rendez vous phases of space missions.

The trajectory optimization problems which have to be solved during the mission design in order to analyze the feasibility of transfer and rendez vous mission phases have begun to be solved with alternative optimization solutions, since the low thrust propulsion systems have to be activated for longer periods of the transfer time. High thrust trajectory optimization problems, typically formulated as discrete, have been replaced with low thrust trajectory optimization problems formulated as continuous and solved by continuous control techniques.

The goal of this thesis is to understand what is the impact of the low thrust propulsion technology on the station keeping phase feasibility analysis performed during the design of a geostationary mission. In particular we study the impact that the low thrust propulsion systems have on the station keeping maneuver planning and on the realization of the whole station keeping control loop. The goal is to deduce whether the maneuver planning related with this technology is competitive with respect to the more classical one based on high thrust level.

Usually the well known long term strategies for the SK maneuver are deduced from simplified propagation orbit models (in function of mean orbital elements) mainly because the following three conditions are met: high thrust level propulsions, SK dead band box sizes not very stringent and the possibility to execute low frequency maneuvers. In the framework of this dissertation, given the low thrust level propulsion and increasingly stringent dead band requirements, we think it is more appropriate to make the hypothesis of a much higher maneuver execution frequency in order to achieve a finer control of the GEO satellite position and to use an orbit propagation model described by the motion equations in terms of osculating elements.

For the maneuver planning we propose a solution based on a direct approach considered as

the transcription in terms of parameter optimization problem of the constrained optimal control problem associated to the planning task. Two optimization techniques have been considered: the fixed horizon optimization under constraints and the receding horizon one. This second is also used with the linearized motion equations appropriately transformed via a Lyapunov variable change on the state space of the osculating equinoctial element deviations. This Lyapunov transformation leads to the definition of a new set of orbital parameters. It makes the planning process more immediately understandable from a control viewpoint and easier to implement from a numerical viewpoint, thanks to the differential flatness and inclusion concepts.

All the low thrust maneuver planning results are obtained in a first time in terms of thrust velocity increments and in a second time directly in terms of thrust, considering typical propulsion system configurations with the goal of determining the more efficient one in nominal conditions and in the condition of failure of one of the thrusters.

The problem of collocation of more geostationary satellites in a same big box has not been explicitly addressed but is implicitly solved once the fine control technique with a relative stringent dead band requirement is proposed for each satellite.

Keywords

Orbital dynamics and perturbation theory. Chemical and electrical propulsion systems. Geostationary satellite station keeping. Orbit control. Control saturation constraints. Trajectory optimization via direct methods. Fixed horizon optimal control with constraints. Receding horizon optimal control with constraints. Differential flatness.

Acknowledgements

I think that this PhD Thesis work is the fruit of my deep interest in problems related to spatial domain and control.

The difficulties I met with during these last three years are many and the results I obtained maybe not fully satisfying. I think that such difficulties come into the normal ones endured by anyone deciding to engage in a PhD Thesis. I think also that a part of these difficulties come into those endured by anyone deciding to engage in a PhD Thesis in an educative universe which is unknown to her and deciding therefore to assume a certain amount of risks related to the ignorance of this universe. I think therefore that this PhD Thesis is also the fruit of my perseverance in willing to achieve the works I undertake and in willing to achieve them in the best possible way. This perseverance and this will have been fed during these three years by the esteem and love that several people have expressed to me. I will thank these people in a separate section since they deserve a different kindness.

I am also deeply convinced that if a succession of events — more or less fortuitous (it depends on the viewpoint) — had not happened, this work wouldn't even have begun. I would like to express my boundless thankfulness toward the people, the educational institutions and the industrial partners who are at the origin of those events. I will do it in the same order they appeared in my professional life.

- To Rémi DRAI, Marco LOVERA, and Jean-Paul MARMORAT, for having thought to me, after I graduated at Politecnico di Milano in Italy, as an engineer able to participate in their collaboration project. Thanks for having introduced me to spatial mechanics problems and for having accepted to be my PhD Thesis supervisors.

- To the École Nationale Supérieure des Mines de Paris, for having offered me the possibility to complete an applied research work in one of its departments: the Centre des Mathématiques Appliquées (CMA) in Sophia Antipolis.

- To the CMA director (Nadia MAÏZI) and to ARMINES, for having done all the necessary to allow me to complete this PhD Thesis work, and for having given to me all the necessary training and granted me the necessary founding.

- To ALCATEL ALENIA SPACE, for having provided me with research subjects strongly

related with industrials realities and for having partially founded me during my PhD.

- To Thierry DARGENT and Roland FRENKIEL of AAS Research and Development department, to Catherine LEGRAND and Joël AMALRIC of AAS Mission Engineering department, to Paul LEGENDRE of CNES, for their precise information and valuable advices on my research topic and, above all, for the great amount of time they dedicated to me and to my problems.

- To Pierre BERNHARD and to Jacques BERNUSSOU for having accepted to be referees of this PhD Thesis work.

- Thierry DARGENT, Paul LEGENDRE, Marco LOVERA, Jean-Paul MARMORAT, for having accepted to be examiners in the committee.

- To Catherine LEGRAND, Joël AMALRIC and Rémi DRAI for having accepted my invitation to my defence.

Contents

List of Figures

List of Tables

Dictionary of Symbols and Mathematical Notations

Minuscule Latin Symbols

a		Semi-major axis
a_a		Modulus of the acceleration vector $\boldsymbol{a}_a$
	or	If with further subscript, component of the acceleration vector $\boldsymbol{a}_a$
a_d		Modulus of the acceleration vector $\boldsymbol{a}_d$
	or	If with further subscript, component of the acceleration vector $\boldsymbol{a}_d$
a_e		Modulus of the acceleration vector $\boldsymbol{a}_e$
	or	If with further subscript, component of the acceleration vector $\boldsymbol{a}_e$
$a_{e_{sk}}$		Modulus of the acceleration vector $\boldsymbol{a}_{e_{sk}}$
	or	If with further subscript, component of the acceleration vector $\boldsymbol{a}_{e_{sk}}$
a_g		Modulus of the acceleration vector $\boldsymbol{a}_g$
	or	If with further subscript, component of the acceleration vector $\boldsymbol{a}_g$
a_i		Thrust acceleration of the ith thruster
a_k		Keplerian semi-major axis (constant)
a_p		Modulus of the acceleration vector $\boldsymbol{a}_p$
	or	If with further subscript, component of the acceleration vector $\boldsymbol{a}_p$
a_t		Modulus of the acceleration vector $\boldsymbol{a}_t$
	or	If with further subscript, component of the acceleration vector $\boldsymbol{a}_t$
$\boldsymbol{a}_a$		Acceleration vector induced by the Sun's and Moon's gravity attraction
$\boldsymbol{a}_d$		Sum of all the disturbing acceleration vectors
$\boldsymbol{a}_e$		Acceleration vector induced by a generic environmental disturbing force
$\boldsymbol{a}_{e_{sk}}$		Nominal station keeping environmental perturbing accelerations
$\boldsymbol{a}_g$		Acceleration vector induced by Earth's gravity attraction
$\boldsymbol{a}_p$		Acceleration vector induced by the solar radiation pressure
$\boldsymbol{a}_t$		Acceleration vector induced by thrusts
b		Function of EOEs in the nonlinear Gauss' VOP equations

c		Effective propellant exhaust velocity
c_e		Effective propellant exhaust velocity
$\boldsymbol{c}$		Generic orbital element vector
e		Eccentricity
$\boldsymbol{e}$		Eccentricity vector
f		Generic scalar function
$\boldsymbol{f}$		Vector of infinitesimal transition functions
g		Sea-level acceleration of gravity on the Earth (constant)
$\boldsymbol{g}$		Vector of output functions in the GEO satellite nonlinear model
h		Modulus of the angular momentum vector
	or	Function of EOEs in the nonlinear Gauss' VOP equations
	or	Sampling interval
i		Inclination
$\boldsymbol{i}$		Inclination vector
l		Mean longitude
l_Θ		Mean longitude net of Θ
$\tilde{l}_\Theta$		Mean longitude deviation from its nominal station keeping value λ_s
m		Spacecraft mass
m_d		Dry mass
m_p		Propellant mass
m_0		Initial spacecraft mass
$\dot{m}$		Mass flow rate of propellant
n		Mean motion
	or	Modulus of the node vector
$\boldsymbol{n}$		Node vector
p		Semi-latus rectum
$\boldsymbol{p}$		Satellite geographical position vector in the ECEF reference frame
r		Modulus of the spacecraft position vector
$\boldsymbol{r}$		Spacecraft position vector
r_{sS}		Distance of the Sun from the spacecraft
$\boldsymbol{r}_{sS}$		Position vector of the Sun respect to the spacecraft
r_{sM}		Distance of the Moon from the spacecraft
$\boldsymbol{r}_{sM}$		Position vector of the Moon respect to the spacecraft
r_M		Modulus of the Moon's position vector
$\boldsymbol{r}_M$		Modulus of the Moon's position vector
r_S		Modulus of the Sun's position vector
$\boldsymbol{r}_S$		Modulus of the Sun's position vector
t		Time
	or	Epoch

t_m^{off}		Switching off instant
t_m^{on}		Switching on instant
t_m		Impulsive maneuver time
t_p		Passage time from the perigee
t_r		Reference epoch
u		Modulus of the control variable vector
	or	If with subscript, component of the control variable vector
$\boldsymbol{u}$		Control variable vector
$\boldsymbol{u}_{sk}$		Nominal station keeping control vector
v_{sk}		Nominal station keeping velocity of a GEO satellite (constant)
v_x, v_y, v_z		Components of the spacecraft velocity vector along the axes of the ECI reference frame
	or	Components of the spacecraft velocity vector along the axes of a CW reference frame
v_t		Velocity magnitude of the spacecraft subject to the only thruster forces
$\boldsymbol{v}$		Spacecraft velocity vector
w		Argument of latitude
x, y, z		Components of the spacecraft position vector along the axes of the ECI reference frame
x_G, y_G, z_G		Components of the spacecraft position vector along the axes of the GEO CW reference frame
x_M, y_M, z_M		Components of the Moon's position vector along the axes of the ECI reference frame
x_S, y_S, z_S		Components of the Sun's position vector along the axes of the ECI reference frame
$\boldsymbol{x}$		Spacecraft state vector in terms on EOEs
	or	Generic spacecraft state vector
$\boldsymbol{x}_e$		State vector of the environmental effect linear system
$\boldsymbol{x}_t$		State vector of the thrust effect linear system
$\boldsymbol{x}_{COE}$		Spacecraft state vector in terms of COEs
$\boldsymbol{x}_{Ksk}$		Keplerian nominal station keeping state vector
$\boldsymbol{x}_{Ssk}$		Synchronous Keplerian nominal station keeping state vector
$\boldsymbol{x}_{PV}$		Spacecraft state vector in terms of position and velocity
$\boldsymbol{y}$		Output vector of a GEO spacecraft dynamical model

Capital Latin Symbols

A_n	Area of the thruster nozzle exit
A_{al_Θ}, A_K	(1,6) and (6,1) elements of matrix $\boldsymbol{A}_c$

$\boldsymbol{A}$, $\boldsymbol{A}_c$, $\boldsymbol{B}$, $\boldsymbol{C}$	Matrices of the continuous time state deviation space linear model of the GEO spacecraft dynamics
$\boldsymbol{A}_d$, $\boldsymbol{B}_d$, $\boldsymbol{C}_d$	Matrices of the discrete time state deviation space linear model of the GEO spacecraft dynamics
$\tilde{\boldsymbol{A}}$, $\tilde{\boldsymbol{B}}$, $\tilde{\boldsymbol{C}}$	Matrices of the Lyapunov transformed continuous time linear model of the GEO spacecraft dynamics
$\boldsymbol{\mathcal{A}}$	Vector of samples of environmental acceleration vectors
$\boldsymbol{\mathcal{B}}$	Matrix in the POP formulation
C_{nm}	Earth's gravity potential coefficients
C_R	Radiation pressure coefficient
C_x, C_y, C_z	Director cosines of the spacecraft position vector in the ECI reference frame
$\boldsymbol{\mathcal{C}}$	Matrix in the POP formulation
D	Mean motion deviation rate
$\boldsymbol{\mathcal{D}}$	Disturbing contribution vector to the nonlinear VOP equations
$\boldsymbol{E}$, $\boldsymbol{Q}$, $\boldsymbol{W}$	Unit vectors along the axes of the equinoctial coordinate system
E	Eccentric anomaly
$\mathcal{E}_a$	Potential function related to the Sun's and Moon's gravity attraction
$\mathcal{E}_e$	Potential function related to a generic environmental disturbing force
$\mathcal{E}_g$	Potential function related to the Earth's gravity attraction
$\mathcal{E}_p$	Potential function related to the solar radiation pressure
F	Thrust
$\boldsymbol{F}$	Thrust vector of a propulsion system
$GM_\oplus$	Gravitational coefficient of the Earth (constant)
$GM_\odot$	Gravitational coefficient of the Sun (constant)
$GM_\circledcirc$	Gravitational coefficient of the Moon (constant)
$\boldsymbol{G}$	State vector dependent matrix, factor of the Gauss' contribution in the nonlinear VOP equations
$\bar{\boldsymbol{G}}$	State vector dependent matrix, factor of the Gauss' contribution in the nonlinear VOP equations
$\boldsymbol{\mathcal{G}}$	Gauss' contribution vector in the nonlinear VOP equations
I	Retrograde factor
I_{sp}	Specific impulse
I_t	Total impulse
J	Performance index
K	Eccentric longitude
K_{sk}	Nominal station keeping eccentric longitude
$\boldsymbol{\mathcal{K}}$	Kepler's contribution vector in the nonlinear VOP equations
L	True longitude

$\boldsymbol{L}$	State vector dependent matrix, factor of the Lagrange's contribution in the nonlinear VOP equations
$\bar{\boldsymbol{L}}$	State vector dependent matrix, factor of the Lagrange's contribution in the nonlinear VOP equations
$\boldsymbol{\mathcal{L}}$	Lagrange's contribution vector in the nonlinear VOP equations
$\mathbf{L_{SK}}$	Station keeping line
M	Mean anomaly
N_t	Thruster number of a propulsion system
$P_\odot$	Solar radiation pressure
P_a	Ambient pressure
P_g	Gas pressure
P_{jet}	Thruster jet power
P_{nm}	Associated Legendre polynomial of degree n and order m
P_{sys}	Propulsion system input power
P_1, P_2	Eccentricity equinoctial orbital elements
$\tilde{P}_1$, $\tilde{P}_2$	Eccentricity vector components in a rotated equinoctial coordinate system
$\mathbf{P_{SK}}$	Station keeping point
Q_1, Q_2	Inclination equinoctial orbital elements
$\tilde{Q}_1$, $\tilde{Q}_2$	Inclination vector components in a rotated equinoctial coordinate system
$\boldsymbol{Q}_c$	State controllability matrix
$R_\oplus$	Equatorial radius of the Earth (constant)
R, T, N	Axes of the RTN coordinate system
$\boldsymbol{R}$, $\boldsymbol{T}$, $\boldsymbol{N}$	Unit vectors along the axes of the RTN coordinate system
$\boldsymbol{\mathcal{R}}_X$, $\boldsymbol{\mathcal{R}}_Y$, $\boldsymbol{\mathcal{R}}_Z$	Elementary rotation matrices around X, Y, Z axes
$\boldsymbol{\mathcal{R}}_{ZXZ}$	Transformation matrix from the ECI to the RTN coordinate system
S	Mean spacecraft surface area exposed to the solar flux
S_{nm}	Earth's gravity potential coefficients
$\boldsymbol{S}$, $\boldsymbol{\mathcal{S}}$	Selection matrices in the POP formulation
$\boldsymbol{S}_c$	Output controllability matrix
T_C	Station keeping correction interval
T_M	Mission life time
T	Number of Julian centuries since J2000 epoch (1.5 January, 2000)
T_m	Maneuver time interval
T_{SK}	Station keeping maneuver planning interval
$\mathcal{U}$	Total potential function related to the Earth's gravity attraction
$\boldsymbol{\mathcal{U}}$	Vector of samples of control variable vectors
$\boldsymbol{W}$	Lyapunov transformation matrix

X, Y, Z	Axes of the ECI coordinate system
$\boldsymbol{X}$, $\boldsymbol{Y}$, $\boldsymbol{Z}$	Unit vectors along the axes of the ECI coordinate system
X_B, Y_B, Z_B	Axes of the SBF coordinate system
$\boldsymbol{X}_B$, $\boldsymbol{Y}_B$, $\boldsymbol{Z}_B$	Unit vectors along the axes of the SBF coordinate system
X_G, Y_G, Z_G	Axes of the geostationary CW coordinate system
X_1, X_2, X_3	Functions of the EOEs in the nonlinear Gauss' VOP equations
Y_1, Y_2, Y_3	Functions of the EOEs in the nonlinear Gauss' VOP equations
$\boldsymbol{\mathcal{Y}}$	Vector of samples of output variable vector deviations
$\boldsymbol{\mathcal{Z}}$	Vector of samples of state variable vector deviations

Minuscule Greek Symbols

α	Geocentric right ascension
β_M	Moon's geographical latitude
β_S	Sun's ecliptic geographical latitude
γ	Cant angle
δ	Geocentric declination
ϵ	Reflectivity coefficient
$\zeta_1, \cdots, \zeta_6$	Components of the spacecraft state vector deviation $\boldsymbol{\zeta}$
$\tilde{\zeta}_1, \cdots, \tilde{\zeta}_6$	Components of the Lyapunov transformed state vector deviation $\tilde{\boldsymbol{\zeta}}$
$\boldsymbol{\zeta}$	Deviation of the spacecraft state variable vector from its nominal station keeping value
$\boldsymbol{\zeta}_e$	State vector deviation of the environmental effect linear system
$\boldsymbol{\zeta}_t$	State vector deviation of the environmental effect linear system
$\tilde{\boldsymbol{\zeta}}$	Lyapunov transformed deviation $\boldsymbol{\zeta}$
$\boldsymbol{\eta}$	Spacecraft output vector in the discrete time CW equations
ε	Mean obliquity of the ecliptic
η_{sys}	Total propulsion system efficiency
θ_{Ms}	Angle between the Moon and the satellite position vectors
θ_{Ss}	Angle between the Sun and the satellite position vectors
λ	Geographical longitude
λ_s	Station geographical longitude
λ_M	Moon's geographical longitude
λ_S	Sun's ecliptic geographical longitude
ν	True anomaly
$\boldsymbol{\xi}$	Spacecraft state vector in the continuous and discrete time CW equations
σ	Slew angle
ς_1, ς_2, ς_3	Components of the spacecraft output vector deviation $\boldsymbol{\varsigma}$

$\boldsymbol{\varsigma}$		Deviation of the spacecraft output variable vector from its nominal station keeping value
φ		Geographical latitude
τ		Bijection function
	or	Time integration variable
$\boldsymbol{\omega}$		Angular velocity vector
ω		Argument of perigee
$\tilde{\omega}$		Longitude of periapsis
$\tilde{\omega}_{true}$		True longitude of periapsis
$\omega_{\oplus}$		Angular velocity of the Earth (constant)

Capital Greek Symbols

$\boldsymbol{\Gamma}$		Thruster system configuration matrix
$\boldsymbol{\Gamma}_i$		Configuration vector of the ith thruster
Δ		Variation
$\tilde{\Delta}$		Total change
Δv_t		Velocity increment induced by a thrust
ΔV		Total velocity increment budget
Θ		Right ascension of the Greenwich meridian
Θ_r		Right ascension of the Greenwich meridian at a reference epoch
$\boldsymbol{\Lambda}$		Vector of samples of longitude deviations
Υ		Vernal equinox
$\boldsymbol{\Phi}$		State transition matrix associated with matrix $\boldsymbol{A}$
	or	Vector of samples of latitude deviations
$\boldsymbol{\Phi}_c$		State transition matrix associated with matrix $\boldsymbol{A}_c$
Ω		Right ascension of the ascending node

Constants

a_k	=	42164.172	km
g	=	9.80665	m/s^2
v_{sk}	=	$\omega_\oplus a_k \approx 3.075$	km/s
$GM_\oplus$	=	398600.4415	km^3/s^2
$GM_\odot$	=	$1.32712440018 \times 10^{11}$	km^3/s^2
$GM_\circledcirc$	=	4902.801	km^3/s^2
$P_\odot$	=	4.56×10^{-6}	N/m^2
$R_\oplus$	=	6378.137	km
$\omega_\oplus$	=	0.7292115×10^{-4}	rad/s
ε	=	23.43929111	deg

Acronyms

AAS	Alcatel Alenia Space
BOL	Beginning of life
B1950	1950 January 0.923, date corresponding to the beginning of a Besselian solar year
CEV	Constant effective Exhaust Velocity
CNES	Centre Nationale d'Études Spatiales
COE	Classical Orbital Element
COV	Calculus Of Variation
CW	Clohessy-Wiltshire
ECI	Earth Centered Inertial
ECEF	Earth Centered Earth Fixed Inertial
EOE	Equinoctial Orbital Element
EOL	End of life
ESA	European Space Agency
EW	East-West
FEEP	Field Emission Electric Propulsion
FHO	Fixed Horizon Optimization
GEO	Geostationary Earth Orbit
GHA	Greenwich Hour Angle
GMST	Greenwich mean sidereal time
GPS	Global Positioning System
JD	Julian date
JPL	Jet Propulsion Laboratory

J2000	2000 January 1.5, date corresponding to the beginning of a Julian solar year
LP	Limited jet Power
LQ	Linear quadratic
LQR	Linear quadratic regulator
LST	Local sidereal time
MEME	Mean Equator and Mean Equinox
MJD	Modified Julian date
MPBVP	Multi-Point Boundary Value Problem
MPDT	Magneto Plasma Dynamics Thruster
NASA	National Aeronautics and Space Administration
NS	North-South
OCP	Optimal Control Problem
POP	Parameter Optimization Problem
PPT	Pulsed Plasma Thruster
RFCS	Reference Frames and Coordinate System
RHO	Receding Horizon Optimization
RTN	Radial Tangent Normal
SBF	Spacecraft Body Fixed
SK	Station Keeping
SPP	Sun pointing perigee
SRP	Solar radiation pressure
TELS	Thrust Effect Linear System
TPBVP	Two-Point Boundary Value Problem
TETE	True Equator and True Equinox
UTC	Universal Time Coordinated
VIPER	Variable IsP (specific impulse) Electric Rocket
VOP	Variation Of Parameter
VSI	Variable Specific Impulse
XIPS	Xenon Ion Propulsion System

Mathematical Notations

Vectors and Matrices

➢ Vectors and matrices are written in bold type.

➢ Identity matrices and vector or matrices of zeros and of ones are written as follows.

$$\begin{array}{ll} \boldsymbol{I}_{n\times n} & n \text{ dimensional identity matrix,} \\ \boldsymbol{0}_{n\times m} & n \times m \text{ matrix of zeros,} \\ \boldsymbol{1}_{n\times m} & n \times m \text{ matrix of ones.} \end{array}$$

➢ The transpose of the $n \times m$ matrix $\boldsymbol{M}$ is the $m \times n$ matrix $\boldsymbol{M}^T$ defined by $\boldsymbol{M}^T_{ij} = \boldsymbol{M}_{ji}$ for $i = 1, 2, \ldots, n$ and $j = 1, 2, \ldots, m$.

➢ Inequalities between vectors have to be interpreted componentwise, i.e.,

$$\begin{bmatrix} a_1 & b_1 \end{bmatrix}^T \leq \begin{bmatrix} a_2 & b_2 \end{bmatrix}^T$$

means

$$\begin{aligned} a_1 &\leq b_1, \\ a_2 &\leq b_2. \end{aligned}$$

➢ The determinant of the square matrix $\boldsymbol{M}$ is indicated with the following notation: $\det \boldsymbol{M}$.

Derivatives

Let be

- v_k a generic scalar quantity;
- $\boldsymbol{v}$ a generic vector with components v_1, v_2, …, v_n

$$\boldsymbol{v} = \begin{bmatrix} v_1 & v_2 & \cdots & v_n \end{bmatrix}^T;$$

- f_k a generic scalar function dependent on the components v_1, v_2, …, v_n of the vector $\boldsymbol{v}$

$$f_k = f_k(v_1, v_2, \ldots, v_n) \equiv f_k(\boldsymbol{v});$$

- $\boldsymbol{f}$ a generic function vector with components f_1, f_2, …, f_m dependent on the components v_1, v_2, …, v_n of the vector $\boldsymbol{v}$

$$\boldsymbol{f} = \boldsymbol{f}(\boldsymbol{v}) = \begin{bmatrix} f_1(\boldsymbol{v}) & f_2(\boldsymbol{v}) & \cdots & f_m(\boldsymbol{v}) \end{bmatrix}^T;$$

- $\boldsymbol{F}$ a generic $p \times m$ function matrix with elements f_{ij} $(i = 1, 2, \ldots, p$ and $j = 1, 2, \ldots, m)$ dependent on the components v_1, v_2, $\ldots$, v_n of the vector $\boldsymbol{v}$

$$\boldsymbol{F} = \boldsymbol{F}(\boldsymbol{v}) = \begin{bmatrix} f_{11}(\boldsymbol{v}) & f_{12}(\boldsymbol{v}) & \cdots & f_{1m}(\boldsymbol{v}) \\ f_{21}(\boldsymbol{v}) & f_{22}(\boldsymbol{v}) & \cdots & f_{2m}(\boldsymbol{v}) \\ \vdots & \vdots & \ddots & \vdots \\ f_{p1}(\boldsymbol{v}) & f_{p2}(\boldsymbol{v}) & \cdots & f_{pm}(\boldsymbol{v}) \end{bmatrix}.$$

➢ The notation for the partial derivative of f w.r.t. the v_k component is

$$f_{v_k} = \frac{\partial f}{\partial v_k}.$$

➢ The notation for the partial derivative of $\boldsymbol{M}$ w.r.t. the v_k component is

$$\boldsymbol{F}_{v_k} = \frac{\partial \boldsymbol{F}}{\partial v_k}$$

where the partial derivative matrix $\boldsymbol{F}_{v_k}$ has elements

$$f_{ij_{v_k}}(\boldsymbol{v}) = \frac{\partial f_{ij}(\boldsymbol{v})}{\partial v_k},$$

for $i = 1, 2, \ldots, p$ and $j = 1, 2, \ldots, m$.

➢ The notation for the Jacobian of f, i.e., the derivative of f w.r.t. the vector $\boldsymbol{v}$ is

$$\begin{aligned} \boldsymbol{\nabla}_{\boldsymbol{v}} f \equiv \boldsymbol{\nabla}_{v_1 v_2 \ldots v_n} f &= \begin{bmatrix} f_{v_1} & f_{v_2} & \ldots & f_{v_n} \end{bmatrix}^T = \\ &= \begin{bmatrix} \frac{\partial f}{\partial v_1} & \frac{\partial f}{\partial v_2} & \ldots & \frac{\partial f}{\partial v_n} \end{bmatrix}^T. \end{aligned}$$

➢ The notation for the Jacobian of $\boldsymbol{f}$, i.e., the derivative of $\boldsymbol{f}$ w.r.t. the vector $\boldsymbol{v}$ is

$$\begin{aligned} \boldsymbol{\nabla}_{\boldsymbol{v}} \boldsymbol{f} \equiv \boldsymbol{\nabla}_{v_1 v_2 \ldots v_n} \boldsymbol{f} &= \begin{bmatrix} \boldsymbol{\nabla}_{\boldsymbol{v}}^T f_1 \\ \boldsymbol{\nabla}_{\boldsymbol{v}}^T f_2 \\ \vdots \\ \boldsymbol{\nabla}_{\boldsymbol{v}}^T f_m \end{bmatrix} = \\ &= \begin{bmatrix} \frac{\partial f_1}{\partial v_1} & \frac{\partial f_1}{\partial v_2} & \cdots & \frac{\partial f_1}{\partial v_n} \\ \frac{\partial f_2}{\partial v_1} & \frac{\partial f_2}{\partial v_2} & \cdots & \frac{\partial f_2}{\partial v_n} \\ \vdots & \vdots & \ddots & \vdots \\ \frac{\partial f_m}{\partial v_1} & \frac{\partial f_m}{\partial v_2} & \cdots & \frac{\partial f_m}{\partial v_n} \end{bmatrix}. \end{aligned}$$

➢ Notation $\boldsymbol{\nabla}_{COE} \boxtimes$ indicates the Jacobian of $\boxtimes$ w.r.t. the classical orbital element state vector

$$\boldsymbol{x}_{COE} = \begin{bmatrix} a & e & i & \Omega & \omega & M \end{bmatrix}^T,$$

i.e.,

$$\boldsymbol{\nabla}_{COE} \boxtimes = \boldsymbol{\nabla}_{aei\Omega\omega M} \boxtimes.$$

➢ Notation $\boldsymbol{\nabla}_{EOE}\boxtimes$ indicates the Jacobian of $\boxtimes$ w.r.t. the equinoctial orbital element state vector

$$\boldsymbol{x} = \begin{bmatrix} a & P_1 & P_2 & Q_1 & Q_2 & l_\Theta \end{bmatrix}^T,$$

i.e.,

$$\boldsymbol{\nabla}_{EOE}\boxtimes = \boldsymbol{\nabla}_{aP_1P_2Q_1Q_2l_\Theta}\boxtimes.$$

➢ The Jacobian of a vector factorized as $\boldsymbol{F}(\boldsymbol{v})\boldsymbol{f}(\boldsymbol{v})$ can be calculated via the chain rule with the following way

$$\boldsymbol{\nabla}_{\boldsymbol{v}}\left[\boldsymbol{F}(\boldsymbol{v})\boldsymbol{f}(\boldsymbol{v})\right] = \begin{bmatrix} \boldsymbol{F}_{v_1}\boldsymbol{f} & \boldsymbol{F}_{v_2}\boldsymbol{f} & \cdots & \boldsymbol{F}_{v_n}\boldsymbol{f} \end{bmatrix} + \boldsymbol{F}(\boldsymbol{\nabla}_{\boldsymbol{v}}\boldsymbol{f}).$$

This calculus rule is used to calculate matrix $\boldsymbol{A}(t)$ of the GEO satellite linear model from the linearization of Gauss's or Lagrange's VOP nonlinear equations (see Chapter 6 at page 201).

➢ Gradient operator ∇ has not to be confused with Jacobian operator $\boldsymbol{\nabla}$. Given for example a potential function $\mathcal{E} = \mathcal{E}(x, y, z)$ dependent on the inertial Cartesian coordinates, the gradient of $\mathcal{E}$ along the axes X, Y, Z of the ECI reference frame with orthogonal basis $\boldsymbol{X}$, $\boldsymbol{Y}$, $\boldsymbol{Z}$ is

$$\nabla\mathcal{E}(x, y, z) = \mathcal{E}_x(x, y, z)\boldsymbol{X} + \mathcal{E}_y(x, y, z)\boldsymbol{Y} + \mathcal{E}_z(x, y, z)\boldsymbol{Z}.$$

➢ First and second time derivatives will be indicated sometimes with dotted notation

$$\begin{aligned} \dot{v}_k &= \frac{dv_k}{dt}, \\ \ddot{v}_k &= \frac{d^2v_k}{dt^2}, \\ \dot{\boldsymbol{v}} &= \frac{d\boldsymbol{v}}{dt} = \begin{bmatrix} \dot{v}_1 & \dot{v}_2 & \dots & \dot{v}_n \end{bmatrix}^T, \\ \ddot{\boldsymbol{v}} &= \frac{d^2\boldsymbol{v}}{dt^2} = \begin{bmatrix} \ddot{v}_1 & \ddot{v}_2 & \dots & \ddot{v}_n \end{bmatrix}^T. \end{aligned}$$

➢ Time derivative of a generic scalar function f_k of $\boldsymbol{v}$ can be calculated via the chain rule as

$$\dot{f}_k = \frac{df_k}{dt} = \left(\boldsymbol{\nabla}_{\boldsymbol{v}}^T f_k\right)\dot{\boldsymbol{v}}.$$

➢ The notation

$$\left[\boxtimes\right]_{\boldsymbol{v}=\boldsymbol{v}_0}$$

means that the function $\boxtimes$ of $\boldsymbol{v}$ is evaluated in $\boldsymbol{v} = \boldsymbol{v}_0$.

➢ The Taylor development of the vector function $\boldsymbol{f}(\boldsymbol{v})$ around $\boldsymbol{v} = \boldsymbol{v}_0$ is calculated and denotated as follows

$$\boldsymbol{f}(\boldsymbol{v}) = \boldsymbol{f}(\boldsymbol{v}_0) + \left[\boldsymbol{\nabla}_{\boldsymbol{v}}\boldsymbol{f}(\boldsymbol{v})\right]_{\boldsymbol{v}=\boldsymbol{v}_0}(\boldsymbol{v} - \boldsymbol{v}_0).$$

Chapter 1

Introduction

1.1 Motivations and Objectives

The operation of geostationary satellites requires that their latitude and longitude remain confined during the whole spacecraft life. To this purpose, a suitable station keeping strategy is implemented, whose objectives are the set of manoeuvres that have to be executed in order to thwart the effects of natural perturbing forces affecting the spacecraft position. The strategy is decided by predicting the changes of the orbital parameters on the basis of simplified models for the spacecraft dynamics which take into account only the main natural perturbing forces: the luni-solar attraction force, the solar radiation pressure and the Earth gravitational force.

Nowadays, in order to achieve the objectives of a station keeping strategy, most geostationary satellites are equipped with chemical propulsion systems: in order to compensate changes in the orbit parameters, chemical thrusters are typically fired once every two weeks during a time interval T_m of few tens of minutes, providing forces of some tens of Newton. Given the small ratio between T_m and the geostationary orbital period, chemical thrusts can be considered with good approximation as impulsive. It thus makes sense to define station keeping strategy by excluding from the dynamics equations the non conservative forces (i.e., the thrusts).

More recently, however, the use of electric propulsion systems is being considered as a viable alternative to the classical chemical actuators and is rapidly becoming the baseline on new telecom satellite platforms. The use of low thrust propulsion systems is compulsory when the dimension of the station keeping box is very small. In this case the accelerations produced by the thrusters have to be of the same order of magnitude as the accelerations induced by the environmental perturbing forces.

Compared to chemical technology, this type of propulsion allows the overall platform to significantly improve their performances both in term of mass and/or lifetime. This is achieved thanks to the increase in specific impulse of a factor between 5 and 10 which makes it possible to reduce by the same factor the propellant mass needed for station keeping throughout the life of the satellite.

Replacing chemical thrusters with electric ones, however, is not without implications from the

control viewpoint. Since electric thrusters can only provide a very low thrust level (of the order of milliNewtons), in order to achieve the same station keeping objectives that would be given for chemical propulsion it is necessary to fire the electric thrusters for some hours every day. It is then important to think again the control strategy as a continuous process to be optimized.

The main goal of this thesis is to evaluate what is the impact in terms of control design of using a low thrust propulsion system instead of an high thrust propulsion system.

1.2 Approache Proposed

The dynamics of a GEO satellite will be studied in detail in order to obtain a dynamical model as accurate as possible. This model will be obtained in terms of Gauss' variation of osculating parameter (VOP) equations containing the environmental perturbing accelerations, instead of the environmental perturbing potential functions of the Lagrange's VOP equations, which are traditionally used to plan the station keeping maneuvers. The idea is to implement a controller for geostationary station keeping purposes based on a model written in terms of osculating orbital elements instead of averaged elements. Such a controller plans in an automatic way the SK maneuvers and it could be integrated on board in view of autonomous station keeping control loop.

We will devote attention to the real performances of an electric propulsion system. In particular, current electric thrusters for station keeping can only provide on off thrust; this constraint implies that the electric station keeping problem has to be formulated as an optimal control problem with mixed constraints: continuous in the state variables and discrete in the control variables.

The approach which we intend to follow to design a fine station keeping controller is the direct approach. We will translate the station keeping problem formulated as optimal control problem into a parameter optimization problem and we will solve it via linear and nonlinear optimization programs.

We will use the receding horizon optimization approach to find the optimal trajectory fulfilling the orbital requirements characterizing the geostationary mission. Then, we will look for a transformation of the spacecraft state space such that the transformed geostationary linear system (initially with time varying coefficients) turns out to be differentially flat and with time invariant coefficients. This means that only three outputs of the system and their derivatives are sufficient to describe all the geostationary satellite dynamics. Moreover, the control variables can be explicitly expressed in function of these outputs and their derivatives.

1.3 Thesis Dissertation Outline

Chapter 1 of the dissertation is an introduction (see page 11 for the French translation). The rest of the thesis dissertation is organized as follows.

Chapter 2. It is a background chapter where some fundamental definitions are given in order to

understand what will be explained in the sequel of the dissertation. We introduce the time systems, the reference frames and the corresponding coordinate systems where and in terms of which the geostationary satellite motion equations will be defined. The satellite state representation in terms of classical and equinoctial orbital elements is given as alternative to the position and velocity vector representation. Conversion formulas that will be used in geostationary dynamics simulator are also listed. The concept of osculating and mean orbital elements is defined and a brief review of the different techniques to examine the effects of perturbations in the orbit propagation is done.

Chapter 3. In this chapter we describe the three main environmental perturbations acting on a geostationary satellite, both in terms of accelerations and in terms of corresponding potential functions. The thrust accelerations are also considered as accelerations provided by a propulsion system able to counteract the disturbing effect of the above ones. We define the main performance parameters of a spacecraft propulsion system and we explain the differences between the chemical propulsion and the electrical one. Thrust accelerations are expressed as a function of the propulsion system configuration and of the thrust forces to give a propulsion system acceleration model. In this chapter, we depict also the commonly employed high thrust propulsion system configurations and those at low thrust more recently proposed for station keeping purposes.

Chapter 4. In this chapter we present different translational dynamical models for a geostationary satellite: nonlinear models in unperturbed Keplerian conditions and nonlinear models in perturbed Keplerian conditions (Gauss' and Lagrange's forms of the variation of osculating parameter equations). A procedure to analytically solve Kepler's equation with small parameters is also described. Geographical position vector components are considered as nonlinear functions of the equinoctial orbital elements. Finally a linearized geostationary orbit model is presented with the environmental perturbing accelerations expanded in Taylor's series up zeroth order. This last model is described by the classical Clohessy-Wiltshire equations also known as Hill's equations of the relative motion of a geostationary spacecraft with respect to the ideal geostationary orbit. Simulation results are presented along all the chapter to show the time histories of the modeled satellite state vector components and of the position vector in geographical spherical coordinates.

Chapter 5. In this chapter we start to deal with the station keeping problem. We define the geostationary satellite orbital requirements. We explain the difference between high and low thrust station keeping maneuvers. We state the station keeping problem as a maneuver planning problem in its most general accepted meanings, leaving out in a first time some important specifications related with operational practice and propulsion system technology. Actually the station keeping maneuver planning becomes part of the geostationary station keeping control loop. It is one of the three main operations that have to be performed to ensure

the functioning of the control loop. The other two operations are the orbit determination and the maneuver execution. In this chapter these last two operations are briefly described by giving some related bibliography references. A survey of the works found in the state of the art about the geostationary station keeping maneuver planning concludes the chapter. The works related with the low thrust maneuver planning are surveyed separately from those ones related with the high thrust maneuver planning. Based on the above categorization three works (relevant to autonomous station keeping control loops) fall outside because they handle the station keeping maneuver planning problem as a formation keeping maneuver planning problem, i.e., as a regulation problem.

Chapter 6. In this chapter we deal with the station keeping maneuver planning problem solving a sequence of optimal control problems over finite time horizons with constraints on the state variables and on the control variables. The first set of constraints is given by the mathematical translation of the mission orbital requirements. Once the spacecraft propulsion system has been chosen, the second set is given by the mathematical translation of the propulsion system technological requirements. In this chapter we first formulate in mathematical terms the SK maneuver planning problem under virtual technological conditions: the propulsion system is composed of six thrusters with infinite specific impulsion, orthogonally mounted along the three axes of the RTN reference frame and, at every instant, able to produce an acceleration vector with unbounded magnitude in any direction. We propose a solution based on direct transcription of the problem in terms of parameter optimization problems. In order to implement the solution with linear programming codes, we will refer to the first order Taylor's expansion of the nonlinear Gauss' VOP equations about the nominal station keeping trajectory; however, to validate the solution the nonlinear model will be used. This chapter also contains a brief survey of the solution methods of the trajectory optimization problems. We present and discuss some simulation results of the above simplified problem, obtained with the fixed horizon optimization approach and with the receding horizon one. We take gradually into account technological specifications relevant to the propulsion system and we perform feasibility studies in presence of new constraints on the control variables. We deal with two idealized models to describe the electrical thrusters. The first model corresponds to that of thrusters which are able to give thrusts that can be modulated. The second model corresponds to that of thrusters which are able to work only in on off conditions. We finally relax the hypothesis of having six thrusters working independently, mounted orthogonally on the spacecraft body. We try to answer the following questions: do privileged thrust directions in the RTN frame exist, such that for thrusters mounted along them the number of thrusters can be reduced by synchronizing the maneuvers in the three directions of the RTN reference frame?

Chapter 7. In this chapter, we explain the way to transform the linear system with time varying coefficients describing the linear dynamics of a GEO satellite in a linear system with time

invariant coefficients. This transformation is a Lyapunov transformation, which does not modify the stability properties of the original system. Moreover, this transformation leads to recognize differential flatness in the GEO satellite dynamics.

Chapter 8 is the conclusion chapter (see page 277 for the French translation).

Chapter 2

Background

In this chapter some fundamental definitions are given as minimum background for the understanding of the sequel of this thesis dissertation.

In Section 2.1 and 2.2 we introduce the time systems, the reference frames and the corresponding coordinate systems where and in terms of which the geostationary satellite dynamics will be defined. In Section 2.3 the satellite state representation in terms of classical and equinoctial orbital elements is given as alternative to the position and velocity vector representation; conversion formulas that will be used in geostationary dynamics simulator are also listed. Section 2.4 introduces the concept of osculating and mean orbital elements. Finally, Section 2.5 is a brief review of the different techniques to examine the effects of perturbations in the orbit propagation.

Further details related with all the topics introduced in this chapter can be found, for example, in [Meeus, 1998], [Zarrouati, 1987], [Soop, 1994], [CNES, 1995a] and [CNES, 1995b], [Sidi, 1997], [Battin, 1999], [Montenbruck and Gill, 2000], [Vallado, 2001].

2.1 Time Systems

2.1.1 Local Sidereal Time (LST) and Coordinated Universal Time (UTC)

The sidereal time is traditionally defined as the time between successive transits of the stars over a particular meridian. Because the stars are several orders of magnitude more distant than the Sun, their relative locations as seen from the Earth does not change much during a year. However, irregularities in the Sun's apparent motion make it difficult to use the Sun's motion for reckoning time. As a result, the concept of universal time (UT) was adopted years ago. It is based on a fictitious mean Sun exhibiting uniform motion in right ascension along the equator. This fictitious mean Sun is now defined mathematically as a function of the sidereal time. So, ultimately, the UT (more precisely its variations UT0, UT1 and UT2) is derived from the sidereal time (see [Vallado, 2001]).

Sidereal time is a direct measure of the Earth's rotation and it is measured positively in the

counter clockwise direction when viewed from the North pole. Ideally, the observations of a star would suffice for determining sidereal time but the changing in the Earth's instantaneous axis of rotation causes station locations to change continually. This produces a small difference in the time of meridian transits, depending on the star declination (see Section 2.2.1). Because this effect vanishes at the equator, it is better to use stars with small declinations: for example the Sun which crosses the intersection between the equator plane and the ecliptic[1] twice a year. This intersection is defined as a line of nodes. The two instants of crossing are called the *equinoxes*. The points of crossing are the ascending node in the spring about March 21 (vernal equinox) and the descending node in the fall about September 23 (autumn equinox). They are on the equatorial plane but the vernal equinox is more suitably defined to be always on the equator. The sidereal time is defined as the hour angle of the vernal equinox relative to the local meridian. The sidereal time associated with the Greenwich meridian is termed Greenwich mean sidereal time (GMST). The sidereal time at a particular longitude is called local sidereal time (LTS).

The Coordinated Universal Time (UTC) is derived from atomic time, it is the basis of civil time systems and it is on ordinary clocks. The UTC is the time scale used for all satellite operations, the time by which also all satellite telemetry and tracking data is labeled at the ground stations. The definition of UTC concept originated in 1962 as a cooperative international effort to provide a consistent time standard for broadcasting. UTC was introduced in January 1972, as a convenient approximation of UT1 (see [Vallado, 2001] pages 184 and 185).

2.1.2 Epoch and Calendar Date

The moment of an event is referred to as the epoch of the event. The epoch designates a particular instant designated with a calendar date expressed in day, local sidereal time of the day, month and year. For example the date

$$\text{2010 January 1.0} \tag{2.1}$$

designates the 1st January 2010 when the Local Sidereal Time expressed in hours (hrs) is equal to 00.00 hrs. The date

$$\text{2010 January 1.75} \tag{2.2}$$

designates the 1st January 2010 when the Local Sidereal Time is equal to 18.00 hrs.

There are mainly two different reference epochs with respect to which a date can be defined:

1. the epoch designated by the date 2000 January 1.5 (J2000) of beginning of a Julian year;
2. the epoch designated by the date 1950 January 0.923 (B1950) of beginning of a Besselian year.

[1] The ecliptic is the plane of the Earth's mean orbit about the Sun.

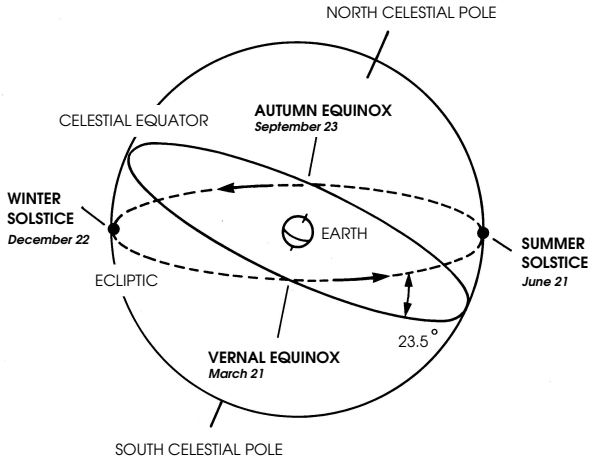

Figure 2.1: *Vernal and autumn equinoxes*

A Julian year is the solar year of 365.25 days, which implies one extra day every four years. A Besselian year is a year of 365.2421988 days, equal to the tropical year, defined as the time for the mean Sun's right ascension to increase by 24 hours. The first one will be used in this thesis.

Another way to designate a date (useful in defining the celestial body ephemerides) is in terms of decimal number of days since a reference date:

1. the Julian Date (JD) is the number of days since noon January 14713 BC including the fraction of day;

2. the Modified Julian Date (MJD) is defined as

$$\mathrm{MJD} = \mathrm{JD} - 2400000.5 \tag{2.3}$$

to have a date number smaller and to start counting at midnight.

2.2 Reference Frames and Coordinate Systems (RFCSs)

2.2.1 Earth Centered Inertial RFCS

Earth Centered Inertial (ECI) reference frame with orthonormal basis $\boldsymbol{XYZ}$ has its origin in the center of the Earth and the fundamental plane coinciding with the Earth's equatorial plane. The unit vectors $\boldsymbol{X}$, $\boldsymbol{Y}$, $\boldsymbol{Z}$ of its orthonormal basis have the same directions of the X, Y, Z axes (see

Fig. 2.2). The Z axis points to the North pole. The X axis is aligned with the line of intersection of the equatorial plane and of the Earth's orbital plane around the Sun, i.e., the vernal equinox or first point of Aries Υ. The Y axis completes a right-handed orthogonal coordinate system.

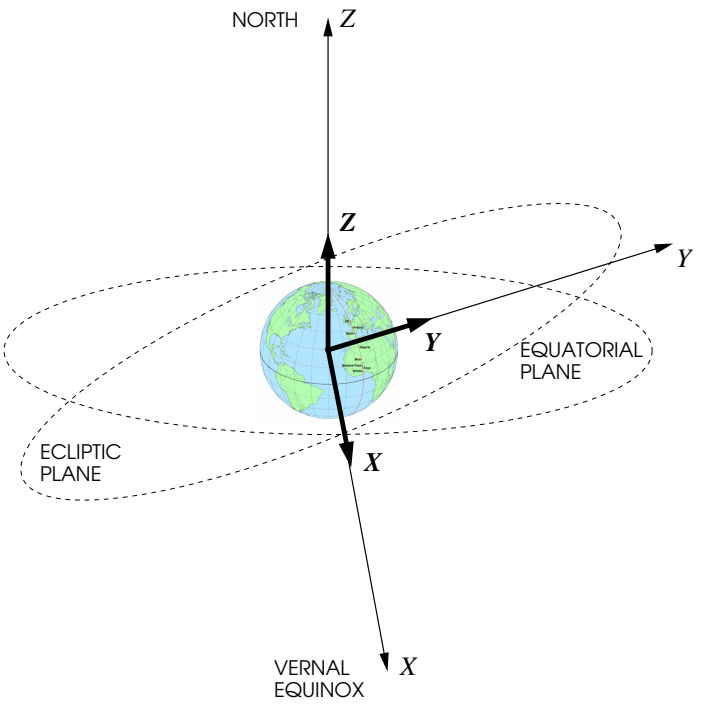

Figure 2.2: *Earth Centered Inertial (ECI) reference frame*

Earth Centered Inertial is actually a bit of a misnomer, due to the fact that the vernal equinox and equatorial plane vary slightly over time. The Earth's equator is not fixed in inertial space. The gravitational force of the Sun, the Moon and other planets on the Earth's equatorial bulge drive the equator motion. This motion consists of both precession and nutation (see Fig. 2.3). The precession of the Earth is the secular effect of the gravitational attraction from the Sun and the planets on the equatorial bulge of the Earth. The main effect is a rotation of the ECI frame in the negative sense in the ecliptic plane by one turn in 26000 years, which is equivalent to 0.014° per year. The nutation is the short-periodic effect of the gravitational attraction of the Moon and, to a lesser degree, the planets on the Earth's equatorial bulge. It has a certain periodicity with important contributions from the Moon's orbital period. The maximum value of anyone of the two nutation angles is 0.006°. Likewise, the ecliptic plane varies due to perturbations by the planets on the Earth's orbital plane. The slow rotation of the ecliptic, called planetary precession, causes an eastward movement of the equinox (approximately 12 arc seconds per century) and a decrease in the obliquity of the ecliptic, ε, which is the angle between the Earth's equator and the ecliptic

(approximately 47 arc seconds per century).

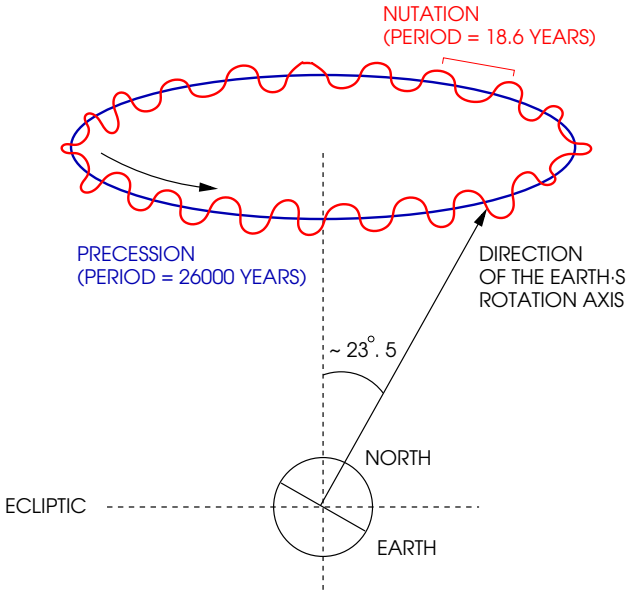

Figure 2.3: *Earth's precession and nutation*

Thus, the ECI frame is time-dependent. The ECI system at a particular time is referred to as either a True-of-Date or Mean-of-Date inertial system. If we account for both precession and nutation effects, we have a True-of-Date system that references the True Equator and True Equinox (TETE) of date. If we ignore the nutation effect, we are left with a Mean-of-Date system that references the Mean Equator and Mean Equinox (MEME) of date.

In order to achieve a sufficiently inertial coordinate system for an accurate enough orbit determination, the equinox and equator are specified at a particular epoch. From 1984 the most commonly used reference epoch is J2000 (i.e., 2000 January 1.5, the beginning of a Julian year). Before 1984, star position catalogs used for a standard epoch the B1950 (i.e., 1950 January 0.923, the beginning of a Besselian year). See Section 2.1.2 for the meaning of the decimal notation of the dates and for the definitions of a Julian and Besselian year.

The position of a point (e.g., the satellite center of mass) in the ECI frame can be specified by either Cartesian coordinates x, y, z or inertial spherical coordinates geocentric distance r, right ascension α, geocentric declination δ (see Fig. 2.4).

The conversion from the inertial spherical coordinates to Cartesian coordinates and vice versa

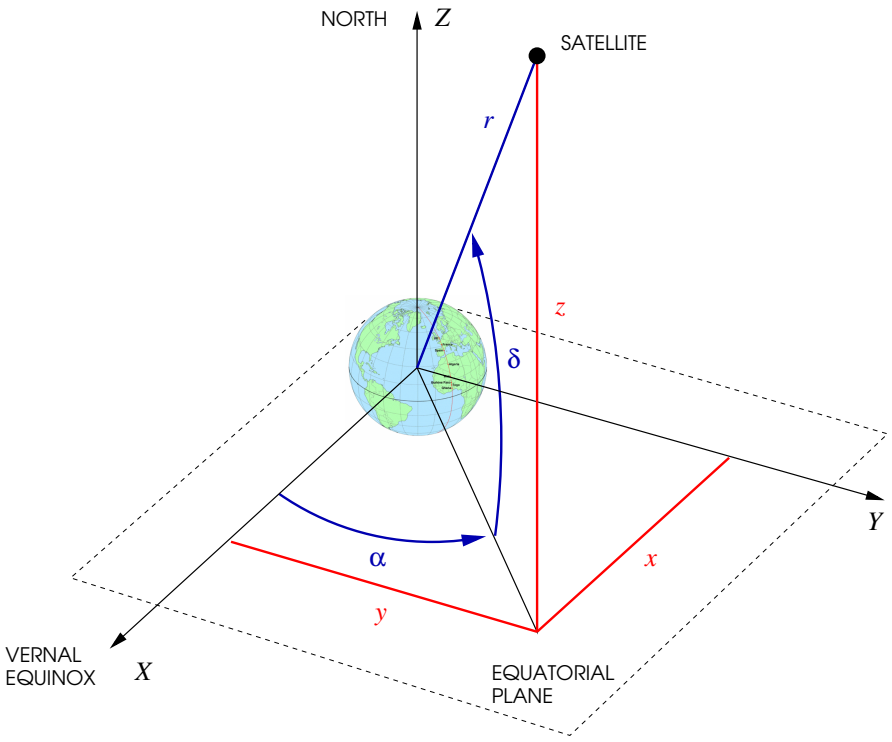

Figure 2.4: *Cartesian (red) and spherical (blue) inertial coordinates*

may be accomplished via the following basic relations

$$\begin{bmatrix} x \\ y \\ z \end{bmatrix} = \begin{bmatrix} r\cos\delta\cos\alpha \\ r\cos\delta\sin\alpha \\ r\sin\delta \end{bmatrix} \tag{2.4}$$

and

$$\alpha = \arctan\frac{y}{x}, \quad \delta = \arctan\frac{z}{\sqrt{x^2+y^2}}, \quad r = \sqrt{x^2+y^2+z^2} \tag{2.5}$$

where the quadrant of α is chosen in such a way that the sign of the denominator x is equal to the sign of $\cos\alpha$, i.e., $-90° < \alpha < 90°$ for $x > 0$ and $90° < \alpha < 270°$ for $x < 0$.

2.2.2 Earth Centered Earth Fixed RFCS

The geocentric coordinate system may be allowed to rotate with the Earth, and is referred to as the Earth Centered Earth Fixed (ECEF) reference frame. The origin is the center of the Earth, and the fundamental plane is the equatorial plane. The principal axis is always aligned with a particular meridian, usually the Greenwich meridian.

Geostationary satellite position on the Earth is defined by the geographical longitude (or subsatellite longitude) λ and the geographical latitude (or subsatellite latitude) φ. Coordinates λ, φ and r are the spherical coordinates in the ECEF reference frame. Longitude λ is counted positively towards the East, and differs from the right ascension α by the right ascension Θ of the Greenwich meridian

$$\lambda = \alpha - \Theta. \tag{2.6}$$

Assuming the Earth with perfectly spherical shape, latitude φ is equal to the satellite declination δ

$$\varphi = \delta. \tag{2.7}$$

Right ascension Θ of the Greenwich meridian, also called Greenwich Hour Angle (GHA), is the angle from $\boldsymbol{X}$ axis to the Greenwich meridian (see Fig. 2.5). It can be calculated as a function of the Coordinated Universal Time UTC with 0.004° accuracy by means of the uniform angular velocity of the Earth $\omega_\oplus$ by the following equation

$$\Theta(t) = \Theta_r + \omega_\oplus (t - t_r) \tag{2.8}$$

where Θ_r is the value of Θ at a reference instant t_r. The right ascension of the Greenwich meridian Θ at time t (in the UTC system) is also known as Greenwich mean sidereal time (GMST). It is the local sidereal time (see Section 2.1.1) associated with the longitude of the Greenwich meridian. Table 1 of [Soop, 1994] shows the values of Θ_r at 0 hours UTC on January 1 for a sequence of years.

The conversion from the geographical spherical coordinates r, λ, φ to the inertial Cartesian coordinates x, y, z may be accomplished via the following basic relation

$$\begin{bmatrix} x \\ y \\ z \end{bmatrix} = \boldsymbol{\mathcal{R}}_Z(-\Theta) \begin{bmatrix} r\cos\varphi\cos\lambda \\ r\cos\varphi\sin\lambda \\ r\sin\varphi \end{bmatrix} \tag{2.9}$$

where matrix $\boldsymbol{\mathcal{R}}_Z(-\Theta)$ describes a rotation around the Z axis of an angle $-\Theta$

$$\boldsymbol{\mathcal{R}}_Z(-\Theta) = \begin{bmatrix} \cos\Theta & -\sin\Theta & 0 \\ \sin\Theta & \cos\Theta & 0 \\ 0 & 0 & 1 \end{bmatrix}. \tag{2.10}$$

The conversion from the inertial Cartesian coordinates x, y, z to the geographical spherical coordinates r, λ, φ may be accomplished via the following basic relations

$$\lambda = \arctan\frac{y\sin\Theta + x\cos\Theta}{y\cos\Theta - x\sin\Theta}, \quad \varphi = \arctan\frac{z}{\sqrt{x^2+y^2}}, \quad r = \sqrt{x^2+y^2+z^2} \tag{2.11}$$

where the quadrant of $\lambda + \Theta$ is chosen in such a way that the sign of the denominator x is equal to the sign of $\cos(\lambda + \Theta)$, i.e., $-90° < \lambda + \Theta < 90°$ for $x > 0$ and $90° < \lambda + \Theta < 270°$ for $x < 0$.

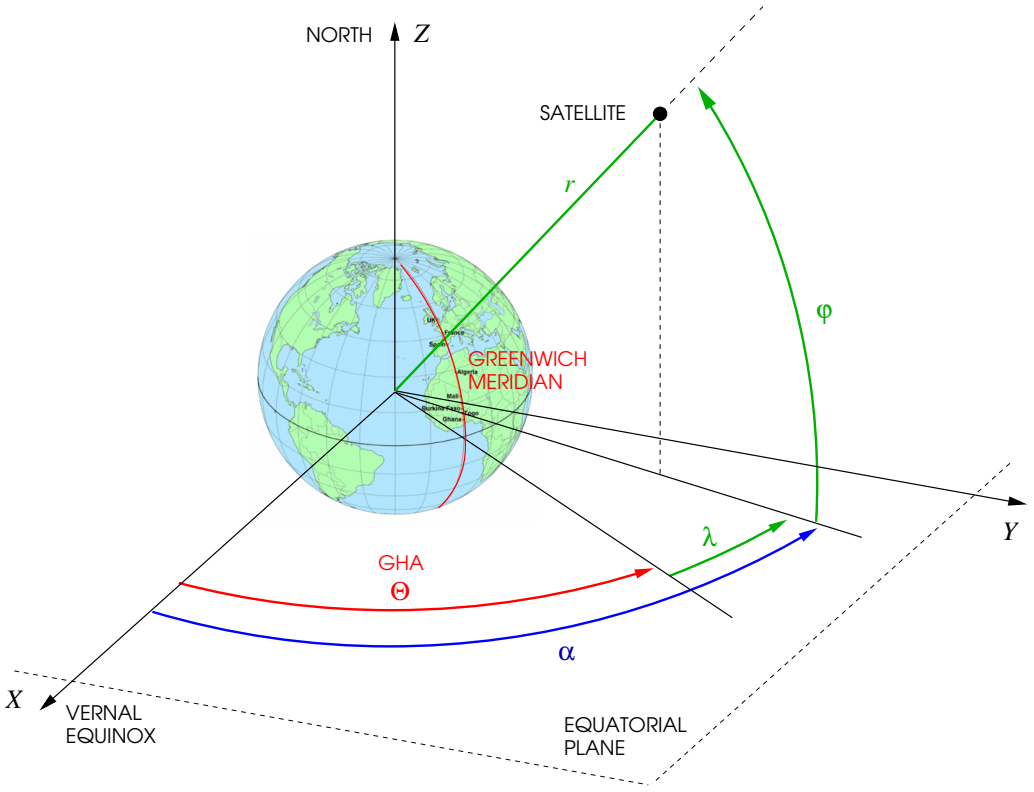

Figure 2.5: *Greenwich Hour Angle, geographical latitude and longitude*

2.2.3 Geostationary Clohessy-Wiltshire RFCS

We define the geostationary Clohessy-Wiltshire (GEO CW) reference frame with X_G, Y_G, Z_G axes as a non inertial reference frame rotating with the Earth (see Fig. 2.6). The fundamental plane is the equatorial plane. The origin is a point of the perfect geostationary orbit with radius $a_k \approx 42164$ km. The X_G axis points in opposite direction of the Earth. The Z_G axis is normal to the equatorial plane with direction toward the North. The Y_G axis completes a right-handed orthogonal coordinate system.

The Cartesian coordinates x_G, y_G, z_G of a point in this RFCS can be expressed in function of the inertial ones x, y, z of the ECI frame, by the following basic conversion formula

$$\begin{bmatrix} x_G \\ y_G \\ z_G \end{bmatrix} = \boldsymbol{\mathcal{R}}_Z \left(\Theta + \lambda_G\right) \begin{bmatrix} x \\ y \\ z \end{bmatrix} - \begin{bmatrix} a_k \\ 0 \\ 0 \end{bmatrix}, \tag{2.12}$$

where λ_G is the geographical longitude of the GEO CW coordinate system origin.

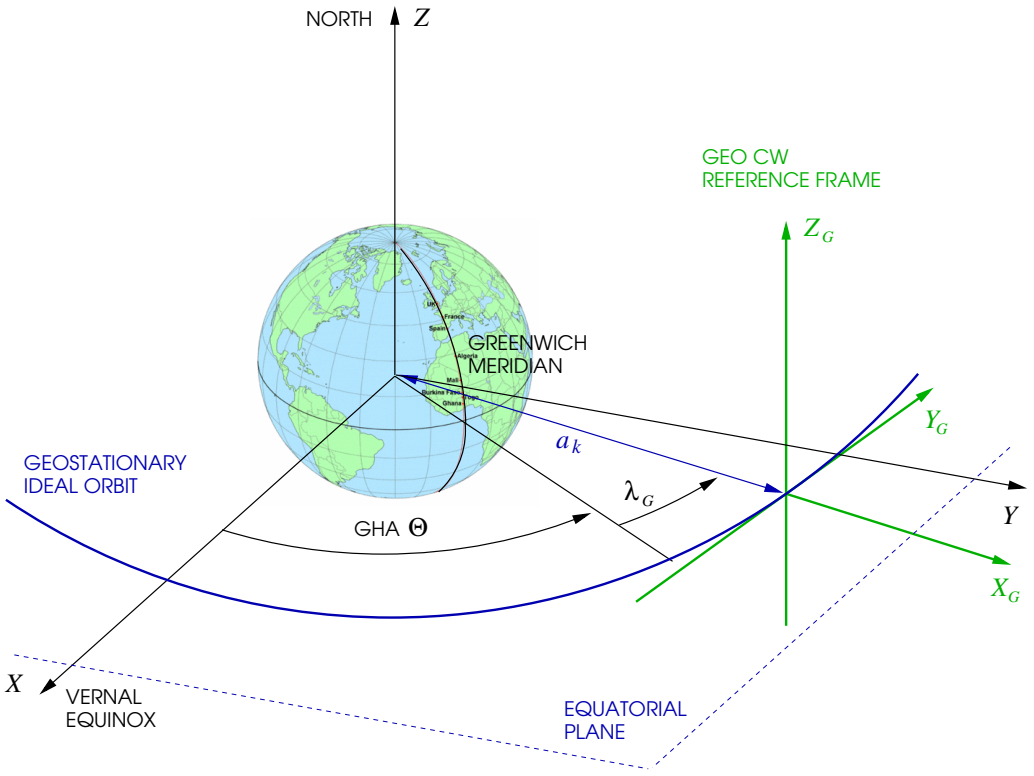

Figure 2.6: *Geostationary Clohessy-Wiltshire (GEO CW) reference frame*

2.2.4 Gaussian and Equinoctial RFCSs

The coordinate system used in this work for describing the perturbing forces is the satellite based Radial Tangent Normal (RTN) coordinate system with orthonormal basis $\boldsymbol{RTN}$, also called Gaussian coordinate system because it is used to express the perturbing accelerations in the Gauss' planetary equations[2]. The origin is fixed to the position of the spacecraft considered as punctiform; the unit vectors $\boldsymbol{R}$, $\boldsymbol{T}$, $\boldsymbol{N}$ of its orthonormal basis have the same directions of the R, T, N axes (see Fig. 2.7). The R axis is defined as always pointing from the Earth's center along the radius vector toward the satellite as it moves through the orbit

$$\boldsymbol{R} = \frac{\boldsymbol{r}}{r}. \tag{2.13}$$

The N axis is normal to the orbit plane with direction of the satellite angular momentum vector h

$$\boldsymbol{N} = \frac{\boldsymbol{h}}{h} \tag{2.14}$$

[2]This coordinate system is also used to study the relative motion between two close-orbiting satellites and to derive the Clohessy-Wiltshire equations. It is often called RSW coordinate system (see, e.g., [Vallado, 2001], [CNES, 1995a], [Zarrouati, 1987]).

with

$$\boldsymbol{h} = \boldsymbol{r} \wedge \boldsymbol{v}. \tag{2.15}$$

The T axis is perpendicular to R in the orbit plane and with the direction toward the satellite movement. It completes, with the unit vectors $\boldsymbol{R}$ and $\boldsymbol{N}$, a right-handed orthogonal basis

$$\boldsymbol{T} = \boldsymbol{N} \wedge \boldsymbol{R}. \tag{2.16}$$

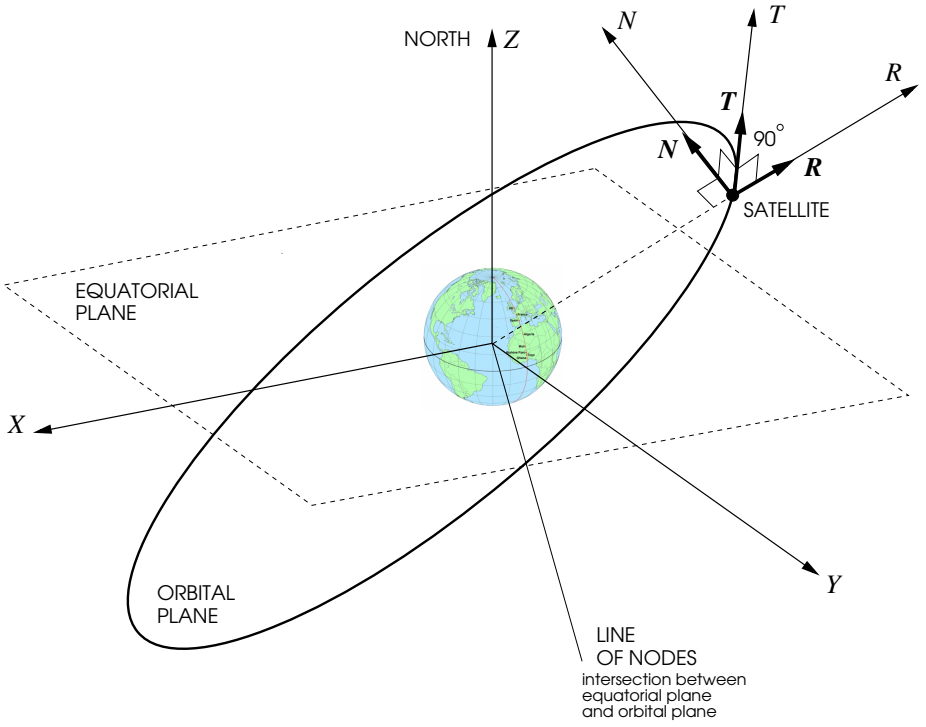

Figure 2.7: *Radial Tangent Normal (RTN) reference frame*

The coordinate system used in this work for analyzing the effect of the perturbing forces is the equinoctial one with orthonormal basis $\boldsymbol{EQW}$ (see Fig. 2.8). The satellite orbit plane is the fundamental plane. The satellite orbital plane is the fundamental plane. The principal axis along the unit vector $\boldsymbol{E}$ forms an angle equal to $-I\Omega$ with the the line of nodes. The angle Ω between the X axis and the line of nodes (intersection between the equatorial plane and the orbit plane) is defined as the right ascension of the ascending node. The coefficient I is a retrograde factor which is $+1$ for direct orbits and -1 for retrograde orbit. The third axis along the unit vector $\boldsymbol{W}$ is normal to the orbit and oriented in the same direction as the angular momentum vector. Unit vector $\boldsymbol{Q}$ completes the right-handed orthogonal coordinate system.

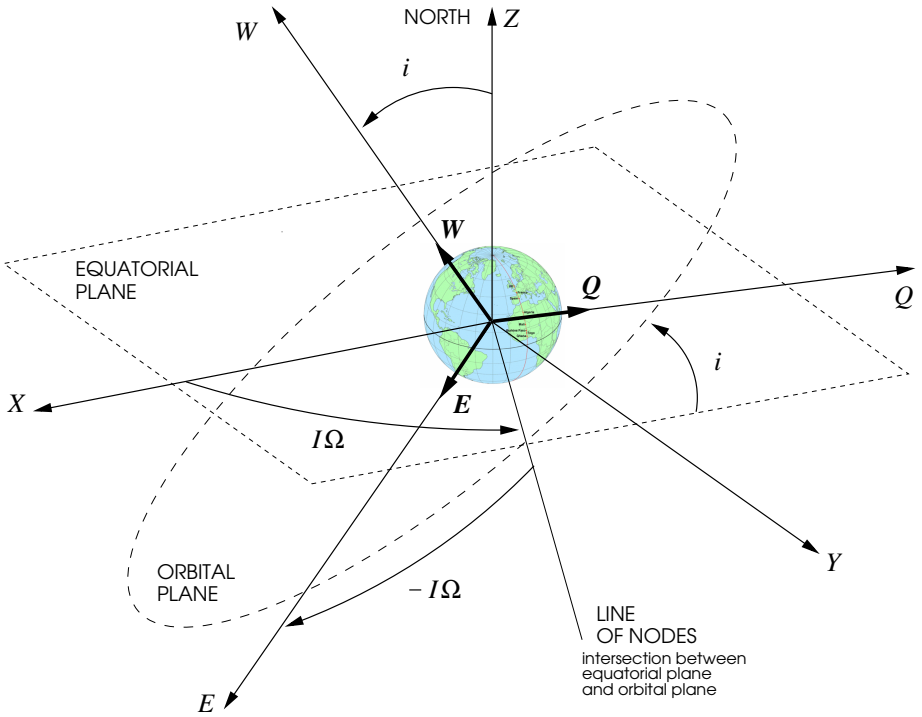

Figure 2.8: *Equinoctial reference frame*

2.2.5 Spacecraft Body Fixed RFCS

In this study, the orientations of the various thrusters of the satellite propulsion system are specified with respect to the Spacecraft Body Fixed (SBF) reference frame with orthonormal basis $\boldsymbol{X}_B\boldsymbol{Y}_B\boldsymbol{Z}_B$. The SBF frame for a typical 3-axis stabilized geostationary spacecraft is shown in figure 2.9. The origin of the SBF frame is the center of mass of the spacecraft, and the fundamental plane is normal to the spacecraft position vector. The principal axis is the X_B axis (roll axis), which points in the along-track direction and is perpendicular to the spacecraft position vector. This means that the X_B axis is not perfectly aligned with the velocity vector, except in the case of a circular orbit or in the case of an elliptical orbit at apogee or perigee. The Y_B axis (pitch axis) points in the cross-track direction, and is perpendicular to the principal axis as well as to the spacecraft position vector. The third axis is the Z_B axis (yaw axis), which is nadir-pointing in the direction opposite to the spacecraft position vector. The X_B, Y_B, Z_B axes are also called the longitudinal, lateral and vertical axes, or roll, pitch, and yaw axes, respectively. The SBF frame is the satellite coordinate system that is generally applied to 3-axis stabilized geostationary spacecraft. This is convenient because instruments on such spacecraft are typically oriented to be nadir-pointing along the Z_B axis, while the solar panels are typically oriented north-south and

rotate about the Y_B axis.

Usually, the satellite body reference frame is used for specifying the attitude control problem, which consist in placing the SBF frame with respect to another reference frame (for example, the inertial one or the orbital one). The geostationary station keeping problem tackled in this thesis is considered as a problem of position and velocity control, i.e., a problem tackled without attitude determination, but by means of the only orbit determination. This assumption is justified by the following hypothesis: for the considered geostationary satellite the attitude determination is not correlated with the characterization of the spacecraft center of mass motion. Moreover, in the thesis work, this simplifying hypothesis will be done: an adequate attitude control system makes the axes of the SBF reference frame aligned with those of the RTN reference frame and such that

$$\boldsymbol{X_B} = +\boldsymbol{T}, \quad \boldsymbol{Y_B} = -\boldsymbol{N}, \quad \boldsymbol{Z_B} = -\boldsymbol{R}. \tag{2.17}$$

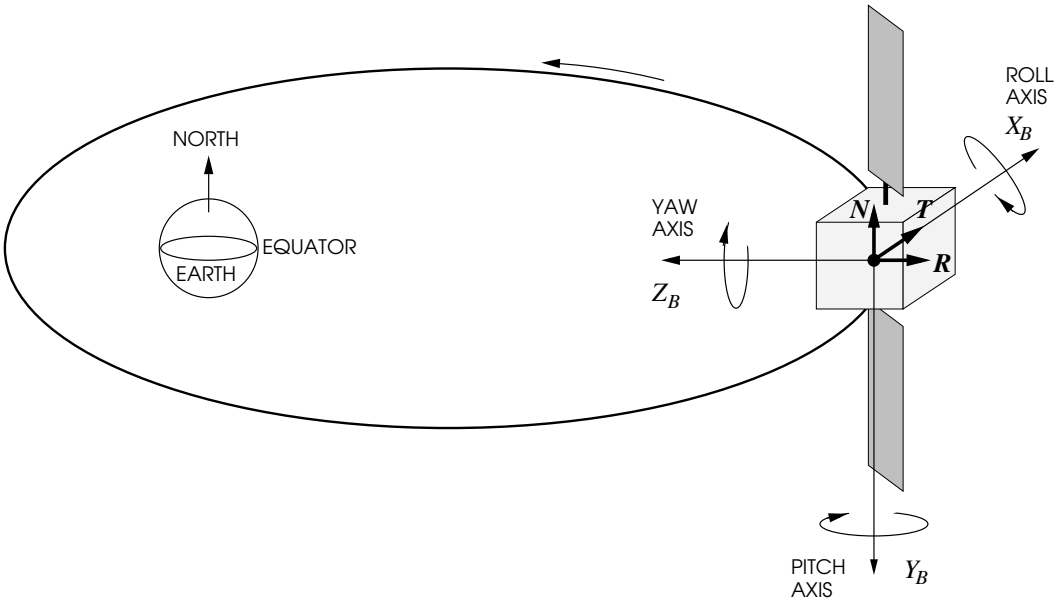

Figure 2.9: *Spacecraft Body Fixed (SBF) reference frame*

2.3 Satellite State Representations

The state of a satellite in space needs six quantities to be defined. These quantities may take on many equivalent forms. Whatever the form, we call the collection of these quantities either a state vector (usually associated with position and velocity vectors) or a set of elements called orbital elements (typically used with scalar magnitude and angular representations of the orbit). Either set of quantities is referenced to a particular reference frame and completely specifies the two-body orbit from a complete set of initial conditions for solving an initial value problem class of differential equations.

In the following four sections we will refer to a spacecraft subject only to the gravitational attraction of the Earth considered with punctiform mass (*unperturbed Keplerian conditions*).

2.3.1 Position and Velocity Coordinates

In the ECI reference frame the position and velocity vectors of a spacecraft influenced only by the gravitational attraction of the Earth considered with punctiform mass will be denotated as follows

$$\boldsymbol{r}_K = \begin{bmatrix} x_K & y_K & z_K \end{bmatrix}^T, \tag{2.18}$$

$$\boldsymbol{v}_K = \begin{bmatrix} v_{Kx} & v_{Ky} & v_{Kz} \end{bmatrix}^T = \frac{d\boldsymbol{r}_K}{dt}. \tag{2.19}$$

The acceleration of such a spacecraft satisfies the equation of two-body motion

$$\frac{d^2\boldsymbol{r}_K}{dt^2} = -GM_\oplus \frac{\boldsymbol{r}_K}{r_K^3} \tag{2.20}$$

where $GM_\oplus$ is the gravitational coefficient of the Earth and r_K is the modulus of the position vector $\boldsymbol{r}_K$. A particular solution of this second order vector differential equation is called an orbit that can be elliptic or parabolic or hyperbolic, depending on the initial values of the spacecraft position and velocity vectors $\boldsymbol{r}_K(t_0)$ and $\boldsymbol{v}_K(t_0)$. Only the elliptic trajectories and its special case, the circle, are of interest in the geostationary context.

The state representation by position and velocity of a spacecraft in unperturbed Keplerian conditions is

$$\boldsymbol{x}_{K_{PV}} = \begin{bmatrix} x_K & y_K & z_K & v_{Kx} & v_{Ky} & v_{Kz} \end{bmatrix}^T \tag{2.21}$$

at a given time t. Time t is always associated with a state vector and it is often considered as a seventh component. A time used as reference for the state vector or orbital elements is called the epoch.

2.3.2 Classical Orbital Elements

The most common element set used to describe elliptical orbits (including circular orbits) are the classical orbital elements (COEs) also called the Keplerian elements. They are described in the

sequel of this section. In all this section and in the following one, the index K (indicating that the spacecraft is in unperturbed Keplerian conditions) will be understood. Names and units of the COEs are

- a : semi-major axis, [km];
- n : mean motion, [sec^{-1}]
- e : eccentricity, [dimensionless];
- i : inclination, [rad];
- Ω : right ascension of the ascending node, [rad];
- ω : argument of perigee, [rad];
- ν : true anomaly, [rad];
- E : eccentric anomaly, [rad];
- M : mean anomaly, [rad];

(see Fig.s 2.10 and 2.11). The definitions of the COEs are referenced to the ECI frame.

- The semi-major axis a specifies the size of the orbit. Alternatively, the mean motion

$$n = \sqrt{\frac{GM_{\oplus}}{a^3}} \tag{2.22}$$

  can be used to specify the size.

- The eccentricity e specifies the shape of the ellipse. It is the magnitude of the eccentricity vector, which points toward the perigee along the line of apsis.

- The inclination i specifies the tilt of the orbit plane. It is defined as the angle between the angular momentum vector $\boldsymbol{h} = \boldsymbol{r} \wedge \boldsymbol{v}$ and unit vector $\boldsymbol{Z}$

$$\cos i = \frac{\boldsymbol{Z} \cdot \boldsymbol{h}}{h}. \tag{2.23}$$

- The right ascension of the ascending node Ω is the angle from the positive X axis to the node vector $\boldsymbol{n}$ pointing toward the ascending node, that is the point on the equatorial plane where the orbit crosses from south to north. The node vector $\boldsymbol{n}$ is defined as

$$\boldsymbol{n} = \boldsymbol{Z} \wedge \boldsymbol{h}. \tag{2.24}$$

  The cosine of the right ascension of the ascending node is then

$$\cos \Omega = \frac{\boldsymbol{X} \cdot \boldsymbol{n}}{n}, \tag{2.25}$$

where n is the modulus of the node vector and it has not to be confused with the mean motion n defined by Eq. (2.22). A quadrant check must be done because Ω can vary from 0 to 2π. If the component of $\boldsymbol{n}$ along the Y axis is negative, then

$$\Omega = 2\pi - \arccos\left(\frac{\boldsymbol{X}\cdot\boldsymbol{n}}{n}\right). \tag{2.26}$$

- The argument of perigee ω is measured from the ascending node to the perigee, i.e. to the eccentricity vector $\boldsymbol{e}$ pointing toward the perigee

$$\cos\omega = \frac{\boldsymbol{n}\cdot\boldsymbol{e}}{ne}. \tag{2.27}$$

A quadrant check must be done because ω can vary from 0 to 2π. If the component of $\boldsymbol{e}$ along the Z axis is negative, then

$$\omega = 2\pi - \arccos\left(\frac{\boldsymbol{n}\cdot\boldsymbol{e}}{ne}\right). \tag{2.28}$$

- The true anomaly ν specifies the position of the satellite within its orbit and it is the angle between the perigee and the current position vector $\boldsymbol{r}$

$$\cos\nu = \frac{\boldsymbol{e}\cdot\boldsymbol{r}}{er}. \tag{2.29}$$

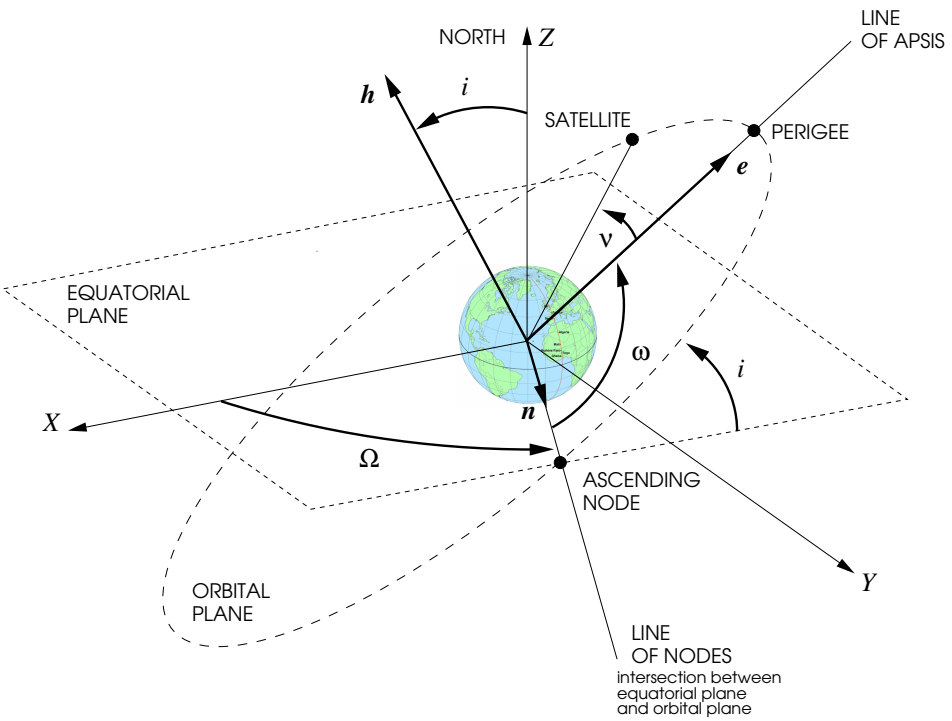

Figure 2.10: *Classical Orbital Elements (COEs)*

A quadrant check must be done because ν can vary from 0 to 2π. If $\boldsymbol{r} \cdot \boldsymbol{v} < 0$, then

$$\nu = 2\pi - \arccos\left(\frac{\boldsymbol{e} \cdot \boldsymbol{r}}{er}\right). \tag{2.30}$$

- The true anomaly is not a constant in the two-body motion. It varies with time and it is sometimes called the fast variable. Other orbital elements can be used instead of the true anomaly to describe the satellite position on the orbit. The first of these is the eccentric anomaly E. This angle is defined on the auxiliary circle of radius a, that can be drawn around the elliptical orbit, as shown in Fig. 2.11. Sine and cosine of eccentric anomaly are related to eccentricity and true anomaly in accordance with the following relations

$$\sin E = \frac{\sin\nu\sqrt{1-e^2}}{1+e\cos\nu} \quad \text{and} \quad \cos E = \frac{e+\cos\nu}{1+e\cos\nu}. \tag{2.31}$$

  Kepler's equation expresses the position in the orbit as a function of time in terms of the eccentric anomaly

$$E - e\sin E = n(t - t_p) \tag{2.32}$$

  where n is the mean motion and t_p is the passage time from the perigee.

- The right-hand side of equation (2.32) is also called the mean anomaly M

$$M = n(t - t_p). \tag{2.33}$$

  The mean anomaly is related to time and corresponds to the angular position of a body moving with constant angular velocity on the auxiliary circle of Fig. 2.11. Kepler's equation (2.32) can be rewritten so that it relates the mean and eccentric anomalies

$$E - e\sin E = M. \tag{2.34}$$

  Calculating the eccentric or true anomaly given the mean anomaly using Kepler's equation is a transcendental operation. One must use an iterative method in order to solve for E to a sufficient accuracy given M and e. With small eccentricity, finding an approximate analytical solution of Kepler's equation consists in solving an algebraic perturbation problem (see the following of this dissertation and [Hull, 2003]).

In this work, satellite state representation in terms of classical orbital elements will be denoted as follows

$$\boldsymbol{x}_{COE} = \begin{bmatrix} a & e & i & \Omega & \omega & \text{anomaly} \end{bmatrix}^T \tag{2.35}$$

with the anomaly component equal to the true anomaly ν or the eccentric anomaly E or the mean anomaly M.

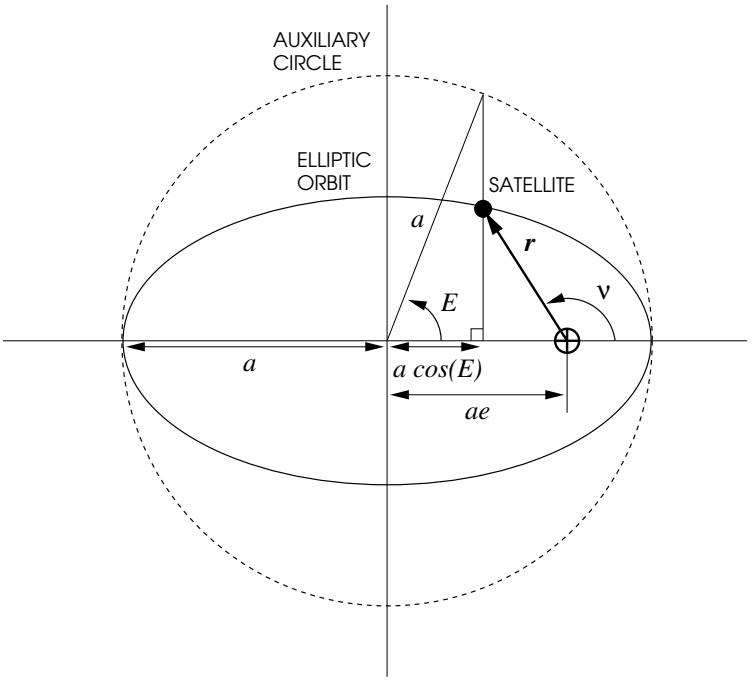

Figure 2.11: *True and eccentric anomalies for elliptic motion*

2.3.3 Equinoctial Orbital Elements

COEs suffer from two main singularities. The first is when the orbit is circular, i.e., when the eccentricity is zero ($e = 0$). In this case the line of apsis is undefined and also the argument of perigee ω. The second occurs when the orbit is equatorial, i.e., when the inclination is zero ($i = 0$). In this case the ascending node is undefined and also the right ascension of the ascending node Ω. See Fig. 2.10.

In the special case of an elliptical equatorial orbit, the ascending node is undefined. In this case, the true longitude of periapsis, $\tilde{\omega}_{true}$, is defined as the angle between the vernal equinox measured positive eastward to the eccentricity vector pointing toward the perigee

$$\tilde{\omega}_{true} = \frac{\boldsymbol{X} \cdot \boldsymbol{e}}{e}. \tag{2.36}$$

For all orbits, the longitude of periapsis, $\tilde{\omega}$, is defined by the following sum

$$\tilde{\omega} = \omega + \Omega. \tag{2.37}$$

It should be noted that this element is not necessarily a true longitude in the normal sense, because ω and Ω are measured in two different planes if the orbit is inclined.

In the case of a circular inclined orbit, there is no perigee, so the argument of perigee and the true anomaly cannot be defined. In this case, the argument of latitude, w, is the angle eastward from the ascending node to the spacecraft position vector. A relation in terms of the classical orbital elements for w is

$$w = \omega - \nu. \tag{2.38}$$

This relation is always true because ω and ν are in the same plane.

For the special case of a circular equatorial orbit, neither the ascending node nor the perigee are defined. The true longitude L, is the angle positive eastward from the positive X axis to the spacecraft position vector $\boldsymbol{r}$

$$\cos L = \frac{\boldsymbol{X} \cdot \boldsymbol{r}}{r}. \tag{2.39}$$

The true longitude can be approximated (because in the ECI reference frame the angles are in different planes when the orbit is inclined) as

$$L = \omega + \Omega + \nu. \tag{2.40}$$

Moreover, when the orbit is close to being equatorial as in the geostationary case, the true longitude L can be approximated with the right ascension α.

The equinoctial orbital elements (EOEs) avoid the singularities encountered when using the classical orbital elements. EOEs were originally developed by Lagrange in 1774. Their definitions in terms of Keplerian elements are given by the following equations

$$a, \tag{2.41}$$

$$P_1 = e \sin(\omega + I\Omega), \tag{2.42}$$

$$P_2 = e \cos(\omega + I\Omega), \tag{2.43}$$

$$Q_1 = \tan(i/2) \sin \Omega, \tag{2.44}$$

$$Q_2 = \tan(i/2) \cos \Omega, \tag{2.45}$$

$$l = \Omega + \omega + M. \tag{2.46}$$

True retrograde equatorial orbits ($i = 180°$) cause problems because Q_1 and Q_2 are undefined. This problem is solved by introducing a retrograde factor I which is $+1$ for direct orbits and -1 for retrograde orbits. In this work, dealing with geostationary satellites, I is equal to $+1$ and the mean longitude net of the GHA $\Theta(t)$

$$l_\Theta = \Omega + \omega + M - \Theta(t) \tag{2.47}$$

will be used instead of the mean longitude l given by Eq. (2.46). GEO satellite state representation in terms of equinoctial orbital elements will be denoted as follows

$$\boldsymbol{x} = \begin{bmatrix} a & P_1 & P_2 & Q_1 & Q_2 & l_\Theta \end{bmatrix}^T. \tag{2.48}$$

The definitions of the EOEs are referenced to the equinoctial reference frame with orthonormal basis $\boldsymbol{EQW}$ introduced in Section 2.2.4. It can be obtained from the ECI reference frame by a rotation through the angle Ω about the Z axis, followed by a rotation through the angle i about the new X axis (which points in the same direction as the node vector $\boldsymbol{n}$ pointing the ascending node), followed by a rotation through the angle $-I\Omega$ about the new Z axis (which points in the same direction as the $\boldsymbol{h}$ vector). In the equinoctial frame the elements P_1 and P_2 represent the projection of the eccentricity vector onto the $\boldsymbol{Q}$ and $\boldsymbol{E}$ directions, respectively. The elements Q_1 and Q_2 represent the projection of the vector oriented in the direction of the ascending node with magnitude $\tan(i/2)$, onto the $\boldsymbol{Q}$ and $\boldsymbol{E}$ directions, respectively. The element l is the mean longitude, which is a variation of the true longitude L defined in the orbital plane as

$$L = \omega + \Omega + \nu \tag{2.49}$$

(see Fig. 2.12).

The equinoctial element set is sometimes expressed in a slightly different fashion. Elements Q_1 and Q_2 can be defined with $\sin(i/2)$ or $\sin i$ or even just i replacing the $\tan(i/2)$ terms in Eq.s (2.44) and (2.45). These differences change the elements Q_1 and Q_2 to represent the projection of the vector oriented in the direction of the ascending node with a different magnitude onto the $\boldsymbol{Q}$ and $\boldsymbol{E}$ directions, respectively.

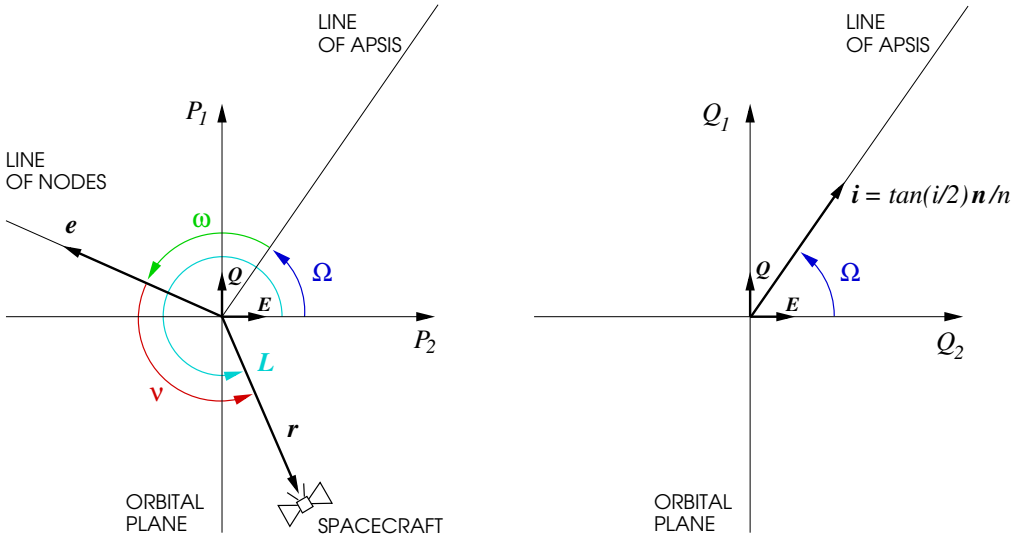

Figure 2.12: *Eccentricity and inclination equinoctial components and true longitude*

2.3.4 Conversion Formulas

Even in this section, index K in all orbital mechanics quantities of the spacecraft (indicating that the spacecraft is in unperturbed Keplerian conditions) will be understood.

From classical orbital elements it is possible to obtain the inertial Cartesian coordinates by means of the following conversion vectorial formula

$$\begin{bmatrix} x \\ y \\ z \end{bmatrix} = r \begin{bmatrix} \cos\Omega\cos(\omega+\nu) - \sin\Omega\sin(\omega+\nu)\cos i \\ \sin\Omega\cos(\omega+\nu) + \cos\Omega\sin(\omega+\nu)\cos i \\ \sin(\omega+\nu)\sin i \end{bmatrix} \tag{2.50}$$

with

$$r = a(1 - e\cos E). \tag{2.51}$$

From classical orbital elements, the representation of a vector in the RTN coordinate system known, it is also possible to convert it into the representation of the same vector in the ECI reference frame and vice versa. As depicted in Fig. 2.13, the orthogonal basis $\boldsymbol{RTN}$ of the Gaussian coordinate system can be obtained from the orthogonal basis $\boldsymbol{XYZ}$ of the ECI frame be means of three successive rotations

$$\begin{bmatrix} \boldsymbol{R} \\ \boldsymbol{T} \\ \boldsymbol{N} \end{bmatrix} = \boldsymbol{\mathcal{R}}_{ZXZ}\left(\boldsymbol{x}_{COE}\right) \begin{bmatrix} \boldsymbol{X} \\ \boldsymbol{Y} \\ \boldsymbol{Z} \end{bmatrix}. \tag{2.52}$$

with

$$\boldsymbol{\mathcal{R}}_{ZXZ}\left(\boldsymbol{x}_{COE}\right) = \boldsymbol{\mathcal{R}}_Z(\omega+\nu)\boldsymbol{\mathcal{R}}_X(i)\boldsymbol{\mathcal{R}}_Z(\Omega) \tag{2.53}$$

where matrix

$$\boldsymbol{\mathcal{R}}_Z(\Omega) = \begin{bmatrix} \cos\Omega & \sin\Omega & 0 \\ -\sin\Omega & \cos\Omega & 0 \\ 0 & 0 & 1 \end{bmatrix} \tag{2.54}$$

describes the first rotation around the Z axis of an angle Ω, matrix

$$\boldsymbol{\mathcal{R}}_X(\Omega) = \begin{bmatrix} 1 & 0 & 0 \\ 0 & \cos i & \sin i \\ 0 & -\sin i & \cos i \end{bmatrix} \tag{2.55}$$

describes the second rotation around the X of an angle i, matrix

$$\boldsymbol{\mathcal{R}}_Z(\omega+\nu) = \begin{bmatrix} \cos(\omega+\nu) & \sin(\omega+\nu) & 0 \\ -\sin(\omega+\nu) & \cos(\omega+\nu) & 0 \\ 0 & 0 & 1 \end{bmatrix} \tag{2.56}$$

describes the third rotation around the Z axis of an angle $\omega+\nu$.

Equations (2.50) and (2.52) are conversion formulas from COEs to Cartesian coordinates in ECI and in RTN frame respectively. Conversion formulas from EOEs to Cartesian coordinates in ECI

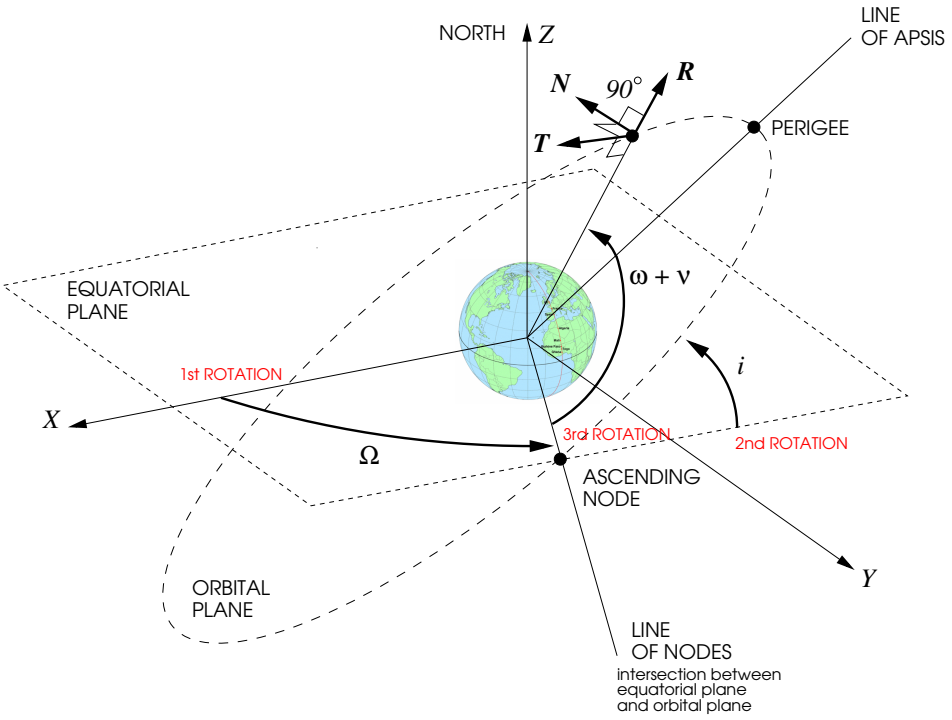

Figure 2.13: *Rotations to convert from ECI to RTN reference frame*

and in RTN will be used to obtain geostationary dynamics models. To this purpose the right-hand side of Eq.s (2.50) and (2.52) have to be expressed in terms of equinoctial elements

$$a, \tag{2.57}$$

$$P_1 = e\sin(\omega + \Omega), \tag{2.58}$$

$$P_2 = e\cos(\omega + \Omega), \tag{2.59}$$

$$Q_1 = \tan(i/2)\sin\Omega, \tag{2.60}$$

$$Q_2 = \tan(i/2)\cos\Omega, \tag{2.61}$$

$$l_\Theta = \Omega + \omega + M - \Theta(t), \tag{2.62}$$

thanks to the following conversion formulas

$$r = a(1 - P_1 \sin K - P_2 \cos K), \tag{2.63}$$

$$\sin\Omega = \frac{Q_1}{\sqrt{Q_1^2 + Q_2^2}} \quad , \quad \cos\Omega = \frac{Q_2}{\sqrt{Q_1^2 + Q_2^2}}, \tag{2.64}$$

$$\sin i = \frac{2\sqrt{Q_1^2 + Q_2^2}}{1 + Q_1^2 + Q_2^2} \quad , \quad \cos i = \frac{1 - Q_1^2 - Q_2^2}{1 + Q_1^2 + Q_2^2}, \tag{2.65}$$

$$\sin(\omega + \nu) = \frac{Q_2 \sin L - Q_1 \cos L}{\sqrt{Q_1^2 + Q_2^2}} \quad , \quad \cos(\omega + \nu) = \frac{Q_1 \sin L + Q_2 \cos L}{\sqrt{Q_1^2 + Q_2^2}}, \tag{2.66}$$

valid when the inclination i is small but different to zero. Parameter K is the eccentric longitude

$$K = \omega + \Omega + E, \tag{2.67}$$

solution of the Kepler's equation

$$l_\Theta + \Theta(t) = K + P_1 \cos K - P_2 \sin K. \tag{2.68}$$

True longitude L is given by

$$L = \omega + \Omega + \nu \tag{2.69}$$

and its sine and cosine are functions of P_1, P_2 and l_Θ according to the following equations

$$\sin L = \frac{\left(\sqrt{1 - P_1^2 - P_2^2} + 1 - P_2^2\right)\sin K + P_1 P_2 \cos K - P_1\left(1 + \sqrt{1 - P_1^2 - P_2^2}\right)}{(1 - P_1 \sin K - P_2 \cos K)\left(1 + \sqrt{1 - P_1^2 - P_2^2}\right)}, \tag{2.70}$$

$$\cos L = \frac{\left(\sqrt{1 - P_1^2 - P_2^2} + 1 - P_1^2\right)\cos K + P_1 P_2 \sin K - P_2\left(1 + \sqrt{1 - P_1^2 - P_2^2}\right)}{(1 - P_1 \sin K - P_2 \cos K)\left(1 + \sqrt{1 - P_1^2 - P_2^2}\right)}. \tag{2.71}$$

Formula (2.63) is being deduced from Eq.s (2.51), (2.58), (2.59) and (2.67); formulas (2.64) and (2.65) from Eq.s (2.60) and (2.61); formula (2.66) from Eq.s (2.64) and (2.69).

When the inclination i is equal to zero, i.e., $Q_1 = 0$ and $Q_2 = 0$, equations (2.50) and (2.52) in terms of EOEs become

$$\begin{bmatrix} x \\ y \\ z \end{bmatrix} = r \begin{bmatrix} \cos L \\ \sin L \\ 0 \end{bmatrix} \tag{2.72}$$

with $r = a(1 - P_1 \sin K - P_2 \cos K)$, and

$$\begin{bmatrix} \boldsymbol{R} \\ \boldsymbol{T} \\ \boldsymbol{N} \end{bmatrix} = \begin{bmatrix} \cos L & \sin L & 0 \\ -\sin L & \cos L & 0 \\ 0 & 0 & 1 \end{bmatrix} \begin{bmatrix} \boldsymbol{X} \\ \boldsymbol{Y} \\ \boldsymbol{Z} \end{bmatrix}. \tag{2.73}$$

2.4 Osculating and Mean Orbital Elements

The perturbing accelerations acting on a spacecraft are induced by all forces except the spherically symmetric Earth's gravity attraction. The exact perturbed motion of the spacecraft can be expressed by the time histories of the position and velocity vectors $\boldsymbol{r}$ and $\boldsymbol{v}$ fulfilling, in perturbed Keplerian conditions, the second order differential equation (2.20) with at the right-hand member the sum $\boldsymbol{a}_d$ of all the disturbing acceleration vectors

$$\frac{d^2\boldsymbol{r}}{dt^2} = -GM_\oplus \frac{\boldsymbol{r}}{r^3} + \boldsymbol{a}_d. \tag{2.74}$$

At each point in time, position and velocity vectors $\boldsymbol{r}$ and $\boldsymbol{v}$ can be converted into classical orbital elements or into equinoctial orbital elements using the same conversion formulas written in the previous section and valid for unperturbed Keplerian coordinates and orbital elements[3]. COEs or EOEs obtained in such a way at any epoch are called osculating orbital elements and they will be correctly indicated without index K because relative to perturbed Keplerian conditions. "Osculate" comes from a Latin word meaning "to kiss". Thus, the orbit defined by the osculating elements at a given instant (also called osculating trajectory) kisses the perturbed trajectory at that instant. The osculating trajectory can be defined as the two-body orbit the satellite would follow if the perturbing forces were suddenly removed at that instant. Each point on the true trajectory has a corresponding set of osculating elements that are the true time-varying orbital elements and they include all periodic (long and short periodic) and secular effects. They represent the high-precision trajectory and are useful for highly accurate simulations, including real-time pointing and tracking operation.

Perturbations on orbital motion result in secular and periodic changes of orbital elements. In perturbation theory osculating orbital elements are distinguished as either fast or slow variables, depending on their relative rate of change.

- **Fast variables** change a lot during one orbital revolution, even in the absence of perturbation. Examples are the true, eccentric and mean anomaly ν, E and M.
- **Slow variables** change very little during one orbital revolution and remain constant without perturbations. Examples are the semi-major axis a, the eccentricity e, the inclination i, the right ascension of the ascending node Ω, the argument of perigee ω.

The following characterization of how the osculating elements vary on time will be useful to better understand the state vector perturbed time history of a geostationary satellite (see Fig.s 2.14 and 2.15).

- **Secular changes** in a particular orbital element vary linearly over time, or in some cases, proportionally to some power of time, such as quadratic. They are the primary contributor to the degradation of analytical theories over long time intervals.

[3] We remember that in the previous section index K has been omitted.

- **Periodic changes** are either short- or long-periodic, depending on the length of time required for an effect to repeat.
  - **Short-periodic changes** typically repeat on the order of the satellite's period or less.
  - **Long-periodic changes** have cycles considerably longer than one orbital period, typically one or two orders of magnitude longer.

Mean elements, in contrast, are averaged over some appropriate time interval. They can also be averaged over an appropriate angular displacement such as true anomaly, eccentric anomaly, mean anomaly, or longitude. As a result, mean elements are smoothly-varying compared to osculating elements, and do not chase the short-periodic variations that the osculating elements experience. Mean elements are useful for orbit propagations with a long time span because they give an idea of the satellite long-term behavior. Additionally, mean elements are useful in recursive estimation and filtering applications because they are slowly-varying and behave more linearly than osculating elements.

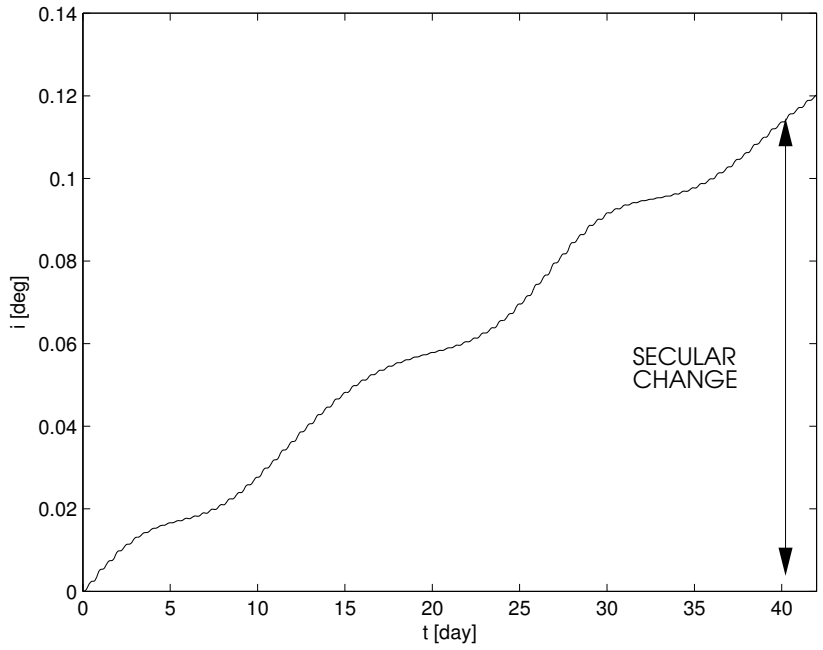

Figure 2.14: *Secular change in a GEO satellite inclination time history over 6 weeks.*

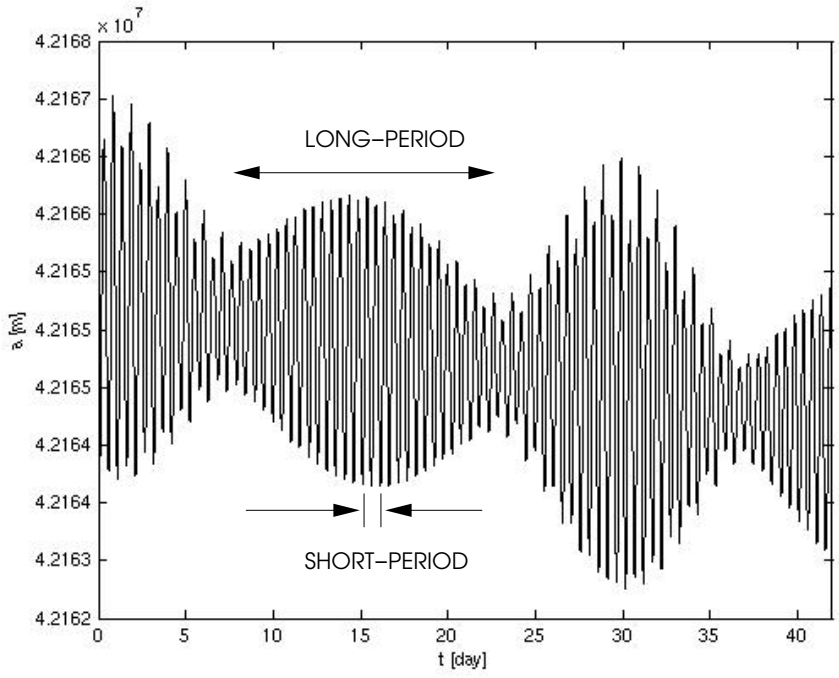

Figure 2.15: *Short and long-periodic changes in a GEO satellite semi-major axis time history over 6 weeks.*

2.5 Perturbation Techniques

Studying and modeling perturbations are key disciplines in astrodynamics. Although most of the solution techniques have been known for a long time, only recently the literature has begun to present with increasing exactness the precise methods needed to satisfactorily solve perturbation problems as the orbit propagation. There are mainly three different techniques to examine the effects of perturbations: special perturbation techniques, general perturbation techniques and semianalytical techniques. In the following the characteristics of each of them will be briefly presented.

I. Special perturbation techniques.

These techniques integrate numerically the equations of motion including all necessary perturbing accelerations. The term "special perturbation" comes from the fact that, because numerical integration is involved, the solution is only valid for the initial conditions and model parameters used as inputs to the problem.

The best-known orbit propagation technique that falls into the special perturbations category is Cowell's method. This method was developed by Philip Herbert Cowell at the end of the nineteenth century by applying integration formulas first given by Carl Friedrich Gauss and it consists in a step-by-step numerical integration method of the planetary equations of motion in Cartesian coordinates. Today, any technique that numerically integrates the equations of motion in Cartesian coordinates is referred to as Cowell's method. In Cowell's formulation, the perturbing accelerations are included in the equations of motion as follows

$$\frac{d^2\boldsymbol{r}}{dt^2} = -\frac{GM_\oplus}{r^3}\boldsymbol{r} + \boldsymbol{a}_d(\boldsymbol{r}, \boldsymbol{v}, t) \tag{2.75}$$

where $\boldsymbol{a}_d$ is the vector sum of the perturbing accelerations on the satellite, which can be a function of position, velocity and time[4]. The three second-order differential equations are sometimes expressed as six first order differential equations.

$$\frac{d\boldsymbol{x}_{PV}}{dt} = \begin{bmatrix} v_x \\ v_y \\ v_z \\ GM_\oplus \frac{x}{\sqrt{(x^2+y^2+z^2)^3}} + a_{dX} \\ GM_\oplus \frac{y}{\sqrt{(x^2+y^2+z^2)^3}} + a_{dY} \\ GM_\oplus \frac{z}{\sqrt{(x^2+y^2+z^2)^3}} + a_{dZ} \end{bmatrix} \quad \text{with} \quad \boldsymbol{x}_{PV} = \begin{bmatrix} x \\ y \\ z \\ v_x \\ v_y \\ v_z \end{bmatrix}. \tag{2.76}$$

This first-order system is a variation of Cowell's formulation, where $\boldsymbol{x}_{PV}$ is the satellite state vector.

[4] Eq. (2.75) holds also for two-body problem with central body different from the Earth.

II. General perturbation techniques.

General perturbation methods to examine the perturbation effects are based on the **Method of Perturbations**. This last describes a class of mathematical techniques for generating analytical approximations to the solution of the motion equations over some definite time intervals. General perturbation techniques replace the original equations of motion with an analytical approximation that captures the essential character of the motion over some limited time intervals and which also permits analytical integration. Such methods rely on series expansions of the perturbing accelerations. The resulting expression are truncated to make simpler expressions in the theory. This trade-off speeds up computation but decreases accuracy. Unlike numerical techniques, analytical methods produce approximate or general results that hold for some limited time intervals and accept any initial input condition.

This method applies to a large variety of perturbed motion equation, in particular to variation of parameter (VOP) equations. VOP equations of motion are a system of first-order differential equations that describe the rate of change for the time-varying orbital (classical or equinoctial) element vector $\boldsymbol{c}$

$$\frac{d\boldsymbol{c}}{dt} = \boldsymbol{f}\left(\boldsymbol{c}, \boldsymbol{a}_d, t\right). \tag{2.77}$$

The rate of change $\dot{\boldsymbol{c}}$ is due to the small disturbing forces on the constants of the unperturbed solution and $\boldsymbol{a}_d$ is the sum of all the disturbing accelerations. Both Gauss and Lagrange developed VOP methods to analyze perturbations. Gauss' technique works for conservative and non conservative accelerations. Lagrange's technique applies only to conservative accelerations and replaces the generic disturbing acceleration $\boldsymbol{a}_d$ with the gradient of its potential function.

Gauss' and Lagrange's VOP equations in terms of equinoctial orbital elements will be used to obtain nonlinear dynamical models of a geostationary satellites (see Chapter 4) and they can also be used in special perturbation techniques. VOP differs from Cowell's method in that, while Cowell's method integrates the Cartesian coordinates of the satellite, VOP integrates the orbital elements or some other set of parameters that specify the satellite's position.

III. Semianalytical techniques.

There is a trade-off between the computational speed and accuracy depending whether special or general perturbations methods are used. Numerical techniques have higher accuracy, but can be computationally expensive. Analytical techniques, in the other hand, are computationally efficient at the expense of accuracy. Semianalytical techniques attempt to combine the best features of special and general perturbation methods to give the best speed and accuracy. The basic approach in semi-analytical methods is to separate the short-periodic perturbations from the long-periodic and secular effects, so that the mean element rates can be numerically integrated. The short-periodic effects constrain the integration step size, so

removing them allows the numerical integration of the equations of motion for the mean elements to use a large step size, typically in the order of a day. The short-periodic contributions are 2π periodic in the fast variable, and they are modeled analytically using a Fourier series. The mean elements are recovered by numerically integrating the averaged equations of motion to the integrator's step size times and interpolating to any desired output time. The short-periodic variations are obtained by evaluating the slowly-varying short periodic coefficients and interpolating to the desired output time. The short-periodic variations are then added to the mean elements to obtain the osculating elements that solve the original equations of motion.

Chapter 3

Environmental and Thrust Perturbing Accelerations

Examples of perturbation forces that would be considered for the orbit problem are the non-sphericity of the central body, atmospheric drag and lift, the forces induced by the presence of another attracting body (third body effects), the solar radiation pressure, the forces of thrust, the forces induced by a magnetic field, by solid-Earth tides, by ocean tides, by Earth re-radiation (albedo), by relativistic effects. But for geostationary satellites, the disturbing forces that need to be considered are:

- the non-spherical part of the Earth's gravitational attraction;
- the gravitational attraction of the Sun and the Moon considered as point masses;
- the solar radiation pressure;
- the forces induced by the on-board thrusters.

Other forces, such as air drag or attraction from other planets, can be neglected.

This chapter is organized as follows. Environmental perturbation potentials and accelerations arising from the main environmental disturbing forces are described in Section 3.1. In Section 3.2, we define the performance parameters of a spacecraft propulsion system and we explain the differences between the chemical propulsion and the electrical one. Thrust accelerations are expressed in function of the propulsion system configuration and of the thrust forces to give a propulsion system acceleration model. In this chapter, we depict also the high thrust propulsion system configurations commonly employed and those at low thrust more recently proposed for station keeping purposes.

Both environmental disturbing potential and accelerations induced by on-board thrusters will be used in Chapter 4 to define nonlinear and linear models describing the orbit evolution of a geostationary satellite.

3.1 Environmental Disturbing Potentials and Accelerations

The total acceleration vector acting on a geostationary satellite and induced by all the disturbing forces, conservative or not, can be written as

$$\boldsymbol{a}_d = \boldsymbol{a}_g + \boldsymbol{a}_a + \boldsymbol{a}_p + \boldsymbol{a}_t \tag{3.1}$$

where $\boldsymbol{a}_t$ is the acceleration induced by the on-board thrusters and $\boldsymbol{a}_g$, $\boldsymbol{a}_a$ and $\boldsymbol{a}_p$ are the accelerations induced respectively by the three environmental disturbing forces: the asymmetric gravity attraction of the Earth, the gravity attraction of the Sun and the Moon, the solar radiation pressure. Calling $\boldsymbol{a}_e$ the acceleration induced by the generic environmental disturbing force, in the three following subsections we will give its expression and the expression of the corresponding potential function $\mathcal{E}_e$. More precisely, for each disturbing environmental function, we will give the following formulas:

A. The potential function $\mathcal{E}_e$ in function of the geographical spherical coordinates

$$\mathcal{E}_e = \mathcal{E}_e(r, \lambda, \varphi). \tag{3.2}$$

B. The potential function $\mathcal{E}_e$ in function of the inertial Cartesian coordinates

$$\mathcal{E}_e = \mathcal{E}_e(x, y, z). \tag{3.3}$$

C. The acceleration components in function of the inertial Cartesian coordinates x, y, z of the acceleration vector $\boldsymbol{a}_e$ expressed in the ECI reference frame

$$\boldsymbol{a}_e = a_{eX}\boldsymbol{X} + a_{eY}\boldsymbol{Y} + a_{eZ}\boldsymbol{Z}. \tag{3.4}$$

The acceleration components a_{eX}, a_{eY}, a_{eZ} are obtained directly in function of the inertial Cartesian coordinates by the derivative of the potential function along the XYZ axes

$$\begin{bmatrix} a_{eX} & a_{eY} & a_{eZ} \end{bmatrix}^T = \boldsymbol{\nabla}_{xyz}\mathcal{E}_e(x, y, z) \tag{3.5}$$

where

$$\boldsymbol{\nabla}_{xyz}\mathcal{E}_e(x, y, z) = \begin{bmatrix} \frac{\partial \mathcal{E}_e}{\partial x} & \frac{\partial \mathcal{E}_e}{\partial y} & \frac{\partial \mathcal{E}_e}{\partial z} \end{bmatrix}^T. \tag{3.6}$$

D. The acceleration components in function of the equinoctial orbital elements (EOEs) of the acceleration vector $\boldsymbol{a}_e$ expressed in the RTN reference frame

$$\boldsymbol{a}_e = a_{eR}\boldsymbol{R} + a_{eT}\boldsymbol{T} + a_{eN}\boldsymbol{N}. \tag{3.7}$$

Firstly, the acceleration components a_{eR}, a_{eT}, a_{eN} are obtained in function of the EOEs using the conversion formula (2.52), i.e., by three successive rotation of the acceleration vector expressed in the ECI reference frame

$$\begin{bmatrix} a_{eR} & a_{eT} & a_{eN} \end{bmatrix}^T = \boldsymbol{\mathcal{R}}_Z(\omega + \nu)\boldsymbol{\mathcal{R}}_X(i)\boldsymbol{\mathcal{R}}_Z(\Omega) \begin{bmatrix} a_{eX} & a_{eY} & a_{eZ} \end{bmatrix}^T. \tag{3.8}$$

Secondly, to obtain the expression of these components in function of the equinoctial orbital elements, the conversion formulas introduced in Section 2.3.4 are used.

E. The partial derivative

$$\boldsymbol{\nabla}_{EOE}\mathcal{E}_e = \left[\frac{\partial\mathcal{E}_e}{\partial a} \quad \frac{\partial\mathcal{E}_e}{\partial P_1} \quad \frac{\partial\mathcal{E}_e}{\partial P_2} \quad \frac{\partial\mathcal{E}_e}{\partial Q_1} \quad \frac{\partial\mathcal{E}_e}{\partial Q_2} \quad \frac{\partial\mathcal{E}_e}{\partial l_\Theta}\right]^T \tag{3.9}$$

of the potential function $\mathcal{E}_e$ with respect to the EOEs, in function of the EOEs. This is obtained by the derivative chain rules and using the conversion formulas introduced in Section 2.3.4.

In Chapter 4 the acceleration components in function of the EOEs (point **D**) will be used to obtain Gauss' variation of parameter (VOP) equations. The partial derivative in function of the EOEs of the potential function (point **E**) will be used to obtain Lagrange's VOP equations.

3.1.1 Gravity Attraction of the Earth

The gravitational attraction of the Earth considered with non homogeneous mass distribution and oblate shape is described by the potential function

$$\mathcal{U}(r,\lambda,\varphi) = \frac{GM_\oplus}{r} + \mathcal{E}_g(r,\lambda,\varphi). \tag{3.10}$$

The expression of the spherical harmonic expansion $\mathcal{E}_g$ is used to correct the part of the Earth's gravitational potential as a mass concentrated in a single point for the Earth's non symmetric mass distribution. Its expression in function of the geographical spherical coordinates is

$$\mathcal{E}_g(r,\lambda,\varphi) = \frac{GM_\oplus}{r}\sum_{n=1}^{\infty}\sum_{m=0}^{n}\left(\frac{R_\oplus}{r}\right)^n P_{nm}(\sin\varphi)[C_{nm}\cos(m\lambda) + S_{nm}\sin(m\lambda)]. \tag{3.11}$$

A. With the geopotential coefficients C_{nm} and S_{nm} and the associated Legendre polynomials $P_{nm}(\sin\varphi)$ given in Table 3.1 up to degree and order three, the expanded expression of the environmental potential function of the gravity attraction of the Earth, in function of the geographical spherical coordinates r, λ, φ (see Fig. 2.5 at page 60), becomes

$$\begin{aligned}
\mathcal{E}_g(r,\lambda,\varphi) = {} & \frac{GM_\oplus R_\oplus^2}{r^3}\left(\frac{3}{2}\sin^2\varphi - \frac{1}{2}\right)C_{20} + \\
& + \frac{GM_\oplus R_\oplus^2}{r^3}\left(3\cos^2\varphi\right)\left[C_{22}\left(\cos^2\lambda - \sin^2\lambda\right) + 2S_{22}\sin\lambda\cos\lambda\right] + \\
& + \frac{GM_\oplus R_\oplus^3}{r^4}\left(\frac{5}{2}\sin^3\varphi - \frac{3}{2}\sin\varphi\right)C_{30} + \\
& + \frac{GM_\oplus R_\oplus^3}{r^4}\left(\frac{15}{2}\sin^2\varphi\cos\varphi - \frac{3}{2}\cos\varphi\right)[C_{31}\cos\lambda + S_{31}\sin\lambda] + \\
& + \frac{GM_\oplus R_\oplus^3}{r^4}\left(15\sin\varphi\cos^2\varphi\right)[C_{32}\left(\cos^2\lambda - \sin^2\lambda\right) + 2S_{32}\sin\lambda\cos\lambda] + \\
& + \frac{GM_\oplus R_\oplus^3}{r^4}\left(15\cos^3\varphi\right)[C_{33}\cos\lambda\left(1 - 4\sin^2\lambda\right) + S_{33}\sin\lambda\left(4\cos^2\lambda - 1\right)].
\end{aligned} \tag{3.12}$$

n	m	C_{nm}	S_{nm}	$P_{nm}(\sin\varphi)$
0	0	$+1.00$	0.00	1
1	0	0.00	0.00	$\sin\varphi$
1	1	0.00	0.00	$\cos\varphi$
2	0	$-1.08\cdot10^{-3}$	0.00	$\frac{3}{2}\sin^2\varphi-\frac{1}{2}$
2	1	0.00	0.00	$3\cos\varphi\sin\varphi$
2	2	$-1.57\cdot10^{-6}$	$-9.03\cdot10^{-7}$	$3\cos^2\varphi$
3	0	$+2.53\cdot10^{-6}$	0.00	$\frac{5}{2}\sin^3\varphi-\frac{3}{2}\sin\varphi$
3	1	$+2.18\cdot10^{-6}$	$+2.68\cdot10^{-7}$	$\frac{15}{2}\cos\varphi\sin^2\varphi-\frac{3}{2}\cos\varphi$
3	2	$+3.11\cdot10^{-7}$	$-2.12\cdot10^{-7}$	$15\cos^2\varphi\sin\varphi$
3	3	$+1.02\cdot10^{-7}$	$+1.98\cdot10^{-7}$	$15\cos^3\varphi$

Table 3.1: *Geopotential coefficients up to degree and order three and corresponding Legendre polynomials.*

B. Using the following conversion formulas

$$r=\sqrt{x^2+y^2+z^2}, \tag{3.13}$$

$$\sin\lambda=\frac{y\cos\Theta-x\sin\Theta}{\sqrt{x^2+y^2}}, \tag{3.14}$$

$$\cos\lambda=\frac{x\cos\Theta+y\sin\Theta}{\sqrt{x^2+y^2}}, \tag{3.15}$$

$$\sin\varphi=\frac{z}{\sqrt{x^2+y^2+z^2}}, \tag{3.16}$$

$$\cos\varphi=\frac{\sqrt{x^2+y^2}}{\sqrt{x^2+y^2+z^2}}, \tag{3.17}$$

the environmental potential function of the gravity attraction of the Earth in function of the inertial Cartesian coordinates x, y, z and of the Greenwich Hour Angle Θ (see Section 2.2.2 page 58) becomes

$$\mathcal{E}_g(x,y,z,\Theta)=\mathcal{E}_{g20}+\mathcal{E}_{g22}+\mathcal{E}_{g30}+\mathcal{E}_{g31}+\mathcal{E}_{g32}+\mathcal{E}_{g33} \tag{3.18}$$

with

$$\mathcal{E}_{g20} = \frac{1}{2} GM_{\oplus} R_{\oplus}^2 \frac{C_{20}(2z^2 - x^2 - y^2)}{\sqrt{(x^2+y^2+z^2)^5}}, \tag{3.19}$$

$$\begin{aligned}\mathcal{E}_{g22} = {} & 3GM_{\oplus} R_{\oplus}^2 \frac{C_{22}\left[(x^2-y^2)\cos(2\Theta) + 2xy\sin(2\Theta)\right]}{\sqrt{(x^2+y^2+z^2)^5}} + \\ & + 3GM_{\oplus} R_{\oplus}^2 \frac{S_{22}\left[(y^2-x^2)\sin(2\Theta) + 2xy\cos(2\Theta)\right]}{\sqrt{(x^2+y^2+z^2)^5}},\end{aligned} \tag{3.20}$$

$$\mathcal{E}_{g30} = \frac{1}{2} GM_{\oplus} R_{\oplus}^3 \frac{C_{30}(2z^2 - 3x^2 - 3y^2)z}{\sqrt{(x^2+y^2+z^2)^7}}, \tag{3.21}$$

$$\begin{aligned}\mathcal{E}_{g31} = {} & \frac{1}{2} GM_{\oplus} R_{\oplus}^3 \frac{C_{31}(x\cos\Theta + y\sin\Theta)(12z^2 - 3x^2 - 3y^2)}{\sqrt{(x^2+y^2+z^2)^7}} + \\ & + \frac{1}{2} GM_{\oplus} R_{\oplus}^3 \frac{S_{31}(y\cos\Theta - x\sin\Theta)(12z^2 - 3x^2 - 3y^2)}{\sqrt{(x^2+y^2+z^2)^7}},\end{aligned} \tag{3.22}$$

$$\begin{aligned}\mathcal{E}_{g32} = {} & 15GM_{\oplus} R_{\oplus}^3 \frac{C_{32} z\left[(x^2-y^2)\cos(2\Theta) + 2xy\sin(2\Theta)\right]}{\sqrt{(x^2+y^2+z^2)^7}} + \\ & + 15GM_{\oplus} R_{\oplus}^3 \frac{S_{32} z\left[(y^2-x^2)\sin(2\Theta) + 2xy\cos(2\Theta)\right]}{\sqrt{(x^2+y^2+z^2)^7}},\end{aligned} \tag{3.23}$$

$$\begin{aligned}\mathcal{E}_{g33} = {} & 15GM_{\oplus} R_{\oplus}^3 \frac{C_{33}(x\cos\Theta + y\sin\Theta)\left[(x^2+y^2) - 4(y\cos\Theta - x\sin\Theta)^2\right]}{\sqrt{(x^2+y^2+z^2)^7}} + \\ & - 15GM_{\oplus} R_{\oplus}^3 \frac{S_{33}(y\cos\Theta - x\sin\Theta)\left[(x^2+y^2) - 4(x\cos\Theta + y\sin\Theta)^2\right]}{\sqrt{(x^2+y^2+z^2)^7}}.\end{aligned} \tag{3.24}$$

C. As explained in point **C** of Section 3.1, the components of the acceleration vector

$$\boldsymbol{a}_g = a_{gX}\boldsymbol{X} + a_{gY}\boldsymbol{Y} + a_{gZ}\boldsymbol{Z} \tag{3.25}$$

induced by the potential function $\mathcal{E}_g$ and expressed in the ECI reference frame are obtained calculating the partial derivative of the potential function with respect to the inertial Cartesian coordinates. The acceleration components are decomposed as follows

$$a_{gX} = GM_{\oplus}\left(R_{\oplus}^2 a_{gX20} + R_{\oplus}^2 a_{gX22} + R_{\oplus}^3 a_{gX30} + R_{\oplus}^3 a_{gX31} + R_{\oplus}^3 a_{gX32} + R_{\oplus}^3 a_{gX33}\right), \tag{3.26}$$

$$a_{gY} = GM_{\oplus}\left(R_{\oplus}^2 a_{gY20} + R_{\oplus}^2 a_{gY22} + R_{\oplus}^3 a_{gY30} + R_{\oplus}^3 a_{gY31} + R_{\oplus}^3 a_{gY32} + R_{\oplus}^3 a_{gY33}\right), \tag{3.27}$$

$$a_{gZ} = GM_{\oplus}\left(R_{\oplus}^2 a_{gZ20} + R_{\oplus}^2 a_{gZ22} + R_{\oplus}^3 a_{gZ30} + R_{\oplus}^3 a_{gZ31} + R_{\oplus}^3 a_{gZ32} + R_{\oplus}^3 a_{gZ33}\right), \tag{3.28}$$

where the explicit expressions of the normalized acceleration components a_{gXnm}, a_{gYnm}, a_{gZnm}, in function of the inertial Cartesian coordinates x, y, z, are given in Table 3.2.

D. The components of the acceleration vector

$$\boldsymbol{a}_g = a_{gR}\boldsymbol{R} + a_{gT}\boldsymbol{T} + a_{gN}\boldsymbol{N} \tag{3.29}$$

a_{gX20}	$\frac{3C_{20}}{2}\frac{x(x^2+y^2-4z^2)}{\sqrt{(x^2+y^2+z^2)^7}}$
a_{gY20}	$\frac{3C_{20}}{2}\frac{y(x^2+y^2-4z^2)}{\sqrt{(x^2+y^2+z^2)^7}}$
a_{gZ20}	$\frac{3C_{20}}{2}\frac{z(3x^2+3y^2-2z^2)}{\sqrt{(x^2+y^2+z^2)^7}}$
a_{gX22}	$\frac{6(y^3+yz^2-4x^2y)[C_{22}\sin(2\Theta)+S_{22}\cos(2\Theta)]+3(2xz^2-3x^3+7xy^2)[C_{22}\cos(2\Theta)-S_{22}\sin(2\Theta)]}{\sqrt{(x^2+y^2+z^2)^7}}$
a_{gY22}	$\frac{6(x^3+xz^2-4y^2x)[C_{22}\sin(2\Theta)+S_{22}\cos(2\Theta)]-3(2yz^2-3y^3+7yx^2)[C_{22}\cos(2\Theta)-S_{22}\sin(2\Theta)]}{\sqrt{(x^2+y^2+z^2)^7}}$
a_{gZ22}	$\frac{-30xyz[C_{22}\sin(2\Theta)+S_{22}\cos(2\Theta)]+15z(y^2-x^2)[C_{22}\cos(2\Theta)-S_{22}\sin(2\Theta)]}{\sqrt{(x^2+y^2+z^2)^7}}$
a_{gX30}	$\frac{5C_{30}}{2}\frac{zx(3x^2+3y^2-4z^2)}{\sqrt{(x^2+y^2+z^2)^9}}$
a_{gY30}	$\frac{5C_{30}}{2}\frac{zy(3x^2+3y^2-4z^2)}{\sqrt{(x^2+y^2+z^2)^9}}$
a_{gZ30}	$\frac{C_{30}}{2}\frac{(24z^2x^2+24z^2y^2-8z^4-3x^4-6x^2y^2-3y^4)}{\sqrt{(x^2+y^2+z^2)^9}}$
a_{gX31}	$\frac{3}{2}\frac{5y(xy^2+x^3-6xz^2)(C_{31}\sin\Theta+S_{31}\cos\Theta)+(-27z^2x^2+4x^4+4z^4-y^4+3y^2x^2+3z^2y^2)(C_{31}\cos\Theta-S_{31}\sin\Theta)}{\sqrt{(x^2+y^2+z^2)^9}}$
a_{gY31}	$\frac{3}{2}\frac{(-27z^2y^2+4y^4+4z^4-x^4+3y^2x^2+3z^2x^2)(C_{31}\sin\Theta+S_{31}\cos\Theta)+5y(xy^2+x^3-6xz^2)(C_{31}\cos\Theta-S_{31}\sin\Theta)}{\sqrt{(x^2+y^2+z^2)^9}}$
a_{gZ31}	$\frac{15}{2}\frac{yz(3x^2+3y^2-4z^2)(C_{31}\sin\Theta+S_{31}\cos\Theta)+xz(3x^2+3y^2-4z^2)(C_{31}\cos\Theta-S_{31}\sin\Theta)}{\sqrt{(x^2+y^2+z^2)^9}}$
a_{gX32}	$\frac{30zy(y^2+z^2-6x^2)[C_{32}\sin(2\Theta)+S_{32}\cos(2\Theta)]+15zx(2z^2-5x^2+9y^2)[C_{32}\cos(2\Theta)-S_{32}\sin(2\Theta)]}{\sqrt{(x^2+y^2+z^2)^9}}$
a_{gY32}	$\frac{30zx(x^2+z^2-6y^2)[C_{32}\sin(2\Theta)+S_{32}\cos(2\Theta)]-15zy(2z^2-5y^2+9x^2)[C_{32}\cos(2\Theta)-S_{32}\sin(2\Theta)]}{\sqrt{(x^2+y^2+z^2)^9}}$
a_{gZ32}	$\frac{30xy(x^2+y^2-6z^2)[C_{32}\sin(2\Theta)+S_{32}\cos(2\Theta)]+15(x^2-y^2)(x^2+y^2-6z^2)[C_{32}\cos(2\Theta)-S_{32}\sin(2\Theta)]}{\sqrt{(x^2+y^2+z^2)^9}}$
a_{gX33}	$\frac{15xy(13y^2-15x^2+6z^2)[C_{33}\sin(3\Theta)+S_{33}\cos(3\Theta)]}{\sqrt{(x^2+y^2+z^2)^9}}+$ $-\frac{15(3y^2z^2+4x^4+3y^4-21x^2y^2-3x^2z^2)[C_{33}\cos(3\Theta)-S_{33}\sin(3\Theta)]}{\sqrt{(x^2+y^2+z^2)^9}}$
a_{gY33}	$\frac{15(3x^2z^2+4y^4+3x^4-21y^2x^2-3y^2z^2)[C_{33}\sin(3\Theta)+S_{33}\cos(3\Theta)]}{\sqrt{(x^2+y^2+z^2)^9}}+$ $-\frac{15yx(13x^2-15y^2+6z^2)[C_{33}\cos(3\Theta)-S_{33}\sin(3\Theta)]}{\sqrt{(x^2+y^2+z^2)^9}}$
a_{gZ33}	$\frac{105zy(y^2-3x^2)[C_{33}\sin(3\Theta)+S_{33}\cos(3\Theta)]-105zx(x^2-3y^2)[C_{33}\cos(3\Theta)-S_{33}\sin(3\Theta)]}{\sqrt{(x^2+y^2+z^2)^9}}$

Table 3.2: *Normalized inertial Cartesian components of the acceleration induced by the Earth's gravity attraction, in function of the inertial Cartesian coordinates.*

induced by the potential function $\mathcal{E}_g$ and expressed in the RTN reference frame are obtained in function of the equinoctial orbital elements a, P_1, P_2, Q_1, Q_2 and l_Θ, using the conversion

formulas introduced in Section 2.3.4.

E. To calculate the partial derivative

$$\boldsymbol{\nabla}_{EOE}\mathcal{E}_g = \begin{bmatrix} \frac{\partial \mathcal{E}_g}{\partial a} & \frac{\partial \mathcal{E}_g}{\partial P_1} & \frac{\partial \mathcal{E}_g}{\partial P_2} & \frac{\partial \mathcal{E}_g}{\partial Q_1} & \frac{\partial \mathcal{E}_g}{\partial Q_2} & \frac{\partial \mathcal{E}_g}{\partial l_\Theta} \end{bmatrix}^T \tag{3.30}$$

in function of the EOEs, the derivative chain rule is applied to the potential function of the Earth's gravity attraction

$$\mathcal{E}_g = \mathcal{E}_g(r, \sin\lambda, \cos\lambda, \sin\varphi, \cos\varphi) \tag{3.31}$$

given by Eq. (3.12). Equation (3.30) becomes

$$\boldsymbol{\nabla}_{EOE}\mathcal{E}_g = \boldsymbol{\nabla}^T_{EOE} \begin{bmatrix} r \\ \sin\lambda \\ \cos\lambda \\ \sin\phi \\ \cos\phi \end{bmatrix} \boldsymbol{\nabla}\mathcal{E}_g \tag{3.32}$$

with

$$\boldsymbol{\nabla}_{EOE} \begin{bmatrix} r \\ \sin\lambda \\ \cos\lambda \\ \sin\varphi \\ \cos\varphi \end{bmatrix} = \begin{bmatrix} \frac{\partial r}{\partial a} & \frac{\partial r}{\partial P_1} & \frac{\partial r}{\partial P_2} & \frac{\partial r}{\partial Q_1} & \frac{\partial r}{\partial Q_2} & \frac{\partial r}{\partial l_\Theta} \\ \frac{\partial \sin\lambda}{\partial a} & \frac{\partial \sin\lambda}{\partial P_1} & \frac{\partial \sin\lambda}{\partial P_2} & \frac{\partial \sin\lambda}{\partial Q_1} & \frac{\partial \sin\lambda}{\partial Q_2} & \frac{\partial \sin\lambda}{\partial l_\Theta} \\ \frac{\partial \cos\lambda}{\partial a} & \frac{\partial \cos\lambda}{\partial P_1} & \frac{\partial \cos\lambda}{\partial P_2} & \frac{\partial \cos\lambda}{\partial Q_1} & \frac{\partial \cos\lambda}{\partial Q_2} & \frac{\partial \cos\lambda}{\partial l_\Theta} \\ \frac{\partial \sin\varphi}{\partial a} & \frac{\partial \sin\varphi}{\partial P_1} & \frac{\partial \sin\varphi}{\partial P_2} & \frac{\partial \sin\varphi}{\partial Q_1} & \frac{\partial \sin\varphi}{\partial Q_2} & \frac{\partial \sin\varphi}{\partial l_\Theta} \\ \frac{\partial \cos\varphi}{\partial a} & \frac{\partial \cos\varphi}{\partial P_1} & \frac{\partial \cos\varphi}{\partial P_2} & \frac{\partial \cos\varphi}{\partial Q_1} & \frac{\partial \cos\varphi}{\partial Q_2} & \frac{\partial \cos\varphi}{\partial l_\Theta} \end{bmatrix} \tag{3.33}$$

and

$$\boldsymbol{\nabla}\mathcal{E}_g = \begin{bmatrix} \frac{\partial \mathcal{E}_g}{\partial r} & \frac{\partial \mathcal{E}_g}{\partial \sin\lambda} & \frac{\partial \mathcal{E}_g}{\partial \cos\lambda} & \frac{\partial \mathcal{E}_g}{\partial \sin\varphi} & \frac{\partial \mathcal{E}_g}{\partial \cos\varphi} \end{bmatrix}^T. \tag{3.34}$$

To calculate matrix (3.33) and vector (3.34) in fucntion of the EOEs, the analytical expressions of quantities r, $\sin\lambda$, $\cos\lambda$, $\sin\varphi$ and $\cos\varphi$ are obtained up to the first order in terms P_1 and P_2 solving Kepler's equations with small eccentricity parameters as algebraic perturbation problems ([Hull, 2003]). Here we quote only the results and the corresponding Kepler's equations, referring to Chapter 4 for the detailed solution procedure.

- Radial position r is

$$r = a(1 - P_1 \sin K - P_2 \cos K) \tag{3.35}$$

where

$$\sin K = \sin(l_\Theta + \Theta) - P_1 \cos^2(l_\Theta + \Theta) + P_2 \sin(l_\Theta + \Theta)\cos(l_\Theta + \Theta), \tag{3.36}$$

$$\cos K = \cos(l_\Theta + \Theta) + P_1 \sin(l_\Theta + \Theta)\cos(l_\Theta + \Theta) - P_2 \sin^2(l_\Theta + \Theta), \tag{3.37}$$

are the first order Taylor's expansions around $P_1 = 0$ and $P_2 = 0$ of sine and cosine of the eccentric longitude

$$K = (l_\Theta + \Theta) - P_1 \cos(l_\Theta + \Theta) + P_2 \sin(l_\Theta + \Theta), \tag{3.38}$$

which is the first order analytical solution in P_1 and P_2 of Kepler's equation

$$K + P_1 \cos K - P_2 \sin K - (l_\Theta + \Theta) = 0 \tag{3.39}$$

(see Section 4.2.1 at page 117 for the detailed solution procedure).

- Geographical longitude

$$\lambda = L - \Theta = \omega + \Omega + \nu - \Theta \tag{3.40}$$

expressed in terms of equinoctial orbital elements up to the first order in P_1 and P_2 is

$$\lambda = l_\Theta - 2P_1 \cos(l_\Theta + \Theta) + 2P_2 \sin(l_\Theta + \Theta), \tag{3.41}$$

thanks to the analytical solution

$$\nu = M + 2e \sin M \tag{3.42}$$

of Kepler's equation

$$E - e \sin E - M = 0 \tag{3.43}$$

with

$$E = 2 \arctan\left(\sqrt{\frac{1-e}{1-e}} \tan\frac{\nu}{2}\right), \tag{3.44}$$

and small values of the eccentricity e (see Section 4.3 at page 125 for the detailed solution procedure). First order Taylor's expansions around $P_1 = 0$ and $P_2 = 0$ of sine and cosine of λ are

$$\sin\lambda = \sin l_\Theta - 2P_1 \cos l_\Theta \cos(l_\Theta + \Theta) + 2P_2 \cos l_\Theta \sin(l_\Theta + \Theta), \tag{3.45}$$

$$\cos\lambda = \cos l_\Theta + 2P_1 \sin l_\Theta \cos(l_\Theta + \Theta) - 2P_2 \sin l_\Theta \sin(l_\Theta + \Theta). \tag{3.46}$$

- Sine and cosine of the true longitude L up to the first order in P_1 and P_2 are the first order Taylor's expansions around $P_1 = 0$ and $P_2 = 0$ of Eq.s (2.70) and (2.71)

$$\sin L = \sin(l_\Theta + \Theta) - 2P_1 \cos^2(l_\Theta + \Theta) + 2P_2 \sin(l_\Theta + \Theta)\cos(l_\Theta + \Theta), \tag{3.47}$$

$$\cos L = \cos(l_\Theta + \Theta) + 2P_1 \sin(l_\Theta + \Theta)\cos(l_\Theta + \Theta) - 2P_2 \sin^2(l_\Theta + \Theta). \tag{3.48}$$

Sine and cosine of geographical latitude (see Section 4.3) are calculated as

$$\sin\varphi = 2\left(Q_2 \sin L - Q_1 \cos L\right), \tag{3.49}$$

$$\cos\varphi = \sqrt{1 - \sin^2\varphi}. \tag{3.50}$$

3.1.2 Gravity Attraction of the Sun and the Moon

To obtain a geostationary satellite dynamical model characterized by a good accuracy, gravity attraction of the Sun and the Moon can be considered as the only third-body perturbation forces acting on the spacecraft.

A. We denote

- the gravitational coefficients of the Sun and the Moon as $GM_\odot$ and $GM_\circledcirc$;
- the position vector of the satellite, of the Sun and of the Moon in the ECI reference frame as $\boldsymbol{r}$, $\boldsymbol{r}_S$ and $\boldsymbol{r}_M$;
- the modulus of the position vectors $\boldsymbol{r}_{sS} = \boldsymbol{r}_S - \boldsymbol{r}$ and $\boldsymbol{r}_{sM} = \boldsymbol{r}_M - \boldsymbol{r}$ of the Sun and the Moon with respect to the spacecraft as r_{sS} and r_{sM}.

With these notations the expressions of the Sun's and Moon's gravity attraction potential is

$$\mathcal{E}_a = GM_\odot \left(\frac{1}{r_{sS}} - \frac{\boldsymbol{r} \cdot \boldsymbol{r}_S}{r_S^3} \right) + GM_\circledcirc \left(\frac{1}{r_{sM}} - \frac{\boldsymbol{r} \cdot \boldsymbol{r}_M}{r_M^3} \right). \tag{3.51}$$

[Cot, 1984] and [Campan et al., 1995b] develop the terms r_{sS}^{-1} and r_{sM}^{-1} of Eq. (3.51) in function of Legendre polynomials up to the second order. Under these hypotheses the Sun's and Moon's gravity attraction potential function becomes

$$\mathcal{E}_a = \frac{GM_\odot}{r_S} \left[1 + \left(\frac{r}{r_S} \right)^2 \left(\frac{3\cos^2 \theta_{sS} - 1}{2} \right) \right] + \frac{GM_\circledcirc}{r_M} \left[1 + \left(\frac{r}{r_M} \right)^2 \left(\frac{3\cos^2 \theta_{sM} - 1}{2} \right) \right]. \tag{3.52}$$

where θ_{Ss} and θ_{Ms} are the angles between the Sun's and Moon's position vector and the spacecraft position vector (see Fig 3.1). In the sequel, we will consider the expression given by equation (3.51) without approximations.

B. It is easy to express the potential function given by Eq. (3.51) in terms of the inertial Cartesian coordinates x, y, z of the satellite, x_S, y_S, z_S of the Sun and x_M, y_M, z_M of the Moon since

$$\boldsymbol{r} = x\boldsymbol{X} + y\boldsymbol{Y} + z\boldsymbol{Z} \tag{3.53}$$

$$\boldsymbol{r}_S = x_S\boldsymbol{X} + y_S\boldsymbol{Y} + z_S\boldsymbol{Z} \tag{3.54}$$

$$\boldsymbol{r}_M = x_M\boldsymbol{X} + y_M\boldsymbol{Y} + z_M\boldsymbol{Z}. \tag{3.55}$$

As it appears clearly from Eq.s (3.54) and (3.55), for the computation of the solar and lunar gravity attraction it is necessary to express in the simulation program the positions of the Sun and the Moon in the ECI reference frame as functions of time. This can be done by transformation of one of the numerical planetary ephemerides available on the web (e.g, by using JPL's HORIZONS system[1]) or by using analytical ephemerides from current literature.

[1] http://ssd.jpl.nasa.gov/?ephemerides

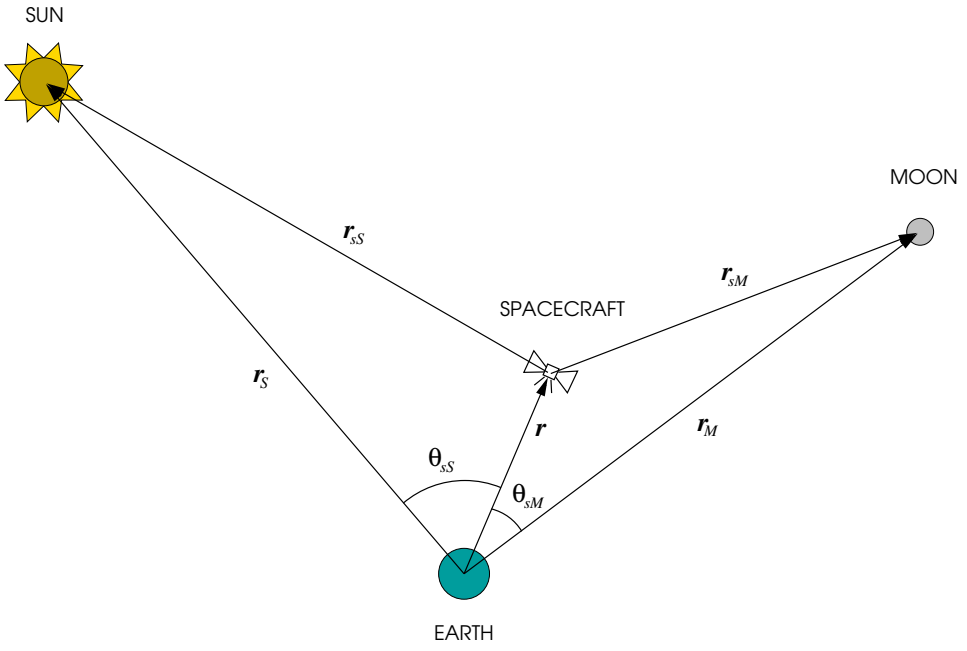

Figure 3.1: *Earth, Sun, Moon and spacecraft relative positions*

In this work, the latter approach will be followed taking the Cartesian coordinates of the Sun and the Moon given in Chapter 3 of [Montenbruck and Gill, 2000] by the following formulas

$$x_S = r_S \cos\lambda_S \cos\beta_S, \tag{3.56}$$

$$y_S = r_S \cos\varepsilon \sin\lambda_S \cos\beta_S - r_S \sin\varepsilon \sin\beta_S, \tag{3.57}$$

$$z_S = r_S \sin\varepsilon \sin\lambda_S \cos\beta_S + r_S \cos\varepsilon \sin\beta_S, \tag{3.58}$$

and

$$x_M = r_M \cos\lambda_M \cos\beta_M, \tag{3.59}$$

$$y_M = r_M \cos\varepsilon \sin\lambda_M \cos\beta_M - r_M \sin\varepsilon \sin\beta_M, \tag{3.60}$$

$$z_M = r_M \sin\varepsilon \sin\lambda_M \cos\beta_M + r_M \cos\varepsilon \sin\beta_M, \tag{3.61}$$

where $\varepsilon = 23°.43929111$ is the obliquity of the ecliptic, i.e., the inclination of the ecliptic relative to the Earth's equator. The solar and lunar spherical ecliptic coordinates r_S, λ_S, β_S and r_M, λ_M, β_M are explicit functions of time. In this work, we will adopt those ones given in function of the number of Julian centuries T since 1.5 January 2000

$$\mathrm{T} = \frac{\mathrm{JD} - 2451545.0}{36525.0} \tag{3.62}$$

where JD is the Julian Date (see pages 70-73 in [Montenbruck and Gill, 2000]). In Fig.s 3.2 and 3.3 the Sun's an Moon's inertial Cartesian coordinates are plotted over 1 year from the epoch $t_0 = 0$ corresponding to the date January 1, 2010, at midnight. They are periodic functions with periodicities equal to 1 year (for the Sun) and 1 month (for the Moon).

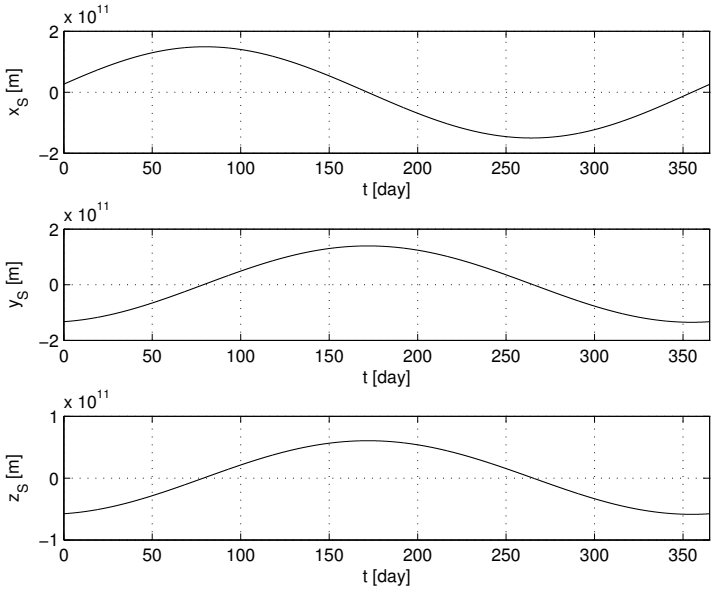

Figure 3.2: *Sun's inertial Cartesian coordinates over 1 year from January 1, 2010, at midnight.*

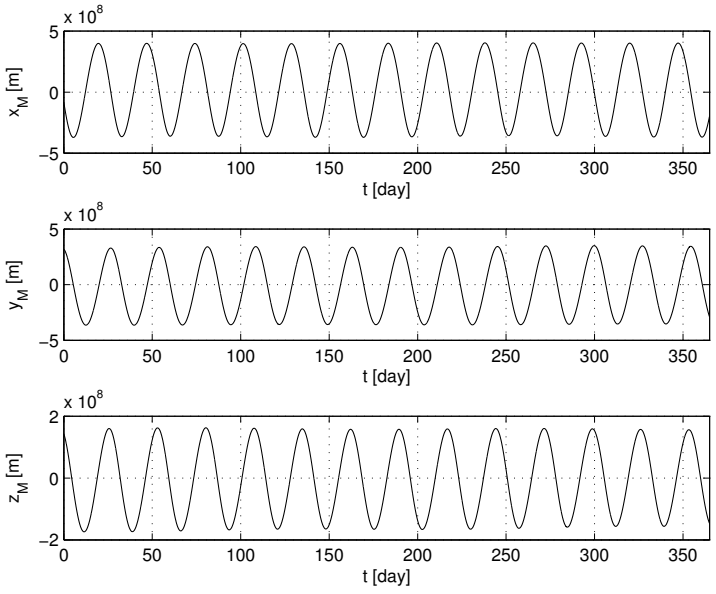

Figure 3.3: *Moon's inertial Cartesian coordinates over 1 year from January 1, 2010, at midnight.*

The expression of the Sun's and Moon's gravity attraction potential function can be written in terms of the inertial Cartesian coordinates replacing Eq.s (3.53)–(3.55) in Eq. (3.51)

$$\mathcal{E}_a(x,y,z,t) = GM_\odot \left[\frac{1}{\sqrt{(x_S-x)^2+(y_S-y)^2+(z_S-z)^2}} - \frac{xx_S+yy_S+zz_S}{\sqrt{(x_S^2+y_S^2+z_S^2)^3}} \right] + \\ + GM_\circledcirc \left[\frac{1}{\sqrt{(x_M-x)^2+(y_M-y)^2+(z_M-z)^2}} - \frac{xx_M+yy_M+zz_M}{\sqrt{(x_M^2+y_M^2+z_M^2)^3}} \right]. \tag{3.63}$$

C. As explained in point **C** of Section 3.1, the components of the acceleration vector

$$\boldsymbol{a}_a = a_{aX}\boldsymbol{X} + a_{aY}\boldsymbol{Y} + a_{aZ}\boldsymbol{Z} \tag{3.64}$$

induced by the potential function $\mathcal{E}_a$ and expressed in the ECI reference frame are obtained calculating the partial derivative of the potential function with respect to the inertial Cartesian coordinates. Decomposing the acceleration components as follows

$$a_{aX} = GM_\odot a_{aX\odot} + GM_\circledcirc a_{aX\circledcirc}, \tag{3.65}$$

$$a_{aY} = GM_\odot a_{aY\odot} + GM_\circledcirc a_{aY\circledcirc}, \tag{3.66}$$

$$a_{aZ} = GM_\odot a_{aZ\odot} + GM_\circledcirc a_{aZ\circledcirc}, \tag{3.67}$$

the explicit expressions of the normalized acceleration components $a_{aX\odot}$, $a_{aX\circledcirc}$, $a_{aY\odot}$, $a_{aY\circledcirc}$, $a_{aZ\odot}$ and $a_{aZ\circledcirc}$, in function of the inertial Cartesian coordinates x, y z are given in Table 3.3. From this table we can see that the acceleration induced by the Sun's and Moon's gravity attraction can be written in vectorial form as the sum

$$\boldsymbol{a}_a = GM_\oplus \left[\frac{\boldsymbol{r_S}-\boldsymbol{r}}{(r_S-r)^3} - \frac{\boldsymbol{r_S}}{r_S^3} \right] + GM_\circledcirc \left[\frac{\boldsymbol{r_M}-\boldsymbol{r}}{(r_M-r)^3} - \frac{\boldsymbol{r_M}}{r_M^3} \right]. \tag{3.68}$$

The first terms in the bracket represent the accelerations induced on the spacecraft by the Sun's and Moon's gravity attraction, in an inertial reference frame where the Earth is affected by the same attraction. This term is positive only during half the day when the spacecraft is at the same side of the Earth as the body and thus is stronger attracted. The other half of the day its distance is greater than that of the Earth and thus is less attracted, so the term is negative. The second terms are independent on the satellite position and they represent the accelerations induced on the Earth by the Sun's and Moon's gravity attraction. The difference between the two terms represents the net acceleration induced on the spacecraft in the ECI reference frame, where the Earth is at rest (see Fig. 3.4). This variable net acceleration on the spacecraft has a positive radial component on either side of the Earth and becomes near to zero when the Earth and the perturbing body are seen at right angles form the spacecraft. There are also time-varying accelerations in the tangential and out-of-plane directions.

$a_{aX\odot}$	$\frac{(x_S-x)}{\sqrt{[(x_S-x)^2+(y_S-y)^2+(z_S-z)^2]^3}} - \frac{x_S}{\sqrt{(x_S^2+y_S^2+z_S^2)^3}}$
$a_{aX\circledcirc}$	$\frac{(x_M-x)}{\sqrt{[(x_M-x)^2+(y_M-y)^2+(z_M-z)^2]^3}} - \frac{x_M}{\sqrt{(x_M^2+y_M^2+z_M^2)^3}}$
$a_{aY\odot}$	$\frac{(y_S-y)}{\sqrt{[(x_S-x)^2+(y_S-y)^2+(z_S-z)^2]^3}} - \frac{y_S}{\sqrt{(x_S^2+y_S^2+z_S^2)^3}}$
$a_{aY\circledcirc}$	$\frac{(y_M-y)}{\sqrt{[(x_M-x)^2+(y_M-y)^2+(z_M-z)^2]^3}} - \frac{y_M}{\sqrt{(x_M^2+y_M^2+z_M^2)^3}}$
$a_{aZ\odot}$	$\frac{(z_S-z)}{\sqrt{[(x_S-x)^2+(y_S-y)^2+(z_S-z)^2]^3}} - \frac{z_S}{\sqrt{(x_S^2+y_S^2+z_S^2)^3}}$
$a_{aZ\circledcirc}$	$\frac{(z_M-z)}{\sqrt{[(x_M-x)^2+(y_M-y)^2+(z_M-z)^2]^3}} - \frac{z_M}{\sqrt{(x_M^2+y_M^2+z_M^2)^3}}$

Table 3.3: *Normalized inertial Cartesian components of the acceleration induced by the Sun's and Moon's gravity attraction, in function of the inertial Cartesian coordinates.*

D. The components of the acceleration vector

$$\boldsymbol{a}_a = a_{aR}\boldsymbol{R} + a_{aT}\boldsymbol{T} + a_{aN}\boldsymbol{N} \tag{3.69}$$

induced by the potential function $\mathcal{E}_a$ and expressed in the RTN reference frame are obtained in function of the equinoctial orbital elements a, P_1, P_2, Q_1, Q_2 and l_Θ, using the conversion formulas introduced in Section 2.3.4.

E. To calculate the partial derivative

$$\boldsymbol{\nabla}_{EOE}\mathcal{E}_a = \left[\frac{\partial\mathcal{E}_a}{\partial a} \quad \frac{\partial\mathcal{E}_a}{\partial P_1} \quad \frac{\partial\mathcal{E}_a}{\partial P_2} \quad \frac{\partial\mathcal{E}_a}{\partial Q_1} \quad \frac{\partial\mathcal{E}_a}{\partial Q_2} \quad \frac{\partial\mathcal{E}_a}{\partial l_\Theta}\right]^T \tag{3.70}$$

in function of the EOEs, the derivative chain rule is applied to the potential function of the Sun's and Moon's gravity attraction

$$\mathcal{E}_a = \mathcal{E}_a(x, y, z) \tag{3.71}$$

written with the inertial Cartesian coordinates in function of the radial position r and of the director cosines C_x, C_y and C_z

$$x = rC_x, \quad y = rC_y, \quad z = rC_z. \tag{3.72}$$

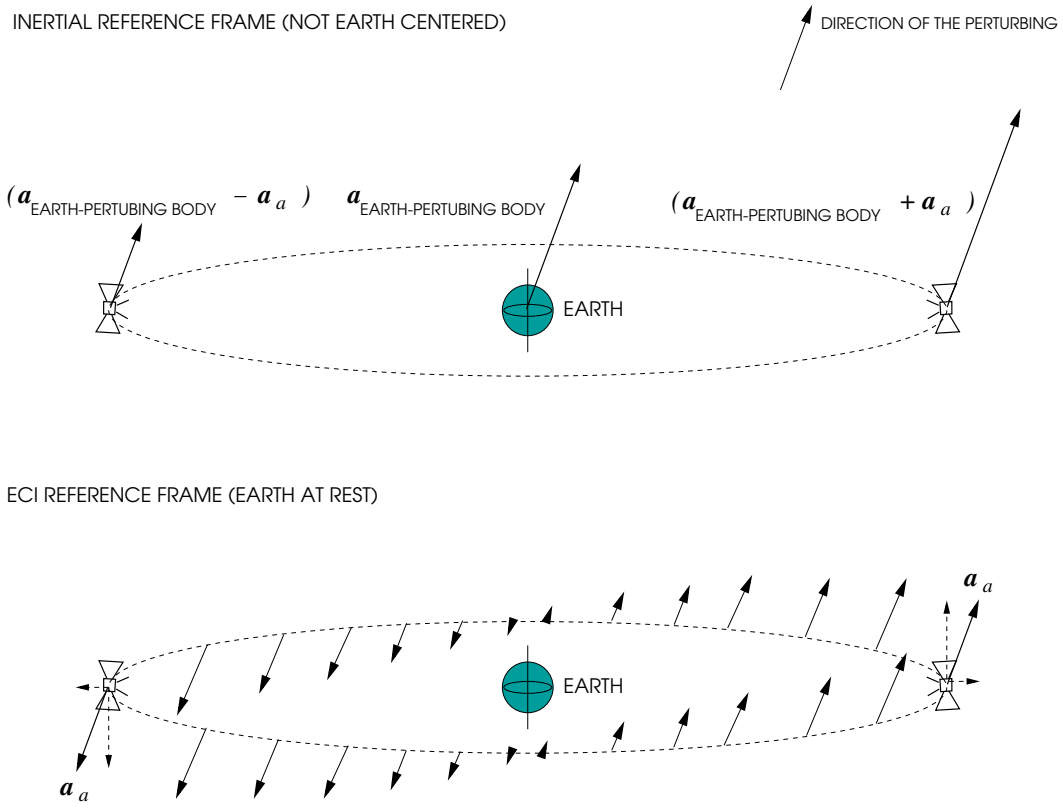

Figure 3.4: *Accelerations induced by the perturbing body gravity attraction*

Equation (3.70) becomes

$$\boldsymbol{\nabla}_{EOE}\mathcal{E}_a = \boldsymbol{\nabla}^T_{EOE}\begin{bmatrix} r \\ C_x \\ C_y \\ C_z \end{bmatrix}\boldsymbol{\nabla}\mathcal{E}_a \tag{3.73}$$

with

$$\boldsymbol{\nabla}_{EOE}\begin{bmatrix} r \\ C_x \\ C_y \\ C_z \end{bmatrix} = \begin{bmatrix} \frac{\partial r}{\partial a} & \frac{\partial r}{\partial P_1} & \frac{\partial r}{\partial P_2} & \frac{\partial r}{\partial Q_1} & \frac{\partial r}{\partial Q_2} & \frac{\partial r}{\partial l_\Theta} \\ \frac{\partial C_x}{\partial a} & \frac{\partial C_x}{\partial P_1} & \frac{\partial C_x}{\partial P_2} & \frac{\partial C_x}{\partial Q_1} & \frac{\partial C_x}{\partial Q_2} & \frac{\partial C_x}{\partial l_\Theta} \\ \frac{\partial C_y}{\partial a} & \frac{\partial C_y}{\partial P_1} & \frac{\partial C_y}{\partial P_2} & \frac{\partial C_y}{\partial Q_1} & \frac{\partial C_y}{\partial Q_2} & \frac{\partial C_y}{\partial l_\Theta} \\ \frac{\partial C_z}{\partial a} & \frac{\partial C_z}{\partial P_1} & \frac{\partial C_z}{\partial P_2} & \frac{\partial C_z}{\partial Q_1} & \frac{\partial C_z}{\partial Q_2} & \frac{\partial C_z}{\partial l_\Theta} \end{bmatrix} \tag{3.74}$$

and

$$\boldsymbol{\nabla}\mathcal{E}_a = \begin{bmatrix} \frac{\partial \mathcal{E}_a}{\partial r} & \frac{\partial \mathcal{E}_a}{\partial C_x} & \frac{\partial \mathcal{E}_a}{\partial C_y} & \frac{\partial \mathcal{E}_a}{\partial C_z} \end{bmatrix}^T. \tag{3.75}$$

To calculate matrix (3.74) and vector (3.75) in fucntion of the EOEs, the analytical expressions of quantities r, C_x, C_y and C_z are obtained up to the first order in terms P_1 and P_2.

- Radial position r is given by equation (3.35).
- Director cosine with respect to the X axis of the ECI reference frame

$$C_x = \cos\Omega\cos(\omega+\nu) - \sin\Omega\sin(\omega+\nu)\cos i \tag{3.76}$$

for small inclination values becomes

$$C_x = \cos L \tag{3.77}$$

with the cosine of the true longitude $L = \omega + \Omega + \nu$ up to the first order in P_1 and P_2 given by Eq. (3.48).

- Director cosine with respect to the Y axis of the ECI reference frame

$$C_y = \sin\Omega\cos(\omega+\nu) + \cos\Omega\sin(\omega+\nu)\cos i \tag{3.78}$$

for small inclination values becomes

$$C_y = \sin L \tag{3.79}$$

with the sine of the true longitude $L = \omega + \Omega + \nu$ up to the first order in P_1 and P_2 given by Eq. (3.47).

- Director cosine with respect to the Z axis of the ECI reference frame

$$C_z = \sin(\omega+\nu)\sin i \tag{3.80}$$

with the approximation

$$\sin i \approx 2\tan(i/2) \tag{3.81}$$

can be expressed in function of the true longitude L, the right ascension of the ascending node Ω and the inclination i as follows

$$C_z = \sin(L-\Omega)2\tan(i/2). \tag{3.82}$$

Finally, using trigonometric formulas and definitions (2.44) and (2.45) of the inclination equinoctial orbital elements Q_1 and Q_2, we obtain

$$C_z = 2\left(Q_2\sin L - Q_1\cos L\right) \tag{3.83}$$

with sine and cosine of the true longitude up to the first order in P_1 and P_2 given by Eq.s (3.47) and (3.48).

3.1.3 Solar Radiation Pressure

A satellite exposed to solar radiation experiences a small force that arises from the absorption and reflection of photons. In contrast to the gravitational perturbations so far discussed, the acceleration due to the solar radiation depends on the spacecraft mass and surface area. One of the more difficult aspects of analyzing solar radiation is accurately modeling and predicting the solar cycles and variations. Moreover, the apparent size of the satellite that faces the Sun is crucial in accurately determining the amount of force. The pressure is simply the force divided by the incident area exposed to the Sun. This means that the pressure distribution depends on the satellite shape and composition. Dividing the force by the mass permits to determine the acceleration. This entire process involves determining the precise location of the Sun, the correct satellite orbital attitude, the exact value of the solar-radiation pressure, the effective time-varying cross-sectional area exposed to the incoming radiation, the correct and usually time-varying coefficients that model the spacecraft reflectivity.

In this work, a simplified expression of the solar radiation acceleration commonly used for numerical simulations (see, e.g., [Montenbruck and Gill, 2000], [Vallado, 2001]) will be adopted

$$\boldsymbol{a}_p = -C_R P_\odot \frac{S}{m} \frac{\boldsymbol{r}_{sS}}{r_{sS}} \tag{3.84}$$

where coefficient $P_\odot \approx 4.56 \cdot 10^{-6}\mathrm{Nm}^{-2}$ is the solar radiation pressure, S and m are the satellite surface and mass and $\boldsymbol{r}_{sS} = \boldsymbol{r}_S - \boldsymbol{r}$ is the position vector of the Sun with respect to the satellite (see Fig. 3.1) and C_R is the radiation pressure coefficient dependent on the reflectivity coefficient ϵ

$$C_R = 1 + \epsilon. \tag{3.85}$$

When the satellite surface absorbs all the solar radiation $\epsilon = 0$. When it reflects all the solar radiation $\epsilon = 1$. In this work, we assume that the geostationary models have a mean reflectivity coefficient $\epsilon = 0.5$. Equation (3.84) is a simplification of the rigorous solar radiation pressure acceleration formula under the assumption that the unit vector normal to the surface points always in the direction of the Sun, i.e., that the satellite surface is always perpendicular to the incoming radiation. This simplified version is commonly used in orbit determination programs with the option of estimating the radiation pressure coefficient C_R as a free parameter. Orbital perturbations due to the solar radiation pressure may thus be accounted for with high precision, even if no details of the satellite structure, orientation and reflectivity are known.

As shown in Fig. 3.5, a simplified decomposition in radial and tangent components of the acceleration induced by the solar radiation pressure gives rise to a deformation of the geostationary orbit shape in terms of eccentricity. Tangent components of the solar radiation pressure are added to the spacecraft tangent accelerations during half the day and they are subtracted during the remaining half.

A. The solar radiation pressure is not a conservative perturbation force as the gravitational forces, because its effect depends on the physical characteristics of the satellite like the amount of

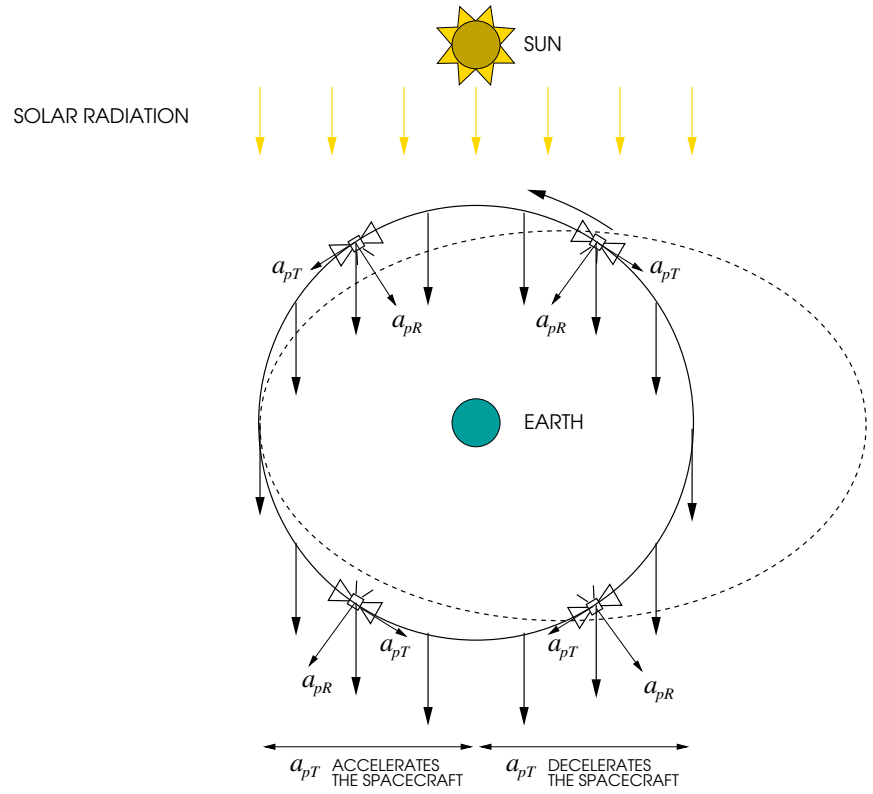

Figure 3.5: *Effect induced on the geostationary orbit eccentricity by the solar radiation pressure*

mass, the amount and type of surface. It could make a work different to zero if integrated along a close trajectory. Nevertheless, for determining the geostationary dynamical model in terms of Lagrange's variation of parameter equations, it is useful to introduce the pseudo-potential function of radiation pressure

$$\mathcal{E}_p = C_R P_\odot \frac{S}{m} \frac{\boldsymbol{r}_{sS}}{r_{sS}}. \tag{3.86}$$

[Cot, 1984] and [Campan et al., 1995b] take the pseudo-potential function of radiation pressure a little different from Eq. (3.86), equal to

$$\mathcal{E}_p = -C_R P_\odot \frac{S}{m} \frac{\boldsymbol{r} \cdot \boldsymbol{r}_S}{r_S}, \tag{3.87}$$

because they approximate in Eq. (3.86) the satellite-Sun position vector $\boldsymbol{r}_{sS}$ with the Earth-Sun position vector $\boldsymbol{r}_S$. In the sequel, the expression without approximations given by Eq. (3.86) will be adopted.

B. The expression of the solar radiation pressure pseudo-potential function can be written in terms of inertial Cartesian coordinates replacing Eq.s (3.53) and (3.54) in Eq. (3.86)

$$\mathcal{E}_p(x, y, z, t) = C_R P_\odot \frac{S}{m} \sqrt{(x_S - x)^2 + (y_S - y)^2 + (z_S - z)^2}. \tag{3.88}$$

The approximate pseudo-potential function (3.87) becomes instead

$$\mathcal{E}_p(x,y,z,t) = -C_R P_\odot \frac{S}{m} \frac{x x_S + y y_S + z z_S}{\sqrt{x_S^2 + y_S^2 + z_S^2}}. \tag{3.89}$$

C. The components of the acceleration vector

$$\boldsymbol{a}_p = a_{pX}\boldsymbol{X} + a_{pY}\boldsymbol{Y} + a_{pZ}\boldsymbol{Z} \tag{3.90}$$

expressed in the ECI reference frame can by straight obtained from Eq. (3.84) rewriting it in terms of the inertial Cartesian coordinates

$$a_{pX} = -C_R P_\odot \frac{S}{m} \frac{x_S - x}{\sqrt{(x_S-x)^2 + (y_S-y)^2 + (z_S-z)^2}}, \tag{3.91}$$

$$a_{pY} = -C_R P_\odot \frac{S}{m} \frac{y_S - y}{\sqrt{(x_S-x)^2 + (y_S-y)^2 + (z_S-z)^2}}, \tag{3.92}$$

$$a_{pZ} = -C_R P_\odot \frac{S}{m} \frac{z_S - z}{\sqrt{(x_S-x)^2 + (y_S-y)^2 + (z_S-z)^2}}. \tag{3.93}$$

It is straightforward to verify that acceleration components (3.91)–(3.93) are the partial derivatives of the pseudo-potential function (3.86) with respect to the inertial Cartesian coordinates, under the assumption of neglecting the satellite transit in shadow zones. By derivation of the approximate pseudo-potential function (3.87), the acceleration components would result independent from the satellite position. They would be equal to Eq.s (3.91)–(3.93) with x, y and z equal to zero. In this thesis, we will consider the acceleration components (3.91)–(3.93) without approximations.

a_{pX}	$-C_R P_\odot \frac{S}{m} \frac{x_S-x}{\sqrt{(x_S-x)^2+(y_S-y)^2+(z_S-z)^2}}$
a_{pY}	$-C_R P_\odot \frac{S}{m} \frac{y_S-y}{\sqrt{(x_S-x)^2+(y_S-y)^2+(z_S-z)^2}}$
a_{pZ}	$-C_R P_\odot \frac{S}{m} \frac{z_S-z}{\sqrt{(x_S-x)^2+(y_S-y)^2+(z_S-z)^2}}$

Table 3.4: *Inertial Cartesian components of the acceleration induced by the solar radiation pressure, in function of the inertial Cartesian coordinates.*

D. The components of the acceleration vector

$$\boldsymbol{a}_p = a_{pR}\boldsymbol{R} + a_{pT}\boldsymbol{T} + a_{pN}\boldsymbol{N} \tag{3.94}$$

induced by the potential function $\mathcal{E}_p$ and expressed in the RTN reference frame are obtained in function of the equinoctial orbital elements a, P_1, P_2, Q_1, Q_2 and l_Θ, using the conversion formulas introduced in Section 2.3.4.

E. To calculate the partial derivative

$$\boldsymbol{\nabla}_{EOE}\mathcal{E}_p = \begin{bmatrix} \frac{\partial \mathcal{E}_p}{\partial a} & \frac{\partial \mathcal{E}_p}{\partial P_1} & \frac{\partial \mathcal{E}_p}{\partial P_2} & \frac{\partial \mathcal{E}_p}{\partial Q_1} & \frac{\partial \mathcal{E}_p}{\partial Q_2} & \frac{\partial \mathcal{E}_p}{\partial l_\Theta} \end{bmatrix}^T \tag{3.95}$$

in function of the EOEs, the derivative chain rule is applied to the pseudo-potential function of the solar radiation pressure written with the inertial Cartesian coordinates in function of the radial position r, the director cosines C_x, C_y, C_z

$$\mathcal{E}_p = C_R P_\odot \frac{S}{m} \sqrt{(x_S - rC_x)^2 + (y_S - rC_y)^2 + (z_S - rC_z)^2} \tag{3.96}$$

and proceeding as explained for potential function $\mathcal{E}_a$ in previous point **E.**. Equation (3.95) becomes

$$\boldsymbol{\nabla}_{EOE}\mathcal{E}_p = \boldsymbol{\nabla}_{EOE}^T \begin{bmatrix} r \\ C_x \\ C_y \\ C_z \end{bmatrix} \boldsymbol{\nabla}\mathcal{E}_p \tag{3.97}$$

with a matrix at the right-hand side of Eq. (3.97) given by Eq. (3.74) and

$$\boldsymbol{\nabla}\mathcal{E}_p = \begin{bmatrix} \frac{\partial \mathcal{E}_p}{\partial r} & \frac{\partial \mathcal{E}_p}{\partial C_x} & \frac{\partial \mathcal{E}_p}{\partial C_y} & \frac{\partial \mathcal{E}_p}{\partial C_z} \end{bmatrix}^T. \tag{3.98}$$

3.2 Thrust Accelerations

Aside from the natural forces discussed in above section, the motion of a spacecraft is also affected by the action of an on-board thruster system. Thrusters are frequently fired for orbit control, attitude control, or a combination of both, and exhibit a variety of performance levels and burns durations. In view of a significant impact on the spacecraft orbit, thrust forces would be taken into account in the trajectory prediction using an adequate mathematical model. In turn, thruster system and maneuver parameters may be calibrated by adjusting them along with other parameters during the orbit determination and estimation.

While attitude thrusters are ideally burned in pairs to produce a pure momentum-free torque, changes in shape and orientation of the orbit are accomplished by thrusters acting primarily in the along-track and cross-track directions. In the case of orbital maneuvers the overall thruster activity is generally confined to a finite time interval, ranging from seconds or minutes for ground track control of remote sensing satellites to several hours for inclination control of geostationary satellites with ionic propulsion. Whenever the thrust duration is small as compared to the orbital period, the maneuvers may conveniently be treated as instantaneous increments of velocity vector

$$\Delta \boldsymbol{v}_t(t_m) = \boldsymbol{v}(t_m^+) - \boldsymbol{v}(t_m^-). \tag{3.99}$$

occurring at the impulsive maneuver time t_m. But for extended maneuvers (e.g., for orbital transfer with large boost maneuvers applied in the positioning of geostationary satellites), an adequate thrust model is required. In these cases a substantial amount of propellant is consumed during a single maneuver, which results in a continuous change of the spacecraft mass along the burn.

In this Section, we describe the main performance parameters of a space propulsion system. We point out the differences between chemical and electric propulsion operation. We express the thrust acceleration vector induced by a propulsion system in function of the propulsion system configuration and of the thrust forces. Finally, we depict the chemical and electric propulsion systems most commonly used and those recently suggested for station keeping purposes.

3.2.1 Performance Parameters of Space Propulsion Systems

In this Section, the concepts of thrust, effective exhaust velocity, total velocity increment budget, total impulse, specific impulse, jet power and total propulsion system efficiency will be explained with a one-dimensional motion analysis. These quantities are collectively referred to as the propulsion system performance parameters.

A spacecraft propulsion system (i.e., any rocket being it chemical, electric, or of different type) accelerates the spacecraft by applying a thrust usually through the expulsion of propellant mass at high velocity. We consider the one-dimensional flight of a rocket-propelled spacecraft as a function of time t with mass $m(t)$, velocity $v_t(t)$ and acceleration $a_t(t)$ in the absence of Earth's gravitational and environmental disturbing forces. **Thrust** F is the amount of force that the propellant expelled at an exhaust velocity c_e with respect to the satellite body applies to the thruster. The amount of thrust can be calculated as follows

$$F = c_e \dot{m} + A_n \left(P_g - P_a\right) = c\dot{m} \tag{3.100}$$

where $\dot{m}$ is the mass flow rate of propellant, A_n denotes the area of the nozzle exit, P_g and P_a are the gas and the ambient pressure respectively. Parameter c is the effective exhaust velocity of the expelled mass with respect to the satellite.

From the conservation of the momentum, the acceleration a_t of the spacecraft resulting from the application of the thrust F is

$$a_t = \frac{dv_t}{dt} = \frac{F}{m} = \frac{\dot{m}}{m} c. \tag{3.101}$$

The expulsion of propellant by the rocket reduces the mass of the spacecraft over time. If the mass flow rate of propellant $\dot{m}$ is constant, the spacecraft mass is

$$m(t) = m_0 - \dot{m}t \tag{3.102}$$

where m_0 is the initial mass of the spacecraft. Differentiating Eq. (3.102) and then substituting into Eq. (3.101) yields the differential equation

$$m\frac{dv_t}{dt} = -\frac{dm}{dt} c \tag{3.103}$$

Canceling the time differentials and integrating over some initial to final spacecraft velocity and mass

$$\int_{v_t(t_0)}^{v_t(t_f)} dv_t = -c \int_{m_0}^{m_f} \frac{dm}{m} \tag{3.104}$$

an expression for the ratio of final to initial vehicle mass is obtained as a function of the velocity increment Δv_t and the effective exit velocity c

$$\frac{m_f}{m_0} = e^{-\frac{\Delta v_t}{c}}. \tag{3.105}$$

Equation (3.105) was first derived by Konstantin Tsiolkovskii in 1895. Also known as the rocket equation, it illustrates the impact of exhaust velocity on the mass ratio of a spacecraft and has always been the basis of all theoretical work on rocket propulsion. The rocket equation implies that effective exhaust velocity should be on the order of the velocity increment to deliver a useful mass fraction at the destination. **Effective exhaust velocity** c is often used as a first-order criterion in space vehicle design.

From an orbit design viewpoint, a space mission is a series of different orbits. Every orbit change in a mission requires energy. **The total velocity increment budget** of a mission ΔV is traditionally used to account for this energy. It is the sum of the velocity increments induced by the on-board propulsion system and required throughout the space mission life

$$\Delta V = \sum_{\text{all thrusts}} \Delta v_t. \tag{3.106}$$

In a broad sense the velocity increment budget represents the cost for each mission orbit scenario. This cost depends on the type of propulsion engine system equipping the satellite. In designing orbits and constellation, it has to be balanced against the utility achieved.

The total impulse delivered to a spacecraft is the thrust integrated over time

$$I_t = \int_{t_0}^{t} F dt \tag{3.107}$$

Total impulse has units of Newton-seconds (Ns) and is often used to report rocket lifetime. For example, the lifetime of a rocket with a total impulse capability of 3×10^6 Ns and a constant thrust of 83 mN would be about 10000 hours.

The specific impulse is the total impulse per unit weight of propellant given by

$$I_{sp} = \frac{\int_{t_0}^{t} F dt}{g \int_{t_0}^{t} \dot{m} dt} \tag{3.108}$$

where the weight force of the propellant is defined by the sea-level acceleration of gravity on the Earth ($g = 9.80665$ m/s^2). Specific impulse has units of seconds, but is really force per unit weight flow rate, that is, specific impulse is a measure of how effectively propellant is converted into useful

thrust. If the thrust and mass flow rate are constant over the thrust time, specific impulse reduces to

$$I_{sp} = \frac{F}{g\dot{m}} = \frac{c}{g} \tag{3.109}$$

Specific impulse is then roughly one-tenth of the effective exit velocity. The two quantities can be used interchangeably in the rocket equation (3.105) via equation (3.109). However, specific impulse should not be interpreted as the exit velocity divided by some arbitrary constant. Unfortunately, equation (3.109) has led some investigators, usually in the absence of reliable thrust measurements, to report specific impulse from measurements of the propellant ion velocity alone. This can significantly overestimate specific impulse if the rocket produces only a very small amount of ions from the propellant or if the ions significantly diverge from the thrust axis. Therefore, using the ion velocity to estimate specific impulse should be avoided.

Besides producing thrust, a rocket can also be thought as an energy converter, since producing thrust requires the conversion of a source of potential energy to kinetic energy. For example, in a chemical rocket potential energy stored in molecular bonds is released to heat propellant gas and converted to kinetic energy by accelerating the gas through a nozzle. In electric propulsion, the potential energy is provided by an external power source. Some fraction of the input power from this external source is converted into the axially directed kinetic power of the exhaust, or **jet power**, given by

$$P_{jet} = \frac{1}{2}\dot{m}c^2 = \frac{1}{2}Fc. \tag{3.110}$$

Due to the second law of thermodynamics, the efficiency of producing the jet power is less than perfect. To characterize the losses of the conversion, **the total system efficiency** (of the power source and thruster) is defined as the ratio of the jet power to the system input power provided by the spacecraft bus

$$\eta_{sys} = \frac{P_{jet}}{P_{sys}} = \frac{\frac{1}{2}Fc}{P_{sys}} = \frac{1}{2}gI_{sp}\frac{F}{P_{sys}}. \tag{3.111}$$

Equation (3.111) shows that the performance of a space propulsion system can be described by specifying the system efficiency via system input power P_{sys}, specific impulse I_{sp} and thrust F.

Typical values of performance parameters of some space propulsion systems are listed in Table 3.5.

3.2.2 Chemical and Electric Propulsion

Chemical propulsion systems can be subdivided into two basic fuel categories, solid and liquid, which are the primary systems used in spacecraft achieving thrust. In the technical literature, rockets using solid propellants are called *motors*, whereas rockets using liquid propellant are called *thrusters* or *jets*. **Solid propellant motors** are used as the upper stage of propulsion system, providing the necessary velocity increment for the injection of the spacecraft from the low-altitude initial orbit into the final operational orbit. The specific impulse I_{ps} of solid motors ranges from 285 to 300 seconds. Thrust level ranges from 9500 and 270000 Newton. **Liquid propulsion systems**

Propulsion system type	F	c	I_{sp}	$\lvert\dot{m}\rvert$
Solid propellant motor	40 kN	3000 m/s	300 s	1.3 kg/s
Liquid propellant motor	400 N	3500 m/s	350 s	130 g/s
Chemical station keeping thruster	10 N	3500 m/s	350 s	3 g/s
Electrostatic station keeping ion thruster	100 mN	25 km/s	4000 s	0.8 mg/s

Table 3.5: *Representative values of the thrust level F, the ejection velocity c, the specific impulse ($I_{sp} = c/9.81\ m/s^2$), and the mass flow rate of various thrust systems.*

must be differentiated between monopropellant and bipropellant fuels. In both cases, the fuel is delivered to the combustion chamber in one of two possible modes: blowdown operation mode and regulated pressure operation mode. In the blowdown operation mode, pressurized gas is stored in the same tank as the propellant; the drawback here is that the pressure decreases as propellant is consumed. In the regulated pressure operation mode, a regulator maintains a constant gas pressure, with the inherent drawback of additional system complexity. **Monopropellant thrusters** use the most popular liquid propellant: the hydrazine (N_2H_4). Hydrazine vaporizes and decomposes when brought into contact with a suitable catalyst, thus producing hydrogen and nitrogen gases under pressure and so generating propulsion. With such a catalytic thruster, a specific impulse ranges between 125 and 250 seconds. Nominal thrust levels range between 0.1 and 500 Newton. **Bipropellant thrusters** are based on combustion resulting from the contact of two propellants; for example, monomethyl hydrazine (MMH) and nitrogen tetroxide (N_2O_4) which is used as oxidant. The primary reason for using such a system is that an augmented specific impulse is achieved: I_{sp} equal to 320 seconds or more. Common monopropellant thrust levels are 10–22 N for the low-thrust type and 400–490 N for the high-thrust type.

Electrical propulsion systems are based on accelerating an ionized mass by an electromagnetic or electrostatic field, where the ions leave the thruster nozzle at very high velocity. The electrical thruster categories are the following.

1. **Electrothermal propulsion**: acceleration of a propellant gas by electrical heat addition and expansion through a convergent/divergent nozzle. Examples include resistojets and arcjets.

2. **Electrostatic propulsion**: acceleration of an ionized propellant gas by the application of electric fields. Examples include gridded ion thrusters, colloid thrusters, and field emission electric propulsion (FEEP).

3. **Electromagnetic propulsion**: acceleration of an ionized propellant gas by the application of both electric and magnetic fields. Examples include Hall thrusters, pulsed plasma thrusters (PPT), and magneto plasma dynamic thrusters (MPDT).

With electric thrusters, specific impulses ranging from 2000 and 6000 seconds can be achieved. However, such propulsion systems have numerous drawbacks. The thrust levels that can be achieved

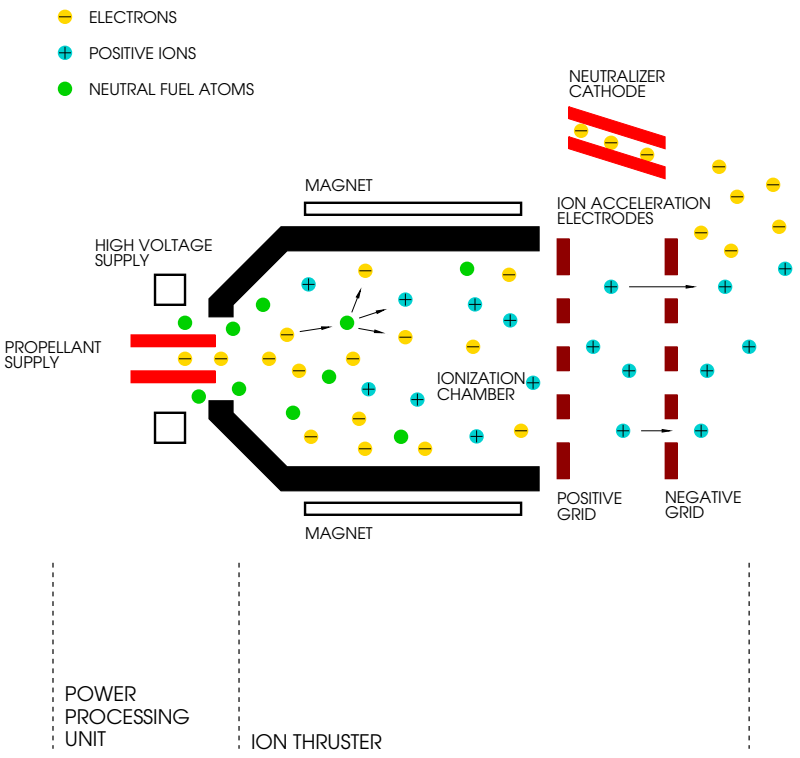

Figure 3.6: *Schematic diagram of an electrostatic ion thruster*

are very low. They range between 5mN and 170 mN. The effective exhaust velocity of the ions must be so high ($c \approx 40$ km/s) that accelerating voltages of about 1500 V are required. This is a complicated and delicate problem in space technology. The expected lifetime of these ion thrusters can exceed 15000 hours, but an increase in power consumption has been observed during this lifetime due to aging of electronic components. Despite all of these technical problems, there is a practical reason for preferring electrical propulsion systems rather than chemical ones: the very low propellant mass to take on-board per mission. For example, a complete ion propulsion system, based on four thrusters supplying 20 mN each and including a propellant mass sufficient to produce a total impulse of 800000 Ns, weights approximatively 90 kg. In contrast, the equivalent mass of chemical propellant needed to produce the same total impulse is nearly 290 kg.

The electrostatic ion thrusters, in particular gridded ion engines, are a kind of highly-efficient low-thrust propulsion running on electrical power that deserve particular attention in the context of this work because they are the good candidates for geostationary station keeping missions. Hughes Aircraft Company has already developed and used the XIPSs (Xenon Ion Propulsion Systems) for performing station keeping on geosynchronous satellites. A simplified diagram of an electrostatic ion thruster is shown in Fig. 3.6. Propellant atoms (of mercury, xenon or argon vapor) are injected into the ionization chamber where they are bombarded with electrons from a hollow cathode,

causing the atoms to lose electrons and become ionized, thus forming a neutral plasma. The side of the exit of the ionization chamber is equipped with two high voltage electrodes that have a grid structure, i.e., an array of aligned apertures. The positively charged ions move towards these gridded electrodes due to diffusion. Ions leak into a plasma sheath just upstream of the positively charged grid; the thruster walls absorb the lost electrons. The high voltage applied to the electrodes extracts ions from the discharged plasma and accelerates them to a high velocity thus forming the thrust beam. Electrons and ions must be injected in the thrust beam in equal numbers to maintain charge neutrality. For this reason electrons are shot from a cathode, called the neutralizer, towards the ions behind the ship to ensure that equal amounts of positive and negative charge are ejected. Neutralizing is needed to prevent the ship from gaining a net negative charge.

Thrust F, specific impulse I_{sp} and power jet P_{jet} of ion thrusters are constrained by the fixed grid gap in the ion accelerator, which limits performance and life to a limited range in I_{sp} and thrust. Additional benefits can be realized if ion thrusters are designed for variable specific impulse (VSI) operation. Sometimes referred to as bimodal or multi-mode operation, VSI usually describes constant power operation for at least two different specific impulses. The first set point is a low-specific impulse (e.g., 1000–2000 s), high-thrust mode suitable for rapid orbit transfers. The second set point is a high-specific impulse (e.g., 3000–4000 s), low thrust mode suitable for station keeping and interplanetary maneuvers. [Goebel et al., 2005] proposed a novel ion optics system to provide operation over a large range in I_{sp} in high power ion thrusters. The Variable IsP Electric Rocket (VIPER) utilizes a space-heritage mechanism to adjust the grid gap of high power ion thrusters during flight to enable operation in two different modes: a high thrust, low specific impulse mode; and a high specific impulse, low thrust mode. A 56 cm grid diameter VIPER thruster can operate at I_{sp} of over 9000 s at a nominal grid gap, and can also operate with a reduced grid gap at an I_{sp} of 5000 seconds at power levels on the order of 25 kW to produce significantly higher thrust than the nominal case ($F > 800$ mN).

3.2.3 Propulsion System Acceleration Model

Attitude control and orbit control maneuvers are performed with a propulsion system mounted on the satellite with a given configuration characterized by a number N_t of thrusters. The ith thruster expels propellant resulting in a thrust F_i. It is mounted on the satellite forming a cant angle γ_i and a slew angle σ_i with respect to the axes of the of the spacecraft body-fixed reference frame (see Fig. 3.7). Cant angle γ_i is the azimuth of thrust direction in the Y_BZ_B plane, measured from Y_B to Z_B about X_B axis. Slew angle σ_i is the azimuth of thrust direction in the X_BZ_B plane, measured from Z_B to X_B about Y_B axis.

Total acceleration vector $\boldsymbol{a}_t$ induced by a thruster system depends on the thrusts, the cant and slew angles of the thrusters and on the satellite mass m. It can be written as

$$\boldsymbol{a}_t = \frac{1}{m}\boldsymbol{\Gamma}\boldsymbol{F} \tag{3.112}$$

where $\mathbf{\Gamma}$ is the thruster system configuration matrix

$$\mathbf{\Gamma} = \begin{bmatrix} \mathbf{\Gamma}_1 & \cdots & \mathbf{\Gamma}_i & \cdots & \mathbf{\Gamma}_{N_t} \end{bmatrix} \tag{3.113}$$

with the configuration vector of the ith thruster given by

$$\mathbf{\Gamma}_i = \begin{bmatrix} \sin\gamma_i \cos\sigma_i & \sin\gamma_i \sin\sigma_i & \cos\gamma_i \end{bmatrix}^T. \tag{3.114}$$

Vector $\boldsymbol{F}$ is the thrust vector of the thruster system in question

$$\boldsymbol{F} = \begin{bmatrix} F_1 & \cdots & F_i & \cdots & F_{N_t} \end{bmatrix}^T. \tag{3.115}$$

In the following the acceleration vector $\boldsymbol{a}_t$ will be expressed in the RTN reference frame under the fundamental hypothesis that an adequate attitude control system makes the axes of the spacecraft body-fixed reference frame aligned with those of the RTN reference frame and such that

$$\boldsymbol{X}_B = +\boldsymbol{T}, \quad \boldsymbol{Y}_B = -\boldsymbol{N}, \quad \boldsymbol{Z}_B = -\boldsymbol{R}. \tag{3.116}$$

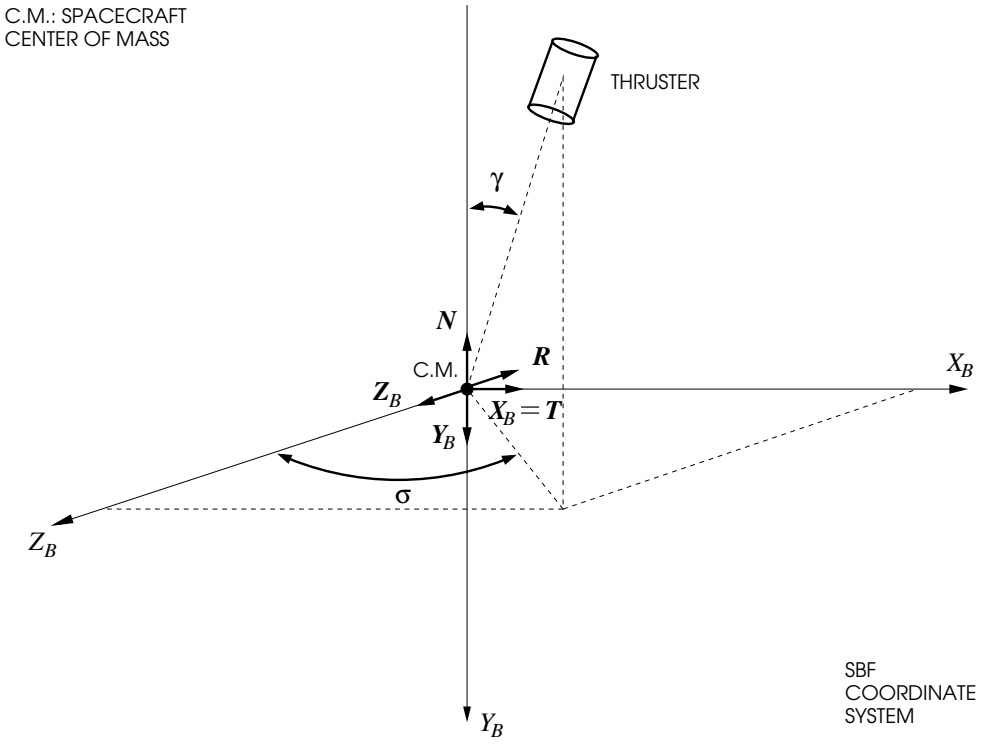

Figure 3.7: *Thruster cant and slew angles*

For geostationary station keeping purposes chemical or electric thrusters are commonly used. The commonly used chemical monopropellant thrusters with hydrazine (N_2H_4) as fuel are often

designed to produce forces of the order of 0.5 to 20 N. A spacecraft with a mass of a few hundreds of kg can be accelerated by the order of mm/s^2 and upwards. Similar performance is obtained with bipropellant chemical propulsion, where the fuel and an oxidant react to produce the thrust. As explained in the previous section, a new type of propulsion system now tried on some space missions is the ion electric propulsion system. It employs an on-board electric field to accelerate ions that are subsequently neutralized before being ejected. The advantage is that more velocity change relative to the launch mass can be obtained for missions of long duration because only a small amount of mass is ejected with high velocity, typically between 30 km/s and 40 km/s. This is combined with the fact that the accelerating power is obtained from the solar cells instead of being carried on-board as chemicals. The disadvantage is the very low force, of the order of 0.01 Newton, leading to thrust times that are a hundred times longer than for chemical propulsion for producing the same effect on the orbit. For more technical details about the chemical and electric thruster technology see above and, e.g., [Sidi, 1997], [Marcuccio et al., 1997], [Martinez-Sanchez and Pollard, 1998], [Wertz and Larson, 1999], [Saccoccia et al., 2000], [Lyszyk and Garnero, 2004]. In general, propulsion systems are called chemical, hybrid or full electrical depending on the nature of its thrusters: chemical, chemical and electrical or only electrical thrusters. In the following we illustrate some of these typical thruster configurations.

3.2.3.1 Chemical, Hybrid, Full Electrical Propulsion Systems

Geostationary satellites TC1 of the first telecom generation (see [Campan et al., 1995a]) have been equipped with two chemical propulsion systems: a system for the station acquisition and a system for the station keeping and attitude control purposes. The first system consists of one motor (a rocket using solid propellant) used during the apogee firing for the station acquisition. The second system consists of a set of sixteen monopropellant thrusters (eight nominal plus eight redundant) powered with hydrazine. Two thrusters are devoted to East-West maneuvers and are mounted on East and West faces. The other six, mounted on North and South faces, are smaller and devoted to the North-South maneuvers and to the attitude control. The hydrazine is stored in a pair of tanks from which the fuel is drawn alternatively. Thruster configuration matrix and thrust vector of the nominal configuration are

$$\mathbf{\Gamma} = \begin{bmatrix} 0 & 0 & 0 & 0 & 0 & 0 & 0 & 0 \\ +1 & -1 & 0 & 0 & 0 & 0 & 0 & 0 \\ 0 & 0 & +1 & +1 & +1 & -1 & -1 & -1 \end{bmatrix}^T \tag{3.117}$$

and

$$\boldsymbol{F} = \begin{bmatrix} F_{-X_B} & F_{+X_B} & F_{-Y_B} & F_{-Y_B} & F_{-Y_B} & F_{+Y_B} & F_{+Y_B} & F_{+Y_B} \end{bmatrix}^T . \tag{3.118}$$

where F_{-X_B} notation indicates that the corresponding thruster is mounted in X_B direction and in its negative side.

Geostationary satellites TC2 of the second telecom generation (see [Campan et al., 1995a]) have been equipped with only one chemical propulsion system used for station acquisition and station keeping purposes. Attitude control is performed via solar sails. The system consists of six nominal and six redundant bi-ergol thrusters. With such a configuration, for each type of maneuver, the combination of one, two or three thrusters supplies a thrust in the desired direction. Thruster configuration matrix $\mathbf{\Gamma}$ and thrust vector $\boldsymbol{F}$ are

$$\mathbf{\Gamma} = \begin{bmatrix} +1 & 0 & 0 & -1 & 0 & 0 \\ 0 & +1 & 0 & 0 & -1 & 0 \\ 0 & 0 & +1 & 0 & 0 & -1 \end{bmatrix}, \tag{3.119}$$

and

$$\boldsymbol{F} = \begin{bmatrix} F_{+Z_B} & F_{-X_B} & F_{+Y_B} & F_{-Z_B} & F_{+X_B} & F_{-Y_B} \end{bmatrix}^T. \tag{3.120}$$

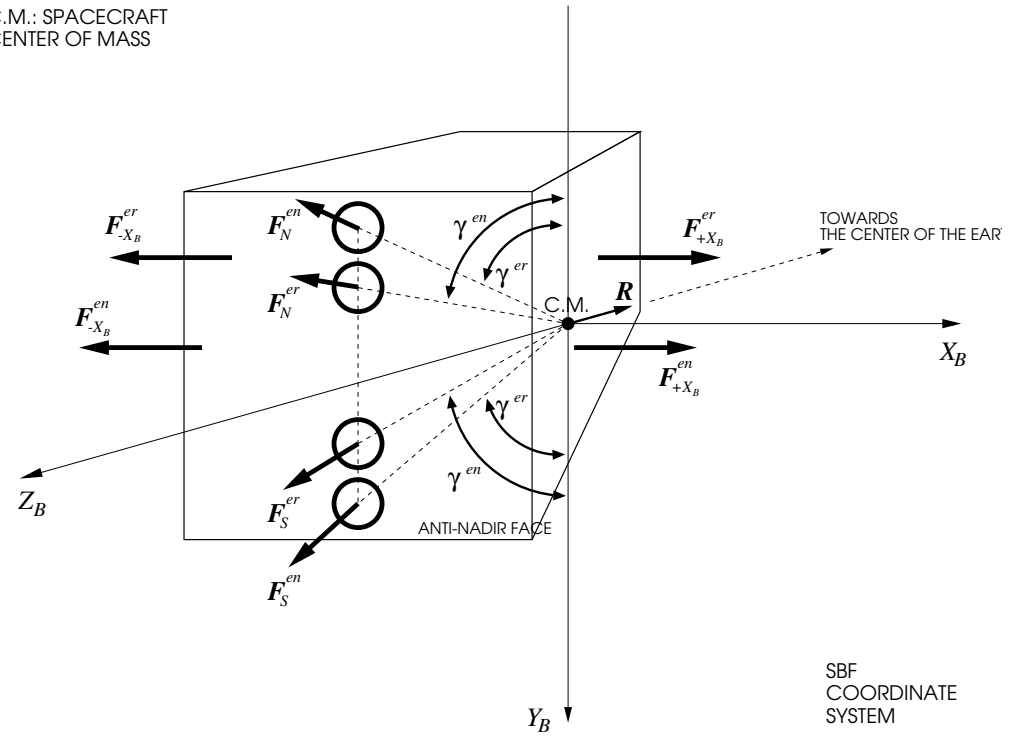

Figure 3.8: *Hybrid electric four-thruster configuration*

In recent years, manufacturers of GEO satellites, as Alcatel Alenia Space (AAS), Astrium, Space System/Loral, Boeing Satellite Systems, have been adding ion electric propulsion system to their original satellite bus design [Skipper et al., 2004]. A typical hybrid electric four-thruster configuration adopted by AAS for station keeping purpose is depicted in Fig. 3.8. This configuration

takes up the XIPS thruster configuration of HS 601HP described in [Anzel, 1998]. It is composed of four electric thrusters mounted on the anti-nadir face of the satellite. All the electric thrust directions lie in the $Y_B Z_B$ plane intersecting the center of mass, which is also nominally in this plane. This design can use the electric propulsion system for inclination and eccentricity station keeping. The feasibility of this simultaneous control of eccentricity and inclination results from the relative large cant angles (ranging typically from 40° to 45°) that imply a significant radial velocity component upon firing. Four bipropellant thrusters are located on the East and West faces (two nominal and two redundant) and provide mean longitude drift station keeping. As we will explain better in Chapter 5, such a configuration allows the system to perform a station keeping technique based on a strategy different from that classical one where the North-South (NS) strategy corrects inclination only and the East-West (EW) strategy corrects eccentricity and mean longitude drift simultaneously. With the hybrid configuration depicted in Fig. 3.8 only two electric thrusters — one North and one South — are used in the event of failure. The first North-South thruster pair has a smaller cant angle value and thus a better efficiency than the second one. Thruster configuration matrix $\boldsymbol{\Gamma}$ and thrust vector $\boldsymbol{F}$ of this propulsion system are

$$\boldsymbol{\Gamma} = \begin{bmatrix} 0 & 0 & 0 & 0 & -\sin\gamma^{en} & -\sin\gamma^{er} & -\sin\gamma^{en} & -\sin\gamma^{er} \\ +1 & +1 & -1 & -1 & 0 & 0 & 0 & 0 \\ 0 & 0 & 0 & 0 & -\cos\gamma^{en} & +\cos\gamma^{er} & -\cos\gamma^{en} & +\cos\gamma^{er} \end{bmatrix}, \tag{3.121}$$

and

$$\boldsymbol{F} = \begin{bmatrix} F^{cn}_{-X_B} & F^{cr}_{-X_B} & F^{cn}_{+X_B} & F^{cr}_{+X_B} & F^{en}_{N} & F^{er}_{N} & F^{en}_{S} & F^{er}_{S} \end{bmatrix}^T \tag{3.122}$$

where c, e, n, r superscripts mean respectively chemical, electric, nominal, redundant and N, S subscripts mean respectively North, South.

The fully electric thruster configuration can be thought as evolved from the hybrid one by simply separating each of two North electric thrusters and of two South electric thrusters laterally and in opposite X_B directions and pointing the thrust axes to intersect the satellite center of mass. With the four electric thrusters mounted as depicted in Fig. 3.9, the thruster configuration matrix $\boldsymbol{\Gamma}$ and the thrust vector $\boldsymbol{F}$ are

$$\boldsymbol{\Gamma} = \begin{bmatrix} -\sin\gamma\cos\sigma & -\sin\gamma\cos\sigma & -\sin\gamma\cos\sigma & -\sin\gamma\cos\sigma \\ +\sin\gamma\sin\sigma & -\sin\gamma\sin\sigma & -\sin\gamma\sin\sigma & +\sin\gamma\sin\sigma \\ -\cos\gamma & -\cos\gamma & +\cos\gamma & +\cos\gamma \end{bmatrix} \tag{3.123}$$

and

$$\boldsymbol{F} = \begin{bmatrix} F_{NW} & F_{NE} & F_{SE} & F_{SW} \end{bmatrix}^T. \tag{3.124}$$

Typical values of cant and slew angles are $\gamma = 50°$ and $\sigma = 13°$ respectively. This thruster configuration has been proposed by [Anzel, 1995] and [Anzel, 1998] with a station keeping technique also that will be explained better in Chapter 5. The basic idea proposed by [Anzel, 1995] is to fire in nominal mode (i.e., in absence of failure) simultaneously the NW and the NE thrusters at a right

ascension α close to 90° and the SW and SE thrusters at a right ascension close to 270°. In the failure mode only two diagonal thrusters are used: either the NW-SE or the NE-SW thruster pair. The North thruster of the pair is fired at $\alpha \approx 90°$ and the South thruster at $\alpha \approx 270°$. Both healthy diagonal thrusters are fired a second time simultaneously and with equal duration at $\alpha \approx 0°$ or $\alpha \approx 180°$ depending on the damaged pair. A total of four firings per orbit are also required in failure mode, two from each thruster.

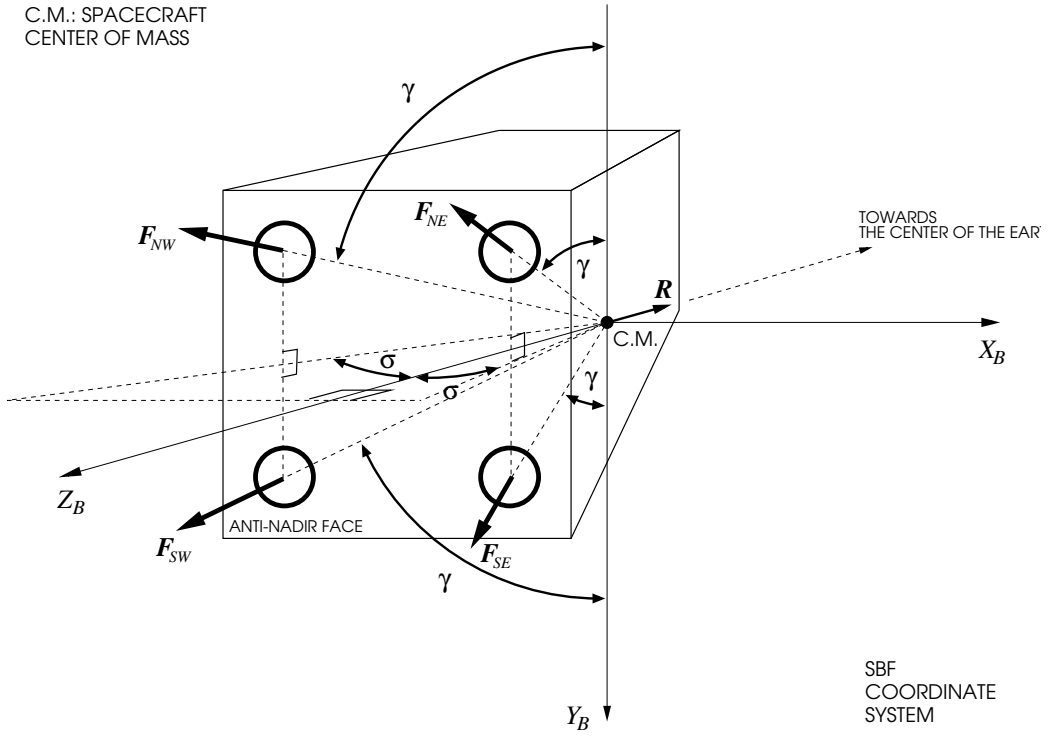

Figure 3.9: *Fully electric thruster configuration proposed in the patent of [Anzel, 1995]*

Chapter 4

Translational Dynamics of GEO Satellites

As their name implies, Geostationary Earth Orbit (GEO) satellites maintain an essentially fixed position with respect to the surface of the Earth. This is made possible by inserting the spacecraft into a circular, equatorial orbit at an altitude of roughly 36000 km. At this altitude, if the main environmental disturbing forces (the Earth's non-spherical gravity attraction, the Moon's and Sun's gravity attraction and the solar radiation pressure) are neglected except the Kepler attraction of the Earth, the geostationary motion is ideal. The satellite remains fixed with respect to the surface of the Earth. The mean motion n matches the Earth's rotation rate $\omega_\oplus$ of one revolution per 23 hours and 56 minutes.

In presence of perturbations, it is a common practice to control a GEO satellite actively via station keeping maneuvers such that it stays confined in a box of 100–150 km width around a nominal geostationary longitude and latitude. Traditionally this is done with an open loop control technique based on a dynamical model of the satellite state vector subject to the only environmental perturbing forces and on a separate dynamical model taking into account the only thrust effects. Moreover, this latter model is derived supposing to use a chemical propulsion system characterized by high thrusts and very short thrust durations relative to the orbital period. These impulsive thrust hypotheses lead to assume that maneuvers induce jumps in the velocity part of the state vector but not in the position part. The GEO station keeping problem is thus dealt with in a discrete way, without considering spacecraft acceleration but only velocity and position vectors.

With a view to substitute chemical propulsion systems with electrical ones, the solution approaches of the GEO station keeping problem should become continuous, in order to gain benefit from the technology change. A GEO satellite dynamics model has to be obtained taking into account all the perturbing forces (environmental or not) acting on the spacecraft.

In this chapter we present different translation dynamical models for a GEO satellite: nonlinear models in unperturbed Keplerian conditions, nonlinear models in perturbed Keplerian conditions written in terms of environmental disturbing potential functions (Lagrange's form) and in terms

of environmental disturbing accelerations (Gauss' form), a linearized geostationary orbit model. Numerical simulations of these models let us obtain the time history of the satellite state vector and of the perturbing accelerations, which depend on orbital parameters; they allow us to identify also from which perturbing force the orbital parameters are mainly affected.

This chapter is organized as follows. In Section 4.1 the unperturbed two-body (Earth and satellite) equations are given in terms of classical orbital parameters and equinoctial ones. The nominal station keeping trajectory is deduced as equilibrium of these equations. In Section 4.2 the perturbing contributions are added to the nonlinear model in unperturbed Keplerian conditions to obtain complete dynamical models in perturbed Keplerian conditions. A procedure to solve analytically Kepler's equation with small parameters is also described. In Section 4.3 geographical longitude and latitude are presented as outputs of the above dynamical models. In Section 4.4 a linearized geostationary orbit model is presented with the environmental perturbing accelerations developed in Taylor's series up to order zero. This last model is described by the classical Clohessy-Wiltshire equations also known as Hill's equations of the relative motion of a geostationary spacecraft with respect to the ideal geostationary orbit.

Simulations are performed with a program implemented in Matlab. The corresponding results are presented over all the chapter, to validate the models. The satellite considered in the simulations is characterized by the following structural parameters: a mass $m = 4500$ km; a mean surface absorbing the solar radiation $S = 300$ m^2; a mean reflectivity coefficient $\epsilon = 0.3$, which entails a radiation pressure coefficient $C_R = 1.3$.

4.1 Nonlinear Models in Unperturbed Keplerian Conditions

Neglecting all the disturbing forces except Kepler attraction of the Earth, given the initial values of position and velocity, the trajectory of a GEO satellite is perfectly defined solving the vectorial unperturbed two-body equations

$$\frac{d\boldsymbol{r}_K}{dt} = \boldsymbol{v}_K \tag{4.1}$$

$$\frac{d\boldsymbol{v}_K}{dt} = -GM_{\oplus}\frac{\boldsymbol{r}_K}{r_K^3}. \tag{4.2}$$

Moreover, this trajectory is a conic univocally defined by the six classical orbital elements in unperturbed Keplerian conditions: a_K (semi-major axis), e_K (eccentricity), i_K (inclination), Ω_K (right ascension of the ascending node), ω_K (argument of perigee), M_K (mean anomaly) or by the equinoctial orbital elements a_K, P_{1K} and P_{2K} (eccentricity vector components), Q_{1K} and Q_{2K} (inclination vector components), $l_{\Theta K}$ (mean longitude net of the GHA). In fact, a one-to-one correspondence exists between position and velocity vector component set and classical orbital element set at a fixed epoch t via a bijection τ

$$\{x_K(t); y_K(t); z_K(t); v_{Kx}(t); v_{Ky}(t); v_{Kz}(t)\} \overset{\tau}{\longleftrightarrow} \{a_K(t); e_K(t); i_K(t); \Omega_K(t); \omega_K(t); M_K(t)\}. \tag{4.3}$$

Then, definitions (2.57)–(2.62) with conversion formulas given in Section 2.3.4 establish a one-to-one correspondence between the COE set and the EOE set

$$\{a_K(t); e_K(t); i_K(t); \Omega_K(t); \omega_K(t); M_K(t)\} \longleftrightarrow \{a_K(t); P_{1K}(t); P_{2K}(t); Q_{1K}(t); Q_{2K}(t); l_{\Theta K}(t)\}. \tag{4.4}$$

First order differential dynamical equations (4.1) and (4.2) are equivalent to the following vectorial differential equation

$$\frac{d\boldsymbol{x}_{K_{COE}}}{dt} = \boldsymbol{K}\left(\boldsymbol{x}_{K_{COE}}\right) \tag{4.5}$$

with

$$\boldsymbol{x}_{K_{COE}} = \begin{bmatrix} a_K & e_K & i_K & \Omega_K & \omega_K & M_K \end{bmatrix}^T, \tag{4.6}$$

$$\boldsymbol{K} = \begin{bmatrix} 0 & 0 & 0 & 0 & 0 & n_K \end{bmatrix}^T, \tag{4.7}$$

where the mean motion n_K is a function of the unperturbed semi-major axis a_K

$$n_K = \sqrt{\frac{GM_\oplus}{a_K^3}}. \tag{4.8}$$

The differential equations (4.5) define the rate of change of the classical orbital element state vector in the two-body (Earth and satellite) problem. Their integrals are all constant except for the fast change of the mean anomaly

$$M_K(t) = M_K(t_0) + \sqrt{\frac{GM_\oplus}{a_K^3(t_0)}}(t - t_0). \tag{4.9}$$

The two-body equations (4.5) can also be written in function of the equinoctial orbit elements, substituting Eq. (4.5) in the following differential conversion formula

$$\frac{d\boldsymbol{x}_K}{dt} = \left(\boldsymbol{\nabla}_{K_{COE}}\boldsymbol{x}_K\right)\frac{d\boldsymbol{x}_{K_{COE}}}{dt} - \boldsymbol{\omega}_\oplus \tag{4.10}$$

where

$$\boldsymbol{x}_K = \begin{bmatrix} a_K & P_{1K} & P_{2K} & Q_{1K} & Q_{2K} & l_{\Theta K} \end{bmatrix}^T, \tag{4.11}$$

$$\boldsymbol{\omega}_\oplus = \begin{bmatrix} 0 & 0 & 0 & 0 & 0 & \omega_\oplus \end{bmatrix}^T \tag{4.12}$$

and Jacobian matrix

$$\boldsymbol{\nabla}_{K_{COE}}\boldsymbol{x}_K = \begin{bmatrix} 1 & 0 & 0 & 0 & 0 & 0 \\ 0 & \frac{P_{1K}}{\sqrt{P_{1K}^2+P_{2K}^2}} & 0 & P_{2K} & P_{2K} & 0 \\ 0 & \frac{P_{2K}}{\sqrt{P_{1K}^2+P_{2K}^2}} & 0 & -P_{1K} & -P_{1K} & 0 \\ 0 & 0 & \frac{Q_{1K}(1+Q_{1K}^2+Q_{2K}^2)}{2\sqrt{Q_{1K}^2+Q_{2K}^2}} & Q_{2K} & 0 & 0 \\ 0 & 0 & \frac{Q_{2K}(1+Q_{1K}^2+Q_{2K}^2)}{2\sqrt{Q_{1K}^2+Q_{2K}^2}} & -Q_{1K} & 0 & 0 \\ 0 & 0 & 0 & 1 & 1 & 1 \end{bmatrix} \tag{4.13}$$

is the partial derivative matrix of the equinoctial orbit element state vector $\boldsymbol{x}_K$ with respect to the classical orbit element state vector $\boldsymbol{x}_{K_{COE}}$. The results is

$$\frac{d\boldsymbol{x}_K}{dt} = \boldsymbol{K}(\boldsymbol{x}_K) - \boldsymbol{\omega}_\oplus \tag{4.14}$$

with $\boldsymbol{x}_K$, $\boldsymbol{K}$ and $\boldsymbol{\omega}_\oplus$ given by Eq.s (4.11), (4.7) and (4.12).

The two-body equations (4.14) define the rate of change of the equinoctial orbit elements in unperturbed Keplerian conditions[1]. For an initial condition

$$\boldsymbol{x}_K(t_0) = \begin{bmatrix} a_{K_0} & P_{1K_0} & P_{2K_0} & Q_{1K_0} & Q_{2K_0} & l_{\Theta K_0} \end{bmatrix}^T, \tag{4.15}$$

the Keplerian EOE evolution is

$$a_K(t) = a_{K_0}, \tag{4.16}$$
$$P_{1K}(t) = P_{1K_0}, \tag{4.17}$$
$$P_{2K}(t) = P_{2K_0}, \tag{4.18}$$
$$Q_{1K}(t) = Q_{1K_0}, \tag{4.19}$$
$$Q_{2K}(t) = Q_{2K_0}, \tag{4.20}$$
$$l_{\Theta K}(t) = l_{\Theta K_0} + \left(\sqrt{\frac{GM_\oplus}{a_{K_0}^3}} - \omega_\oplus \right) (t - t_0). \tag{4.21}$$
$$\tag{4.22}$$

For an initial semi-major axis equal to the root of the equation

$$\sqrt{\frac{GM_\oplus}{a_K^3}} - \omega_\oplus = 0, \tag{4.23}$$

the mean longitude remains equal to its initial value $l_{\Theta K_0}$ forever. This particular value of semi-major axis is called *Keplerian semi-major axis* and it will be denoted as a_k

$$a_k = \sqrt[3]{\frac{GM_\oplus}{\omega_\oplus^2}} = 42164.172 \quad \text{km}. \tag{4.24}$$

Moreover, in the unperturbed Keplerian conditions, if a satellite has an initial state vector with

$$a_{K_0} = a_k, \quad P_{1K_0} = 0, \quad P_{2K_0} = 0, \quad Q_{1K_0} = 0, \quad Q_{2K_0} = 0 \quad (\textit{geostationary conditions}),$$

and with $l_{\Theta K_0}$ equal to the station longitude λ_s, then the satellite remains in a nominal station keeping condion (see Fig. 4.1), i.e., in geostationary conditions and with a longitude equal to its

[1] The spacecraft is subject only to the gravitational attraction of the Earth considered with punctiform mass.

station value. Such a state vector will be called *Keplerian nominal station keeping state* and will be denoted as

$$\begin{aligned} \boldsymbol{x}_{Ksk} &= \begin{bmatrix} a_{Ksk} & P_{1Ksk} & P_{2Ksk} & Q_{1Ksk} & Q_{2Ksk} & l_{\Theta Ksk} \end{bmatrix}^T = \\ &= \begin{bmatrix} a_k & 0 & 0 & 0 & 0 & \lambda_s \end{bmatrix}^T . \end{aligned} \tag{4.25}$$

We observe that the Keplerian nominal station keeping state is an unstable equilibrium point for the nonlinear system (4.14), because for $a_{K_0} \neq a_k$ the mean longitude diverges linearly to the infinity with a slope equal to $(\sqrt{GM_\oplus / a_{K_0}^3} - \omega_\oplus)$.

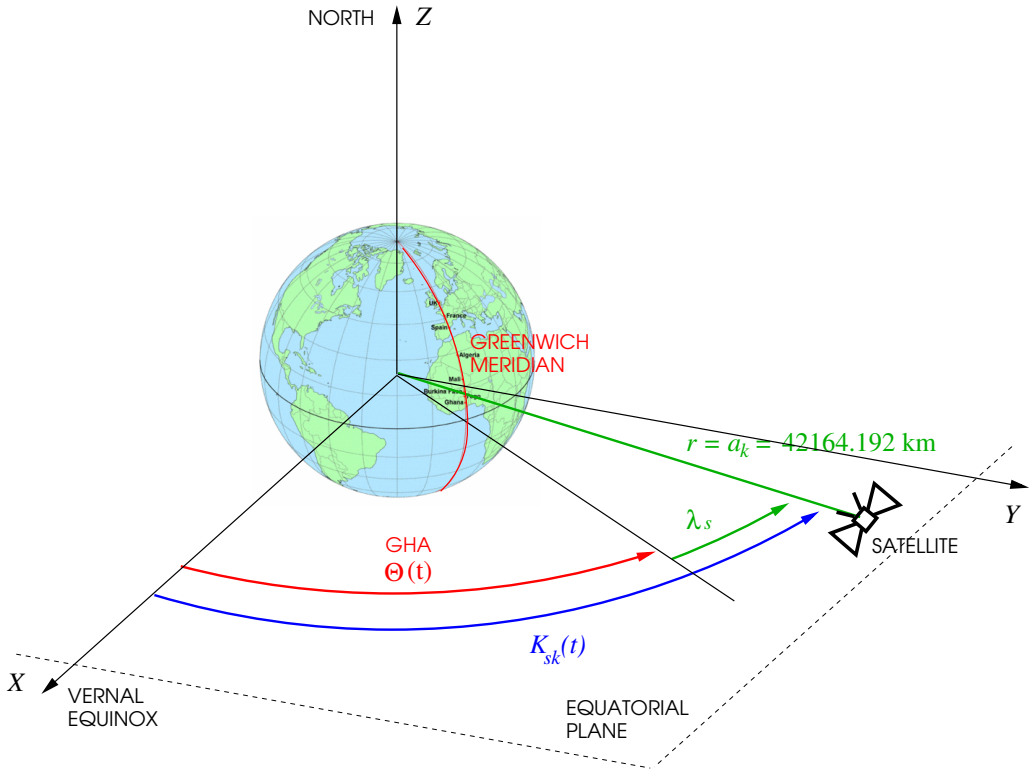

Figure 4.1: *Nominal station keeping condition*

4.2 Nonlinear Models in Perturbed Keplerian Conditions

When the satellite is subject to disturbing forces different to the Keplerian Earth's gravity attraction, the above properties of orbital elements are no longer true. Under the hypothesis that the disturbing forces are weak with respect to the main Keplerian two-body term, it is reasonable to think that the satellite trajectory is slightly different from a conic, i.e., that the six first integrals of the unperturbed two-body equations undergo only weak variations. To express this concept

mathematically, the satellite osculating elements are defined at an epoch t as the image, via the bijection τ (see relation (4.3)), of the position and the velocity vectors $\boldsymbol{r}_K$ and $\boldsymbol{v}_K$ obtained solving the unperturbed Kepler's two-body problem from the epoch t. As explained in Chapter 2, the adjective "osculating" should not be interpreted in geometrical sense. At an epoch t the osculating elements are the orbital elements of the trajectory which the satellite will follow if it is no more subject to disturbing forces from the instant t. The osculating elliptic trajectory defined by the osculating elements is tangent to the actual trajectory (i.e., it has the same velocity vector) but it doesn't have the same curvature radius (i.e., it has a different acceleration vector). According to the variation of parameter (VOP) methods originally developed by Euler and later improved by Lagrange and Gauss in the 18^{th} century to analyse the perturbation effects, the vectorial first order differential dynamical equations valid for a GEO satellite subject to the Keplerian Earth's gravity attraction and to the generic not Keplerian disturbing acceleration $\boldsymbol{a}_d$ are

$$\frac{d\boldsymbol{r}}{dt} = \boldsymbol{v} \tag{4.26}$$

$$\frac{d\boldsymbol{v}}{dt} = -GM_{\oplus}\frac{\boldsymbol{r}}{r^3} + \boldsymbol{a}_d\left(\boldsymbol{r}, \boldsymbol{v}, t\right) \tag{4.27}$$

and they are equivalent to the set of differential equations

$$\frac{d\boldsymbol{x}}{dt} = \boldsymbol{K}(\boldsymbol{x}) - \boldsymbol{\omega}_{\oplus} + \boldsymbol{\mathcal{D}}\left(\boldsymbol{x}, t\right) \tag{4.28}$$

with

$$\boldsymbol{x} = \begin{bmatrix} a & P_1 & P_2 & Q_1 & Q_2 & l_{\Theta} \end{bmatrix}^T, \tag{4.29}$$

$$\boldsymbol{\omega}_{\oplus} = \begin{bmatrix} 0 & 0 & 0 & 0 & 0 & \omega_{\oplus} \end{bmatrix}^T, \tag{4.30}$$

$$\boldsymbol{K} = \begin{bmatrix} 0 & 0 & 0 & 0 & 0 & n \end{bmatrix}^T, \tag{4.31}$$

where the mean motion n is function of the unperturbed semi-major axis a

$$n = \sqrt{\frac{GM_{\oplus}}{a^3}}. \tag{4.32}$$

Vector $\boldsymbol{\mathcal{D}}$ is the disturbing contribution to the VOP equations, small with respect to the Keplerian part. We will call this perturbing contribution $\boldsymbol{\mathcal{G}}$ (as Gauss) when the VOP equations contain directly the disturbing acceleration $\boldsymbol{a}_d$

$$\boldsymbol{\mathcal{D}}\left(\boldsymbol{x}, t\right) \equiv \boldsymbol{\mathcal{G}}\left(\boldsymbol{x}, t\right) \propto \boldsymbol{a}_d(\boldsymbol{x}, t). \tag{4.33}$$

We will call the perturbing contribution $\boldsymbol{\mathcal{L}}$ (as Lagrange) when the conservative disturbing accelerations are modeled as the gradient vector of a potential function $\mathcal{E}_d$

$$\boldsymbol{\mathcal{D}}\left(\boldsymbol{x}, t\right) \equiv \boldsymbol{\mathcal{L}}\left(\boldsymbol{x}, t\right) \propto \boldsymbol{\nabla}_{EOE}\mathcal{E}_d(\boldsymbol{x}, t). \tag{4.34}$$

In the following two subsections, a GEO satellite nonlinear model is first deduced in terms of Gauss' VOP equations in order to compare the magnitude of the environmental disturbing accelerations and that of the accelerations provided by the thrusters. Second, the model is deduced in terms of Lagrange's and Gauss' VOP equations. More precisely, Lagrange's and Gauss' forms will be used to model the environmental force and the thrust effects respectively. This last modeling choice is common practice in GEO satellite modeling used in standard station keeping strategy. Actually, in the thesis work, it has been followed before calculating the Gauss' VOP equations.

4.2.1 Gauss' Variation of Parameter (VOP) Equations

The Gauss' variation of parameter equations (or Gauss' planetary equations) give the variations over time of the classical orbit elements characterizing the motion of a spacecraft subject to the Keplerian gravity attraction of the Earth's *and* subject to small perturbing accelerations.

Let be

$$\boldsymbol{a}_d = a_{dR}\boldsymbol{R} + a_{dT}\boldsymbol{T} + a_{dN}\boldsymbol{N}, \tag{4.35}$$

the sum of all the disturbing acceleration vectors expressed in the RTN reference frame. The disturbing acceleration components perturb the solution $\boldsymbol{x}_{K_{COE}}$ of the unperturbed Kepler's problem (see Eq. (4.5)). This new perturbed solution fulfils the Gauss' variation of parameter equations

$$\frac{d\boldsymbol{x}_{COE}}{dt} = \boldsymbol{K}\left(\boldsymbol{x}_{COE}\right) + \bar{\boldsymbol{G}}\left(\boldsymbol{x}_{COE}\right)\boldsymbol{a}_d\left(\boldsymbol{x}_{COE}, t\right) \tag{4.36}$$

where

$$\boldsymbol{x}_{COE} = \begin{bmatrix} a & e & i & \Omega & \omega & M \end{bmatrix}^T, \tag{4.37}$$

$$\boldsymbol{K} = \begin{bmatrix} 0 & 0 & 0 & 0 & 0 & n \end{bmatrix}^T \quad \text{with} \quad n = \sqrt{\frac{GM_\oplus}{a^3}}, \tag{4.38}$$

$$\bar{\boldsymbol{G}} = \begin{bmatrix} \frac{2}{n\sqrt{1-e^2}} e\sin\nu & \frac{2}{n\sqrt{1-e^2}}(1+e\cos\nu) & 0 \\ \frac{\sqrt{1-e^2}}{na}\sin\nu & \frac{\sqrt{1-e^2}}{na}(\cos E+\cos\nu) & 0 \\ 0 & 0 & \frac{r}{na^2\sqrt{1-e^2}}\cos(\omega+\nu) \\ 0 & 0 & \frac{r}{na^2\sqrt{1-e^2}}\frac{\sin(\omega+\nu)}{\sin i} \\ -\frac{\sqrt{1-e^2}}{nae}\cos\nu & \frac{\sqrt{1-e^2}}{nae}\left(1+\frac{1}{1+e\cos\nu}\right)\sin\nu & -\frac{r\cos i}{na^2\sqrt{1-e^2}}\frac{\sin(\omega+\nu)}{\sin i} \\ \frac{1-e^2}{nae}\left(\cos\nu - \frac{2e}{1+e\cos\nu}\right) & -\frac{1-e^2}{nae}\left(1+\frac{1}{1+e\cos\nu}\right)\sin\nu & 0 \end{bmatrix}, \tag{4.39}$$

$$\boldsymbol{a}_d = \begin{bmatrix} a_{dR_{COE}} & a_{dT_{COE}} & a_{dN_{COE}} \end{bmatrix}^T. \tag{4.40}$$

The dependence of the matrix $\bar{\boldsymbol{G}}$ on the mean anomaly M is not explicit. In fact, sine and cosine of the true anomaly ν depend on sine and cosine of the eccentric anomaly E, via the inverse formulas of Eq.s (2.31)

$$\sin\nu = \frac{\sin E\sqrt{1-e^2}}{1-e\cos E} \quad \text{and} \quad \cos\nu = \frac{\cos E - e}{1-e\cos E}. \tag{4.41}$$

In its turn, the eccentric anomaly E is solution of Kepler's equation

$$E - e\sin E = M, \tag{4.42}$$

which, for small eccentricity, can be solved analytically with a Taylor series expansion process or with a differential process ([Hull, 2003], pages 322–324). It can also be easily solved numerically, using the method of successive substitutions ([Battin, 1999], pages 196–197) or using Newton's method to calculate successive refinements of E values until the result changes by less than a specified amount from one iteration to the next ([Montenbruck and Gill, 2000], pages 23–24). In this last solution way, an auxiliary function

$$f(E) = E - e\sin E - M \tag{4.43}$$

is defined and solved for a given value of M. Applying Newton's method for this purpose, an approximate root E_i of f may be improved by computing

$$E_{i+1} = E_i - \frac{f(E_i)}{f'(E_i)} = E_i - \frac{E_i - e\sin E_i - M}{1 - e\cos E_i}. \tag{4.44}$$

Gauss' VOP equations (4.36) can also be written in terms of the equinoctial orbit elements thanks to the following differential conversion formula

$$\frac{d\boldsymbol{x}}{dt} = \left(\boldsymbol{\nabla}_{COE}\boldsymbol{x}\right)\frac{d\boldsymbol{x}_{COE}}{dt} - \boldsymbol{\omega}_{\oplus} \tag{4.45}$$

where

$$\boldsymbol{x} = \begin{bmatrix} a & P_1 & P_2 & Q_1 & Q_2 & l_\Theta \end{bmatrix}^T, \tag{4.46}$$

$$\boldsymbol{\omega}_{\oplus} = \begin{bmatrix} 0 & 0 & 0 & 0 & 0 & \omega_{\oplus} \end{bmatrix}^T \tag{4.47}$$

and Jacobian matrix

$$\boldsymbol{\nabla}_{COE}\boldsymbol{x} = \begin{bmatrix} 1 & 0 & 0 & 0 & 0 & 0 \\ 0 & \frac{P_1}{\sqrt{P_1^2+P_2^2}} & 0 & P_2 & P_2 & 0 \\ 0 & \frac{P_2}{\sqrt{P_1^2+P_2^2}} & 0 & -P_1 & -P_1 & 0 \\ 0 & 0 & \frac{Q_1(1+Q_1^2+Q_2^2)}{2\sqrt{Q_1^2+Q_2^2}} & Q_2 & 0 & 0 \\ 0 & 0 & \frac{Q_2(1+Q_1^2+Q_2^2)}{2\sqrt{Q_1^2+Q_2^2}} & -Q_1 & 0 & 0 \\ 0 & 0 & 0 & 1 & 1 & 1 \end{bmatrix} \tag{4.48}$$

is the partial derivative matrix of the equinoctial orbit element state vector $\boldsymbol{x}$ with respect to the classical orbit element state vector $\boldsymbol{x}_{COE}$. The right-hand side of Eq. (4.36) has to be replaced in the conversion formula (4.45) by matrix $\bar{\boldsymbol{G}}$ and disturbing acceleration vector $\boldsymbol{a}_d$ expressed in terms of equinoctial elements

$$\bar{\boldsymbol{G}}\left(\boldsymbol{x}_{COE}\right) \quad \longrightarrow \quad \bar{\boldsymbol{G}}(\boldsymbol{x}, t), \tag{4.49}$$

$$\boldsymbol{a}_d\left(\boldsymbol{x}_{COE}, t\right) \quad \longrightarrow \quad \boldsymbol{a}_d(\boldsymbol{x}, t) \tag{4.50}$$

The transformation (4.49) is obtained using the conversion formulas (3.53), (2.65), (2.66) and the following

$$e = \sqrt{P_1^2 + P_2^2}, \tag{4.51}$$

$$\sin\nu = \frac{P_2 \sin L - P_1 \cos L}{\sqrt{P_1^2 + P_2^2}}, \tag{4.52}$$

$$\cos\nu = \frac{P_1 \sin L + P_2 \cos L}{\sqrt{P_1^2 + P_2^2}}, \tag{4.53}$$

$$\cos E = \frac{e + \cos\nu}{1 + e\cos\nu}. \tag{4.54}$$

The explicit dependence of matrix $\bar{\boldsymbol{G}}$ on time comes from the implicit dependence of the conversion formulas (4.52) and (4.53) on the Greenwich Hour Angle Θ. The disturbing accelerations $\boldsymbol{a}_d(\boldsymbol{x}, t)$ acting on GEO satellites are obtained in function of equinoctial orbital elements using the procedure described in point **D** of Section 3.1. Their explicit dependence on time comes also from the dependence on Sun's and Moon's ephemerides.

Gauss' VOP equations in terms of equinoctial orbital elements are as follows

$$\frac{d\boldsymbol{x}}{dt} = \boldsymbol{K}(\boldsymbol{x}) - \boldsymbol{\omega}_{\oplus} + \boldsymbol{\mathcal{G}}(\boldsymbol{x}, t) \tag{4.55}$$

where $\boldsymbol{x}$, $\boldsymbol{K}$, $\boldsymbol{\omega}_{\oplus}$ are given by Eq.s (4.46), (4.38), (4.47) and

$$\boldsymbol{\mathcal{G}}(\boldsymbol{x}, t) = \boldsymbol{G}(\boldsymbol{x}, t)\boldsymbol{a}_d(\boldsymbol{x}, t), \quad \text{with} \quad \boldsymbol{G}(\boldsymbol{x}, t) = (\boldsymbol{\nabla}_{COE}\boldsymbol{x})\,\bar{\boldsymbol{G}}(\boldsymbol{x}, t); \tag{4.56}$$

more precisely

$$\boldsymbol{G}(\boldsymbol{x}, t) = \begin{bmatrix} \frac{2a^2}{h} X_1 & \frac{2a^2}{h}\frac{p}{r} & 0 \\ -\frac{r}{h}\frac{p}{r}\cos L & \frac{r}{h}\left[P_1 + \left(1 + \frac{p}{r}\right)\sin L\right] & -\frac{r}{h}P_2 Y_1 \\ \frac{r}{h}\frac{p}{r}\sin L & \frac{r}{h}\left[P_2 + \left(1 + \frac{p}{r}\right)\cos L\right] & \frac{r}{h}P_1 Y_1 \\ 0 & 0 & \frac{r}{2h} Y_2 \sin L \\ 0 & 0 & \frac{r}{2h} Y_2 \cos L \\ -\frac{r}{h}\left[\frac{a}{a+b}\left(\frac{p}{r}\right) X_2 + \frac{2b}{a}\right] & \frac{r}{h}\frac{a}{a+b}\left(1 + \frac{p}{r}\right) X_1 & -\frac{r}{h} Y_1 \end{bmatrix} \tag{4.57}$$

where

$$b = a\sqrt{1 - P_1^2 - P_2^2}, \tag{4.58}$$

$$h = nab \quad \text{with} \quad n = \sqrt{\frac{GM_\oplus}{a^3}}, \tag{4.59}$$

$$\frac{p}{r} = 1 + P_1 \sin L + P_2 \cos L, \tag{4.60}$$

$$\frac{r}{h} = \frac{h}{GM_\oplus(1 + P_1 \sin L + P_2 \cos L)}, \tag{4.61}$$

$$X_1 = P_2 \sin L - P_1 \cos L, \tag{4.62}$$

$$X_2 = P_1 \sin L + P_2 \cos L, \tag{4.63}$$

$$Y_1 = Q_1 \cos L - Q_2 \sin L, \tag{4.64}$$

$$Y_2 = 1 + Q_1^2 + Q_2^2. \tag{4.65}$$

Sine and cosine of the true longitude L are defined by Eq.s (2.70) and (2.71), which are implicit functions of $(l_\Theta + \Theta)$ via the eccentric longitude

$$K = (l_\Theta + \Theta) - P_1 \cos(l_\Theta + \Theta) + P_2 \sin(l_\Theta + \Theta), \tag{4.66}$$

first order analytical solution in P_1 and P_2 of Kepler's equation

$$f\,(K; P_1, P_2) = K + P_1 \cos K - P_2 \sin K - (l_\Theta + \Theta) = 0. \tag{4.67}$$

Considering P_1 and P_2 as small parameters, the solution of Kepler's equation above has the functional form $K_* = g(P_1, P_2)$ that can be expanded in Taylor series about $P_1 = 0$ and $P_2 = 0$

$$K_* = K_0 + K_{11}P_1 + K_{12}P_2 + K_{21}P_1^2 + K_{22}P_2^2 + K_{23}P_1P_2 + \cdots \tag{4.68}$$

where K_0 is called the zeroth-order solution, $K_0 + K_{11}P_1 + K_{12}P_2$ is called the first-order solution and so on. Equation (4.68) can be rewritten as $K_* = K_0 + \Delta K$ with

$$\Delta K = K_{11}P_1 + K_{12}P_2 + K_{21}P_1^2 + K_{22}P_2^2 + K_{23}P_1P_2 + \cdots. \tag{4.69}$$

Then, K_* is substituted into Eq. (4.67) which in turn is expanded in terms of small quantities ΔK, P_1 and P_2 around $\Delta K = K_0$, $P_1 = 0$ and $P_2 = 0$

$$\begin{aligned} f(K; P_1, P_2) &= f(K_0 + \Delta K; P_1, P_2) = \\ &= f(K_0; 0, 0) + f_K(K_0; 0, 0)\Delta K + f_{P_1}(K_0; 0, 0)P_1 + f_{P_2}(K_0; 0, 0)P_2 + \\ &+ f_{P_1K}(K_0; 0, 0)P_1\Delta K + f_{P_2K}(K_0; 0, 0)P_2\Delta K + f_{P_1P_2}(K_0; 0, 0)P_1P_2 + \\ &+ \frac{1}{2!}\left[f_{KK}(K_0; 0, 0)\Delta K^2 + f_{P_1P_1}(K_0; 0, 0)P_1^2 + f_{P_2P_2}(K_0; 0, 0)P_2^2\right] + \cdots = 0. \end{aligned} \tag{4.70}$$

Finally, Eq. (4.70) is written only in terms of powers of P_1 and P_2 thanks to Eq. (4.69), and the coefficients of the various powers are equated to zero. This process gives the equations

$$f(K_0;0,0)=0, \tag{4.71}$$
$$f_K K_{11}+f_{P_1}=0, \tag{4.72}$$
$$f_K K_{12}+f_{P_2}=0, \tag{4.73}$$
$$f_K K_{21}+f_{P_1K}K_{11}+\frac{1}{2!}f_{KK}K_{11}^2+\frac{1}{2!}f_{P_1P_1}=0, \tag{4.74}$$
$$f_K K_{22}+f_{P_2K}K_{12}+\frac{1}{2!}f_{KK}K_{12}^2+\frac{1}{2!}f_{P_2P_2}=0, \tag{4.75}$$
$$f_K K_{23}+f_{P_2K}K_{11}+f_{P_1K}K_{12}+f_{KK}K_{11}K_{12}+f_{P_1P_2}=0, \tag{4.76}$$
$$\vdots$$

which can be solved sequentially for K_0, K_{11}, K_{12}, etc.. All the partial derivatives in the above Eq.s (4.71)–(4.76) are evaluated in $K=K_0$, $P_1=0$ and $P_2=0$. At the first order in P_1 and P_2 one obtains the coefficients

$$K_0=l_\Theta+\Theta, \tag{4.77}$$
$$K_{11}=-\frac{f_{P_1}(K_0;0,0)}{f_K(K_0;0,0)}=-\frac{\cos K_0}{1}=-\cos\left(l_\Theta+\Theta\right), \tag{4.78}$$
$$K_{12}=-\frac{f_{P_2}(K_0;0,0)}{f_K(K_0;0,0)}=\frac{\sin K_0}{1}=\sin\left(l_\Theta+\Theta\right), \tag{4.79}$$

which are those of solution (4.66).

Fig.s 4.3-4.8 show the equinoctial element time histories obtained by numerical integration of Gauss' VOP equations over 2 years, for a satellite with mass $m=4500$ kg, $S=300$ m^2, $C_R=1.3$. Gauss' VOP equations have been integrated with the disturbing accelerations vector $\boldsymbol{a}_d$ equal to the sum of the three main environmental acceleration vectors described in Section 3.1

$$\boldsymbol{a}_d(\boldsymbol{x},t)=\boldsymbol{a}_g(\boldsymbol{x},t)+\boldsymbol{a}_a(\boldsymbol{x},t)+\boldsymbol{a}_p(\boldsymbol{x},t). \tag{4.80}$$

The initial dynamical conditions are

$$a(t_0)=a_k,\quad P_1(t_0)=P_2(t_0)=Q_1(t_0)=Q_2(t_0)=0,\quad l_\Theta(t_0)=60^\circ, \tag{4.81}$$

at the initial epoch $t_0=0$ corresponding to the date 2010 January 1.0.

Fig.s 4.17–4.22 show the equinoctial element time histories obtained by numerical integration of Gauss' VOP equations over 2 years with initial dynamical conditions

$$a(t_0)=a_k,\quad P_1(t_0)=P_2(t_0)=Q_1(t_0)=Q_2(t_0)=0,\quad l_\Theta(t_0)=180^\circ, \tag{4.82}$$

for a satellite, a disturbing acceleration vector and a t_0 value like the ones above.

With those EOE time histories obtained above, we have evaluated numerically the components F_{dR}, F_{dT}, F_{dN} and the modulus F_d of the vector of the environmental forces acting on the spacecraft. These quantities depend on the EOEs and explicitly on time because the environmental disturbing accelerations are dependent too (see Eq. (4.55), (4.56) and Chapter 3). They have been calculated as follows

$$F_{dR}(\boldsymbol{x},t) = ma_{dR}(\boldsymbol{x},t), \quad F_{dT}(\boldsymbol{x},t) = ma_{dT}(\boldsymbol{x},t), \quad F_{dN}(\boldsymbol{x},t) = ma_{dN}(\boldsymbol{x},t), \tag{4.83}$$

$$F_d(\boldsymbol{x},t) = \sqrt{[F_{dR}(\boldsymbol{x},t)]^2 + [F_{dT}(\boldsymbol{x},t)]^2 + [F_{dN}(\boldsymbol{x},t)]^2}. \tag{4.84}$$

Fig.s 4.9 and 4.10 show the time histories of F_{dR}, F_{dT}, F_{dN} and F_d over 2 years, obtained with the EOEs starting from conditions (4.81). Fig.s 4.23 and 4.24 show those ones obtained with the EOEs starting from conditions (4.82). We observe that the amplitudes of these force components vary in the same range for both the initial conditions and that they have the same periodic behavior. Fig.s 4.12 and 4.26 are a zoom of Fig.s 4.10 and 4.24 over the first 4 weeks and they show that a change of initial longitude results in a change of phase of the force component time histories.

4.2.2 Lagrange's VOP Equations

Lagrange's variation of parameter equations (or Lagrange's planetary equations) give the variations over time of the classical orbit elements characterizing the motion of a spacecraft subject to the Keplerian gravity attraction of the Earth's *and* subject to small conservatives perturbing accelerations.

If the sum $\boldsymbol{a}_d$ of all the disturbing accelerations is conservative, it can also be written in the RTN reference frame as the gradient of the potential function $\mathcal{E}_d$:

$$\boldsymbol{a}_d = \nabla\mathcal{E}_d = \mathcal{E}_{dR}\boldsymbol{R} + \mathcal{E}_{dT}\boldsymbol{T} + \mathcal{E}_{dN}\boldsymbol{N} \tag{4.85}$$

where $\mathcal{E}_{dR}$, $\mathcal{E}_{dT}$ and $\mathcal{E}_{dN}$ are the partial derivatives of $\mathcal{E}_d$ (sum of all the potential functions) along the axes R, T, N of the Gaussian coordinate system. The partial derivatives of the potential function $\mathcal{E}_d$ perturb the solution $\boldsymbol{x}_{K_{COE}}$ of the unperturbed Kepler's problem (see Eq. (4.5)). This new perturbed solution fulfils Gauss' variation of parameter equations

$$\frac{d\boldsymbol{x}_{COE}}{dt} = \boldsymbol{K}\left(\boldsymbol{x}_{COE}\right) + \bar{\boldsymbol{L}}\left(\boldsymbol{x}_{COE}\right)\boldsymbol{\nabla}_{COE}\mathcal{E}_d(\boldsymbol{x}_{COE},t) \tag{4.86}$$

where

$$\boldsymbol{x}_{_{COE}} = \begin{bmatrix} a & e & i & \Omega & \omega & M \end{bmatrix}^T, \tag{4.87}$$

$$\boldsymbol{K} = \begin{bmatrix} 0 & 0 & 0 & 0 & 0 & n \end{bmatrix}^T \quad \text{with} \quad n = \sqrt{\frac{GM_\oplus}{a^3}}, \tag{4.88}$$

$$\bar{\boldsymbol{L}} = \begin{bmatrix} 0 & 0 & 0 & 0 & 0 & \frac{-2}{na} \\ 0 & 0 & 0 & 0 & \frac{\sqrt{1-e^2}}{na^2e} & \frac{e^2-1}{na^2e} \\ 0 & 0 & 0 & \frac{1}{na^2\sqrt{1-e^2}\sin i} & \frac{-\cos i}{na^2\sqrt{1-e^2}\sin i} & 0 \\ 0 & 0 & \frac{-1}{na^2\sqrt{1-e^2}\sin i} & 0 & 0 & 0 \\ 0 & \frac{-\sqrt{1-e^2}}{na^2e} & \frac{\cos i}{na^2\sqrt{1-e^2}\sin i} & 0 & 0 & 0 \\ \frac{2}{na} & \frac{1-e^2}{na^2e} & 0 & 0 & 0 & 0 \end{bmatrix}, \tag{4.89}$$

$$\boldsymbol{\nabla}_{_{COE}}\mathcal{E}_d = \begin{bmatrix} \frac{\partial \mathcal{E}_d}{\partial a} & \frac{\partial \mathcal{E}_d}{\partial e} & \frac{\partial \mathcal{E}_d}{\partial i} & \frac{\partial \mathcal{E}_d}{\partial \Omega} & \frac{\partial \mathcal{E}_d}{\partial \omega} & \frac{\partial \mathcal{E}_d}{\partial M} \end{bmatrix}^T. \tag{4.90}$$

Lagrange's VOP equations (4.86) can also be written in function of the equinoctial orbit elements thanks to the differential conversion formula (4.45). The right-hand side of Eq. (4.86) has to be replaced in the conversion formula (4.45) with the matrix $\bar{\boldsymbol{L}}$ and the Jacobian vector $\boldsymbol{\nabla}_{_{COE}}\mathcal{E}_d$ expressed in terms of equinoctial elements. The transformation

$$\bar{\boldsymbol{L}}\left(\boldsymbol{x}_{_{COE}}\right) \quad \longrightarrow \quad \bar{\boldsymbol{L}}(\boldsymbol{x}) \tag{4.91}$$

is obtained using the conversion formulas (2.65) and (4.51). The Jacobian vector $\boldsymbol{\nabla}_{_{COE}}\mathcal{E}_d$ is obtained in terms of equinoctial elements with the following derivative chain rule

$$\boldsymbol{\nabla}_{_{COE}}\mathcal{E}_d = \left(\boldsymbol{\nabla}_{_{COE}}\boldsymbol{x}\right)^T \boldsymbol{\nabla}_{_{EOE}}\mathcal{E}_d, \tag{4.92}$$

where $\boldsymbol{\nabla}_{_{COE}}\boldsymbol{x}$ is given by equation (4.48) and

$$\boldsymbol{\nabla}_{_{EOE}}\mathcal{E}_d = \begin{bmatrix} \frac{\partial \mathcal{E}_d}{\partial a} & \frac{\partial \mathcal{E}_d}{\partial P_1} & \frac{\partial \mathcal{E}_d}{\partial P_2} & \frac{\partial \mathcal{E}_d}{\partial Q_1} & \frac{\partial \mathcal{E}_d}{\partial Q_2} & \frac{\partial \mathcal{E}_d}{\partial l_\Theta} \end{bmatrix}^T \tag{4.93}$$

for GEO satellites is directly obtained using the procedure described in point **E** of Section 3.1.

Lagrange's VOP equations in terms of equinoctial orbital elements are as follows

$$\frac{d\boldsymbol{x}}{dt} = \boldsymbol{K}(\boldsymbol{x}) - \boldsymbol{\omega}_\oplus + \boldsymbol{\mathcal{L}}(\boldsymbol{x}, t) \tag{4.94}$$

where $\boldsymbol{x}$, $\boldsymbol{K}$, $\boldsymbol{\omega}_\oplus$ are given by Eq.s (4.46), (4.88), (4.47) and

$$\boldsymbol{\mathcal{L}}(\boldsymbol{x}, t) = \boldsymbol{L}(\boldsymbol{x})\boldsymbol{\nabla}_{_{EOE}}\mathcal{E}_d(\boldsymbol{x}, t), \quad \text{with} \quad \boldsymbol{L}(\boldsymbol{x}) = \left(\boldsymbol{\nabla}_{_{COE}}\boldsymbol{x}\right)\bar{\boldsymbol{L}}(\boldsymbol{x})\left(\boldsymbol{\nabla}_{_{COE}}\boldsymbol{x}\right)^T. \tag{4.95}$$

The explicit dependence of matrix $\boldsymbol{\mathcal{L}}$ on time only comes from the explicit dependence on time of the potential function $\mathcal{E}_d$. A GEO satellite undergoes the effect of the aspherical Earth's gravity attraction which depends on the Greenwich Hour Angle Θ (see Section 3.1.1). It is also affected from Sun's and Moon's gravity attraction and the solar radiation pressure which depend on the

Sun's and Moon's ephemerides (see Section 3.1.2 and 3.1.3). Expanded expression of matrix $\bar{\boldsymbol{L}}$ multiplying the Jacobian vector of the potential function $\mathcal{E}_d$ is time independent and given by

$$\boldsymbol{L}(\boldsymbol{x}) = \begin{bmatrix} 0 & 0 & 0 & 0 & 0 & \frac{2}{na} \\ 0 & 0 & \frac{X_3}{na^2} & \frac{Y_2}{X_3}\frac{P_2Q_1}{2na^2} & \frac{Y_2}{X_3}\frac{P_2Q_2}{2na^2} & \frac{X_3-X_3^2}{X_3^2-1}\frac{P_1}{na^2} \\ 0 & -\frac{X_3}{na^2} & 0 & -\frac{Y_2}{X_3}\frac{P_1Q_1}{2na^2} & -\frac{Y_2}{X_3}\frac{P_1Q_2}{2na^2} & \frac{X_3-X_3^2}{X_3^2-1}\frac{P_2}{na^2} \\ 0 & -\frac{Y_2}{X_3}\frac{P_2Q_1}{2na^2} & \frac{Y_2}{X_3}\frac{P_1Q_1}{2na^2} & 0 & \frac{Y_2^2}{X_3}\frac{1}{4na^2} & -\frac{Y_2}{X_3}\frac{Q_1}{2na^2} \\ 0 & -\frac{Y_2}{X_3}\frac{P_2Q_2}{2na^2} & \frac{Y_2}{X_3}\frac{P_1Q_2}{2na^2} & -\frac{Y_2^2}{X_3}\frac{1}{4na^2} & 0 & -\frac{Y_2}{X_3}\frac{Q_2}{2na^2} \\ -\frac{2}{na} & -\frac{X_3-X_3^2}{X_3^2-1}\frac{P_1}{na^2} & -\frac{X_3-X_3^2}{X_3^2-1}\frac{P_2}{na^2} & \frac{Y_2}{X_3}\frac{Q_1}{2na^2} & \frac{Y_2}{X_3}\frac{Q_2}{2na^2} & 0 \end{bmatrix} \tag{4.96}$$

with $n = \sqrt{GM_\oplus/a^3}$, $X_3 = \sqrt{1-P_1^2-P_2^2}$ and $Y_2 = 1+Q_1^2+Q_2^2$.

For orbits with very small eccentricity and inclination like the geostationary ones, matrix (4.96) can be taken at order zero in P_1, P_2, Q_1 and Q_2

$$\boldsymbol{L}(\boldsymbol{x}) = \begin{bmatrix} 0 & 0 & 0 & 0 & 0 & \frac{2}{na} \\ 0 & 0 & \frac{1}{na^2} & 0 & 0 & 0 \\ 0 & -\frac{1}{na^2} & 0 & 0 & 0 & 0 \\ 0 & 0 & 0 & 0 & \frac{1}{4na^2} & 0 \\ 0 & 0 & 0 & -\frac{1}{4na^2} & 0 & 0 \\ -\frac{2}{na} & 0 & 0 & 0 & 0 & 0 \end{bmatrix}, \tag{4.97}$$

which leads to the following Legendre's VOP contributions

$$\boldsymbol{\mathcal{L}}(\boldsymbol{x},t) = \begin{bmatrix} \frac{2}{na}\frac{\partial \mathcal{E}_d}{\partial l_\Theta} \\ \frac{1}{na^2}\frac{\partial \mathcal{E}_d}{\partial P_2} \\ -\frac{1}{na^2}\frac{\partial \mathcal{E}_d}{\partial P_1} \\ \frac{1}{4na^2}\frac{\partial \mathcal{E}_d}{\partial Q_2} \\ -\frac{1}{4na^2}\frac{\partial \mathcal{E}_d}{\partial Q_1} \\ -\frac{2}{na}\frac{\partial \mathcal{E}_d}{\partial a} \end{bmatrix}. \tag{4.98}$$

This is the approximation adopted by [Legendre, 1980a] (see also [Kamel et al., 1973], [Kamel and Tibbitts, 1973], [Kamel, 1975], [Legendre, 1983], [Cot, 1984]) to find simplified analytical solutions of the linearized Lagrange's VOP equations. The simplified time histories of the EOEs thus obtained are than used by [Legendre, 1980b] (see also [Campan et al., 1995b] and [Sidi, 1997]) to design in open loop the classical discrete-time control laws for the geostationary satellite station keeping.

Fig. 4.31 show the differences between the equinoctial orbital elements obtained numerically integrating the nonlinear Gauss' VOP equations and those obtained numerically integrating Lagrange's ones over $T = t_f - t_0 = 2$ years with $\mathcal{E}_d$ given by the sum of the three main environmental potential functions described in Section 3.1

$$\mathcal{E}_d(\boldsymbol{x},t) = \mathcal{E}_g(\boldsymbol{x},t) + \mathcal{E}_a(\boldsymbol{x},t) + \mathcal{E}_p(\boldsymbol{x},t). \tag{4.99}$$

Even if the nonlinear Gauss's and Lagrange's VOP equations are the equations of the same models but written in two different forms, the simulation results are not exactly the same. This is induced by the different degree of the approximations done in writing the models. In Gauss' equations the only approximation done is about the eccentric longitude K, developed up to the first order in P_1 and P_2 (see Eq. (4.66)). In Lagrange's equations, we have approximated up to the first order in P_1 and P_2

- the sine and cosine of the eccentric longitude $\sin K$ and $\cos K$ (see Eq.s (3.36) and (3.37) at page 87);
- the sine and cosine of true longitude $\sin L$ and $\cos L$ (see Eq.s (3.47) and (3.48) at page 88);
- the sine and cosine of geographical longitude $\sin\lambda$ and $\cos\lambda$ (see Eq.s (3.45) and (3.46) at page 88);
- the satellite director cosines C_x, C_y, C_z (see Eq.s (3.77), (3.79) and (3.80) at page 95) .

4.3 Geographical Position Vector

In the previous sections we have presented a series of nonlinear systems of first order differential equations describing the translational dynamics of a GEO satellite. Integrating over time one of these system (for example Gauss' VOP equations), we obtain the time histories of the EOEs of a GEO satellite subject to disturbing accelerations. However, to formalize mathematically the station keeping problem as an optimal control problem, it is suitable to know the satellite position in the Earth Centred Earth Fixed inertial frame (see page 58). In fact, the goal of a GEO station keeping controller is to maintain longitude and latitude confined in a rectangular box of the (λ, φ) plane centered in $(\lambda_s, 0)$ and with sides equal to $2\lambda_{max}$ and $2\varphi_{max}$

$$\lambda_s - \lambda_{max} \leq \lambda \leq \lambda_s + \lambda_{max} \quad \text{and} \quad -\varphi_{max} \leq \varphi \leq \varphi_{max}. \tag{4.100}$$

We denote the satellite geographical position vector in the ECEF reference frame as

$$\boldsymbol{p} = \begin{bmatrix} r & \lambda & \varphi \end{bmatrix}^T, \tag{4.101}$$

where the components r, λ and φ are respectively the radial, longitudinal and latitudinal position of the spacecraft. In the following of this section, $\boldsymbol{p}$ will be expressed as a nonlinear function of the EOEs and it will be considered as an output nonlinear vectorial equation of the differential equation system describing the GEO satellite translational dynamics.

Radius r

The cosine of eccentric anomaly E and the cosine of true anomaly ν are related in accordance with the following relation

$$\cos\nu = \frac{\cos E - e}{1 - e\cos E}. \tag{4.102}$$

From Fig. 4.2 we can deduce that

$$r\cos\left(180^\circ - \nu\right) = ae - a\cos E. \tag{4.103}$$

Replacing Eq. (4.102) in the one above, one obtains

$$r = a(1 - e\cos E). \tag{4.104}$$

Using trigonometric identities and definition of eccentric longitude and eccentricity equinoctial parameters

$$K = \omega + \Omega + E, \quad P_1 = e\sin(\omega + \Omega), \quad P_2 = e\cos(\omega + \Omega),$$

equation (4.104) becomes

$$r = a(1 - P_1\sin K - P_2\cos K). \tag{4.105}$$

Taking $\sin K$ and $\cos K$ at order zero in P_1 and P_2 (see Eq.s (3.36) and (3.37) at page 87), radius r can be expressed exclusively as function of equinoctial orbital parameters

$$r = a\left[1 - P_1\sin(l_\Theta + \Theta) - P_2\cos(l_\Theta + \Theta)\right]. \tag{4.106}$$

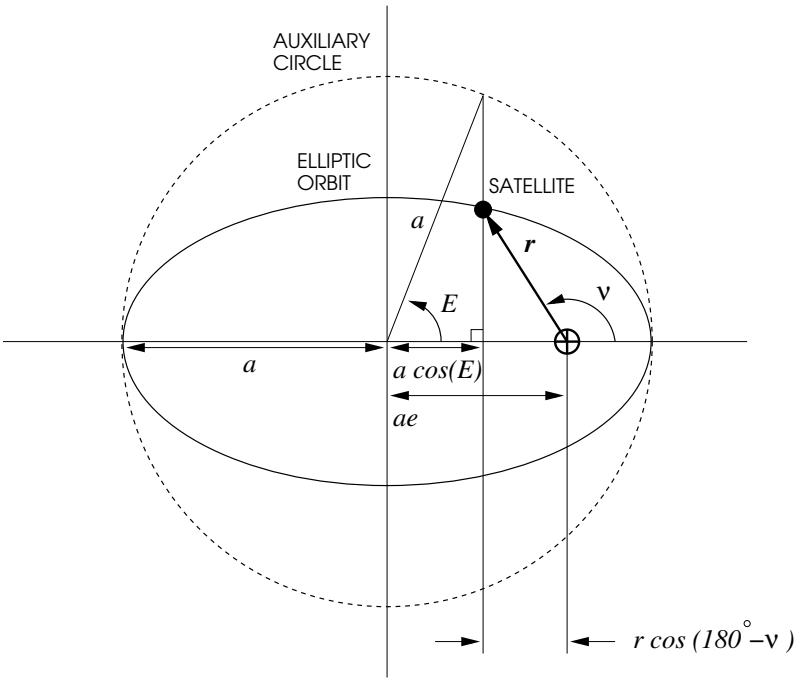

Figure 4.2: *Link between radius, semi-major axis, true and eccentric anomaly*

Geographical longitude λ

Geographical longitude has been defined in Chapter 2 as the geocentric right ascension α net of the Greenwich Hour Angle Θ

$$\lambda = \alpha - \Theta \tag{4.107}$$

(see Fig. 2.5). For small values of inclination i, when the orbit is close to being equatorial as in the geostationary case, we can write

$$\lambda = L - \Theta = \omega + \Omega + \nu - \Theta \tag{4.108}$$

because the right ascension α can be approximated with the true longitude L (see Fig. 2.5 and Fig. 2.12 at pages 60 and Fig. 71). For small values of eccentricity e, analytical expression of the true anomaly ν in function of mean anomaly M can be found solving Keper's equation

$$E - e \sin E - M = 0 \tag{4.109}$$

with

$$E = 2 \arctan \left(\sqrt{\frac{1-e}{1-e}} \tan \frac{\nu}{2} \right), \tag{4.110}$$

following the procedure proposed by [Hull, 2003] to solve algebraic perturbation problems. Replacing folmula (4.110) in Eq. (4.109) we obtain

$$f(\nu; e) = 2 \arctan \left(\sqrt{\frac{1-e}{1-e}} \tan \frac{\nu}{2} \right) - e \sin \left[2 \arctan \left(\sqrt{\frac{1-e}{1-e}} \tan \frac{\nu}{2} \right) \right] - M = 0 \tag{4.111}$$

where ν is the unknown and e is a small parameter. The solution of this equation has the functional form $\nu_* = g(e)$ that can be expanded in a Taylor series about $e = 0$

$$\nu_* = \nu_0 + \nu_1 e + \nu_2 e^2 + \cdots , \tag{4.112}$$

where ν_0 is called the zeroth-order solution, $\nu_0 + \nu_1 e$ is called the first-order solution and so on. Equation (4.112) can be rewritten as $\nu_* = \nu_0 + \Delta\nu$ where

$$\Delta\nu = \nu_1 e + \nu_2 e^2 + \cdots . \tag{4.113}$$

Then, ν_* is substituted into Eq. (4.111), which in turn is expanded in terms of the small quantities $\Delta\nu$ and e, around $\Delta\nu = \nu_0$ and $e = 0$

$$\begin{aligned} f(\nu; e) &= f(\nu_0 + \Delta\nu; e) = \\ &= f(\nu_0; 0) + f_\nu(\nu_0; 0)\Delta\nu + f_e(\nu_0; 0)e + \\ &+ \frac{1}{2!} \left[f_{\nu\nu}(\nu_0; 0)\Delta\nu^2 + 2 f_{e\nu}(\nu_0; 0) e \Delta\nu + f_{ee}(\nu_0; 0) e^2 \right] + \cdots = 0. \end{aligned} \tag{4.114}$$

Finally, Eq. (4.114) is written in terms of powers of e only thanks to Eq. (4.113), and coefficients of the various powers of e are equated to zero. This process gives the equations

$$f(\nu_0;0) = 0 \tag{4.115}$$

$$f_\nu(\nu_0;0)\nu_1 + f_e(\nu_0;0) = 0 \tag{4.116}$$

$$f_\nu(\nu_0;0)\nu_2 + \frac{1}{2!}\left[f_{\nu\nu}(\nu_0;0)\nu_1^2 + 2f_{e\nu}(\nu_0;0)\nu_1 + f_{ee}(\nu_0;0)\right] = 0 \tag{4.117}$$

$$\vdots \tag{4.118}$$

which can be solved sequentially for ν_0, ν_1, etc.. At the first order in e one obtains the coefficients

$$\nu_0 = M, \tag{4.119}$$

$$\nu_1 = -\frac{f_e(\nu_0;0)}{f_\nu(\nu_0;0)} = 2\sin M, \tag{4.120}$$

which lead to the following true anomaly expression

$$\nu = M + 2e\sin M. \tag{4.121}$$

To express true longitude λ in function of mean longitude l_Θ, we replace the first order true anomaly in definition (4.108). The results is

$$\lambda = \omega + \Omega + M + 2e\sin M - \Theta, \tag{4.122}$$

which can be written in function of $l_\Theta = \Omega + \omega + M - \Theta(t)$

$$\lambda = l_\Theta + 2e\sin\left[l_\Theta + \Theta - (\Omega + \omega)\right]. \tag{4.123}$$

Finally, using trigonometric formulas and definitions of eccentricity equinoctial parameters

$$P_1 = e\sin(\omega + \Omega), \quad P_2 = e\cos(\omega + \Omega),$$

geographical longitude up to the first order in P_1 and P_2 can be expressed exclusively as a nonlinear function of the equinoctial orbital parameters and of time

$$\lambda = l_\Theta - 2P_1\cos(l_\Theta + \Theta) + 2P_2\sin(l_\Theta + \Theta). \tag{4.124}$$

Geographical latitude φ

Assuming the Earth with perfectly spherical shape, geographical latitude φ is equal to the satellite declination δ

$$\varphi = \delta$$

(see chapter 2). From third equations of definition (2.4) and conversion formulas (2.50)

$$\begin{aligned} z &= r \sin \delta, \\ z &= r \sin(\omega + \nu) \sin i, \end{aligned} \tag{4.125}$$

we obtain

$$\sin \varphi = \frac{z}{r} = \sin i \sin(\omega + \nu). \tag{4.126}$$

With the following approximations

$$\sin \varphi \approx \varphi, \tag{4.127}$$

$$\sin i \approx 2 \tan(i/2), \tag{4.128}$$

and the definition of the true longitude $L = \omega + \Omega + \nu$, the geographical longitude can be expressed as follows

$$\varphi = 2 \tan(i/2) \sin(\omega + \nu) = 2 \tan(i/2) \sin(L - \Omega). \tag{4.129}$$

Finally, using trigonometric formulas and the definitions of inclination equinoctial parameters

$$Q_1 = \tan(i/2) \sin \Omega, \quad Q_2 = \tan(i/2) \cos \Omega,$$

the geographical latitude φ can be expressed exclusively as a nonlinear function of the equinoctial orbital parameters and of time

$$\varphi = -2Q_1 \cos L + 2Q_2 \sin L \tag{4.130}$$

where sine and cosine of the true longitude L are defined by Eq.s (2.70)–(2.71). Taking $\cos L$ and $\sin L$ up to the zeroth order in P_1 and P_2, geographical latitude can be expressed exclusively as a nonlinear function of the equinoctial orbital parameters and of time

$$\varphi = -2Q_1 \cos(l_\Theta + \Theta) + 2Q_2 \sin(l_\Theta + \Theta) \tag{4.131}$$

Position Vector

The spacecraft position vector expressed in geographical spherical coordinates

$$\boldsymbol{p} = \begin{bmatrix} r & \lambda & \varphi \end{bmatrix}^T, \tag{4.132}$$

is a nonlinear vectorial function of the equinoctial orbital elements and it depends explicitly on time

$$\boldsymbol{p} = \boldsymbol{p}(\boldsymbol{x}, t) \tag{4.133}$$

with

$$\boldsymbol{x} = \begin{bmatrix} a & P_1 & P_2 & Q_1 & Q_2 & l_\Theta \end{bmatrix}^T, \tag{4.134}$$

$$\boldsymbol{p}(\boldsymbol{x},t) = \begin{bmatrix} 1 & -a\sin(l_\Theta+\Theta) & -a\cos(l_\Theta+\Theta) & 0 & 0 & 0 \\ 0 & -2\cos(l_\Theta+\Theta) & 2\sin(l_\Theta+\Theta) & 0 & 0 & 1 \\ 0 & 0 & 0 & -2\cos(l_\Theta+\Theta) & 2\sin(l_\Theta+\Theta) & 0 \end{bmatrix} \boldsymbol{x}, \tag{4.135}$$

where the Greenwich Hour Angle Θ depends on time as follows

$$\Theta = \omega_\oplus t + (\Theta_r - \omega_\oplus t_r) \tag{4.136}$$

(see also page 59).

Fig. 4.13 is the plot of the time histories of radius r, longitude λ and latitude φ obtained with the nonlinear equation (4.133) and with the EOEs drawn in Fig.s 4.3–4.8. Fig. 4.27 is the plot of the time histories of the spherical geographical coordinates of the satellite with EOEs drawn in Fig.s 4.17–4.22. A zoom over the first 4 weeks of Fig. 4.13 and Fig. 4.27 is plotted in Fig. 4.14 and 4.28, to show more clearly the radius and latitude daily oscillations. Fig.s 4.15 and 4.29 are the 3-D pictures of the zoomed spherical coordinates. In Fig.s 4.16 and 4.30 latitude φ is drawn in function of longitude λ in the (λ, φ) plane perpendicular to the equatorial plane and to the nominal radial position of the spacecraft.

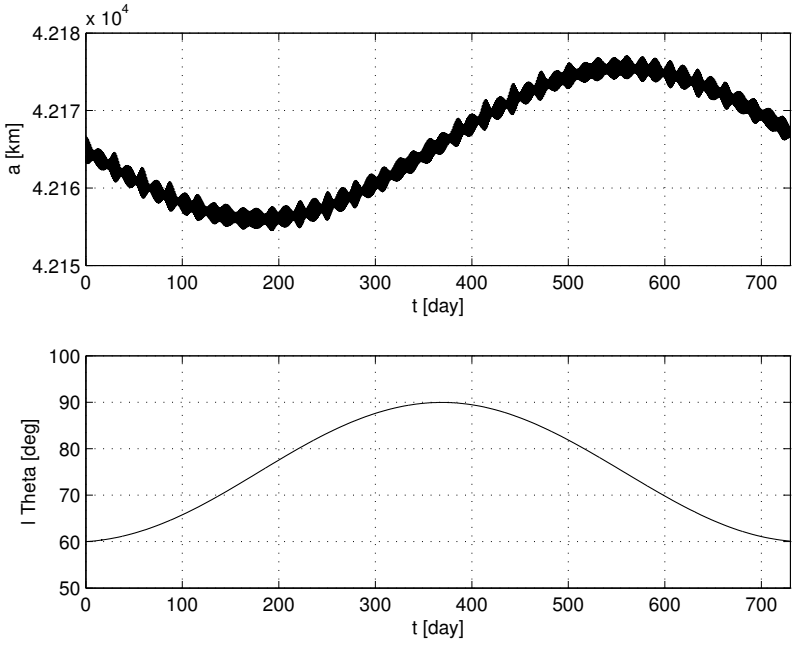

Figure 4.3: *Semi-major axis a and mean latitude l_Θ time histories as results of the numerical integration of Gauss' VOP equations over 2 years. Initial conditions: $a(t_0) = a_k$, $P_1(t_0) = P_2(t_0) = Q_1(t_0) = Q_2(t_0) = 0$, $l_\Theta(t_0) = 60°$, at the initial epoch $t_0 = 0$ corresponding to the date 2010 January 1.0.*

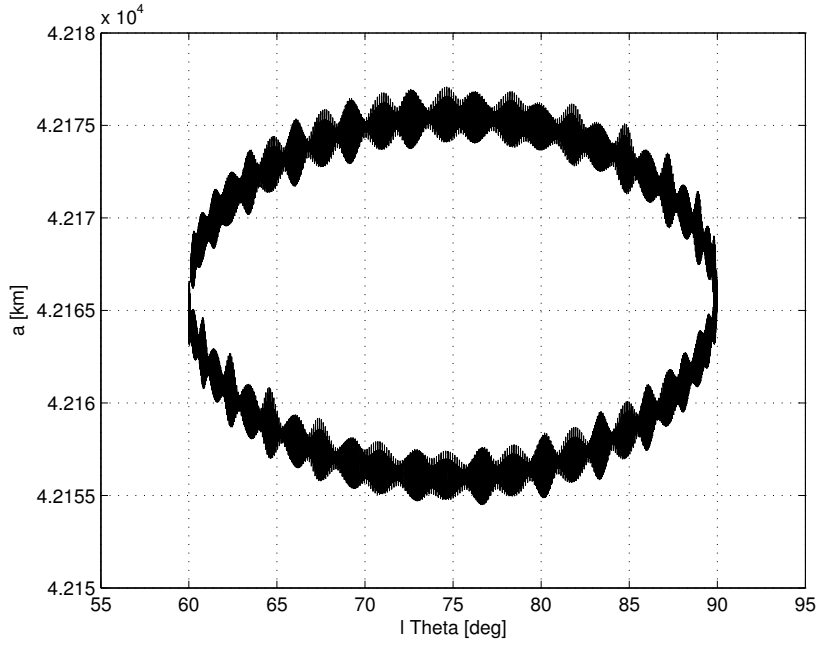

Figure 4.4: *Semi-major axis a vs mean latitude l_Θ relevant to the simulation results above.*

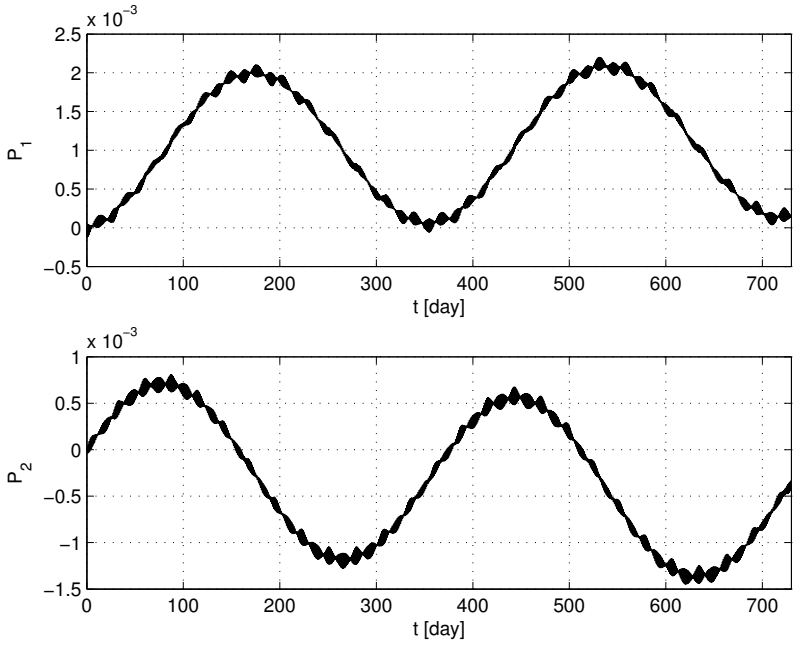

Figure 4.5: *Time histories of the eccentricity vector components P_1 and P_2 as results of the numerical integration of Gauss' VOP equations over 2 years. Initial conditions: $a(t_0) = a_k$, $l_\Theta(t_0) = 60°$, $P_1(t_0) = P_2(t_0) = Q_1(t_0) = Q_2(t_0) = 0$ at the initial epoch $t_0 = 0$ corresponding to the date 2010 January 1.0.*

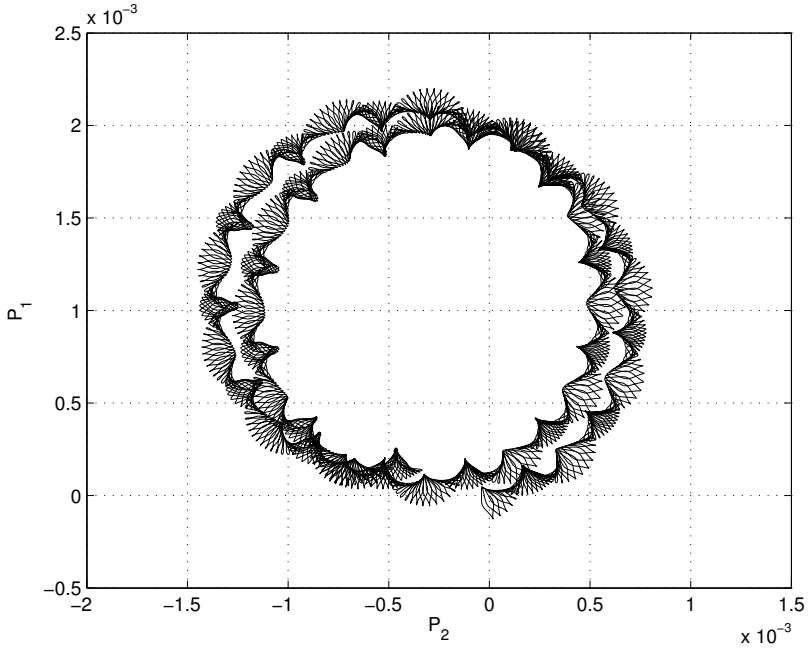

Figure 4.6: *P_1 vs P_2 relevant to the simulation results above.*

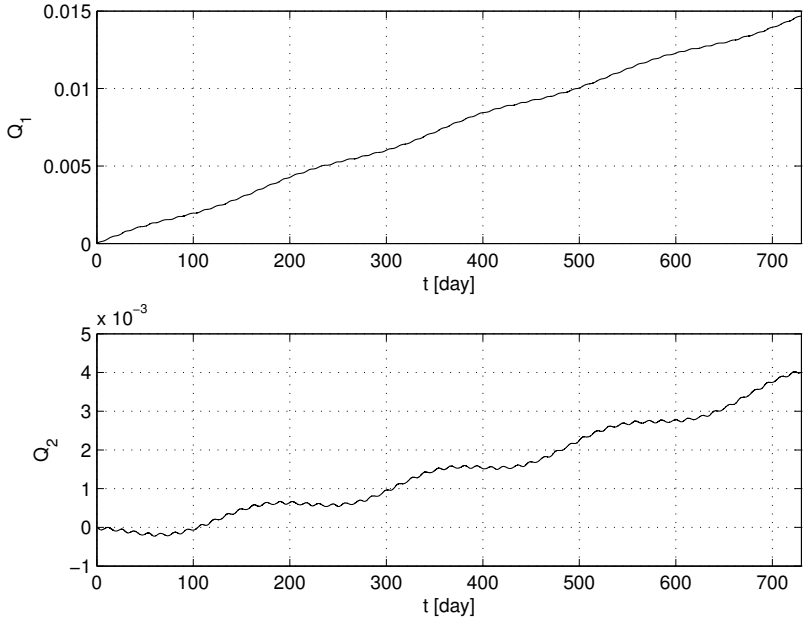

Figure 4.7: *Time histories of the inclination vector components Q_1 and Q_2 as results of the numerical integration of Gauss' VOP equations over 2 years. Initial conditions: $a(t_0) = a_k$, $l_\Theta(t_0) = 60^\circ$, $P_1(t_0) = P_2(t_0) = Q_1(t_0) = Q_2(t_0) = 0$ at the initial epoch $t_0 = 0$ corresponding to the date 2010 January 1.0.*

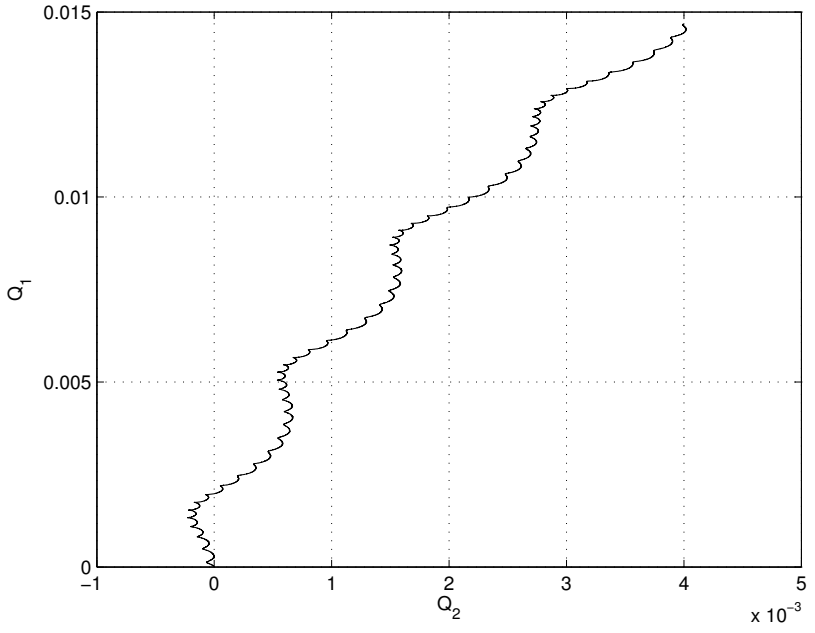

Figure 4.8: *Q_1 vs Q_2 relevant to the simulation results above.*

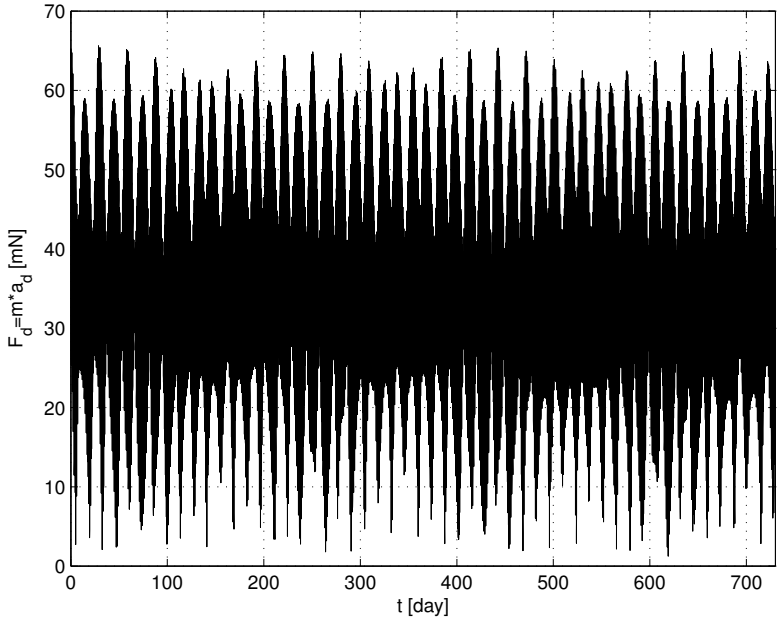

Figure 4.9: *Time history over 2 years of the modulus of the environmental disturbing force vector acting on a spacecraft with mass* $m = 4500$ *kg and modifying its EOEs as depicted in Fig. s 4.3–4.8.*

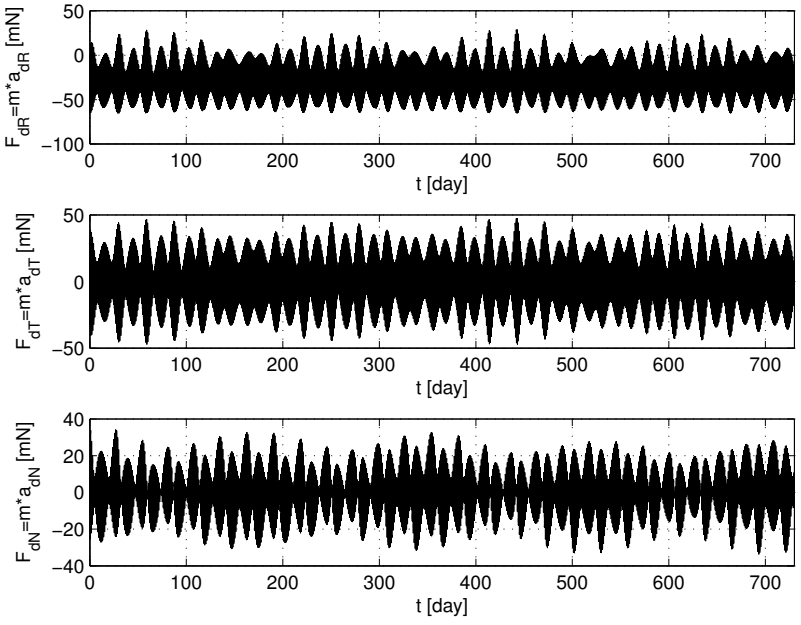

Figure 4.10: *Time history over 2 years of the Gaussian components of the environmental disturbing force vector acting on a spacecraft with mass* $m = 4500$ *kg and modifying its EOEs as depicted in Fig. s 4.3–4.8.*

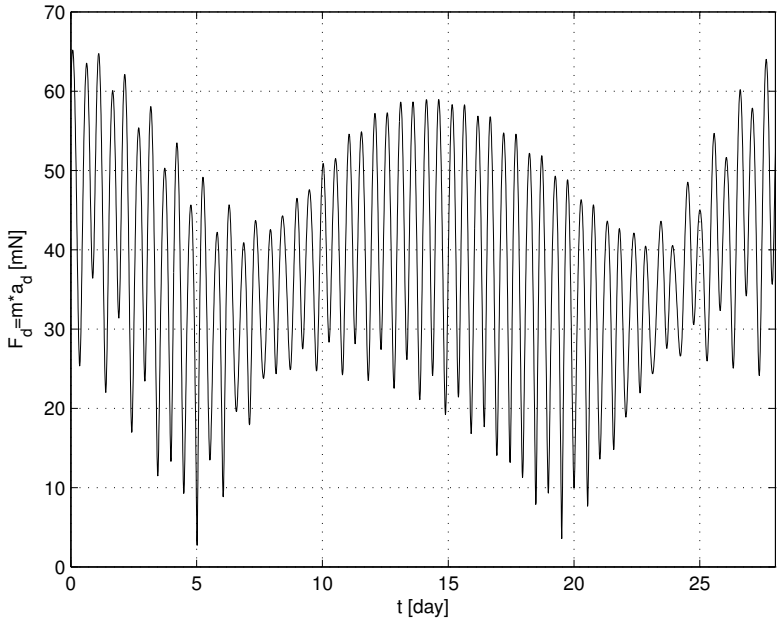

Figure 4.11: *Zoom of Fig. 4.9 over 4 weeks.*

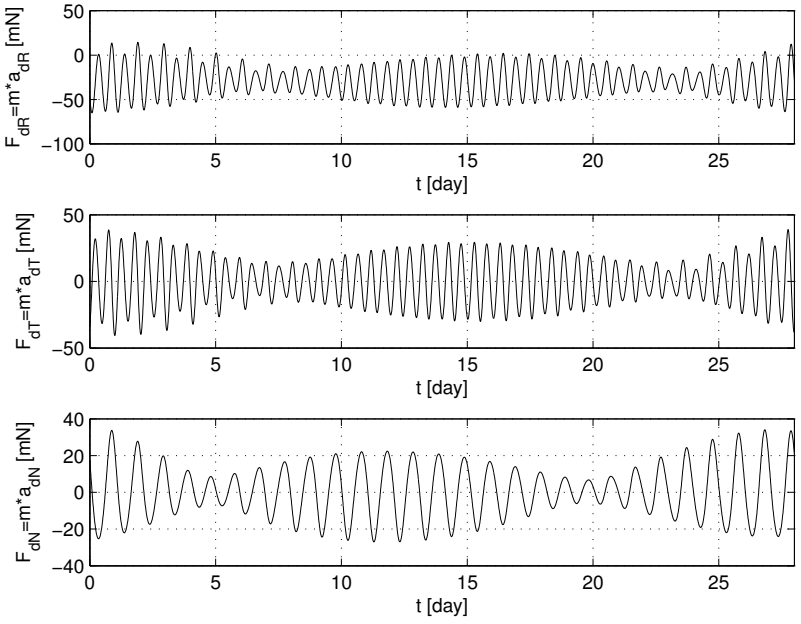

Figure 4.12: *Zoom of Fig. 4.10 over 4 weeks.*

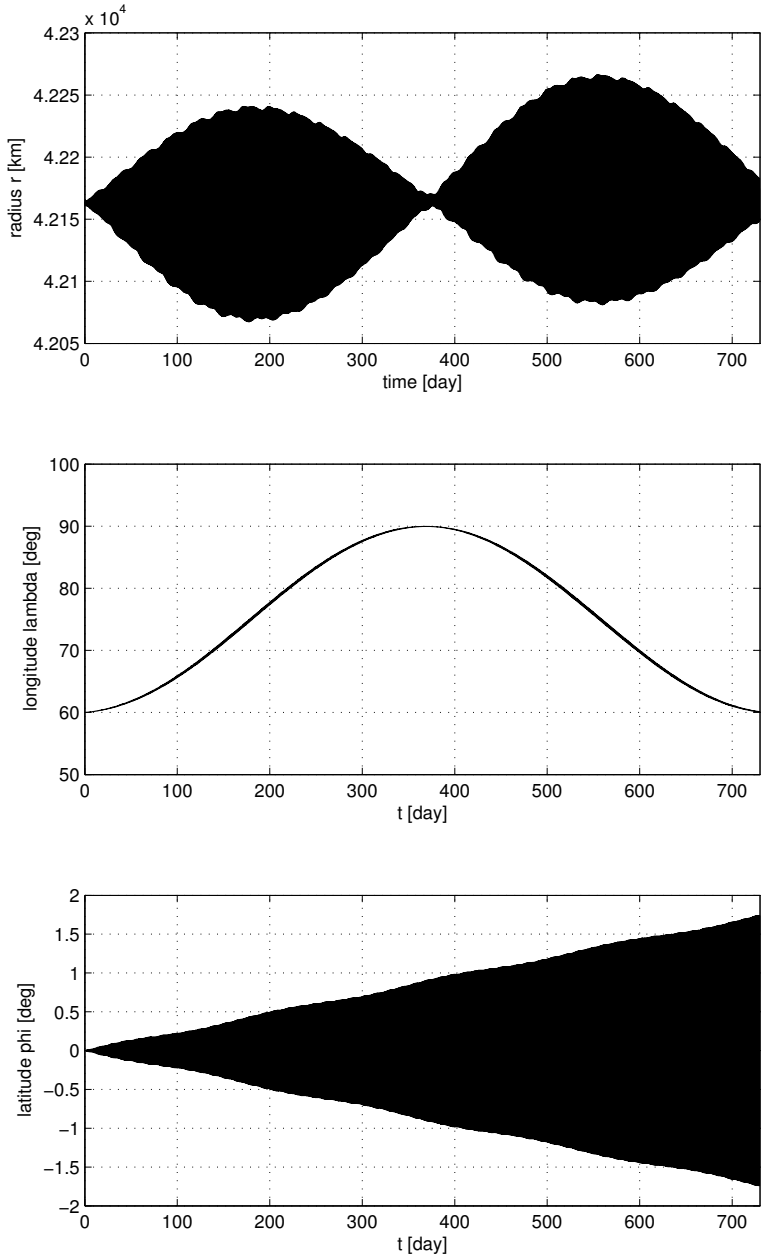

Figure 4.13: *Time histories of the radius r, longitude λ, latitude φ, calculated as nonlinear functions of EOEs obtained by numerical integration of the Gauss' VOP equations over 2 years. Initial conditions:* $a(t_0) = a_k$, $l_\Theta(t_0) = 60^\circ$, $P_1(t_0) = P_2(t_0) = Q_1(t_0) = Q_2(t_0) = 0$ *at the initial epoch* $t_0 = 0$ *corresponding to the date 2010 January 1.0.*

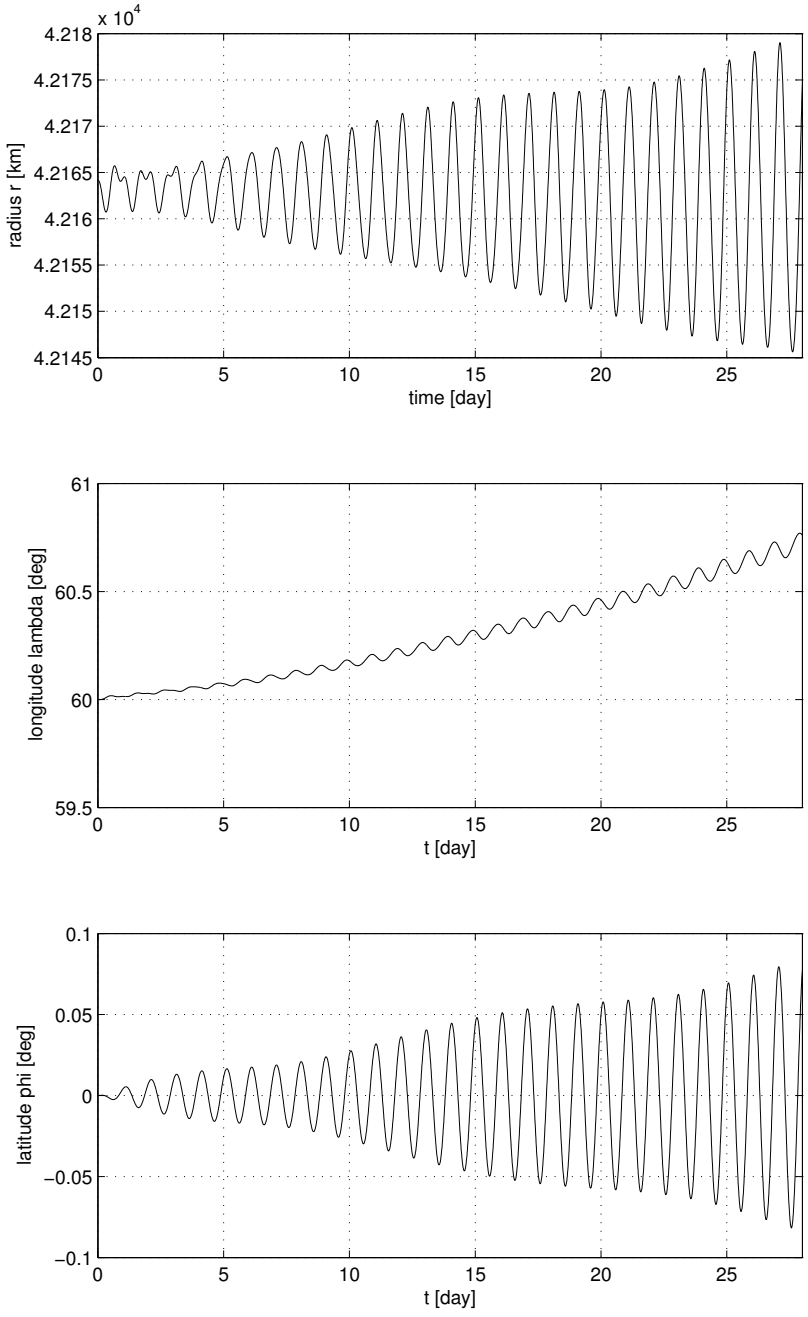

Figure 4.14: *Zoom of Fig. 4.13 over 4 weeks.*

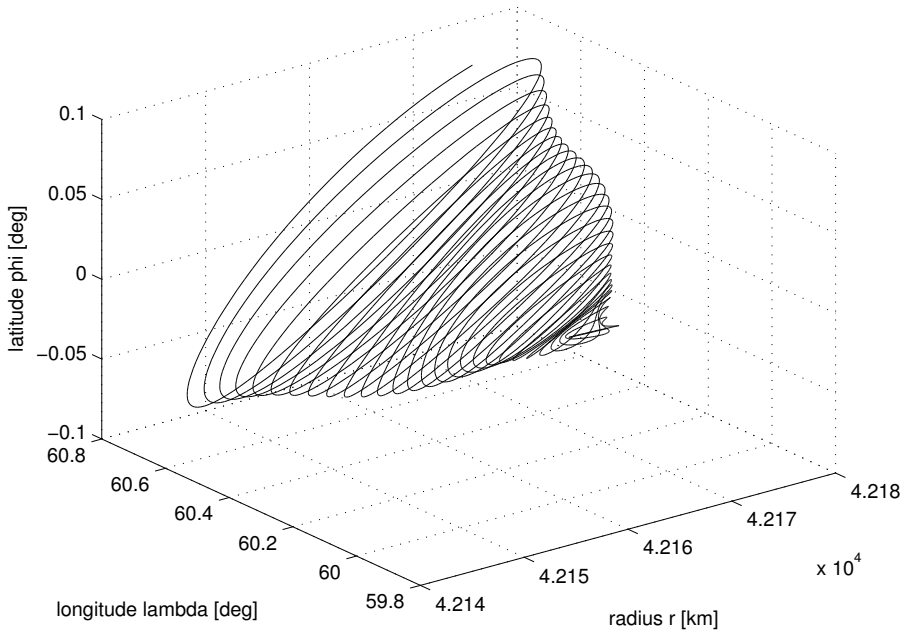

Figure 4.15: *r vs λ vs φ relevant to the simulation results above.*

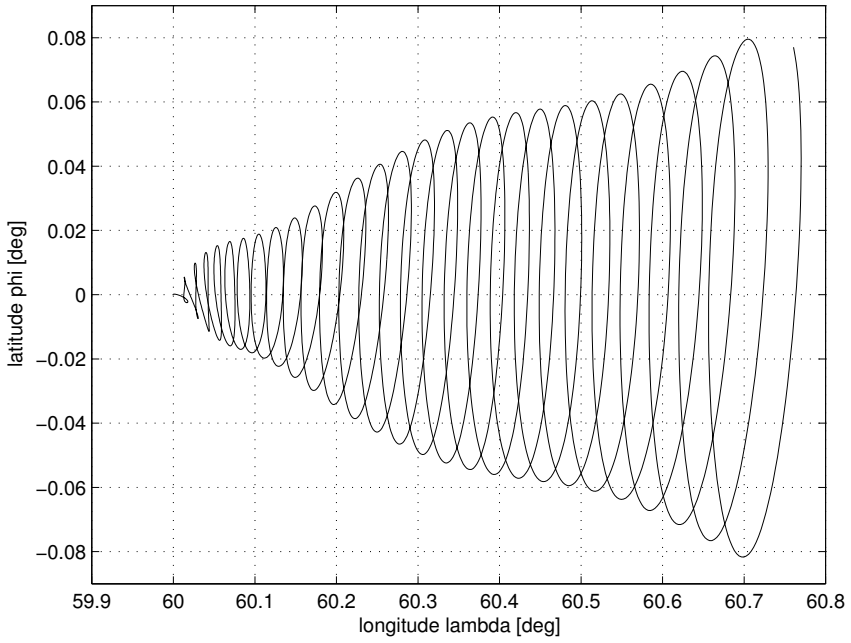

Figure 4.16: *λ vs φ relevant to the simulation results above.*

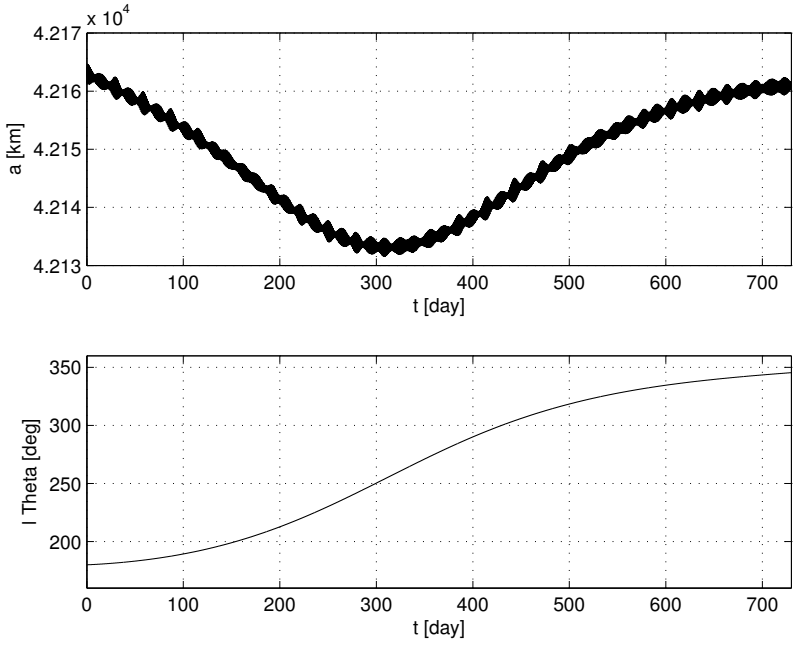

Figure 4.17: *Semi-major axis a and mean latitude l_Θ time histories as results of the numerical integration of Gauss' VOP equations over 2 years. Initial conditions: $a(t_0) = a_k$, $P_1(t_0) = P_2(t_0) = Q_1(t_0) = Q_2(t_0) = 0$, $l_\Theta(t_0) = 180°$, at the initial epoch $t_0 = 0$ corresponding to the date 2010 January 1.0.*

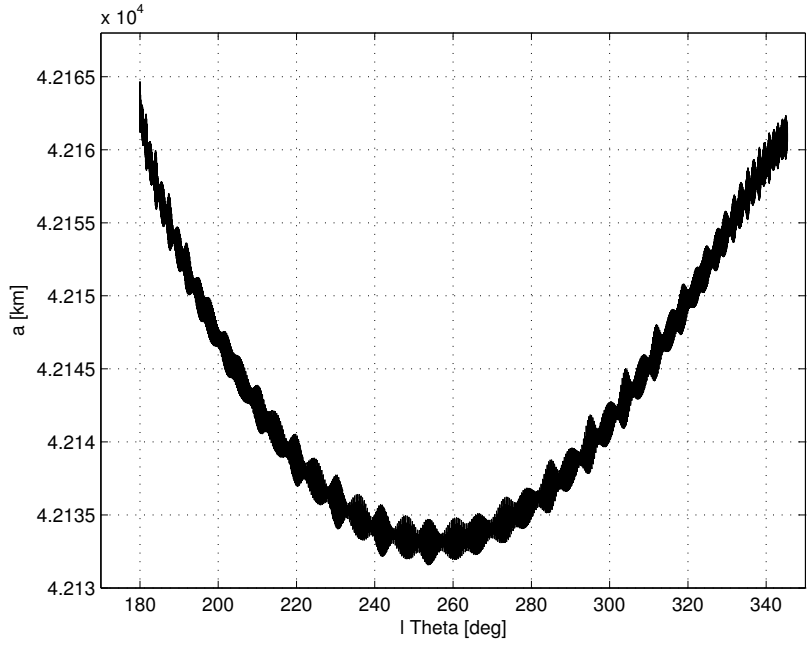

Figure 4.18: *Semi-major axis a vs mean latitude l_Θ relevant to the simulation results above.*

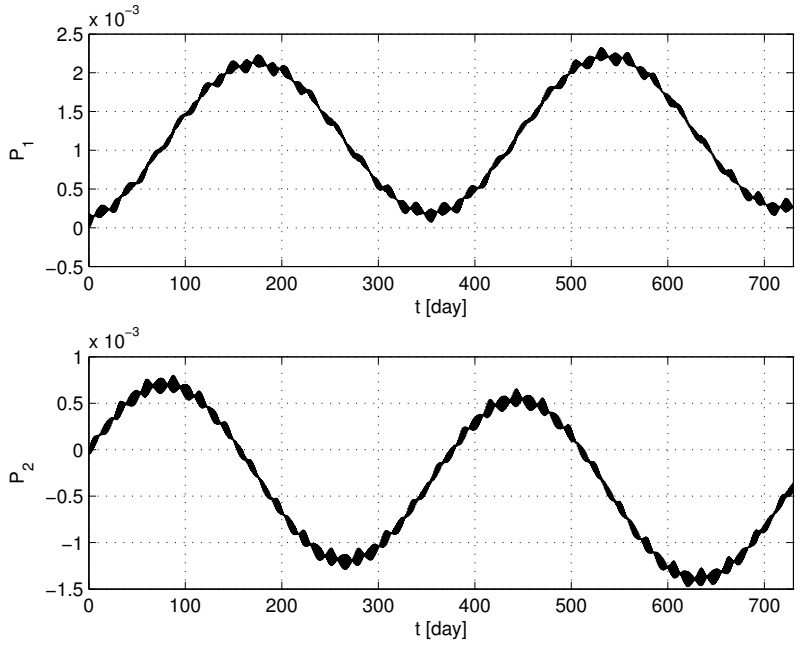

Figure 4.19: *Time histories of the eccentricity vector components P_1 and P_2 as results of the numerical integration of Gauss' VOP equations over 2 years. Initial conditions: $a(t_0) = a_k$, $l_\Theta(t_0) = 180°$, $P_1(t_0) = P_2(t_0) = Q_1(t_0) = Q_2(t_0) = 0$ at the initial epoch $t_0 = 0$ corresponding to the date 2010 January 1.0.*

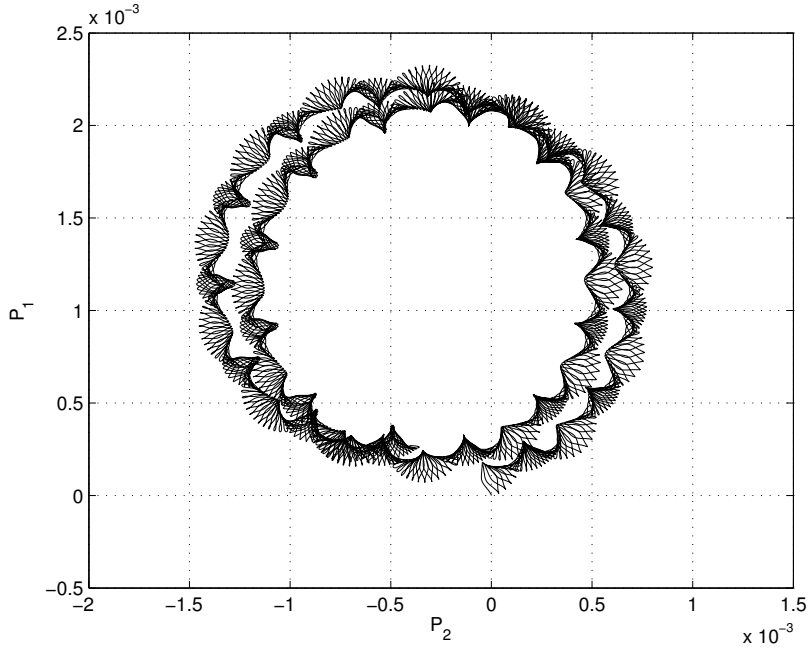

Figure 4.20: *P_1 vs P_2 relevant to the simulation results above.*

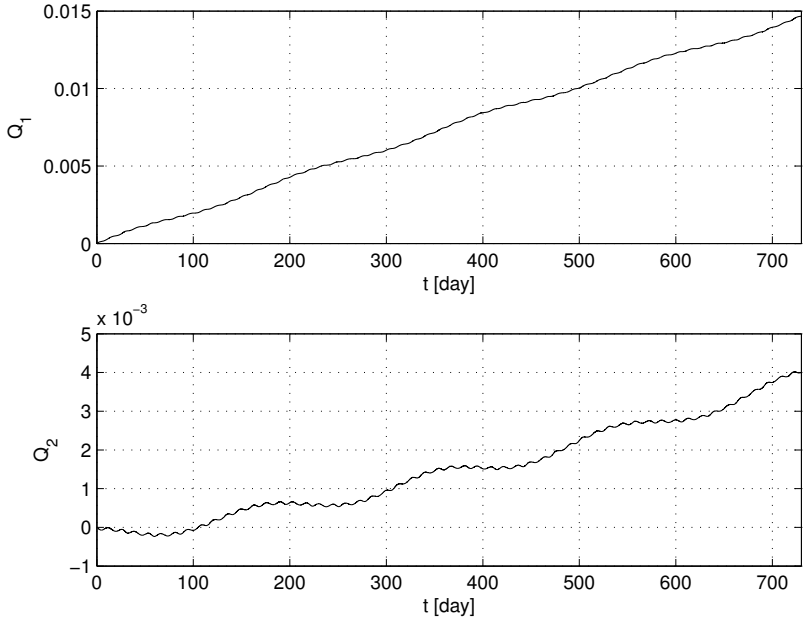

Figure 4.21: *Time histories of the inclination vector components Q_1 and Q_2 as results of the numerical integration of Gauss' VOP equations over 2 years. Initial conditions: $a(t_0) = a_k$, $l_\Theta(t_0) = 180^\circ$, $P_1(t_0) = P_2(t_0) = Q_1(t_0) = Q_2(t_0) = 0$ at the initial epoch $t_0 = 0$ corresponding to the date 2010 January 1.0.*

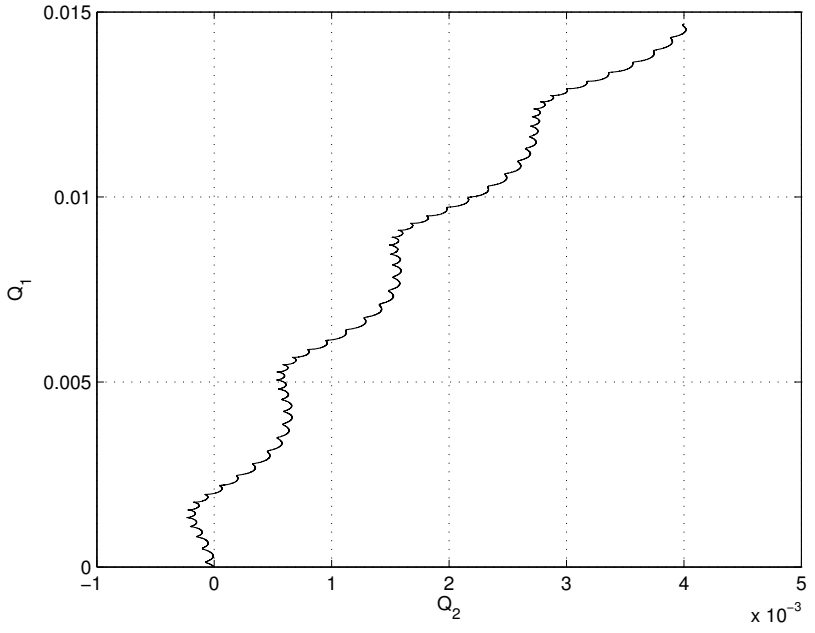

Figure 4.22: *Q_1 vs Q_2 relevant to the simulation results above.*

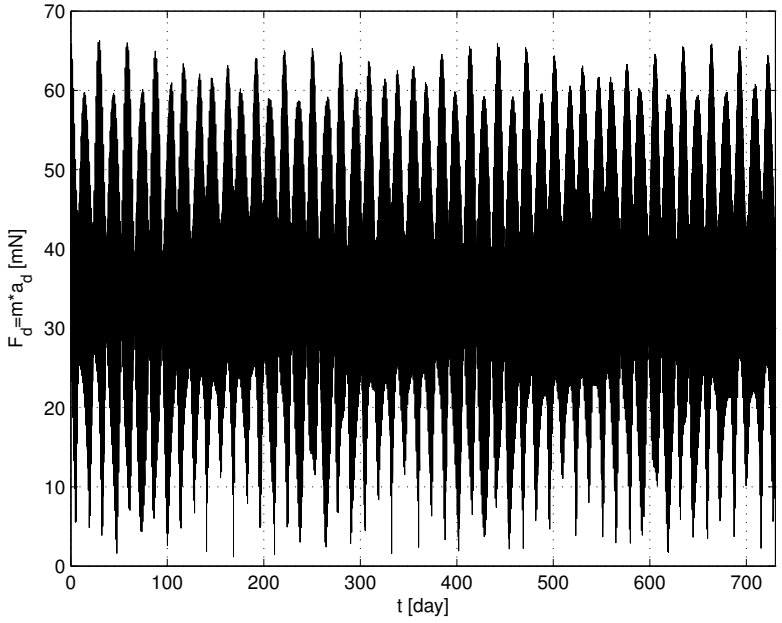

Figure 4.23: *Time history over 2 years of the modulus of the environmental disturbing force vector acting on a spacecraft with mass* $m = 4500$ *kg and modifying its EOEs as depicted in Fig. s 4.17–4.22.*

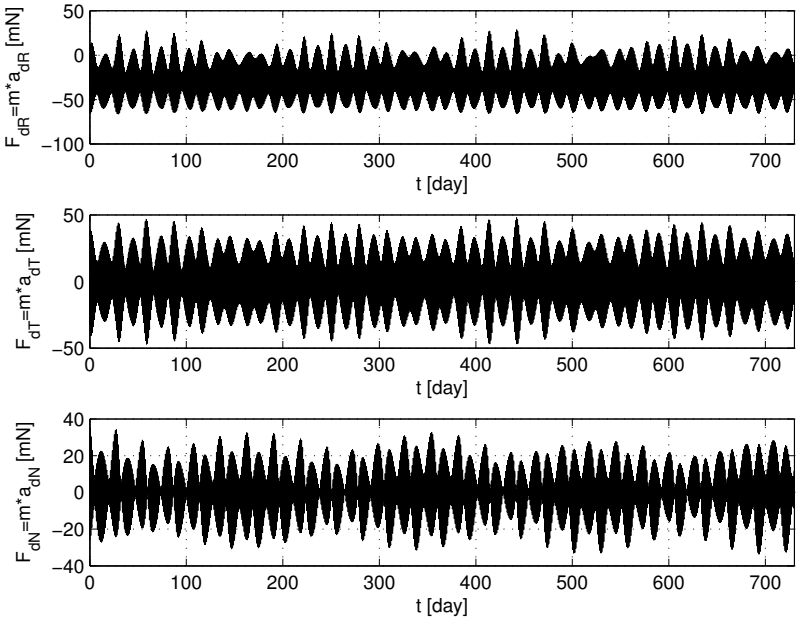

Figure 4.24: *Time history over 2 years of the Gaussian components of the environmental disturbing force vector acting on a spacecraft with mass* $m = 4500$ *kg and modifying its EOEs as depicted in Fig. s 4.17–4.22.*

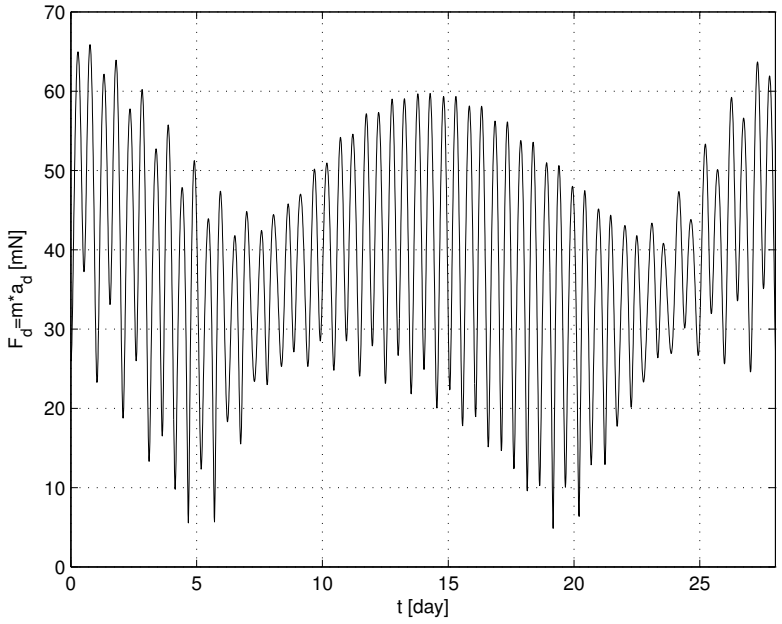

Figure 4.25: *Zoom of Fig. 4.23 over 4 weeks.*

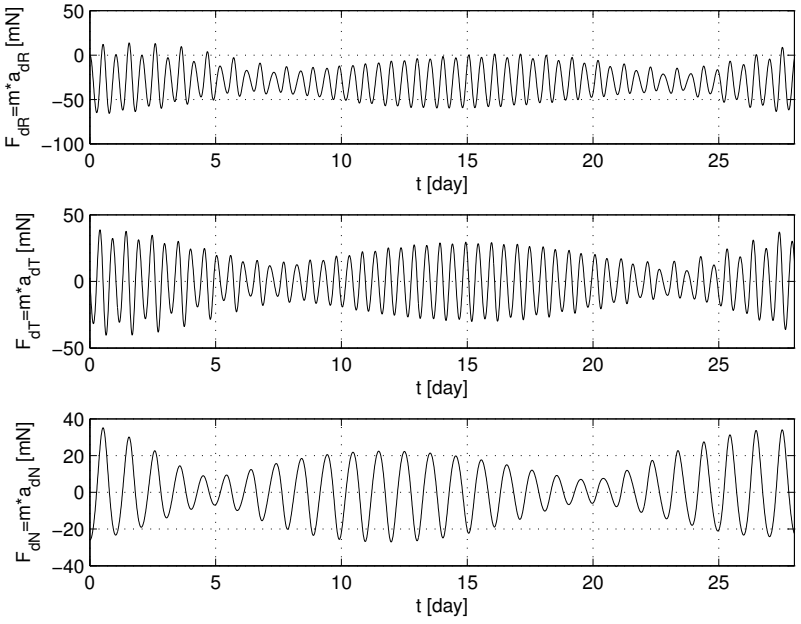

Figure 4.26: *Zoom of Fig. 4.24 over 4 weeks.*

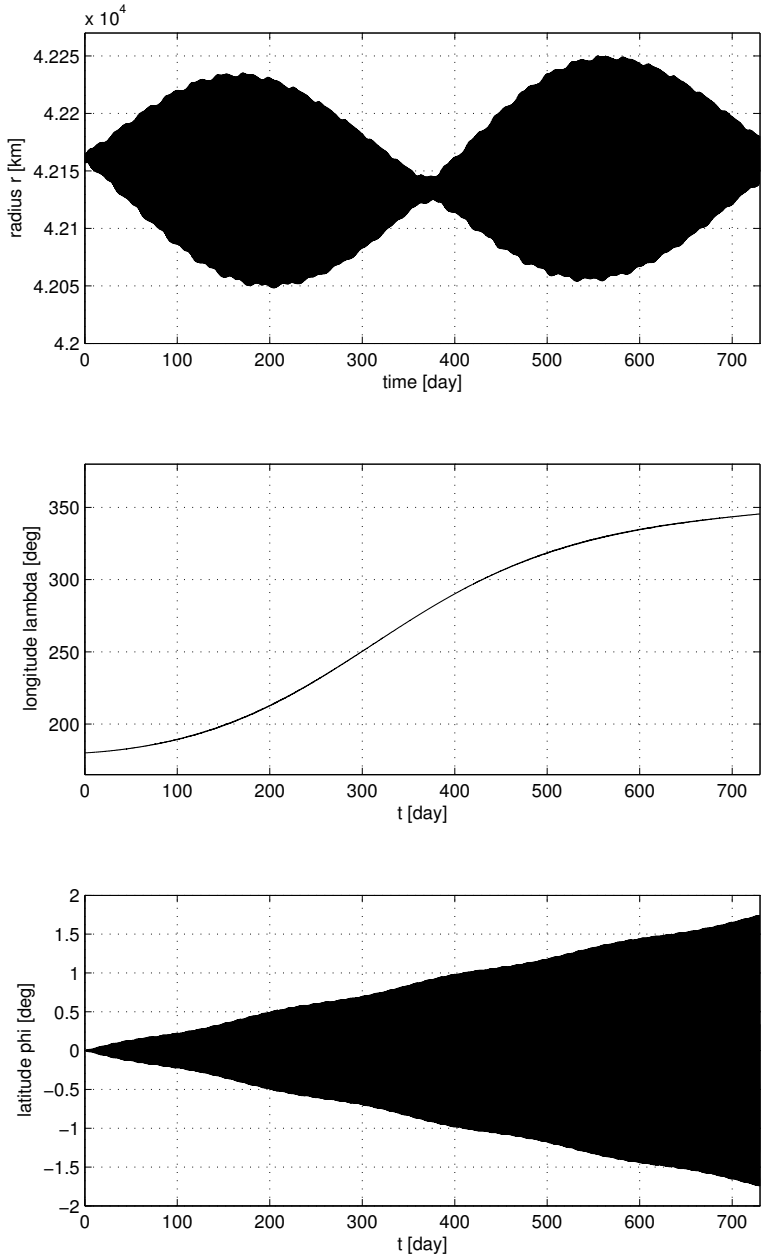

Figure 4.27: *Time histories of the radius r, longitude λ, latitude φ, calculated as nonlinear functions of the EOEs obtained by numerical integration of Gauss' VOP equations over 2 years. Initial conditions: $a(t_0) = a_k$, $l_\Theta(t_0) = 180°$, $P_1(t_0) = P_2(t_0) = Q_1(t_0) = Q_2(t_0) = 0$ at the initial epoch $t_0 = 0$ corresponding to the date 2010 January 1.0.*

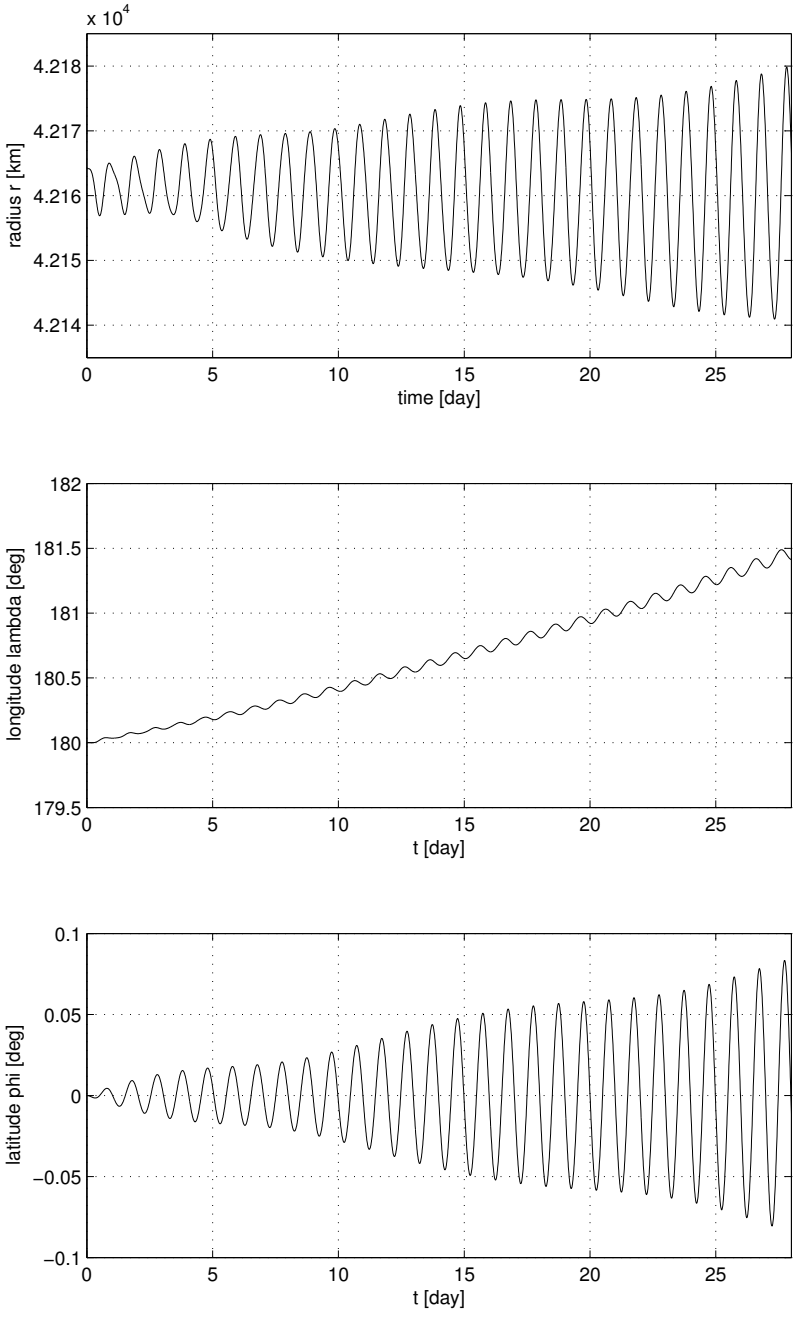

Figure 4.28: *Zoom of Fig. 4.27 over 4 weeks.*

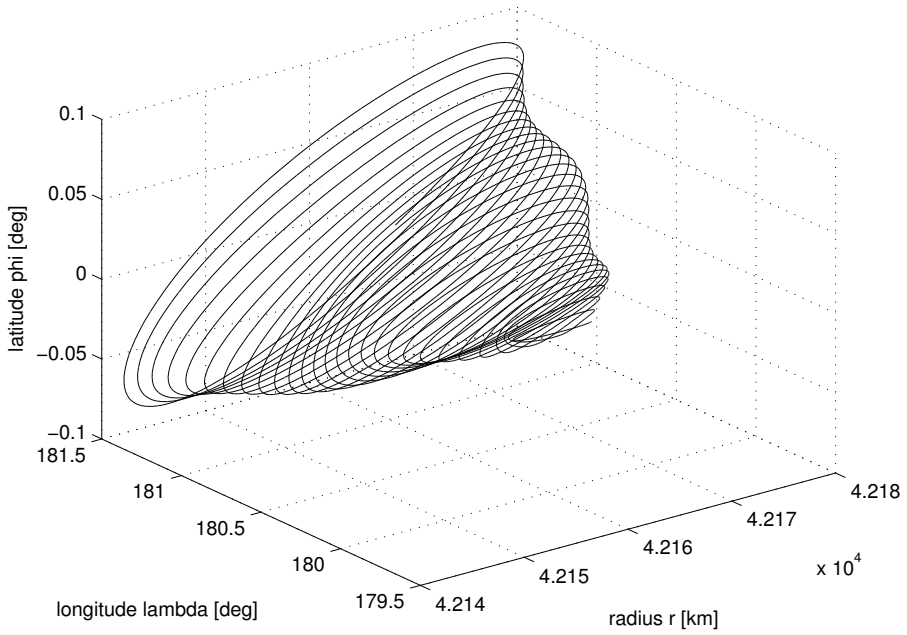

Figure 4.29: *r vs λ vs φ relevant to the simulation results above.*

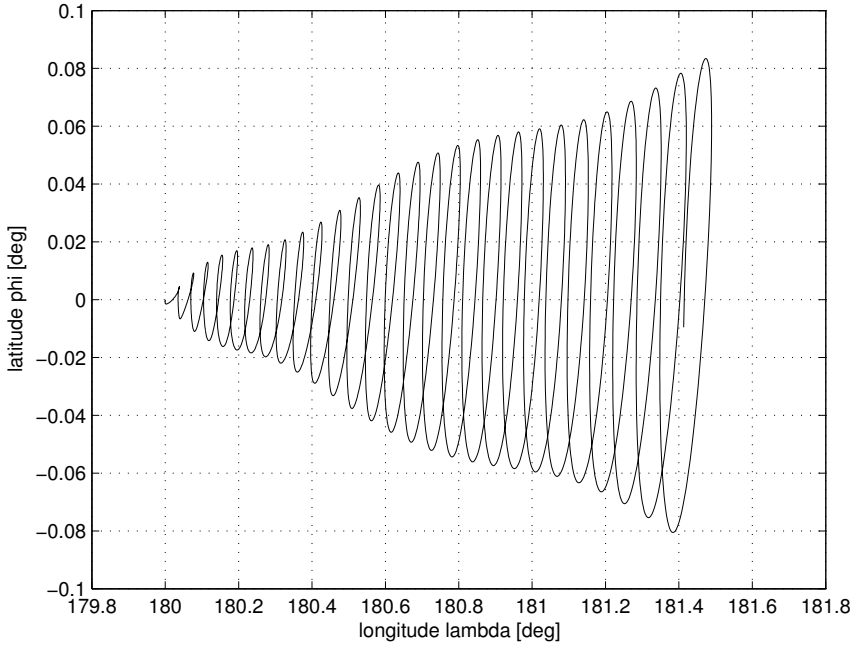

Figure 4.30: *λ vs φ relevant to the simulation results above.*

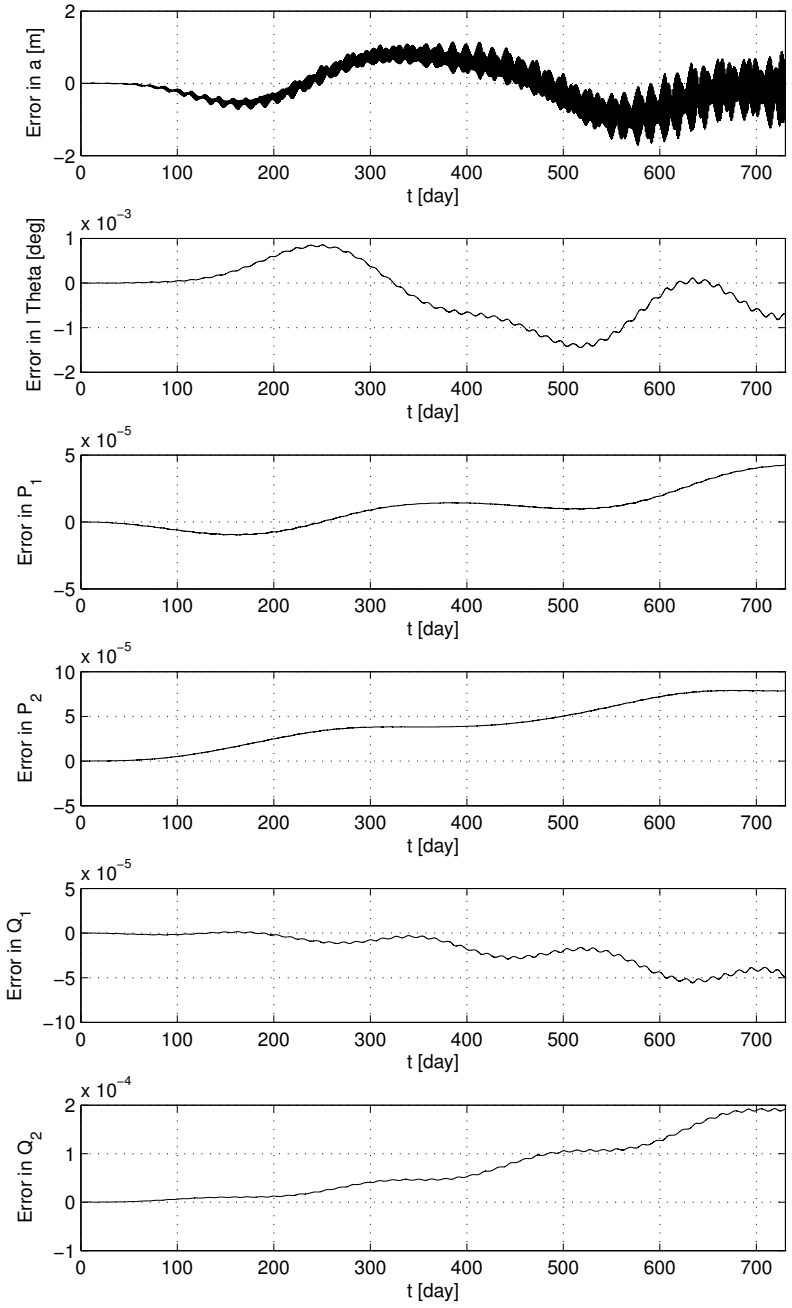

Figure 4.31: *Differences between the EOE time histories obtained numerically integrating the nonlinear Gauss' VOP equations and those obtained numerically integrating the nonlinear Lagrange's VOP equations over $T = 2$ years. Initial conditions: $a(t_0) = a_k$, $l_\Theta(t_0) = 60°$, $P_1(t_0) = P_2(t_0) = Q_1(t_0) = Q_2(t_0) = 0$ at the initial epoch $t_0 = 0$ corresponding to the date 2010 January 1.0.*

4.4 A Linearized Geostationary Orbit Model

In this section, we give the well known Clohessy-Wiltshire (or Hill's) equations of motion of a GEO satellite in the geostationary Clohessy-Wiltshire reference frame described in Section 2.2.3 and centered at the ideal geostationary position with station longitude λ_s. These equations are those of the relative motion of a GEO satellite with respect to another which is permanently in nominal geostationary station keeping conditions, i.e., with zero position and velocity components in the GEO CW reference frame (see [Montenbruck and Gill, 2000] at page 294 or [Vallado, 2001] at page 372). Their form includes Coriolis terms and centripetal accelerations. It is as follows

$$\frac{d\boldsymbol{\xi}}{dt} = \boldsymbol{A}_{CW}\boldsymbol{\xi} + \boldsymbol{B}_{CW}\boldsymbol{a_d} \tag{4.137}$$

where

$$\boldsymbol{\xi} = \begin{bmatrix} x_G & y_G & z_G & \dot{x}_G & \dot{y}_G & \dot{z}_G \end{bmatrix}^T, \tag{4.138}$$

$$\boldsymbol{A}_{CW} = \begin{bmatrix} 0 & 0 & 0 & 1 & 0 & 0 \\ 0 & 0 & 0 & 0 & 1 & 0 \\ 0 & 0 & 0 & 0 & 0 & 1 \\ 3\omega_\oplus^2 & 0 & 0 & 0 & 2\omega_\oplus & 0 \\ 0 & 0 & 0 & -2\omega_\oplus & 0 & 0 \\ 0 & 0 & -\omega_\oplus^2 & 0 & 0 & 0 \end{bmatrix}, \tag{4.139}$$

$$\boldsymbol{B}_{CW} = \begin{bmatrix} \boldsymbol{0}_{3\times3} & \boldsymbol{I}_{3\times3} \end{bmatrix}^T, \tag{4.140}$$

$$\boldsymbol{a_d} = \begin{bmatrix} a_{dX_G} & a_{dY_G} & a_{dZ_G} \end{bmatrix}^T. \tag{4.141}$$

The vector $\boldsymbol{a_d}$ is the sum of all the disturbing acceleration vectors acting on the satellite. Its components a_{dX_G}, a_{dY_G}, a_{dZ_G}, along the X_G, Y_G, Z_G axes, have to be expressed in terms of the Cartesian coordinates x_G, y_G and z_G of the GEO CW coordinate system.

In Fig.s 4.32 and 4.33 we have plotted the 3-D trajectory (x_G vs y_G vs z_G) and the velocity vector tip trace ($\dot{x}_G$ vs $\dot{y}_G$ vs $\dot{z}_G$) obtained integrating over one week the Eq. (4.137) for a spacecraft with mass 4500 kg, an initial condition $\boldsymbol{\xi}(t_0) = \boldsymbol{0}_{6\times1}$ at the initial epoch $t_0 = 0$ corresponding to the date 2010 January 1.0 and subject to the environmental perturbing acceleration vector

$$\boldsymbol{a}_d(x_G, y_G, z_G, t) = \boldsymbol{a}_g(x_G, y_G, z_G, t) + \boldsymbol{a}_a(x_G, y_G, z_G, t) + \boldsymbol{a}_p(x_G, y_G, z_G, t). \tag{4.142}$$

The inertial Cartesian components of the Earth's gravity acceleration $\boldsymbol{a}_g$ (see Table 3.2), of the Sun's and Moon's gravity acceleration $\boldsymbol{a}_a$ (see Table 3.3) and of the solar radiation pressure $\boldsymbol{a}_p$ (see Table 3.4) have been transformed in geostationary CW Cartesian components using the conversion formula

$$\begin{bmatrix} x \\ y \\ z \end{bmatrix} = \boldsymbol{\mathcal{R}}_Z^T(\Theta + \lambda_s) \left(\begin{bmatrix} x_G \\ y_G \\ z_G \end{bmatrix} + \begin{bmatrix} a_k \\ 0 \\ 0 \end{bmatrix} \right), \tag{4.143}$$

which is the inverse of Eq. (2.12) at page 60.

In Fig. 4.34 we have drawn the spacecraft state vector components respectively in the phase planes $(x_G, \dot{x}_G)$, $(y_G, \dot{y}_G)$ and $(z_G, \dot{z}_G)$.

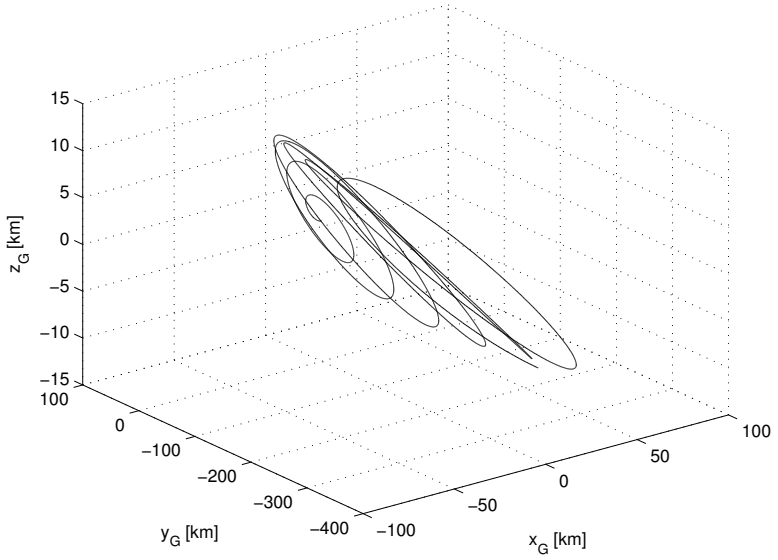

Figure 4.32: *Spacecraft trajectory obtained integrating the CW equations over one week (x_G vs y_G vs z_G).*

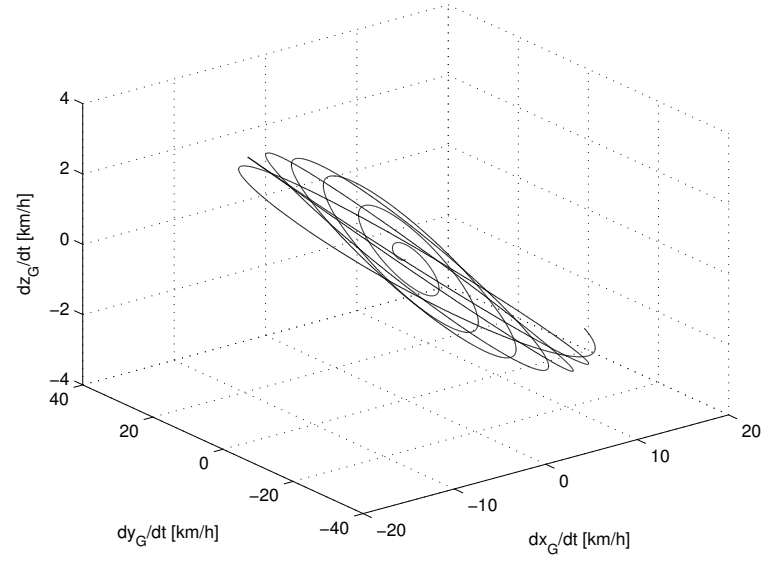

Figure 4.33: *Spacecraft velocity vector tip trace obtained integrating the CW equations over one week ($\dot{x}_G$ vs $\dot{y}_G$ vs $\dot{z}_G$).*

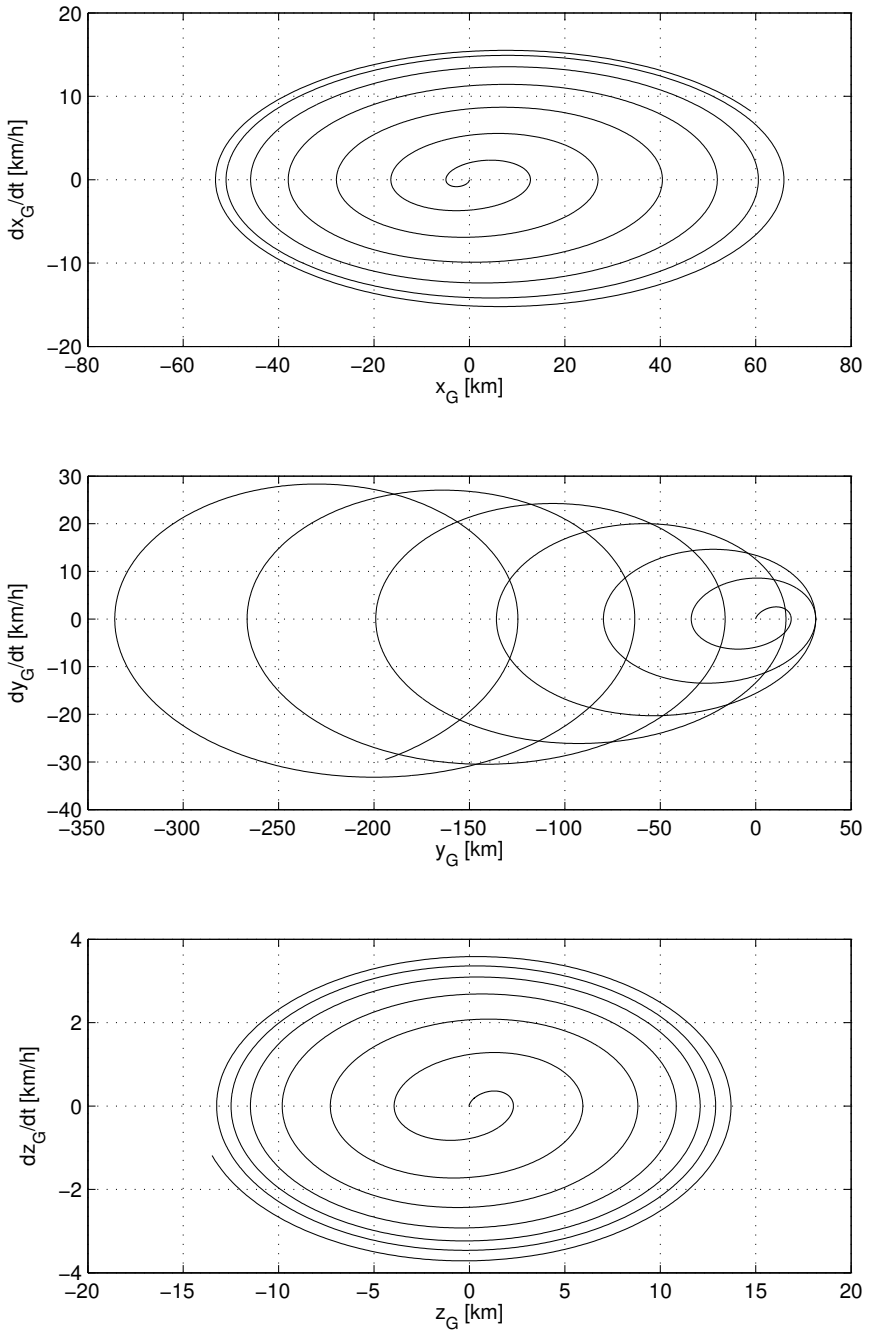

Figure 4.34: *State vector components drawn in the phase planes* $(x_G, \dot{x}_G)$, $(y_G, \dot{y}_G)$ *and* $(z_G, \dot{z}_G)$, *obtained integrating the CW equations over one week.*

Chapter 5

GEO Satellite Station Keeping: Problem Statement and State of the Art

In this chapter we describe the satellite station keeping problem using the orbital mechanics concepts which have been introduced in the previous chapters. Moreover, we present a short survey of the works related to this problem which have been done during the last three decades.

5.1 GEO Satellite Orbital Requirements

The main requirement of a geostationary satellite consists in having, during its whole life, longitudinal and latitudinal position confined in a rectangular box of (λ, φ) plane centered in $(\lambda_s, 0)$ and with dimensions equal to $2\lambda_{max}$ and $2\varphi_{max}$

$$-\lambda_{max} \leq \lambda - \lambda_s \leq +\lambda_{max}, \tag{5.1}$$

$$-\varphi_{max} \leq \varphi \leq +\varphi_{max} \tag{5.2}$$

(see Fig. 5.1). This box is called *deadband box* or *station keeping window* and its sides of magnitude $2\lambda_{max}$ and $2\varphi_{max}$ (usually specified in degrees) are respectively called the *longitude* and *latitude deadbands*. A circular confinement area may also be prescribed for the latitude and longitude, but this is usually handled like the previous case by using the square box inscribed in the circle. The orbital requirement (5.2) on the latitude φ can be replaced with a requirement of spacecraft inclination $0 \leq i \leq i_{max}$. This last requirement is translated in a constraint on the magnitude of the inclination vector which is $\tan(i/2) = \sqrt{Q_1^2 + Q_2^2}$

$$0 \leq \sqrt{Q_1^2 + Q_2^2} \leq \tan(i_{max}/2) \tag{5.3}$$

(see Fig. 5.2).

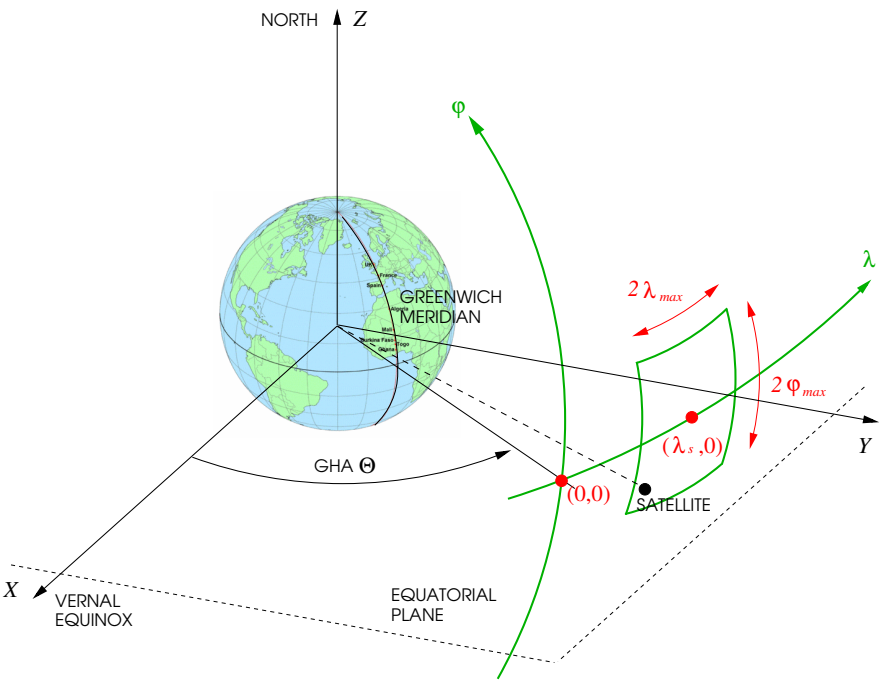

Figure 5.1: *Deadband rectangular box in* (λ, φ) *plane*

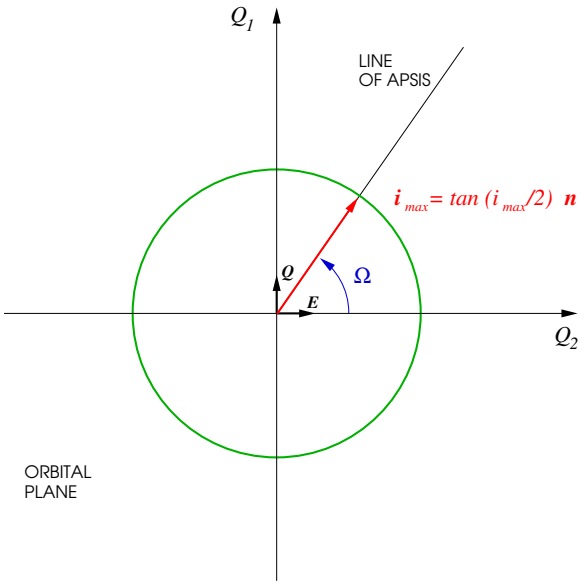

Figure 5.2: *Inclination tolerance circle in* (Q_2, Q_1) *plane*

In order to be able to evaluate in linear terms the angular constraints on geographic longitude and latitude (5.1)–(5.2) we will refer to the Earth fixed equatorial reference frame centered at the ideal geostationary position with axes X_G, Y_G, Z_G (see Fig. 5.3). The Cartesian coordinates x_G, y_G, z_G in this reference frame are related to the geographical spherical coordinates r, λ, φ as follows

$$\begin{bmatrix} x_G \\ y_G \\ z_G \end{bmatrix} = \begin{bmatrix} r\cos\varphi\cos(\lambda-\lambda_s) \\ r\cos\varphi\sin(\lambda-\lambda_s) \\ r\sin\varphi \end{bmatrix} - \begin{bmatrix} a_k \\ 0 \\ 0 \end{bmatrix} \tag{5.4}$$

where a_k is the Keplerian semi-major axis and λ_s the station longitude. Consequently, as depicted in Fig. 5.3, an allowed range in longitude given by (5.1) entails an allowed range along the Y_G axis given by

$$-a_k \tan\lambda_{max} \leq y_G \leq +a_k \tan\lambda_{max}. \tag{5.5}$$

An allowed range in latitude given by (5.2) entails an allowed range along the Z_G axis given by

$$-a_k \tan\varphi_{max} \leq z_G \leq +a_k \tan\varphi_{max}. \tag{5.6}$$

Values of λ_{max} and φ_{max} equal to 0.05° entail a square box in the (Y_G, Z_G) plane with a side nearly 73.6 km long. Values equal to 0.005° entail a square with a side 10 times smaller than the previous one. The ground track[1] of a geostationary satellite is confined in an Earth ellipsoidal spot surface with semi-major axes along Y_G and Z_G given respectively by

$$R_\oplus \sin\varphi_{max} \quad \text{and} \quad R_\oplus \sin\lambda_{max} \tag{5.7}$$

(see Fig. 5.4). For values of λ_{max} and φ_{max} equal to 0.05° this spot is a circle with a radius nearly 5.5 km long. For values equal to 0.005° the circular spot has a diameter of about 1 km.

Besides the longitudinal and latitudinal position keeping requirements, additional constraints may apply to the velocity with which the spacecraft is allowed to move inside the deadband box. These constraints are expressed as upper limits to the orbit eccentricity and to the mean longitude drift rate

$$D = -\frac{3}{2}\frac{a-a_k}{a_k}, \tag{5.8}$$

which is a measure of the deviation between the orbital period and the Earth rotation period. Mean longitude drift rate D comes from the Taylor expansion up to the first order of the mean motion $n = \sqrt{GM_\oplus/a^3}$ around $a = a_k$

$$\frac{n-n_k}{n_k} = -\frac{3}{2}\frac{a-a_k}{a_k}, \tag{5.9}$$

with $n_k = \sqrt{GM_\oplus/a_k^3} = \omega_\oplus$. For this reason in the sequel we prefer to call the quantity D as "mean motion deviation rate" instead of "mean longitude drift rate" as [Soop, 1994] does. We will

[1] Ground track is the locus of points on the Earth surface which are directly below a satellite as it travels through its orbit.

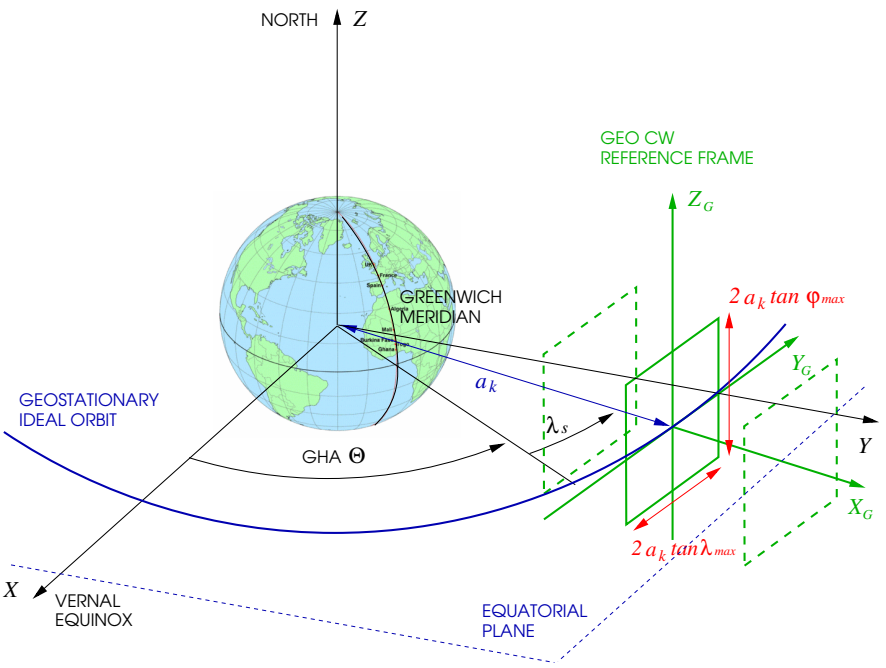

Figure 5.3: *Tolerance ranges along Y_G and Z_G axes of the geostationary CW reference frame*

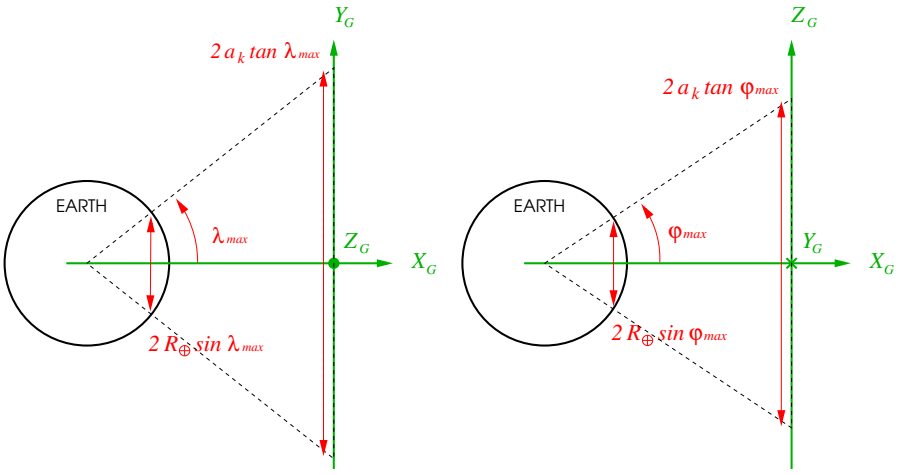

Figure 5.4: *Sizes of the ground track region of a GEO satellite*

use the expression "mean longitude drift" to indicate the time derivative $\dot{l}_\Theta$ of the mean longitude l_Θ.

Moreover, a geostationary satellite may be required to perform a longitude shift maneuver in order, for example, to bring into service a spare spacecraft or because of other changes in the mission. Also a reacquisition of station longitude may be necessary if the spacecraft has drifted outside the longitude deadband. This could follow upon some mistakes in the station keeping performance or as a result of an attitude change.

In this work the attitude control is considered decoupled from the orbit control. However, in some cases, attitude control should be planned with consideration of its influence on the orbit. An example are the spin axis inversions of ESA's GEOS-2 spacecraft, which operated between 1978 and 1984 (see [Soop, 1994]). At each equinox the spin axis was changed from north-pointing in summer to south-pointing in winter, and vice versa. The manoeuvres had to be performed with an unbalanced propulsion system, which perturbed considerably the spacecraft velocity.

5.2 High and Low Thrust Station Keeping Maneuvers

As shown in previous chapters, there are several environmental forces which act to alter over time the orbit of a satellite initially placed in an ideal geostationary orbit. Since the geostationary orbital plane is not coincident with the orbital plane of the Earth around the Sun — the ecliptic — and with the orbital plane of the Moon, the gravitational attraction of the Sun and the Moon act to pull a GEO satellite out of its equatorial orbit, gradually increasing its orbital inclination. In addition, the non circular shape of the Earth's equator, the non-homogeneous Earth's mass distribution and the solar radiation pressure cause a GEO satellite to be slowly drawn to one of two equilibrium points along the equator, resulting in an East-West libration about these points.

To counteract the undesirable effects of the environmental perturbing forces, sufficient fuel is loaded into the geostationary satellites to periodically activate the on board propulsion system and to correct the satellite trajectory over all the planned mission duration. The making of these periodic GEO satellite trajectory corrections are also called station keeping maneuvers. North-South (NS) station keeping (SK) maneuvers counteract the changes of latitude and keep the satellite in the assigned position range around zero latitude value; they consist in thrust accelerations along the N axis of the RTN reference frame. East-West (EW) station keeping maneuvers counteract the variations inlongitude and keep the satellite in the assigned position range around the station longitude on the geostationary belt; they consist in thrust accelerations along the R axis and/or the T axis of the RTN reference frame. Once a GEO satellite has exhausted its fuel, it becomes unusable and it is no more operational, because no control prevents its inclination to grow and the satellite to drift in longitude. A number of guidelines and recommendations for end-of-mission disposal were issued by national and international institutions to protect the geostationary orbit environment. In 1997 an international consensus was found within the Inter-Agency Space Debris Coordination Committee (IADC). The recommended minimum altitude increase (in km) is given

as

$$\Delta H = 235 + 1000 \left(C_R \frac{S}{m} \right) \tag{5.10}$$

where C_R is the solar radiation pressure coefficient, S is the average cross-section area and m is the mass of the satellite. In view of these guidelines and recommendations one would expect that the geostationary ring is a well protected space. However, only about one third of all the satellites follows the internationally agreed recommendations. Two out of three satellites are re-boosted into an orbit so low above the geostationary one that they will sooner or later interfere with GEO satellites (see, e.g., [Jehn et al., 2005]).

Station keeping maneuvers can be performed activating propulsion systems at high thrust level or at low thrust level. The former systems are the chemical ones with typical thrust level of few dozens of Newton. The latter are the electrical ones with typical thrust level of few hundreds of milli-Newton. In both cases a thrust acceleration induces a change of the spacecraft velocity vector and consequently a deflection of the spacecraft trajectory. However, since for the same spacecraft the accelerations induced by chemical thrusters are one hundred times stronger then those induced by electrical ones, a given change in the velocity vector can take place with a single high thrust maneuver in a time interval one hundred times shorter then the time interval which is necessary with a single low thrust maneuver. For example, let suppose to be interested in compensating, over 2 days and with a single maneuver, the effect in terms of velocity modulus change of an environmental perturbing force of constant modulus $F_e = 35$ mN acting on a spacecraft of mass 4500 kg. The value of 35 mN is the average value of the time history plotted in Fig. 4.9 or in Fig. 4.23. Considering the spacecraft mass constant, over two days such an environmental force delivers to the spacecraft a total impulse $I_t \approx 6000$ Ns, corresponding to a spacecraft velocity modulus change $\Delta v_e \approx 1.3$ m/s

$$I_t = \int_{2 \text{ days}} F_e dt = m \int_{2 \text{ days}} \dot{v} dt = m \Delta v_e. \tag{5.11}$$

A velocity modulus change Δv_t equal to 1.3 m/s can be induced by a chemical thruster with constant thrust level $F = 10$ N over a maneuver time interval $T_m \approx 9.75$ minutes or by an electrical thruster with constant thrust level $F = 100$ mN over a maneuver time interval $T_m \approx 16.25$ hours

$$\Delta v_t = \frac{F}{m} T_m. \tag{5.12}$$

In spacecraft maneuvering theory (see, e.g., [Rauschenbakh et al., 2003]) the term of "high thrust maneuver" is used if a change in the spacecraft velocity vector caused by a thruster takes place during a time interval T_m which is short in comparison with the typical time scale of the spacecraft motion (e.g., the period of revolution). High thrust maneuvers can be considered as produced by the application of instantaneous thrust pulses which induce instantaneous acceleration pulses. In the sequel we will refer to one generic acceleration component a_t induced by a thrust F.

In the geostationary station keeping a maneuver performed by an acceleration with time history like that of a pulse centered in t_m and with duration T_m shorter than fifteen minutes can be

considered with good approximation like an impulse applied in t_m with area Δv_t

$$a_t(t) = \Delta v_t \delta(t - t_m) \tag{5.13}$$

i.e.,

$$a_t(t) = \begin{cases} \infty & \text{if} \quad t = t_m \\ 0 & \text{otherwise} \end{cases} \qquad \text{and such that} \qquad \int_{t_m^-}^{t_m^+} a_t(t)dt = \Delta v_t \tag{5.14}$$

(see Fig. 5.5). Such an acceleration produces an impulsive station keeping maneuver. The instantaneous character of the spacecraft velocity change has the consequence that, in the equations of motion, the change of velocity is not related to a change of position. In other words, executing an impulsive maneuver with high thrust we don't have an arc of trajectory where velocity changes induced by thrusts combine with velocity changes induced by perturbing forces. Instead, we simply have a point in which instantaneously velocity changes combine in order to change brusquely the trajectory slope. In that point we can refer to a velocity variation that is a fixed-time velocity differential.

A station keeping maneuver could be non-impulsive and produced by accelerations having time histories that can be approximated as pulses[2] of area Δv_t and duration $T_m = t_m^{off} - t_m^{on}$

$$a_t(t) = \begin{cases} \dfrac{\Delta v_t}{T_m} & \text{if} \quad t_m^{on} \leq t \leq t_m^{off} \\ 0 & \text{otherwise} \end{cases} \tag{5.15}$$

(see Fig. 5.5). In this case for times from t_m^{on} to t_m^{off} the spacecraft trajectory (i.e., the spacecraft coordinates) varies under the effect of both the accelerations induced by thrusts and the ones induced by the environmental forces. Over T_m we have a total velocity change on an arc of trajectory.

Typically impulsive station keeping maneuvers are performed with thrusters at high thrust level (chemical thrusters) and non-impulsive maneuvers are performed with thrusters at low thrust level (electrical thrusters). However, nothing prevents from executing an impulsive maneuver with thrusters at low thrust switching them on for less than fifteen minutes.

5.3 GEO Satellite Station Keeping (SK) Problem Statement

The GEO satellite station keeping problem is a maneuver planning problem. The goal is to find the thrust time histories of each thruster of the propulsion system over all the spacecraft life time. Such thrust time histories must generate thrust acceleration components such that the GEO satellite orbital requirements are met minimizing the propellant mass consumption. The advantage of this minimization is twofold: one can choose to increase the spacecraft life time for the same propellant mass or to reduce the necessary amount of propellant mass allowing the spacecraft to take extra payload mass on board[3].

[2] Pulse wave shape is only an approximation because spacecraft mass has been considered constant over T_m.

[3] Payload mass is the mass of load useful for the GEO spacecraft mission, e.g., mass of communication equipment.

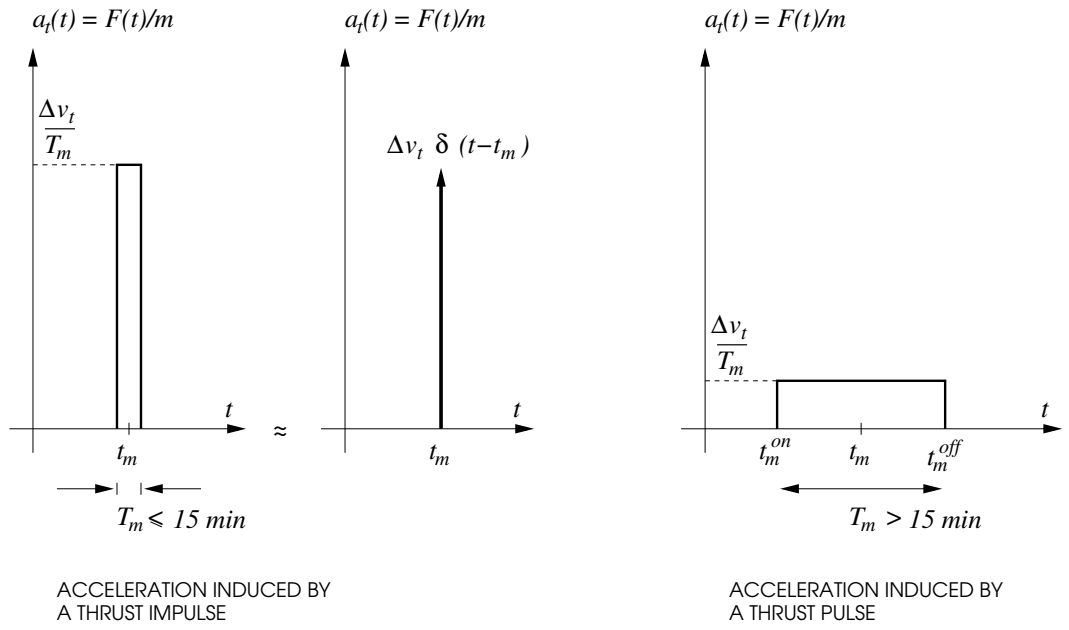

Figure 5.5: *Accelerations induced by a thrust impulse and by a thrust pulse*

During the whole mission life time T_M, spacecraft drift intervals without maneuvers alternate with spacecraft drift intervals with maneuvers. The first ones are under the effect of the environmental perturbing accelerations only. The second ones are under the effect of the environmental perturbing accelerations and the thrust accelerations. This is true for both maneuvers performed by acceleration impulses and maneuvers performed by acceleration pulses. For the first ones the spacecraft drift intervals with maneuvers narrow to points where instantaneous changes of the velocity vector take place.

The station keeping problem can be seen, instead of a problem of maneuver planning, as a problem of trajectory optimization. In this second formulation the problem consists in finding the optimal GEO trajectory meeting the orbital requirements and minimizing the duration and/or the number of the spacecraft drift intervals with maneuvers.

Under the light of what has been inferred about the propulsion system acceleration model (see Section 3.2 at page 99) and about the models of the translational dynamics of a GEO satellite (see Chapter 4 at page 111), we give in the following the expression in mathematical terms of the station keeping maneuver planning problem. The following formulation does not consider some factors belonging to the following two specification types.

1. Operational practice specifications[4].

Factor left out: how the spacecraft state vector is estimated. This estimate is performed by the so called *orbit determination*. Orbit determination can be ground-based or on-board. In the ground-based orbit determination the six orbital elements are deduced from a set of measurements provided by satellite tracking systems. In the on-board orbit determination the position and velocity vectors of the spacecraft are usually deduced in real-time from a set of navigation measurements.

2. Propulsion system technological specifications.

Factors left out: thruster technology type (chemical or electric); on board thruster disposition (that can generate thrust acceleration components along directions coinciding or not with the three main directions of a Cartesian reference frame).

The following formulation of the SK maneuver planning problem is based on an orbit propagation model and does not take into account the measures of the spacecraft state vector which are actually provided by a measured orbit model (also called orbit determination model). In other words, at this time, we make the hypothesis that the orbit found by orbit propagation (which is obtained integrating the equations of motion) coincides during the whole mission life time $T_M = t_{fM} - t_{iM}$ with the orbit found by orbit determination (which provides the best estimate of the spacecraft state vector).

Let be

$$\frac{d\boldsymbol{s}}{dt} = \boldsymbol{f}\left(\boldsymbol{s}, \boldsymbol{a}_t\right), \quad \boldsymbol{s}(t_{iM}) = \boldsymbol{s}_i \tag{5.16}$$

a system of nonlinear differential equations describing the translational dynamics of a GEO satellite subject to the effect of the environmental perturbing accelerations and to the effect of the acceleration vector $\boldsymbol{a}_t$ induced by a propulsion system composed by N_t thrusters.

The vector $\boldsymbol{s}$ of the system (5.16) is

$$\boldsymbol{s} = \begin{bmatrix} \boldsymbol{x} & \Theta & \mathrm{T} & m_{p_1} & \cdots & m_{p_i} & \cdots & m_{p_{N_t}} \end{bmatrix}^T. \tag{5.17}$$

It is made up of the following quantities.

- ➢ The spacecraft state vector $\boldsymbol{x}$, whose components can be given by the three position components plus the three velocity components or by the six equinoctial orbital elements. Its dynamics is described by one of the GEO satellite models in perturbed Keplerian conditions (see Section 4.2 page 115).
- ➢ The Greenwich mean sidereal time Θ, which has a dynamics given by

$$\frac{d\Theta}{dt} = \omega_{\oplus} \tag{5.18}$$

[4]The operational practice is the set of operations which are performed in order to achieve the entire station keeping process.

(see Eq. (2.8) at page 59 and the time dependence of the inertial Cartesian components of the acceleration induced by the Earth's gravity attraction in Table 3.2 at page 86).

➢ The number of Julian centuries T since 1.5 January 2000, which has a dynamics given by

$$\frac{d\mathrm{T}}{dt} = 1 \tag{5.19}$$

(see Eq. (3.62) at page 90 and the time dependence of inertial Cartesian components of the accelerations induced by the Sun's and Moon's gravity attraction and by the solar radiation pressure in Tables 3.3 and 3.4 at pages 93 and 98).

➢ The propellant masses $m_{p_1}, \ldots, m_{p_i}, \ldots, m_{p_{N_t}}$ of the N_t thrusters, which have a dynamics given by

$$\frac{dm_{p_1}}{dt} = -\frac{F_1}{gI_{sp_1}}, \quad \cdots, \quad \frac{dm_{p_i}}{dt} = -\frac{F_i}{gI_{sp_i}}, \quad \cdots, \quad \frac{dm_{p_{N_t}}}{dt} = -\frac{F_{N_t}}{gI_{sp_{N_t}}} \tag{5.20}$$

(see Section 3.2 at page 99).

The vector $\boldsymbol{a}_t$ of the system (5.16) is the acceleration vector induced by the propulsion system.

$$\boldsymbol{a}_t(t) = \boldsymbol{\Gamma}_1(\gamma_1, \sigma_1)\frac{F_1(t)}{m(t)} + \cdots + \boldsymbol{\Gamma}_i(\gamma_i, \sigma_i)\frac{F_i(t)}{m(t)} + \cdots + \boldsymbol{\Gamma}_{N_t}(\gamma_{N_t}, \sigma_{N_t})\frac{F_{N_t}(t)}{m(t)}. \tag{5.21}$$

It depends on the following quantities.

➢ The loaded spacecraft mass m, which is the sum of the constant spacecraft dry mass m_d and of the time varying propellant masses of each thruster m_p

$$m(t) = m_d + \sum_{i=1}^{N_t} m_{p_i}(t). \tag{5.22}$$

The loaded spacecraft mass m is maximum at the beginning of the spacecraft life and equal to the so called Beginning of Life (BOL) mass. The dry mass m_d is constant and composed by the payload mass (i.e., mass of load useful for the mission) and by the spacecraft bus dry mass (e.g., vehicle dry mass, propulsion system mass).

➢ The configuration vector $\boldsymbol{\Gamma}_i$ of the ith thruster, which is function of the cant γ and slew σ angles of the thruster

$$\boldsymbol{\Gamma}_i(\gamma_i, \sigma_i) = \begin{bmatrix} \sin\gamma_i \cos\sigma_i & \sin\gamma_i \sin\sigma_i & \cos\gamma_i \end{bmatrix}^T \quad \text{with} \quad i = 1, \ldots, N_t \tag{5.23}$$

(see Fig. 3.7 of Section 3.2 at page 106).

➢ The scalar quantity $F_i(t)/m(t)$, which is the time history of magnitude a_i of the acceleration vector induced by the ith thrust F_i

$$a_i(t) = \frac{F_i(t)}{m(t)} \quad \text{with} \quad i = 1, \ldots, N_t. \tag{5.24}$$

In the following we will call a_i the thrust acceleration of the ith thruster.

The problem of station keeping maneuver planning consists in determining the N_p time histories of thrusts $F_i(t)$ over a time horizon equal to the mission duration $T_M = t_{fM} - t_{iM}$ such that over T_M the inequality constraints on the state $\boldsymbol{s}$ variables

$$\begin{array}{c} \textit{translation of longitude requirements} \\ -\lambda_{max} \leq \lambda - \lambda_s \quad \textit{and} \quad \lambda - \lambda_s \leq +\lambda_{max} \end{array} \quad \begin{cases} S_{\lambda^+}(\boldsymbol{s}) \leq 0 \\ S_{\lambda^-}(\boldsymbol{s}) \leq 0 \end{cases} \tag{5.25}$$

$$\begin{array}{c} \textit{translation of latitude requirements} \\ -\varphi_{max} \leq \varphi \quad \textit{and} \quad \varphi \leq +\varphi_{max} \end{array} \quad \begin{cases} S_{\varphi^+}(\boldsymbol{s}) \leq 0 \\ S_{\varphi^-}(\boldsymbol{s}) \leq 0 \end{cases} \tag{5.26}$$

$$\textit{translation of further orbital requirements} \quad \begin{cases} S_1(\boldsymbol{s}) \leq 0 \\ \vdots \\ S_n(\boldsymbol{s}) \leq 0 \end{cases} \tag{5.27}$$

are fulfilled, and such that over T_M the total fuel consumption over the mission duration

$$-\sum_{i=1}^{N_t} [m_{p_i}(t_{fM}) - m_{p_i}(t_{iM})] \tag{5.28}$$

is minimum, i.e., the End of Life (EOL) mass $m(t_{fM})$ is maximum.

In the formulation of the SK maneuver planning problem over the total life time T_M (global planning problem), we have left out the factors of specifications **1** and **2** given above. Such factors play a fundamental role in the entire station keeping control loop, which we will depict and explain in the following section. In this section, where the station keeping problem is only stated, we want to present in some general terms the impacts of these factors from the solution viewpoint of the global planning problem.

1. Operational practice specifications.

Impact of the factor left out: the orbit determination plays the role of a controlled variable transducer in the station keeping control system. The timing of the restitution of the spacecraft state vector estimate has an impact on how to partition the global planning problem in partial planning sub-problems of duration T_{SK}. These sub-problems have to be solved in sequence as constrained optimal control problems in a piecewise open loop. The solution of each maneuver planning problem is followed by the execution of the planned maneuvers.

2. Propulsion system technological specifications.

Impact of the factors left out: the technology type and the on board disposition of each thruster have an impact on how to formulate the partial planning sub-problems in terms of optimal control problems over each station keeping cycle T_{SK}. In particular they have an impact on the choice of the control variables and on the definition of constraints related to the control variables.

5.4 GEO Satellite Station Keeping Control Loop

In Fig. 5.6, the three main operations characterizing a GEO satellite station keeping control loop are depicted.

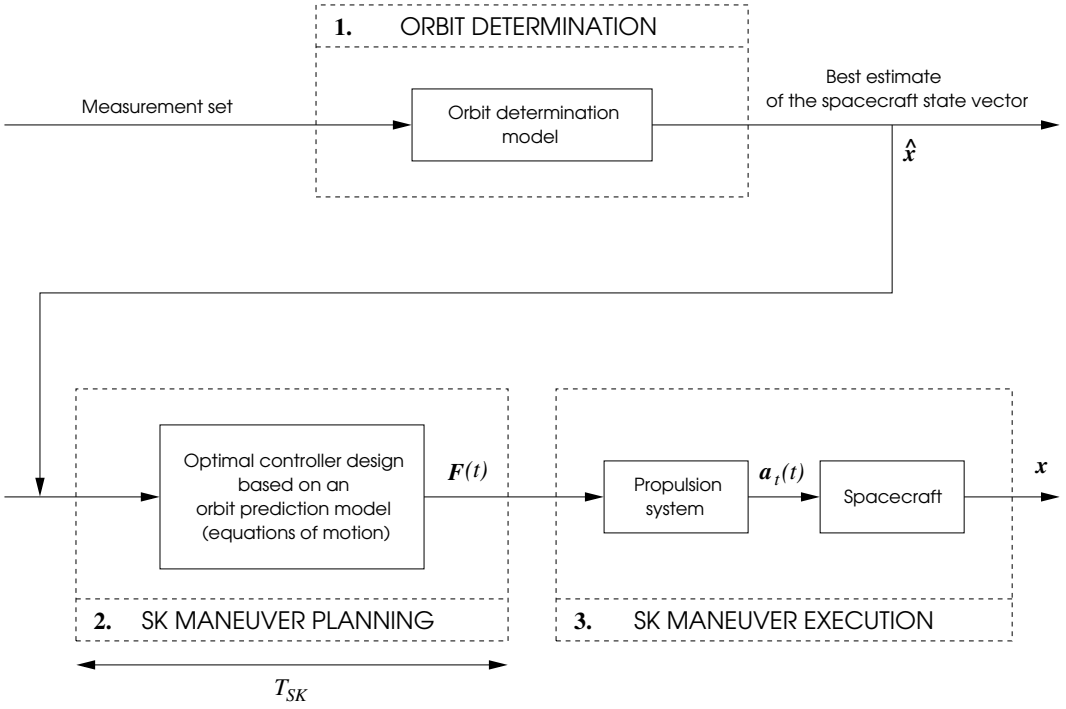

Figure 5.6: *GEO satellite station keeping control loop*

1. The orbit determination. It can be performed from the ground or on board.

In the ground based orbit determination a preliminary orbit determination precedes the definitive orbit estimate which provides the best estimate of the state vector at some earlier time as well as the solar radiation pressure and the velocity increment budgets $\Delta \boldsymbol{v}$ of the high thrust maneuvers. Ground based orbit determination is normally the largest and most complex of the orbit control programs. It applies the idea of least-square estimate to find the trajectory and the parameters of the orbit determination model, i.e., a measurement model function of the time, of a set of parameters and of osculating orbital elements. Trajectory and parameters are deduced from the tracking system data such that the difference between the modeled observations and the actual measurements becomes as small as possible. In other words, the orbit determination finds a trajectory which fits best the spacecraft tracking observations in the sense of the residual least-squares. Actually, since different measurements

have different units and reliability, a weighting factor is applied to each residual and it is the square of the weighted residuals which is minimized. A storage of a large measurement batch is necessary to allow multiple iterations. Typically, an orbit determination program runs regularly, at least every week, using eight days of accumulated tracking data (see [Soop, 1994] and [Campan et al., 1995b]).

The on board orbit determination is usually performed in real-time. It provides the best estimate of where a satellite is at the present time using an extended Kalman filter with an appropriate orbit determination model. Kalman filter processes each measurement exactly once as soon as it is collected by the GPS receiver on board. The inherent measurement noise[5] may be reduced considerably and a much more accurate state vector estimate can be obtained. The concept of on board GEO satellite orbit determination using GPS receivers has been explored for the first time by [Chao and Bernstein, 1994], which propose a GPS receiver as means of on board ephemeris determination due to its portability, accuracy and low cost. In their paper they perform also a covariance analysis of the on board GPS ephemeris determination.

[Eckstein et al., 1981] follows a slightly more sophisticated approach to determine the orbit on board in an autonomous station keeping control loop. They propose to collect navigational data from Sun, Earth and Polaris sensors mounted on the spacecraft body. The data are then evaluated by an epoch mean element filter which combines a batch least square estimator algorithm with the benefits of a sequential estimator algorithm. Such an orbit determination is attitude independent.

2. **The SK maneuver planning.** This is the definition of the station keeping problem which we have given in the previous section. It is performed designing an optimal controller based on an orbit prediction model (see Eq. (5.16)). This orbit prediction model can be more or less sophisticated. It is written in terms of the spacecraft motion equations with the initial spacecraft state vector value equal to its best estimate (the estimate provided by the orbit determination). The programs implementing the designed optimal controller can run on the ground or on board depending on the type of orbit determination. Reasonably, they run on board if the orbit determination is performed on board and on the ground if the the orbit determination is performed from the ground. In the first case the geostationary orbit control loop is defined as *ground based* and in the second case as *autonomous*.

3. **The SK maneuver execution.** It is performed activating the propulsion system.

   In the ground based station keeping, the transmission to the spacecraft of the planned maneuver activation controls is typically performed at the end of each station keeping cycle with duration T_{SK} of one or two weeks (see [Soop, 1994] and [Campan et al., 1995b]). The

[5] In general, position values are provided by the GPS receiver with a spherical 1σ accuracy of about 100 m, whereas velocity is only accurate to 1 m/s in representative spaceborne receivers.

accuracy of the planned maneuver activation depends on the amount of on board clock drift[6]. However, under some particular conditions, the duration cycle T_{SK} can be increased up to several months. In this case the satellite is autonomous during that period. In this situation the geostationary orbit control loop is defined as *semi autonomous*. The feasibility of the concept of semi autonomous station keeping depends primarily on the accuracies of orbit prediction, maneuver execution and the on board clock. [Chao, 1984] performs a feasibility study of a semi autonomous station keeping control loop over six months.

In the autonomous station keeping, the maneuver activation controls can be executed in the same time or just after the end of the maneuver planning without caring about the control transmission phase. Since the SK maneuver planning is performed on board, the on board clock drift is no more an issue from the maneuver execution viewpoint.

5.5 GEO Satellite SK Maneuver Planning: a Survey of Related Work

In this section we will review some works done in the last three decades and relating to the planning of SK maneuvers. We will distinguish the works related to the planning of high thrust maneuvers (typically performed with chemical thrusters) from those related to the planning of low thrust maneuvers (typically performed with electrical thrusters).

Three works do not fit into the the above categorization because they handle the station keeping maneuver planning problem as a formation keeping maneuver planning problem, i.e., as a regulation problem. These last works (written by [Chao and Bernstein, 1994], [Kluever and Tanck, 1997] and [Park et al., 2005]) are relevant to autonomous station keeping control loops. They will be deeply described in Section 5.5.3 and illustrated by some simulation results obtained with our GEO satellite translational dynamics model.

5.5.1 High Thrust SK Manoeuvre Planning

[Soop, 1994], [Campan et al., 1995b] and [Sidi, 1997] explain how the station keeping maneuvers are habitually planned in ground based station keeping control systems for GEO satellites equipped with high thrust propulsion systems consisting of chemical thrusters able to achieve radial, tangent and normal thrust acceleration components in unrelated ways (e.g., a propulsion system with a configuration matrix given by Eq. (3.119)). In the following we will call *ground based SK maneuver planning* the SK maneuver planning of a ground based SK control system.

[6]The spacecraft shall maintain a spacecraft reference time (also called *Spacecraft Elapsed Time*) for the purpose of time tagging several events. The Spacecraft Elapsed Time is maintained by the central spacecraft on board clock, which is a free running counter from an arbitrary starting epoch. The on board clock supplies reference timing to switching and processing units on the spacecraft; Earth stations must in turn synchronize their burst transmissions to the on board timing so that all bursts arrive at the satellite at the proper instant.

The ground based SK maneuver planning is executed to reach the two main ground based SK control system goals: to minimize the overall fuel consumption and to minimize the operational effort at the control center in order to achieve the GEO satellite orbital requirements. The way to execute the ground based SK maneuver planning consists in solving a series of parameter optimization problems in different phases of the planning: strategic (**A**) and tactical (**B**) phases.

A. During the strategic phases the planning is independently performed for the East-West SK maneuvers and for the North-South SK maneuvers. In both cases, the strategic planning (**A1**) defines the objectives for reaching the main ground based SK goals and (**A2**) develops action plans for reaching those objectives over SK correction cycles with duration T_C. We will denote T_{Ck} the duration of the kth correction cycle.

A1. The objectives are expressed in terms of start and end epochs t_{iCk} and t_{fCk} of the station keeping correction intervals and in terms of spacecraft state vector target values $\boldsymbol{x}(t_{fCk})$ at the end of each station keeping correction interval of duration $T_{Ck} = t_{fCk} - t_{iCk}$. The definition of the objectives for minimizing the operational effort at the control center depends clearly on the particular requirements of the control center. For example, if the requirement is to minimize the number of correction executions, the objectives are defined maximizing the SK correction cycle durations T_{Ck}. On the other hand, if the requirement is to regularize the number of correction executions, the objectives are defined imposing constant duration of the station keeping correction cycles: $T_{Ck} = T_C$ for every cycle. In all cases the definition of the target values $\boldsymbol{x}(t_{fCk})$ is performed using simplified models of the evolution of the orbital parameters under the effect of the only environmental perturbing accelerations. These models do not provide the evolution of the osculating orbital parameters but the evolution of the averaged orbital parameters. They are a heavily simplified version of the VOP equations described in the previous chapter. In these models the environmental perturbing forces do not indiscriminately affect all the orbital elements but each equinoctial element is affected only by the predominant perturbation acting on it. Typically, the inclination orbital elements are affected by the Sun's and Moon's gravity attraction only; the eccentricity orbital elements by the solar radiation pressure only; the semi-major axis and mean longitude by the Earth's gravity attraction only.

A2. The action plans for reaching the above objectives are expressed in terms of maneuver execution dates (days d and times of the days t_m) and in terms of sizes of the maneuver executed with high thrust accelerations. The hypothesis of high thrust is translated to the hypothesis of impulsiveness of thrust acceleration components which consequently are assumed to have the following time histories

$$a_{tR}(t) = \Delta v_{tR}\delta(t - t_{mR}), \tag{5.29}$$

$$a_{tT}(t) = \Delta v_{tT}\delta(t - t_{mT}), \tag{5.30}$$

$$a_{tN}(t) = \Delta v_{tN}\delta(t - t_{mN}) \tag{5.31}$$

when radial, tangent and normal maneuvers are respectively executed at the instant of the day t_{mR}, t_{mT} and t_{mN}. Therefore the sizes of the maneuvers are nothing else than the amount of thrust velocity increments Δv_{tR}, Δv_{tT}, Δv_{tN} along the main directions of the RTN reference frame at each times t_{mR}, t_{mT}, t_{mN} of the prefixed correction days d_R, d_T, d_N. In case of high thrust corrections, such days are those corresponding to the time t_{iCk} of the beginning of the SK correction interval T_{Ck}. The determination of all the other quantities is done basing on a simplified model of thrust acceleration effect on orbital parameters. The equations of such a model comes from the linearization of Gauss' VOP equations

$$\frac{d\boldsymbol{x}_t}{dt} = \boldsymbol{K}(\boldsymbol{x}_t) - \boldsymbol{\omega}_\oplus + \boldsymbol{G}(\boldsymbol{x}_t, t)\boldsymbol{a}_t(t) \tag{5.32}$$

(see Section 4.2.1 at page 117) around the Keplerian nominal station keeping state vector

$$\boldsymbol{x}_{Ksk} = \begin{bmatrix} a_k & 0 & 0 & 0 & 0 & \lambda_s \end{bmatrix}^T \tag{5.33}$$

and the zero thrust acceleration vector $\boldsymbol{a}_t = \boldsymbol{0}_{3\times 1}$:

$$\frac{da_t}{dt} = 2a_k\frac{a_{tT}(t)}{v_{sk}}, \tag{5.34}$$

$$\frac{dP_{1t}}{dt} = -\cos K_{sk}(t)\frac{a_{tR}(t)}{v_{sk}} + 2\sin K_{sk}(t)\frac{a_{tT}(t)}{v_{sk}}, \tag{5.35}$$

$$\frac{dP_{2t}}{dt} = +\sin K_{sk}(t)\frac{a_{tR}(t)}{v_{sk}} + 2\cos K_{sk}(t)\frac{a_{tT}(t)}{v_{sk}}, \tag{5.36}$$

$$\frac{dQ_{1t}}{dt} = \frac{1}{2}\sin K_{sk}(t)\frac{a_{tN}(t)}{v_{sk}}, \tag{5.37}$$

$$\frac{dQ_{2t}}{dt} = \frac{1}{2}\cos K_{sk}(t)\frac{a_{tN}(t)}{v_{sk}}, \tag{5.38}$$

$$\frac{dl_{\Theta t}}{dt} = -\frac{3}{2}\frac{n_k}{a_k}(a_t - a_k) - 2\frac{a_{tR}(t)}{v_{sk}}, \tag{5.39}$$

with $K_{sk}(t) = \lambda_s + \Theta(t)$ (Θ here is the right ascension of the Greenwich meridian), $v_{sk} = \omega_\oplus a_k$ and $n_k = \sqrt{GM_\oplus/a_k^3} = \omega_\oplus$. [Kamel et al., 1973], [Legendre, 1980a], [Legendre, 1983], [Campan et al., 1995b], linearize the equation (5.32) around the synchronous Keplerian nominal station keeping state

$$\boldsymbol{x}_{Ssk} = \begin{bmatrix} a_s & 0 & 0 & 0 & 0 & \lambda_s \end{bmatrix}^T \tag{5.40}$$

where a_s is the semi-major axis which does not null the zeroth order term of the sixth equation in unperturbed Keplerian conditions

$$\sqrt{\frac{GM_\oplus}{a^3}} - \omega_\oplus \tag{5.41}$$

but the zeroth order term of the sixth Lagrange's VOP equation with $\mathcal{E}_d = \mathcal{E}_g$

$$\sqrt{\frac{GM_\oplus}{a^3}} - \omega_\oplus - \frac{2}{na}\left[\frac{\partial \mathcal{E}_g}{\partial a}\right]_{l_\Theta = \lambda_s}. \tag{5.42}$$

The integration of equations (5.34)–(5.39) with impulsive accelerations (5.29)–(5.31), leads to express the equinoctial parameter variation induced by thrust accelerations (orbital element impulsive corrections) in function of the velocity change budgets Δv_t and of the maneuver instants t_m

$$\Delta a_t = 2a_k \frac{\Delta v_{tT}}{v_{sk}}, \tag{5.43}$$

$$\Delta P_{1t} = -\cos K_{sk}(t_{mR}) \frac{\Delta v_{tR}}{v_{sk}} + 2 \sin K_{sk}(t_{mT}) \frac{\Delta v_{tT}}{v_{sk}}, \tag{5.44}$$

$$\Delta P_{2t} = +\sin K_{sk}(t_{mR}) \frac{\Delta v_{tR}}{v_{sk}} + 2 \cos K_{sk}(t_{mT}) \frac{\Delta v_{tT}}{v_{sk}}, \tag{5.45}$$

$$\Delta Q_{1t} = \frac{1}{2} \sin K_{sk}(t_{mN}) \frac{\Delta v_{tN}}{v_{sk}}, \tag{5.46}$$

$$\Delta Q_{2t} = \frac{1}{2} \cos K_{sk}(t_{mN}) \frac{\Delta v_{tN}}{v_{sk}}, \tag{5.47}$$

$$\Delta l_{\Theta t} = -2 \frac{\Delta v_{tR}}{v_{sk}}. \tag{5.48}$$

Moreover, the first term at the right-hand side of Eq. (5.39) is the mean motion deviation induced by thrust effect. With impulsive accelerations, its integration entails a variation not of the mean longitude $l_{\Theta t}$ but of the mean longitude drift $\dot{l}_{\Theta t}$ given by

$$\Delta \dot{l}_{\Theta t} = -3 n_k \frac{\Delta v_{tT}}{v_{sk}}. \tag{5.49}$$

This formula is deduced from the variation (5.43) of the semi-major axis and it is very useful in the high thrust EW maneuver planning.

The structure of the above equations and the hypothesis of non-correlation between the generations of the RTN thrust acceleration components justify the practice of doing the strategic planning of East-West SK maneuvers independently from the strategic planning of North-South SK maneuvers. Moreover the structure of the previous equations shows that the eccentricity and the inclination corrections are sensitive to the correction instants.

B. During the tactical phases the attention is focused on the immediate execution of the individual detailed activities. The operator at the control center determines which thrusters of the propulsion system have to be switched on and how long. In this phase a more realistic model of the on-board propulsion system is used. In this model the duration and amplitude of the accelerations are non-infinitesimal.

$$a_t(t) = \begin{cases} \dfrac{\Delta v_t}{T_m} & \text{if} \quad t_m^{on} \le t \le t_m^{off} \\ 0 & \text{otherwise} \end{cases}, \tag{5.50}$$

with $T_m = t_m^{off} - t_m^{on}$ (see Fig. 5.5). Hence, when

$$\begin{bmatrix} a_{tR}(t) \\ a_{tT}(t) \\ a_{tN}(t) \end{bmatrix} = \frac{1}{m} \begin{bmatrix} +1 & 0 & 0 & -1 & 0 & 0 \\ 0 & +1 & 0 & 0 & -1 & 0 \\ 0 & 0 & +1 & 0 & 0 & -1 \end{bmatrix} \begin{bmatrix} F_{+Z_B} \\ F_{-X_B} \\ F_{+Y_B} \\ F_{-Z_B} \\ F_{+X_B} \\ F_{-Y_B} \end{bmatrix} \tag{5.51}$$

and when a single maneuver (in terms of Δv_t) is executed by switching on a single thruster, the choice of the thruster to switch on and the duration of the on interval is trivial and depends on thrust levels of each thruster and on the spacecraft mass only. Presumably the thrust durations T_m will be short given that in the strategic planning phase the maneuvers in terms of Δv_t budgets have been computed under the impulsiveness hypothesis. The strategic planning is moreover coherent with the hypothesis of the independence between EW and NS maneuvers.

5.5.1.1 Strategic Planning of North-South High Thrust SK Maneuvers

North-South high thrust maneuvers (also called inclination or latitude maneuvers) require fuel 20 times as much as required for the East-West maneuvers. Inclination high thrust maneuvers can be planned by maneuver optimization programs of various degrees of sophistication.

Most of the inclination maneuvers are planned to compensate only the secular drift of the inclination vector (see, e.g., [Slavinskas et al., 1984], who determine and tabulate the impulse requirements obtained with various methods of compensation for inclination drift). [Soop, 1985] uses a model to describe the evolution of the orbital pole (three-dimensional inclination vector perpendicular to the orbital plane) not only under the effect of the Sun's and Moon's attraction but also of the Earth's precession. He proposes a strategic planning at high degree of optimization where only the direction of the inclination vector variation (i.e., the time of the correction day) is calculated. Neither the day of an inclination maneuver nor its intensity does not influence the total amount of station keeping fuel devoted to North-South maneuvers.

[Campan et al., 1995b] propose a waiting strategy to plan the North-South maneuvers, i.e. a strategy maximizing the SK correction cycles T_{Ck}. We illustrate this strategy with a simple example.

Example. In Fig. 5.7 we have plotted (dashed line) the trace described by the tip of the inclination vector $\boldsymbol{i} = \tan(i/2)\boldsymbol{n}$ in the (Q_2, Q_1) plane over eight weeks. The trace of $\boldsymbol{i}$ reaches the inclination tolerance circle after 36 day. Day 36 after the start of the simulation will be the day of the NS maneuver. The size of maneuver will be such that the instantaneous change $\Delta\boldsymbol{i}$ of the inclination vector $\boldsymbol{i}$ is equal to the maximum amplitude of the inclination dead band box $(2\tan i_{max}/2)$ and such that the inclination vector after the maneuver points at the

opposite side of the tolerance circle in the direction of the natural drift. Than, from

$$|\Delta \boldsymbol{i}|^2 = \Delta {Q_{1t}}^2 + \Delta {Q_{1t}}^2 = \frac{\Delta v_{tN}^2}{4 v_{sk}^2} = 4 \tan^2 \frac{i_{max}}{2} \tag{5.52}$$

we deduce

$$\Delta v_{tN} = 4 v_{sk} \tan \frac{i_{max}}{2}. \tag{5.53}$$

The time of the day for the impulsive maneuver is obtained from the argument of the vector change $\Delta \boldsymbol{i}$, i.e., from the slope of the natural inclination drift whose time history can be approximated as a straight line. Than, from

$$\Delta Q_{1t} = \frac{1}{2} \sin K_{sk}(t_{mN}) \frac{\Delta v_{tN}}{v_{sk}} \quad \text{and} \quad \Delta Q_{2t} = \frac{1}{2} \cos K_{sk}(t_{mN}) \frac{\Delta v_{tN}}{v_{sk}} \tag{5.54}$$

we obtain

$$\arg(\Delta \boldsymbol{i}) = \frac{\Delta Q_{1t}}{\Delta Q_{2t}} = \tan \left[\lambda_s + \Theta(t_{mN}) \right] \tag{5.55}$$

and consequently

$$\Theta(t_{mN}) = \arctan \left[\arg(\Delta \boldsymbol{i}) \right] - \lambda_s. \tag{5.56}$$

Fig.s 5.7 and 5.8 show the results over eight weeks of such a NS maneuver with $i_{max} = 0.1$ deg in the (Q_2, Q_1) and (t, φ) planes respectively. The initial value of inclination is zero. The maneuver found in terms of Δv_{tN} gives $\Delta v_{tN} = 10.73$ m/s to perform at $t_{mN} = -16.2$ hours of the 36th day, i.e., at $t_{mN} = 7.8$ hours of the 35th day (after the beginning of the simulation for a spacecraft with mass $m = 4500$ kg). We have assumed to execute this velocity variation with a chemical thruster at high thrust $F_{+Y_B} = 80$ Newton which gives a maneuver duration $T_{mN} = 10$ minutes

$$T_{mN} = \frac{m \Delta v_{tN}}{F_{+Y_B}}. \tag{5.57}$$

The simulation results plotted in Fig.s 5.7 and 5.8 have been obtained integrating over eight weeks the Gauss' VOP equations with a normal acceleration component given by

$$a_{tN}(t) = \begin{cases} \dfrac{F_{+Y_B}}{m} & \text{if} \quad t_{mN} - \frac{T_{mN}}{2} \leq t \leq t_{mN} + \frac{T_{mN}}{2} \\ 0 & \text{otherwise} \end{cases} \tag{5.58}$$

by a Simulink variable-step solver based on an explicit Runge-Kutta (4,5) formula: ode45. Relative and absolute tolerance have been chosen equal to 10^{-12}. Fig. 5.9 is a zoom of the latitude time history over the maneuver day. We can observe the instantaneous change in the latitude time history derivative (i.e., in the spacecraft latitudinal velocity) at the maneuver instant.

Actually, to plan NS maneuvers, [Campan et al., 1995b] apply the simple considerations above directly to the simplified linear time history of the inclination vector tip trace in the (Q_2, Q_1) plane and to a tolerance window with reduced amplitude in order to take modeling errors into account.

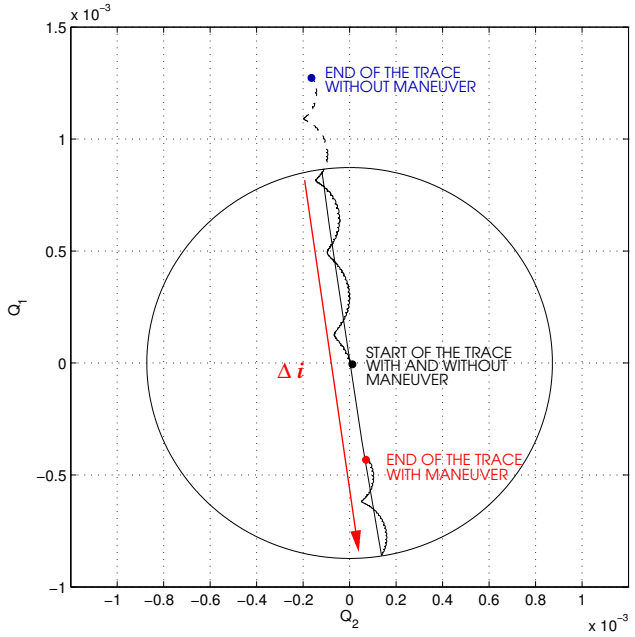

Figure 5.7: *Trace described by the tip of the inclination vector without maneuver (dashed line) and with impulsive maneuver (solid line). The circle is the inclination tolerance circle of radius* $\tan(i_{max}/2)$ *with* $i_{max} = 0.1$ *deg.*

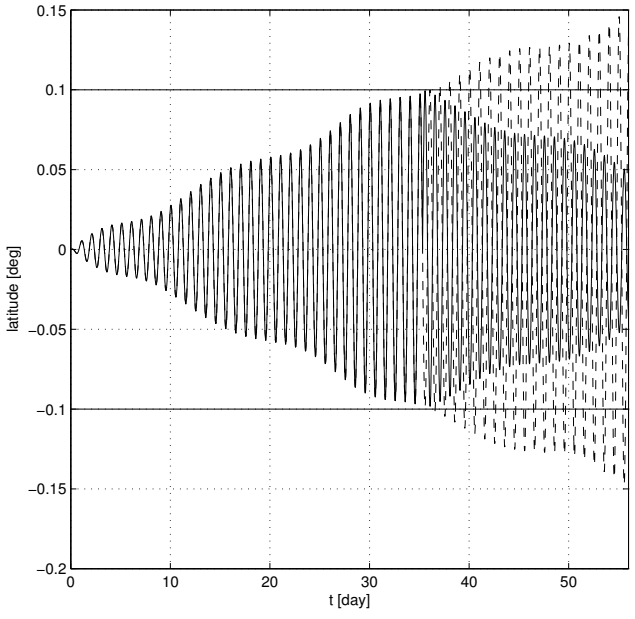

Figure 5.8: *Latitude time histories without maneuver (dashed line) and with impulsive maneuver (solid line). The horizontal lines are the limits of the latitude tolerance range* $2\arcsin[2\tan(i_{max}/2)] \approx 2i_{max}$ *in width.*

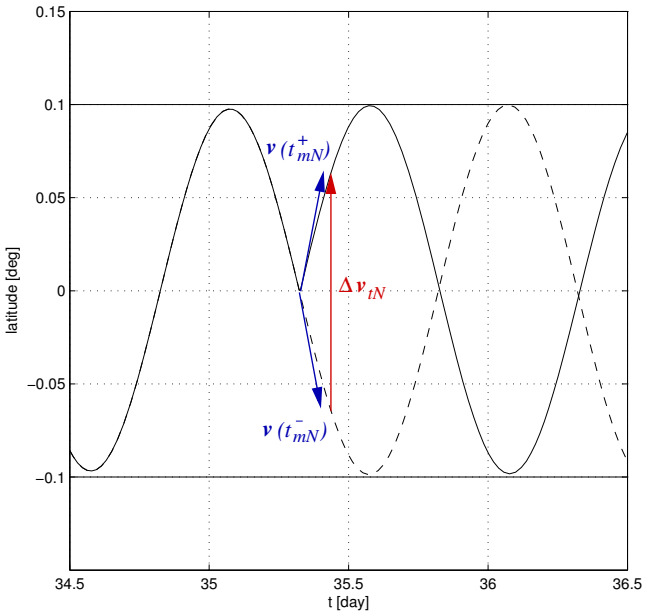

Figure 5.9: *Zoom of Fig. 5.8 over the maneuver day.*

They propose also to perform North-South maneuvers at fixed schedule (constant duration of the SK correction cycles) such that North-South correction cycles T_C are contained in East-West SK correction cycles. Further, they propose different strategic planning based on geometrical considerations in presence of constraints which prevent from performing maneuvers over a fixed period.

5.5.1.2 Strategic Planning of East-West High Thrust SK Maneuvers

[Soop, 1994] and [Campan et al., 1995b] propose to perform East-West high thrust maneuvers (latitude and eccentricity maneuvers) by only tangent thrust accelerations that are twice more efficient than radial ones (see Eq.s (5.43)–(5.45) and (5.48)). East-West high thrust maneuvers uses generally less fuel than inclination maneuvers but they are more complex to plan for several reasons:

1. a tangent thrust acceleration does not change directly the mean longitude l_Θ but only the mean motion drift
$$n - n_k = n_k D = -\frac{3}{2}\frac{n_k}{a_k}(a - a_k) \tag{5.59}$$
(see Eq. (5.8) and the first term at the right-hand side in Eq. (5.39));

2. a tangent thrust acceleration changes also the eccentricity components and consequently the geographical longitude (see definition of the geographical longitude (4.124) at page 128 and

Eq.s (5.35)–(5.36));

3. the longitude drift is sensitive to disturbances from maneuvers of attitude and inclination.

[Soop, 1994] and [Campan et al., 1995b] plan high thrust maneuvers to control the drift rate with a simplified model of the mean longitude evolution under the effect of the Earth's gravity attraction only. Such attraction induces a tangent drift variable with the station longitude but nearly constant over the time. We will have a closer look at this aspect at the beginning of the following chapter. Consequently, the EW maneuver contribution required to compensate this constant effect is also constant. Moreover, from equation 5.48 we can see that the effect induced by a tangent maneuver on the mean longitude is independent from the time instant over the maneuver day. It can be performed at any point of the orbit. [Emma and Pernicka, 2003] and [Romero and Gambi, 2004] assume this hypothesis too and they calculate the target values $l_\Theta(t_{fCk})$ at the end of each correction cycle based on a simplified parabolic time history of the mean longitude. Imposing that the simplified parabolic trend of the spacecraft longitude time history without maneuvers repeats itself under the effect of a constant acceleration, the target values are always the same for each impulsive correction cycle. The correction cycles are chosen with constant duration $T_C = t_{fCk} - t_{iCk}$ in order to define the constant target values $l_\Theta(t_{fCk}) = l_\Theta(t_{fC})$. In such a EW maneuver strategic planning, we recognize the need of regularizing the number of corrections to be performed at the beginning of each correction cycle. Moreover, the correction cycle duration T_C is maximized following a waiting strategy, which consists in deciding to execute a tangent maneuver when the longitude reaches the dead band box border and in using all the allowed range during the spacecraft longitudinal drift without maneuvers. We illustrate this strategy with a simple example based on a simplified version of our Gauss' VOP equations of motion.

Example. In Fig. 5.10 we have plotted the time histories of the mean longitude l_Θ and its derivative $\dot{l}_\Theta$ obtained integrating between $t_0 = 0$ and $t_f = 28$ day the nonlinear Gauss' VOP equations with eccentricity components equal to zero and with only the Earth's gravity acceleration acting on semi-major axis a and mean longitude l_Θ. The mean longitude time history can be approximated with a parabola

$$l_\Theta(t) = \alpha + \beta t + \frac{\gamma}{2} t^2. \tag{5.60}$$

The time history of its derivative (also known as the mean longitude drift) can be approximated with the straight line

$$\dot{l}_\Theta(t) = \beta + \gamma t. \tag{5.61}$$

The coefficients α, β and γ can be extrapolated by the simulation time histories to give

$$\alpha = l_\Theta(t_0), \qquad \beta = \dot{l}_\Theta(t_0), \qquad \gamma = \frac{\dot{l}_\Theta(t_f) - \beta}{(t_f - t_0)}, \tag{5.62}$$

for $t_0 = 0$. The second derivative $\ddot{l}_\Theta(t)$ (the mean longitude acceleration) is equal to γ and it is nearly constant because it depends on the nearly constant tangent acceleration component

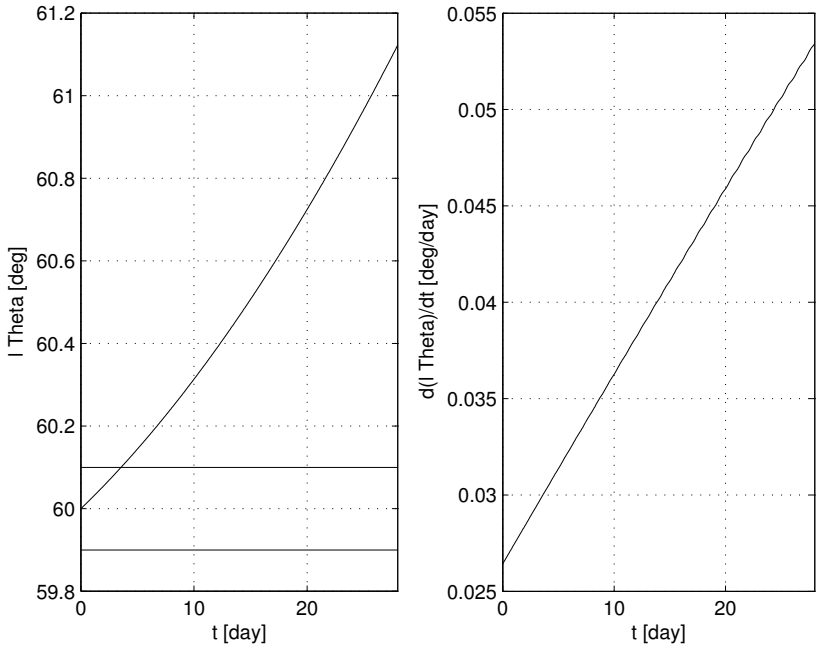

Figure 5.10: *Time histories of the mean longitude l_Θ and of the mean longitude drift $\dot{l}_\Theta$ obtained integrating over 4 weeks simplified nonlinear Gauss' VOP equations.*

induced by the non uniform Earth's gravity attraction. To strategically plan the high thrust maneuvers under the impulsiveness hypothesis, we can not modify the second derivative of the parabola (i.e., its concavity) because the high thrust maneuvers induce only velocity variations (i.e., instantaneously velocity changes) and not total velocity changes resulting in finite accelerations. We can act only on coefficients α and β. Coefficient β modifies the mean longitude drift $\dot{l}_\Theta$. Coefficients α fixes the position of the parabola in the (t, l_Θ) plane. Moreover, because in this phase of the strategic planning we have assumed eccentricity always equal to zero, the mean longitude l_Θ coincides with the geographical longitude λ and the mean longitude drift $\dot{l}_\Theta$ coincides with the longitudinal angular velocity of the spacecraft. In Fig. 5.10 the limits of the allowed zone in the (t, λ) plane are also drawn (horizontal lines). Longitude λ reaches its maximum allowed value

$$\lambda_s + \lambda_{max} = 60.1 \text{ deg} \quad \text{with} \quad \lambda_s = 60 \text{ deg} \quad \text{and} \quad \lambda_{max} = 0.1 \text{ deg}, \tag{5.63}$$

at the instant

$$t_{iC1} = 3.5483 \text{ day} \tag{5.64}$$

(i.e., at the 7th minute of the 13th hour in the 3rd day after the simulation beginning). At this instant an EW maneuver is needed such that the longitude slope changes brusquely and a new parabolic trend begins. Two arcs of trajectory juxtapose without interruption in the

longitude component

$$\lambda(t) = \begin{cases} \alpha + \beta t + \frac{\gamma}{2}t^2 & \text{if} \quad t_0 \le t \le t_{iC1} \\ \tilde{\alpha} + \tilde{\beta} t + \frac{\gamma}{2}t^2 & \text{if} \quad t_{iC1} \le t \le t_{fC1} = t_{iC1} + T_C \end{cases}, \tag{5.65}$$

which entails the following continuity condition

$$\Delta\alpha + t_{iC1}\Delta\beta = 0 \tag{5.66}$$

where $\Delta\alpha = (\alpha - \tilde{\alpha})$, $\Delta\beta = (\beta - \tilde{\beta})$ and t_{iC1} is known. The variation $\Delta\beta$ is the variation of the mean longitude drift $\dot{l}_{\Theta t}$ induced by an impulsive tangent thrust at the maneuver instant $t_{mT} = t_{iC1}$

$$\Delta\beta = \Delta\dot{l}_{\Theta t}(t_{mT}) = \dot{l}_{\Theta t}(t_{mT}^+) - \dot{l}_{\Theta t}(t_{mT}^-). \tag{5.67}$$

Once the amount of $\Delta\beta$ is known, the amount of tangent velocity variation Δv_{tT} induced by a thruster executing an impulsive EW maneuver is known too. In fact, from Eq. (5.49) we have

$$\Delta\dot{l}_{\Theta t}(t_{mT}) = -3n_k\frac{\Delta v_{tT}}{v_{sk}}, \tag{5.68}$$

which entails

$$\Delta v_{tT} = -\frac{a_k\Delta\beta}{3}. \tag{5.69}$$

To find the variation $\Delta\beta$, the target condition

$$\lambda(t_{mT} + T_C) = \lambda(t_{mT}) = \lambda_s + \lambda_{max} \tag{5.70}$$

and the maximum range condition

$$\lambda(t_{mT} + T_C/2) = \lambda_s - \lambda_{max} \tag{5.71}$$

have to be imposed. From the target condition (5.70) and the continuity condition (5.66) we obtain

$$\tilde{\beta} + \gamma t_{mT} + \frac{\gamma}{2}T_C = 0. \tag{5.72}$$

Subtracting term by term the maximum range condition

$$\tilde{\alpha} + \tilde{\beta}t_{mT} + \tilde{\beta}T_C/2 + \frac{\gamma}{2}(t_{mT}^2 + t_{mT}T_C + T_C^2/4) = \lambda_s - \lambda_{max} \tag{5.73}$$

from the target condition

$$\tilde{\alpha} + \tilde{\beta}t_{mT} + \tilde{\beta}T_C + \frac{\gamma}{2}(t_{mT}^2 + 2t_{mT}T_C + T_C^2) = \lambda_s + \lambda_{max}, \tag{5.74}$$

we obtain

$$T_C/2(\tilde{\beta} + \gamma t_{mT}) + \frac{\gamma}{2}3T_C^2/4 = 2\lambda_{max}. \tag{5.75}$$

Thanks to Eq. (5.72), we find from Eq. (5.75) the duration T_C of the correction cycle

$$T_C = 4\sqrt{\frac{\lambda_{max}}{\gamma}}. \tag{5.76}$$

As the values of β and T_C are known, we find $\Delta\beta = (\beta - \tilde{\beta})$ from Eq. (5.72)

$$\Delta\beta = \beta + \gamma t_{mT} + 2\sqrt{\gamma\lambda_{max}}. \tag{5.77}$$

In this example, such a variation is induced by a high thrust maneuver with $\Delta v_{tT} = -0.14$ m/s. Fig. 5.11 shows the effect of this tangent high thrust maneuver on the mean longitude and the mean longitude drift time histories approximated respectively as a parabola and a straight line.

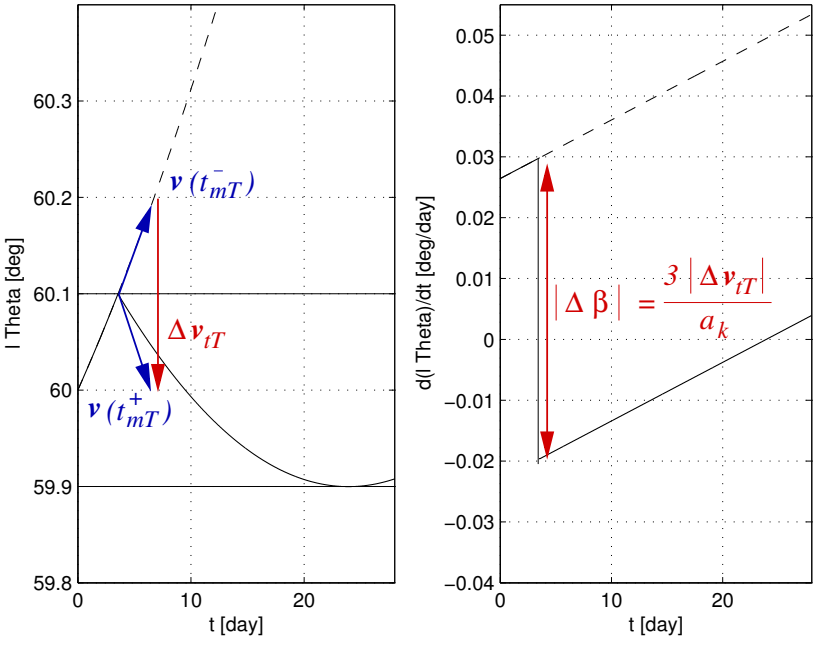

Figure 5.11: *Effect of a tangent high thrust maneuver on the mean longitude l_Θ and on the mean longitude drift $\dot{l}_\Theta$ (solid lines).*

Apropos of drift rate control, [Kelly et al., 1994] address the more general case of time varying longitudinal accelerations by including the effect of the Sun's and Moon's gravity attraction in the model of the environmental force effects. In their work they discuss a strategic planning of East-West SK maneuvers dependent on any particular station longitude value. Most of all, this is necessary when the station longitude is near to the equilibrium points where the Sun's and Moon's gravity effect dominates on the Earth's gravity one. Under this assumption, clearly, the target values for the mean longitude at the end of correction cycle has to be considered variable.

However, a careful strategic planning of the East-West maneuver timing is needed to control the contribution brought in geographical longitude by the eccentricity vector components, which are mainly affected by the solar radiation pressure (SRP) . In the state of the art ([Gartrell, 1981], [Kamel and Wagner, 1981], [Soop, 1994], [Kelly et al., 1994], [Campan et al., 1995b], [Emma and Pernicka, 2003]) we have found two methods to strategically plan the eccentricity control by high thrust tangent maneuvers: (**1**) the orbit circularizing method and (**2**) the method based on the Sun Pointing Perigee strategy.

1. **Orbit Circularizing Method.** This method is based on the idea of mitigating the effect of the SRP performing the drift control maneuvers with tangent thrust acceleration vectors opposite in direction to the tangent perturbing acceleration vectors caused by SRP. As depicted in Fig. 5.12, if the drift control tangent maneuver is a prograde maneuver (that increases the spacecraft tangent velocity) it is an advantageous plan to execute it at 06.00 hrs local sidereal time (LST), i.e., at the apogee of the perturbed orbit. But if the drift control tangent maneuver is retrograde (that decreases the spacecraft tangent velocity) it is advantageous to execute this one at 18.00 hrs LST, i.e., at the perigee of the perturbed orbit. This method is also known as the orbit circularization method because the goal is to reduce the magnitude of the eccentricity vector to make the orbit as circular as possible.

2. **Method Based on the Sun Pointing Perigee (SPP) Strategy.** This second strategical planning method is based on the so called Sun Pointing Perigee (SPP) strategy. It is used instead of the method **1** when the ratio A/m is big or when the SK orbital requirements on the eccentricity are very strict. In these cases SRP causes the orbit eccentricity to increase more than the amount that can be reduced with the circularization method and it is necessary to choose for the longitude drift correction a position on the orbit more optimal than apogee or perigee. To do that, the natural tendency of the eccentricity vector to place itself perpendicular to the Earth-Sun line is exploited. In the SPP strategy the eccentricity vector target values at the end of each correction cycle $\boldsymbol{e}(t_{fCk})$ is chosen in order to make the eccentricity vector to librate about the Earth-Sun line. The EW maneuver sequence is initiated with the eccentricity vector pointing in the same direction of the Earth-Sun line (in general). These maneuvers are performed to set the eccentricity vector to lag the Earth-Sun line. The effects of solar radiation pressure will naturally drive the eccentricity vector to lead the Earth-Sun line once again, and the process is repeated. In this way the eccentricity vector points on average the Sun. What we have just explained is illustrated in Fig. 5.13.

Usually, when the solar radiation pressure effect is extremely high, the mean eccentricity obtained with the SPP strategy performed with only one correction per cycle may cause a geographical longitude libration too large for the longitude orbital requirements. One must spend more fuel to counteract the eccentricity growth than to compensate for the mean longitude drift rate change. Typically, instead of a single tangent thrust maneuver, at least two tangential thrusts are per-

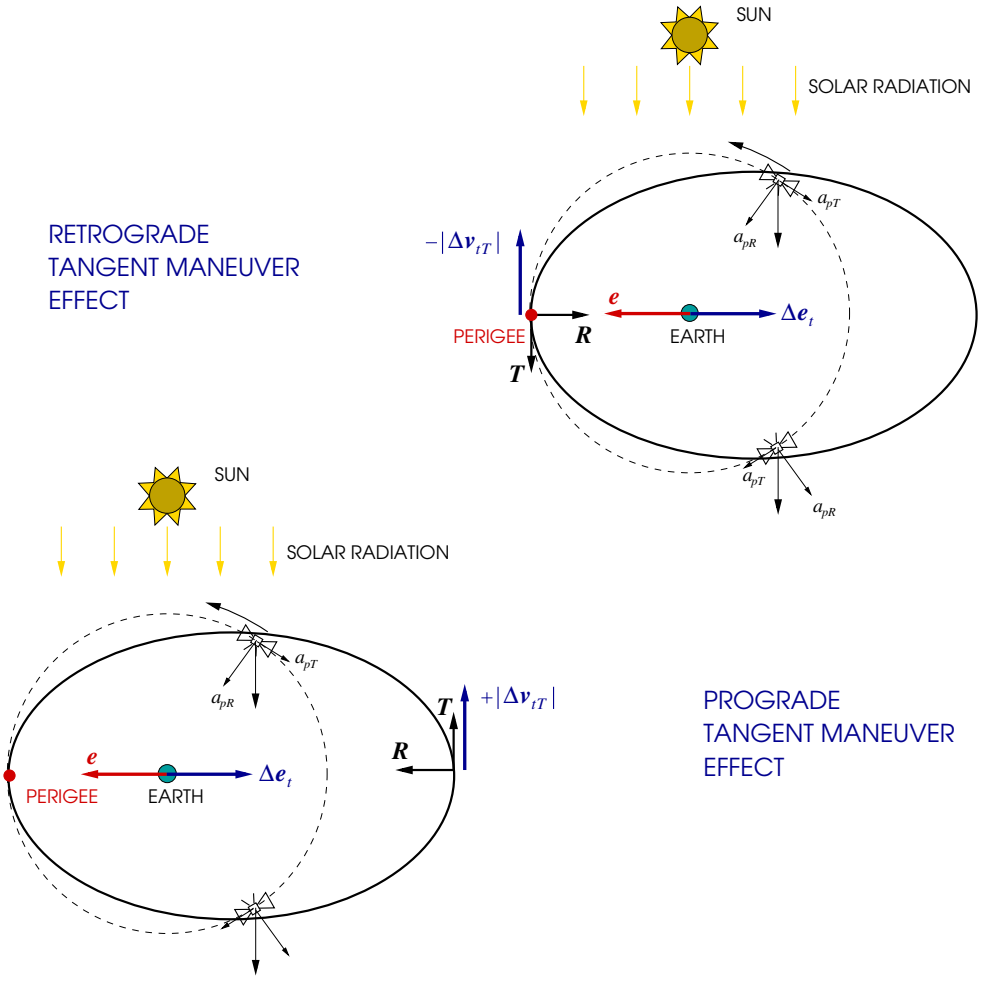

Figure 5.12: *Retrograde and prograde tangent maneuver effects on the eccentricity vector in the orbit circularizing method.*

formed. With two tangent thrusts the performed corrections are separated by a half a sidereal day (see [Kamel and Wagner, 1981], [Soop, 1994], [Campan et al., 1995b]). [Emma and Pernicka, 2003] propose a SPP strategy to be performed with two tangential high thrust maneuvers. They take also the effect of radial thrust components into account, which could be intrinsically generated by propulsion systems which do not allow for a tangential maneuver without a radial component.

In general the strategic assignment of eccentricity vector targets to reach at the end of each correction cycle is performed based on a simplified time history over one year of the eccentricity vector tip trace in the (P_2, P_1) plane. This simplified pattern is a circle. It is usually obtained taking into account the effect of the solar radiation pressure on the eccentricity vector only. The tip of the eccentricity vector draws a circle during one year maintaining its direction always perpendicular to the Earth-Sun line. Fig. 5.14 shows such a circle in dashed line and in solid line the true evolution

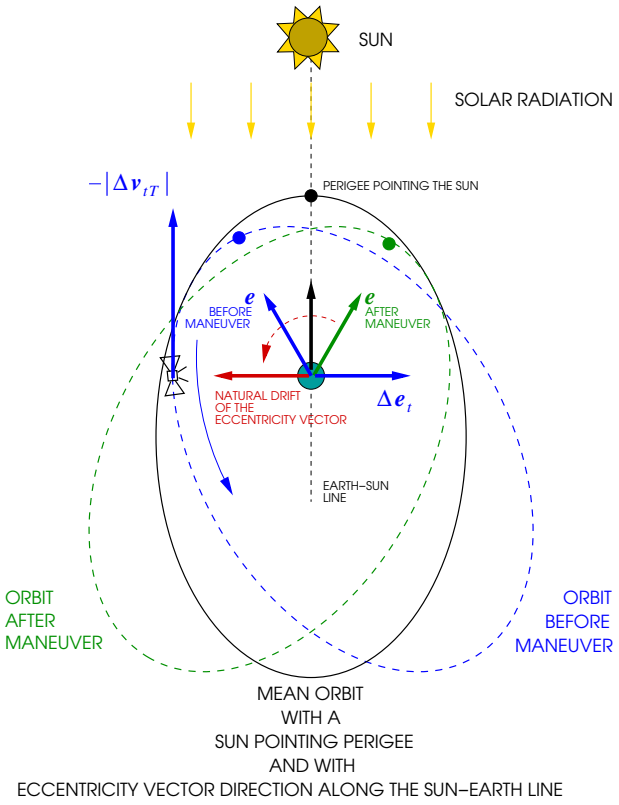

Figure 5.13: *Illustration of the basic idea behind the Sun Pointing Perigee strategy to plan the high thrust EW maneuvers for the eccentricity control.*

of the eccentricity component P_1 versus P_2. The first one has been obtained integrating Lagrange's VOP equations with only the SRP affecting the eccentricity components. The second one has been obtained integrating the Gauss' VOP equations with all the three perturbing accelerations acting on P_1 and P_2. Given the regular shape of the simplified pattern P_2 vs P_1 the parameters are considered in the mean sense. We deduce that the targeting strategy will be nearly the same from one correction cycle to another. But, if we consider the osculating behavior of the eccentricity vector, the targeting strategy varies from a cycle to another. As the eccentricity vector approaches a cusp (see the zoom in Fig. 5.15), its rate of rotation decreases, completely stops momentarily, and may even track counter to the Sun's direction. In between the cusps, $\boldsymbol{e}$ rotates faster than the average. Because the natural rotation of the eccentricity vector varies over a month, the targeting strategy for high thrust control of the eccentricity also needs to vary from one cycle to the next. In their work, [Kelly et al., 1994] take into account this important aspect.

5.5.2 Low Thrust SK Manoeuvre Planning

When speaking of low thrust maneuvers, [Campan et al., 1995b] and [Soop, 1994] limit themselves to stating that the model which gives the variation (5.34)–(5.39) of the orbital parameters

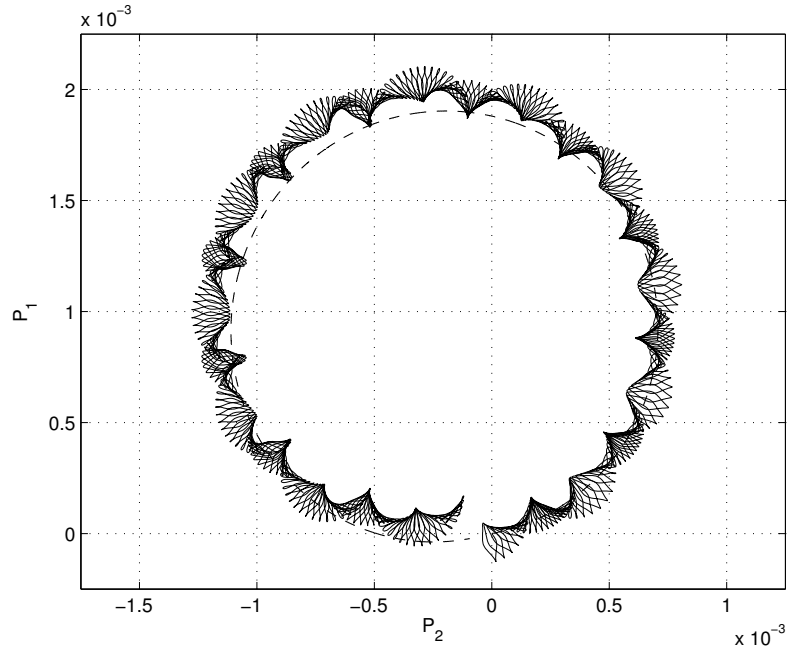

Figure 5.14: *Traces described over one year by the tip of the mean eccentricity vector (dashed line) and by the osculating eccentricity vector (solid line).*

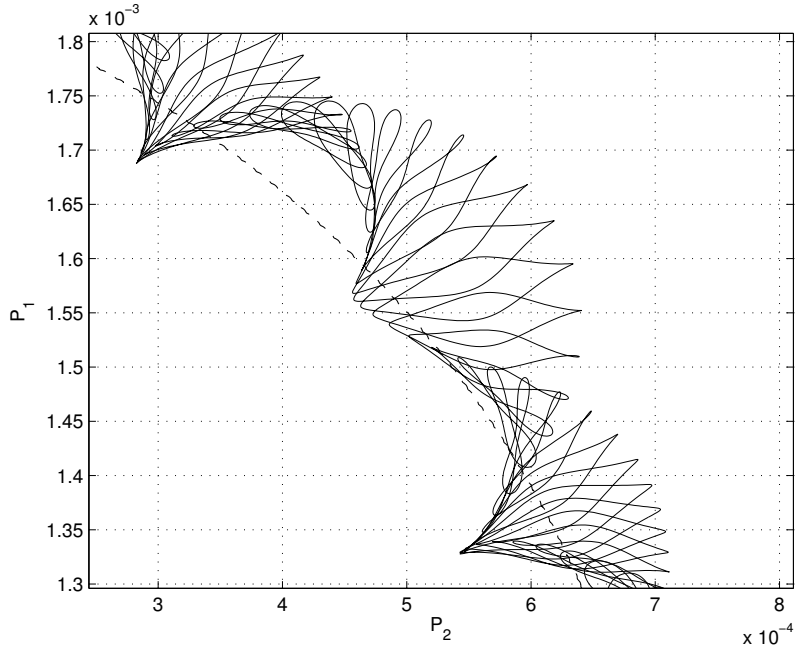

Figure 5.15: *Zoom of Fig. 5.14 highlighting the cusp of the osculating trace.*

as a function of the velocity change components induced by the thrusters is no more valid because presumably the low thrust velocity changes can no more be considered as instantaneous. The authors modify this model making the hypothesis that the thrust acceleration components have no more impulsive but pulse waveforms whose duration is $T_m = t_m^{off} - t_m^{on}$

$$a_{tR}(t) = \begin{cases} \dfrac{\Delta v_{tR}}{T_{mR}} & \text{if} \quad t_{mR}^{on} \le t \le t_{mR}^{off} \\ 0 & \text{otherwise} \end{cases}, \tag{5.78}$$

$$a_{tT}(t) = \begin{cases} \dfrac{\Delta v_{tT}}{T_{mT}} & \text{if} \quad t_{mT}^{on} \le t \le t_{mT}^{off} \\ 0 & \text{otherwise} \end{cases}, \tag{5.79}$$

$$a_{tN}(t) = \begin{cases} \dfrac{\Delta v_{tN}}{T_{mN}} & \text{if} \quad t_{mN}^{on} \le t \le t_{mN}^{off} \\ 0 & \text{otherwise} \end{cases}, \tag{5.80}$$

The differential equations which model the effects of the thrust accelerations on the orbital parameters are still taken as equal to the linearization of the Gauss' VOP equations under only the effect of the thrust accelerations $\dot{\boldsymbol{x}}_t = \boldsymbol{K}(\boldsymbol{x}_t) - \boldsymbol{\omega}_\oplus + \boldsymbol{G}(\boldsymbol{x}_t, t)\boldsymbol{a}_t$ around $\boldsymbol{x}_t = \boldsymbol{x}_{Ksk}$ [Soop, 1994] or $\boldsymbol{x}_t = \boldsymbol{x}_{Ssk}$ [Campan et al., 1995b] and $\boldsymbol{a}_t = \boldsymbol{0}_{3\times 1}$. The total change of the semi-major axis induced by a non-impulsive thrust has the same dependence on Δv_{tT} of the variation (5.43) because we have

$$a_t(t) = a_t(t_{mT}^{on}) + \int_{t_{mT}^{on}}^{t} 2a_k \frac{\Delta v_{tT}/T_{mT}}{v_{sk}} dt = a_t(t_{mT}^{on}) + 2a_k \frac{\Delta v_{tT}/T_{mT}}{v_{sk}} (t - t_{mT}^{on}) \tag{5.81}$$

and when $t = t_{mT}^{off}$

$$\tilde{\Delta} a_t = a_t(t_{mT}^{off}) - a_t(t_{mT}^{on}) = 2a_k \frac{\Delta v_{tT}}{v_{sk}}. \tag{5.82}$$

The total change of the mean longitude induced by a non-impulsive thrust depends not only on a radial but also on a tangent acceleration component, indirectly via the integration of the mean motion deviation over a finite interval of duration T_{mT}. The total change of the mean longitude induced by a radial acceleration pulse is

$$\tilde{\Delta} l_{\Theta tR} = l_{\Theta tR}(t_{mR}^{off}) - l_{\Theta tR}(t_{mR}^{on}) = -2 \frac{\Delta v_{tR}}{v_{sk}} \tag{5.83}$$

obtained evaluating in $t = t_{mR}^{off}$ the following integration results

$$l_{\Theta tR}(t) = l_{\Theta tR}(t_{mR}^{on}) - \int_{t_{mR}^{on}}^{t} 2 \frac{\Delta v_{tR}/T_{mR}}{v_{sk}} dt = l_{\Theta tR}(t_{mR}^{on}) - 2 \frac{\Delta v_{tR}/T_{mR}}{v_{sk}} (t - t_{mT}^{on}). \tag{5.84}$$

The total change of the mean longitude induced by a tangent acceleration pulse is

$$\tilde{\Delta} l_{\Theta tT} = l_{\Theta tT}(t_{mT}^{off}) - l_{\Theta tT}(t_{mT}^{on}) = -\frac{3}{2} \frac{n_k}{a_k} \left[a_t(t_{mT}^{on}) - a_k \right] T_{mT} - \frac{3}{2} n_k \frac{\Delta v_{tT}}{v_{sk}} T_{mT} \tag{5.85}$$

obtained evaluating in $t = t_{mT}^{off}$ the following integration result

$$l_{\Theta tT}(t) = l_{\Theta tT}(t_{mT}^{on}) - \frac{3}{2}\frac{n_k}{a_k}\int_{t_{mT}^{on}}^{t} [a_t(t) - a_k]\, dt \tag{5.86}$$

with $a_t(t)$ given by Eq. (5.81). The total changes of the eccentricity and inclination equinoctial orbital element

$$\tilde{\Delta}P_{1t} = \tilde{\Delta}P_{1tR} + \tilde{\Delta}P_{1tT} = \left[P_{1tR}(t_{mR}^{off}) - P_{1tR}(t_{mR}^{on})\right] + \left[P_{1tT}(t_{mT}^{off}) - P_{1tT}(t_{mT}^{on})\right], \tag{5.87}$$

$$\tilde{\Delta}P_{2t} = \tilde{\Delta}P_{2tR} + \tilde{\Delta}P_{2tT} = \left[P_{2tR}(t_{mR}^{off}) - P_{2tR}(t_{mR}^{on})\right] + \left[P_{2tT}(t_{mT}^{off}) - P_{2tT}(t_{mT}^{on})\right], \tag{5.88}$$

$$\tilde{\Delta}Q_{1t} = \tilde{\Delta}Q_{1tR} + \tilde{\Delta}Q_{1tT} = \left[Q_{1tR}(t_{mR}^{off}) - Q_{1tR}(t_{mR}^{on})\right] + \left[Q_{1tT}(t_{mT}^{off}) - Q_{1tT}(t_{mT}^{on})\right], \tag{5.89}$$

$$\tilde{\Delta}Q_{2t} = \tilde{\Delta}Q_{2tR} + \tilde{\Delta}Q_{2tT} = \left[Q_{2tR}(t_{mR}^{off}) - Q_{2tR}(t_{mR}^{on})\right] + \left[Q_{2tT}(t_{mT}^{off}) - Q_{2tT}(t_{mT}^{on})\right], \tag{5.90}$$

induced by the single thrust acceleration components (5.78)–(5.80) becomes the following

$$\tilde{\Delta}P_{1t} = -\left(\frac{\sin\frac{\omega_\oplus T_{mR}}{2}}{\frac{\omega_\oplus T_{mR}}{2}}\right)\frac{\Delta v_{tR}}{v_{sk}}\cos K_{sk}(t_{mR}) + 2\left(\frac{\sin\frac{\omega_\oplus T_{mT}}{2}}{\frac{\omega_\oplus T_{mT}}{2}}\right)\frac{\Delta v_{tT}}{v_{sk}}\sin K_{sk}(t_{mT}), \tag{5.91}$$

$$\tilde{\Delta}P_{2t} = +\left(\frac{\sin\frac{\omega_\oplus T_{mR}}{2}}{\frac{\omega_\oplus T_{mR}}{2}}\right)\frac{\Delta v_{tR}}{v_{sk}}\sin K_{sk}(t_{mR}) + 2\left(\frac{\sin\frac{\omega_\oplus T_{mT}}{2}}{\frac{\omega_\oplus T_{mT}}{2}}\right)\frac{\Delta v_{tT}}{v_{sk}}\cos K_{sk}(t_{mT}), \tag{5.92}$$

$$\tilde{\Delta}Q_{1t} = \frac{1}{2}\left(\frac{\sin\frac{\omega_\oplus T_{mN}}{2}}{\frac{\omega_\oplus T_{mN}}{2}}\right)\frac{\Delta v_{tN}}{v_{sk}}\sin K_{sk}(t_{mN}), \tag{5.93}$$

$$\tilde{\Delta}Q_{2t} = \frac{1}{2}\left(\frac{\sin\frac{\omega_\oplus T_{mN}}{2}}{\frac{\omega_\oplus T_{mN}}{2}}\right)\frac{\Delta v_{tN}}{v_{sk}}\cos K_{sk}(t_{mN}), \tag{5.94}$$

with epochs t_m located in the middle of the corresponding intervals T_m

$$t_m = \frac{t_m^{on} + t_m^{off}}{2} = t_m^{on} + \frac{T_m}{2}. \tag{5.95}$$

In order to follow the main ground based SK goals, [Campan et al., 1995b] and [Soop, 1994] do not propose a strategic maneuver planning which is different from the one proposed for the high thrust maneuvers and which takes into account the reduced level of thrust (at a strategic level). One can deduce that the proposed solution is to realize the effects of the thruster velocity changes obtained planning the high thrust maneuvers through low thrust propulsion systems. [Soop, 1994] points out the correction efficiency loss that would be present when correcting inclination and eccentricity components through the adoption of a simple solution of "spreading" the impulsive accelerations over the time axes around the impulsive thrust instant and until having reached the necessary level of low thrust (see Fig. 5.16). Fig.s (5.17) and (5.18) show some simulation results obtained "spreading" the normal impulsive acceleration used to obtained the results plotted in Fig.s (5.7) and (5.9). We have tried to reduce the thrust level $F_{+Y_B} = 80$ N by a factor 20, then 40 and finally 80

$$\textbf{A)}\ F_{+Y_B} = 4\text{ N}, \qquad \textbf{B)}\ F_{+Y_B} = 2\text{ N}, \qquad \textbf{C)}\ F_{+Y_B} = 1\text{ N}, \tag{5.96}$$

and to increase the corresponding thrust interval T_{mN} by the same factors

$$\textbf{A)}\ T_{mN} \approx 3.3 \text{ hours}, \qquad \textbf{B)}\ T_{mN} \approx 6.6 \text{ hours}, \qquad \textbf{C)}\ T_{mN} \approx 13.3 \text{ hours}. \tag{5.97}$$

[Soop, 1994] underlines that it would be appropriate for this reason to split the thrusts in several parts separated by one sidereal day or, in case of inclination correction, to alternate North and South thrusts twice per sidereal day. [Eckstein, 1980] also points out that if the station keeping cycle extends over several days, it is appropriate to generate the orbital correction with several thrusting periods instead of with an unique thrust period of long duration. It is easy to realize that by observing the efficiency loss induced by the dependence of the corrections on the sinus of the maneuver interval (see the factors $\sin(\omega_\oplus T_m/2)/(\omega_\oplus T_m/2)$ of efficiency losses in Eq.s (5.91)–(5.94)). Hence splitting the effect induced by a maneuver of duration T_m in k effects induced by maneuvers of duration τ_m

$$k \sin\frac{\omega_\oplus \tau_m}{2} = \sin\frac{\omega_\oplus T_m}{2} \tag{5.98}$$

one obtains

$$\tau_m = \arcsin\left(\frac{\sin T_m}{k}\right) < \frac{T_m}{k}. \tag{5.99}$$

[Eckstein, 1980] considers a propulsion system composed of two thrusters pointing in two different fixed directions and symmetrically attached to the East and West walls of a three-axis-stabilized geostationary satellite. He solves an optimization problem in order to determine the optimum

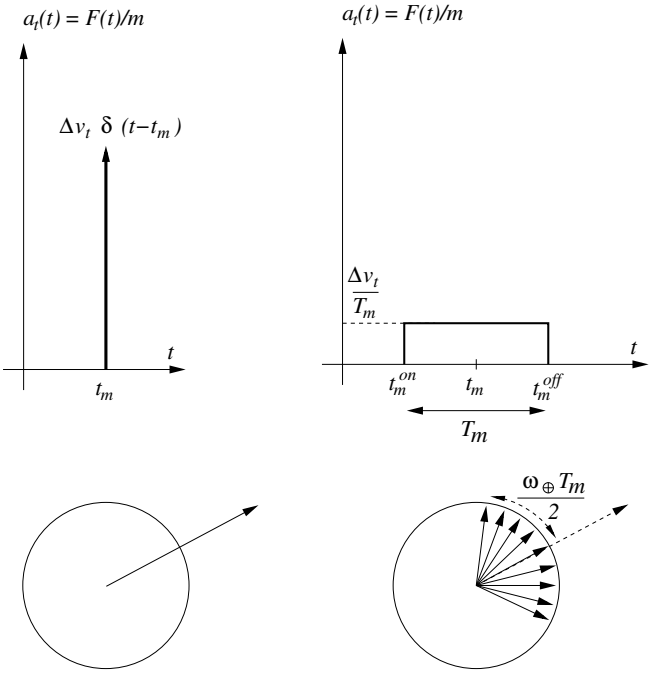

Figure 5.16: *Correction efficiency loss in "spreading" the impulsive accelerations*

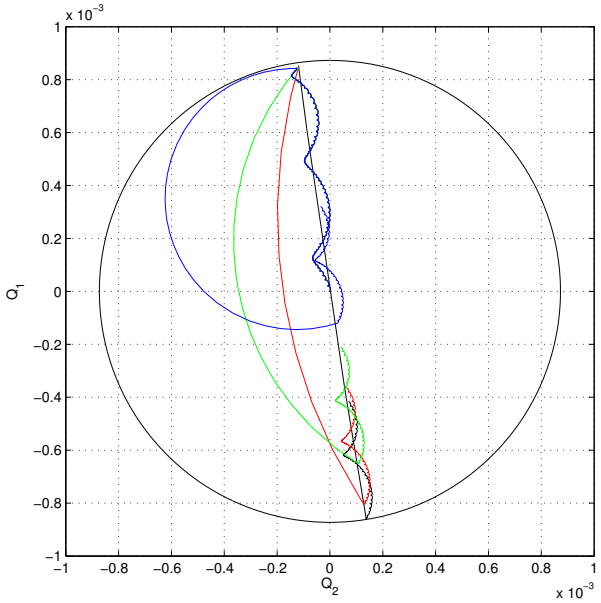

Figure 5.17: *Simulation results obtained "spreading" the normal impulsive acceleration used to obtained the results plotted in Fig. (5.7). In red the case* **A**. *In green the case* **B**. *In blue the case* **C**. *In black the case with impulsive acceleration. The circle is the inclination tolerance circle of radius* $\tan(i_{max}/2)$ *with* $i_{max} = 0.1$ *deg.*

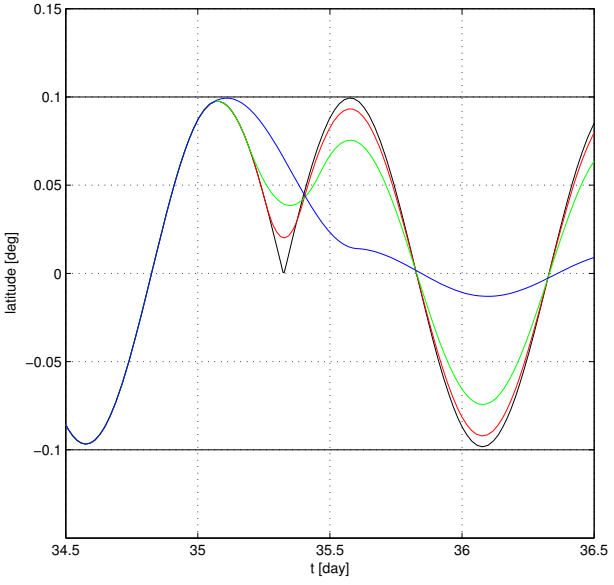

Figure 5.18: *Simulation results obtained "spreading" the normal impulsive acceleration used to obtained the results plotted in Fig. (5.9). In red the case* **A**. *In green the case* **B**. *In blue the case* **C**. *In black the case with impulsive acceleration.*

times for switching on and off the different thrusters, in presence of different operation constraints. The cost function to be minimized over a station keeping cycle is a weighted combination of fuel consumption and the equinoctial element deviation at the end of the cycle from target values.

[Eckstein and Hechler, 1981] wonder about the opportunity of modifying the maneuver planning strategy if the thrusters of the propulsion system dedicated to the station keeping are low thrust. For the correction of the secular effects, instead of proposing a planning strategy based on a minimum correction frequency (i.e., with maneuvers to execute whenever one of the equinoctial secular evolutions reaches the boundary of its admissible range), they prefer to define a strategy based on the minimization of the efficiency loss due to the realization of low thrust maneuvers. For the first time in literature, someone proposed a planning strategy taking into account the maximum variation of equinoctial elements that can effectively be achieved by a single low thrust. This leads to orbital parameter corrections which are very small and carried out very frequently, up to twice a day. The authors give also some strategies to plan the long periodic eccentricity corrections with maneuvers which are frequent and which depend on the initial value of the modulus of an eccentricity vector $\boldsymbol{e}$ which must stay within a tolerance circle of radius R_t during all the mission. Depending on the fact the initial eccentricity value is smaller or greater than R_t, one solves a fuel optimal control problem or a time optimal problem. Considerations of geometric character lead to the determination of the eccentricity variations to induce with the low thrust accelerations.

[Eckstein et al., 1981] investigate the feasibility and performance of a fully autonomous station keeping system for GEO satellites equipped with a fully electrical propulsion system composed of four thrusters mounted in pair on the East and West walls of the spacecraft and inclined to avoid the contamination of the solar generators. Such thrusters provide acceleration components in the main directions without coupling among them by operating in pair. [Eckstein et al., 1981] propose a maneuver planning strategy different from that based on maneuvers executed at the lowest possible frequency. These maneuvers are executed whenever one of the equinoctial secular evolutions reaches the boundary of its admissible range. They define their strategy as "precaution strategy" because it prevents the orbit from exceeding the range of corrections attainable by a single thrust. The target values of the equinoctial orbital elements are defined by a long term strategy and the variations of parameters that can be induced with the maneuvers are deduced from a simplified model used also during the orbit determination phase. The switching times are obtained solving an optimization problem minimizing the fuel consumption over a station keeping cycle of 10 days.

The first fully electrical propulsion system composed of thrusters mounted only on the anti nadir face is proposed by [Anzel, 1988]. [Anzel, 1988] gives also a rough plan of maneuver. To perform inclination vector control the South thruster with a zero slew angle is fired over an arc centered about a right ascension of 90 deg and the North thruster is fired over an arc centered about a right ascension of 270 deg. For equal burn arcs the radial acceleration components are equal, so the eccentricity doesn't change. Partial eccentricity control is performed with unequal burn arcs. The longitude drift rate is controlled altering the semi-major axis with a tangent component of acceleration made swerving one thruster about the North-South axis.

The version with four thrusters of the propulsion system just described has been patented by [Anzel, 1995]. This configuration is oversized with respect to the previous one by adding two redundant thrusters in order to be able to cope with thruster failures and it guarantees a complete control of inclination, eccentricity and mean longitude.

[Gopinath and Srinivasamuthy, 2003] also consider the same configuration carrying out simultaneously in-plane and out-plane station keeping maneuvers. For some given orbit control requirements in terms of drift rate, eccentricity and inclination vector components, they calculate the four thruster durations for different values of right ascension at the middle points of the firing intervals.

The same anti nadir four thruster propulsion system is mounted on satellites of the HS 702 series[7]. [Anzel, 1998] explains how the four ion thrusters mounted in rectangular pattern on the anti-nadir face can be used to perform not only station keeping but also momentum damping maneuvers precluding wheel saturation.

5.5.3 A Different Approach to Plan SK Maneuvers

[Chao and Bernstein, 1994], [Kluever and Tanck, 1997] and [Park et al., 2005] deal with the SK maneuver planning with the goal of executing it on board in autonomous geostationary orbit control loops. To perform the maneuver planning in an autonomous control loop, they underline the disadvantages of embedding on board the SK maneuver planning algorithms employed by the ground based mission analysis software through a long history of satellite operation. These disadvantages are the heavy computational burden, the high complexity of the algorithm and the lack of reliability tests because an autonomous station keeping control loop does not allow the ground maneuver evaluation before and after the execution of the planned maneuvers. [Chao and Bernstein, 1994], [Kluever and Tanck, 1997] and [Park et al., 2005] apply the concept of formation keeping of two nearby spacecraft by means of closed loop feedback control algorithms. More precisely, they exploit this concept to keep in formation a satellite with a fictitious spacecraft whose ephemerides are predetermined as reference orbit. The station keeping problem is handled as a regulation problem. The spacecraft state vector must follow a predefined set point value.

[Chao and Bernstein, 1994] and [Kluever and Tanck, 1997] consider as set point the nominal station keeping state vector. In the [Park et al., 2005] work, the goal is to follow predetermined reference range orbital data generated through a ground based computer simulation with typical SK maneuver planning strategies and embedded or up loaded on board with time tag. While [Chao and Bernstein, 1994] and [Kluever and Tanck, 1997] plan the SK maneuvers to follow the target orbit strictly, [Park et al., 2005] plan the maneuvers to follow the reference trajectory by fast ground computer and plan on board only the correction maneuvers to remove the deviations

[7] In October 1995 Hughes Space and Communications Company, now Boeing Satellite Systems, announced an innovative new satellite series: the Hughes 702, which evolved from Hughes 601 and Hughes 601HP (high power) spacecraft. The body stabilized Hughes 702 is a giant in size, performance, and cost efficiency. The satellites are now known as the Boeing 601, 601HP, and 702. As of April 2001, twelve of these powerful satellites had been ordered, with options for eight more. The first satellite was launched in 1999.

from the reference orbit caused mainly by maneuver uncertainty and perturbing force modeling errors. In each of these three works a state feedback regulator is designed via a discrete time asymptotic LQR approach based on the discrete version

$$\boldsymbol{\xi}(k+1) = \boldsymbol{A}_{CWd}\boldsymbol{\xi}(k) + \boldsymbol{B}_{CWd}\boldsymbol{\eta}(k) \tag{5.100}$$

of the linear Clohessy-Wiltshire equations of a GEO spacecraft motion under the only effect of the thrust acceleration vector $\boldsymbol{a_t}$

$$\frac{d\boldsymbol{\xi}}{dt} = \boldsymbol{A}_{CW}\boldsymbol{\xi} + \boldsymbol{B}_{CW}\boldsymbol{a_t}(t) \tag{5.101}$$

where

$$\boldsymbol{\xi} = \begin{bmatrix} x_G & y_G & z_G & \dot{x}_G & \dot{y}_G & \dot{z}_G \end{bmatrix}^T. \tag{5.102}$$

Matrices $\boldsymbol{A}_{CW}$ and $\boldsymbol{B}_{CW}$ are those defined in Section 4.4 at page 148. Thrust acceleration vector

$$\boldsymbol{a}_t(t) = \begin{bmatrix} a_{tXG}(t) & a_{tYG}(t) & a_{tZG}(t) \end{bmatrix}^T \tag{5.103}$$

is defined with components

$$a_{tX_G}(t) = \begin{cases} \dfrac{\Delta v_{tX_G}}{T_{mX_G}} & \text{if} \quad t^{on}_{mX_G} \le t \le t^{off}_{mX_G} \\ 0 & \text{otherwise} \end{cases}, \tag{5.104}$$

$$a_{tY_G}(t) = \begin{cases} \dfrac{\Delta v_{tY_G}}{T_{mT_G}} & \text{if} \quad t^{on}_{mY_G} \le t \le t^{off}_{mY_G} \\ 0 & \text{otherwise} \end{cases}, \tag{5.105}$$

$$a_{tZ_G}(t) = \begin{cases} \dfrac{\Delta v_{tZ_G}}{T_{mZ_G}} & \text{if} \quad t^{on}_{mZ_G} \le t \le t^{off}_{mZ_G} \\ 0 & \text{otherwise} \end{cases}, \tag{5.106}$$

where Δv_t quantities are the velocity increments induced by thrusts over time intervals $T_m = t^{off}_m - t^{on}_m$. The components of the discrete control variable vector $\boldsymbol{\eta}(k)$ are the velocity increments induced by the thrust accelerations at each sample instant along the axes of the GEO CW coordinate system

$$\boldsymbol{\eta}(k) = \begin{bmatrix} \Delta v_{tX_G}(k) & \Delta v_{tY_G}(k) & \Delta v_{tZ_G}(k) \end{bmatrix}^T. \tag{5.107}$$

[Chao and Bernstein, 1994] consider the control problem formulated with the CW equations (5.100) as decoupled for the in plane components

$$\begin{bmatrix} x_G(k) & y_G(k) & \dot{x}_G(k) & \dot{y}_G(k) \end{bmatrix}^T = \boldsymbol{\xi}_{xy}(k) \tag{5.108}$$

and the out of plane components

$$\begin{bmatrix} z_G(k) & \dot{z}_G(k) \end{bmatrix}^T = \boldsymbol{\xi}_z(k). \tag{5.109}$$

The feedback control laws proposed by [Chao and Bernstein, 1994] are two steady state feedback control laws

$$\boldsymbol{\eta}_{xy}(k) = -\boldsymbol{R}_{xy}^{-1}\boldsymbol{B}_{xy}^{T}\boldsymbol{P}_{xy}\boldsymbol{\xi}_{xy}(k), \tag{5.110}$$

$$\eta_{z}(k) = -\boldsymbol{R}_{z}^{-1}\boldsymbol{B}_{z}^{T}\boldsymbol{P}_{z}\boldsymbol{\xi}_{z}(k), \tag{5.111}$$

minimizing respectively the two performance indexes

$$J_{xy} = \frac{1}{2}\sum_{k=1}^{\infty}\left[\boldsymbol{\xi}_{xy}^{T}(k)\boldsymbol{Q}_{xy}\boldsymbol{\xi}_{xy}(k) + \boldsymbol{\eta}_{xy}^{T}(k)\boldsymbol{R}_{xy}\boldsymbol{\eta}_{xy}(k)\right] \tag{5.112}$$

$$J_{z} = \frac{1}{2}\sum_{k=1}^{\infty}\left[\boldsymbol{\xi}_{z}^{T}(k)\boldsymbol{Q}_{z}\boldsymbol{\xi}_{z}(k) + R_{z}\eta_{z}^{2}(k)\right] \tag{5.113}$$

with

$$\boldsymbol{\eta}_{xy}(k) = \begin{bmatrix}\Delta v_{tX_G}(k) & \Delta v_{tY_G}(k)\end{bmatrix}^{T}, \quad \eta_{z}(k) = \Delta v_{tZ_G}(k), \tag{5.114}$$

$$\boldsymbol{Q}_{xy} = \begin{bmatrix}0 & 0 & 0 & 0\\ 0 & 1 & 0 & 0\\ 0 & 0 & 0 & 0\\ 0 & 0 & 0 & 0\end{bmatrix}^{T}, \quad \boldsymbol{Q}_{z} = \begin{bmatrix}1 & 0\\ 0 & 0\end{bmatrix}^{T}, \tag{5.115}$$

$$\boldsymbol{R}_{xy} = \boldsymbol{I}_{2\times 2}/\omega_{\oplus}^{2}, \quad R_{z} = 1/\omega_{\oplus}^{2}. \tag{5.116}$$

Matrices $\boldsymbol{P}_{xy}$ and $\boldsymbol{P}_{z}$ are the solution of the algebraic Riccati equations

$$\boldsymbol{A}_{xy}^{T}\boldsymbol{P}_{xy} + \boldsymbol{P}_{xy}\boldsymbol{A}_{xy} - \boldsymbol{P}_{xy}\boldsymbol{B}_{xy}\boldsymbol{R}_{xy}^{-1}\boldsymbol{B}_{xy}^{T}\boldsymbol{P}_{xy} + \boldsymbol{Q}_{xy} = \boldsymbol{0}_{4\times 4} \tag{5.117}$$

$$\boldsymbol{A}_{z}^{T}\boldsymbol{P}_{z} + \boldsymbol{P}_{z}\boldsymbol{A}_{z} - \boldsymbol{P}_{z}\boldsymbol{B}_{z}\boldsymbol{R}_{z}^{-1}\boldsymbol{B}_{z}^{T}\boldsymbol{P}_{z} + \boldsymbol{Q}_{z} = \boldsymbol{0}_{2\times 4} \tag{5.118}$$

where $\boldsymbol{A}_{xy}$, $\boldsymbol{B}_{xy}$, $\boldsymbol{A}_{z}$ and $\boldsymbol{B}_{z}$ are deduced from the matrices $\boldsymbol{A}_{CWd}$ and $\boldsymbol{B}_{CWd}$ of the discrete dynamics (5.100). [Chao and Bernstein, 1994] show simulation results obtained with a discrete dynamics with sampling intervals $h = 6$ hours and $h = 8$ hours. These sampling intervals are also the thrust frequency. In fact, in such a maneuver planning the sampling interval of the equations of motion coincides with a station keeping cycle.

[Kluever and Tanck, 1997] do not decouple the control problem in and out of the equatorial plane. They deal directly with the discrete system (5.100) obtained by discretization of the continuous dynamics (5.101) with sampling interval $h = 12$ minutes. They find a steady state feedback control law minimizing the performance index

$$J = \frac{1}{2}\sum_{k=0}^{\infty}\left[\boldsymbol{\xi}(k)^{T}\boldsymbol{Q}\boldsymbol{\xi}(k) + \boldsymbol{\eta}(k)^{T}\boldsymbol{R}\boldsymbol{\eta}(k)\right]. \tag{5.119}$$

Matrix $\boldsymbol{Q}$ is a diagonal matrix with (nondimensional) weights of 100 for the displacement variables and 10 for the velocity variables. Matrix $\boldsymbol{R}$ is also a diagonal matrix with (nondimensional) weights

of 10^{11} for all Δv_t control variables. The state feedback control in terms of Δv_t is a posteriori carried into effect by a set of electric propulsion thrusters that operate in an on off mode with constant thrust magnitude. Once the amount of each Δv_t component found and the spacecraft mass and the thrust levels F_{X_G}, F_{Y_G}, F_{Z_G} of the thrusters mounted along X_G, Y_G, Z_G axes known, the actual thrust intervals are calculated with the following approximations

$$T_{mX_G} \approx m\frac{\Delta v_{tX_G}}{F_{X_G}}, \quad T_{mY_G} \approx m\frac{\Delta v_{tY_G}}{F_{Y_G}}, \quad T_{mZ_G} \approx m\frac{\Delta v_{tZ_G}}{F_{Z_G}}. \tag{5.120}$$

To obtain simulation results investigating the SK maneuvers about the nominal geostationary target orbit, [Kluever and Tanck, 1997] do not use a dynamical model taking into account the environmental perturbing accelerations. The effect of these last ones is taken into account only by the off target initial conditions of the spacecraft state vector at the beginning of a sequence of 100 station keeping cycles. Actually the validation is performed with an unreal spacecraft model, which left the counteracted perturbations out of consideration.

5.5.3.1 An Example

With the Matlab function *lqr* we have designed a linear quadratic state feedback regulator

$$\boldsymbol{a}_t = -\boldsymbol{K}_\infty \boldsymbol{\xi} \tag{5.121}$$

for the continuous model

$$\frac{d\boldsymbol{\xi}}{dt} = \boldsymbol{A}_{CW}\boldsymbol{\xi} + \boldsymbol{B}_{CW}\boldsymbol{a_t} \tag{5.122}$$

The gain matrix $\boldsymbol{K}_\infty$ has been obtained minimizing the quadratic cost function

$$J = \int_0^\infty \left(\boldsymbol{\xi}^T \boldsymbol{Q}\boldsymbol{\xi} + \boldsymbol{a}_t^T \boldsymbol{R}\boldsymbol{a}_t\right) dt \tag{5.123}$$

with

$$\boldsymbol{Q} = \begin{bmatrix} 100\boldsymbol{I}_{3\times3} & \boldsymbol{0}_{3\times3} \\ \boldsymbol{0}_{3\times3} & 10\boldsymbol{I}_{3\times3} \end{bmatrix} \quad \text{and} \quad \boldsymbol{R} = \boldsymbol{I}_{3\times3}. \tag{5.124}$$

The gain results approximatively as follows

$$\boldsymbol{K}_\infty \approx \begin{bmatrix} 88.6 & -9.68 & 0 & 7.54 & 4.41 & 0 \\ 150 & -2.5 & 0 & 4.41 & 9.82 & 0 \\ 0 & 0 & 1.24 & 0 & 0 & 3.53 \end{bmatrix}. \tag{5.125}$$

In Fig.s 5.19 and 5.20 we have plotted the 3-D trajectory (x_G vs y_G vs z_G) and the velocity vector tip trace ($\dot{x}_G$ vs $\dot{y}_G$ vs $\dot{z}_G$) of a spacecraft with mass $m = 4500$ kg obtained integrating over four weeks the differential equations

$$\frac{d\boldsymbol{\xi}}{dt} = \left(\boldsymbol{A}_{CW} - \boldsymbol{B}_{CW}\boldsymbol{K}_\infty\right)\boldsymbol{\xi} + \boldsymbol{B}_{CW}\boldsymbol{a_d} \tag{5.126}$$

with initial conditions

$$\boldsymbol{\xi}(t_0) = \begin{bmatrix} x_G(t_0) \\ y_G(t_0) \\ z_G(t_0) \\ \dot{x}_G(t_0) \\ \dot{y}_G(t_0) \\ \dot{z}_G(t_0) \end{bmatrix} = \begin{bmatrix} 100 \text{ m} \\ 0 \\ 100 \text{ m} \\ 0 \\ -3.75 \times 10^{-3} \text{ m/s} \\ 0 \end{bmatrix} \tag{5.127}$$

at the initial epoch $t_0 = 0$ corresponding to the date 2010 January 1.0 and subject to the environmental perturbing acceleration vector

$$\boldsymbol{a}_d(x_G, y_G, z_G, t) = \boldsymbol{a}_g(x_G, y_G, z_G, t) + \boldsymbol{a}_a(x_G, y_G, z_G, t) + \boldsymbol{a}_p(x_G, y_G, z_G, t). \tag{5.128}$$

The inertial Cartesian components of the Earth's gravity acceleration $\boldsymbol{a}_g$ (see Table 3.2), of the Sun's and Moon's gravity acceleration $\boldsymbol{a}_a$ (see Table 3.3) and of the solar radiation pressure $\boldsymbol{a}_p$ (see Table 3.4) have been transformed in geostationary CW Cartesian components using the conversion formula

$$\begin{bmatrix} x \\ y \\ z \end{bmatrix} = \boldsymbol{\mathcal{R}}_Z^T(\Theta + \lambda_s) \left(\begin{bmatrix} x_G \\ y_G \\ z_G \end{bmatrix} + \begin{bmatrix} a_k \\ 0 \\ 0 \end{bmatrix} \right), \tag{5.129}$$

which is the inverse of Eq. (2.12) at page 60.

In Fig. 5.21 we have drawn the spacecraft state vector components respectively in the phase planes $(x_G, \dot{x}_G)$, $(y_G, \dot{y}_G)$ and $(z_G, \dot{z}_G)$.

In Fig.s 5.22–5.24 we have plotted both the spacecraft state vector components (black) obtained over four weeks with the previous LQ state feedback controller and those ones (gray) obtained over one week without any control action.

In Fig. 5.25 the three components of the control vector $\boldsymbol{a}_t = -\boldsymbol{K}_\infty \boldsymbol{\xi}$ (along the X_G, Y_G and Z_G axes) have been plotted after having been multiplied by the mass value in order to evaluate the control in terms of milli Newton.

The above linear quadratic regulator gives a closed loop control law able to keep the spacecraft position in a confined area around the nominal station keeping position. However, it solves a problem without constraints. Neither specific orbital requirements on the state variable $\boldsymbol{\xi}$ nor specific technological requirements on the control variable $\boldsymbol{a}_t$ have been taken into account in the control problem formulation. In the next chapters we will face up to this drawback choosing an open loop control approach which will lead to formulate and solve a set of optimization problems taking into account constraints.

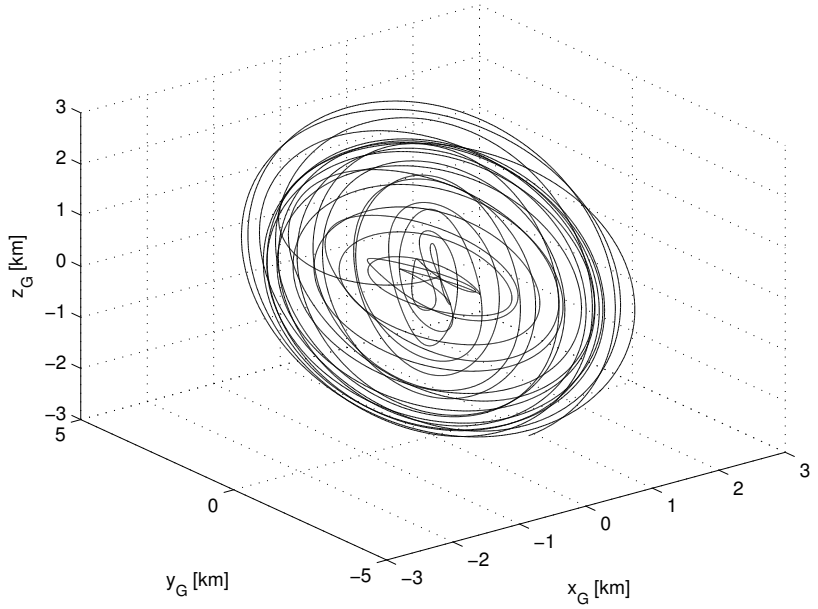

Figure 5.19: *Spacecraft trajectory (x_G vs y_G vs z_G) obtained integrating over four weeks the CW equations with an LQ regulator as thrust control action ($\boldsymbol{a}_t = -\boldsymbol{K}_\infty \boldsymbol{\xi}$).*

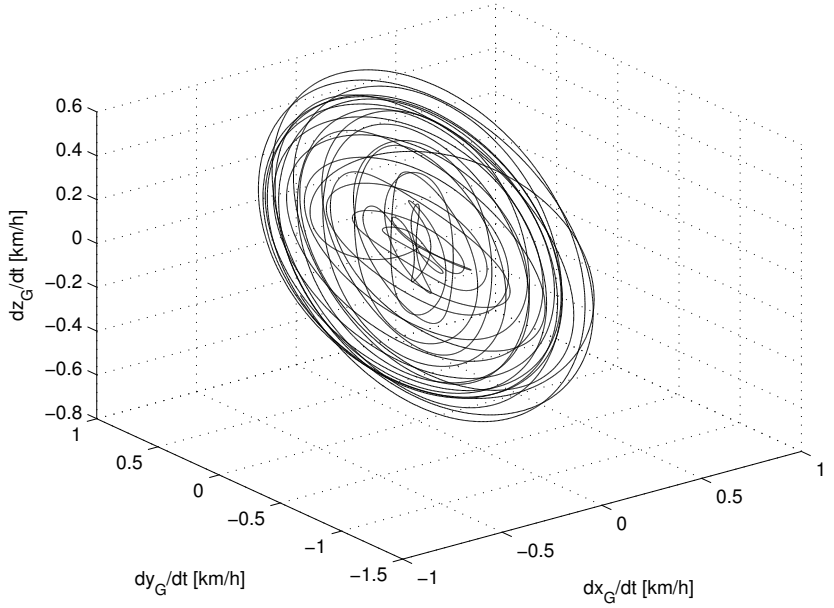

Figure 5.20: *Spacecraft velocity vector tip trace ($\dot{x}_G$ vs $\dot{y}_G$ vs $\dot{z}_G$) obtained integrating over four weeks the CW equations with an LQ regulator as thrust control action ($\boldsymbol{a}_t = -\boldsymbol{K}_\infty \boldsymbol{\xi}$).*

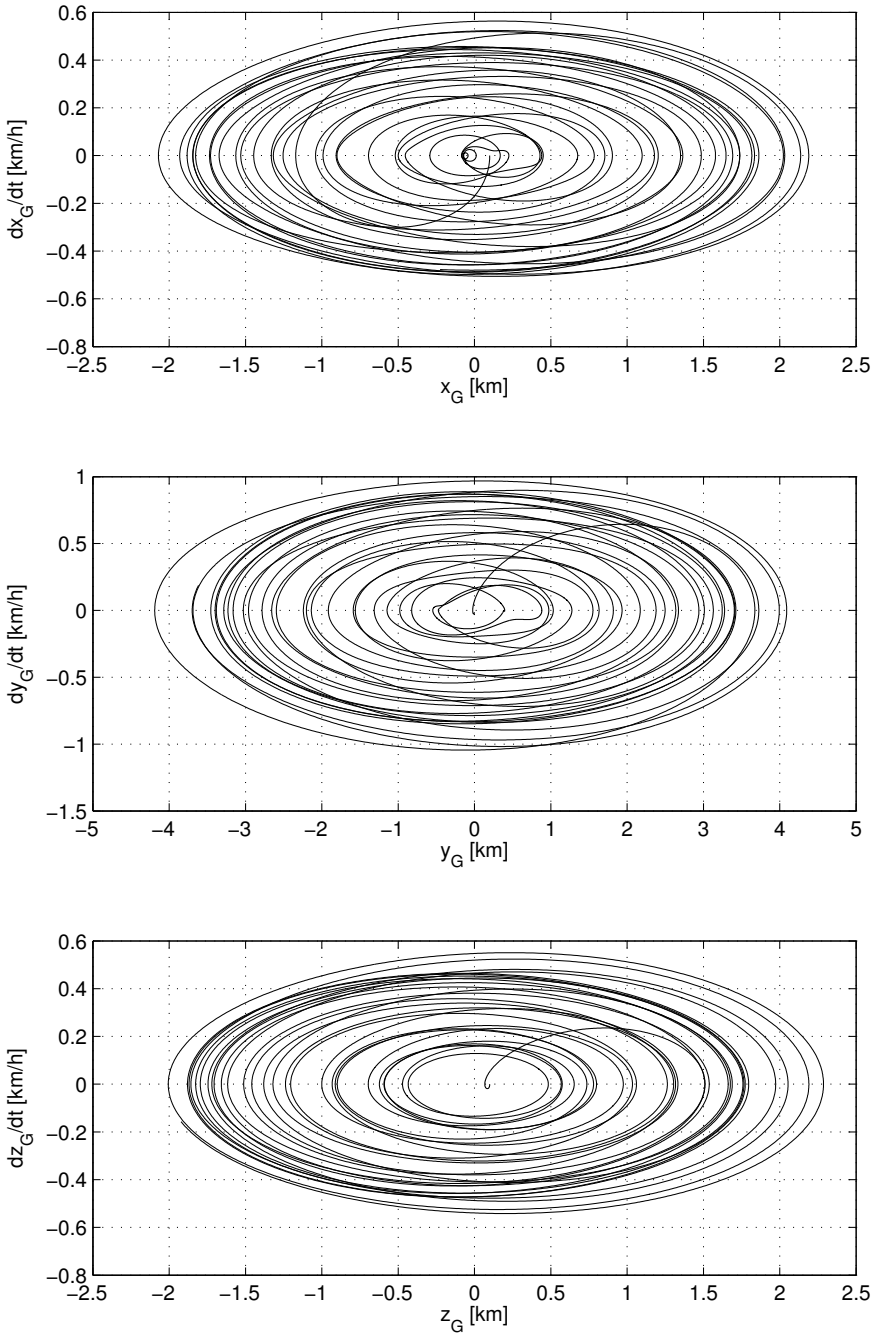

Figure 5.21: *State vector components drawn in the phase planes* $(x_G, \dot{x}_G)$, $(y_G, \dot{y}_G)$ *and* $(z_G, \dot{z}_G)$, *obtained integrating the CW equations over four weeks with an LQ regulator as thrust control action* ($\boldsymbol{a}_t = -\boldsymbol{K}_\infty \boldsymbol{\xi}$).

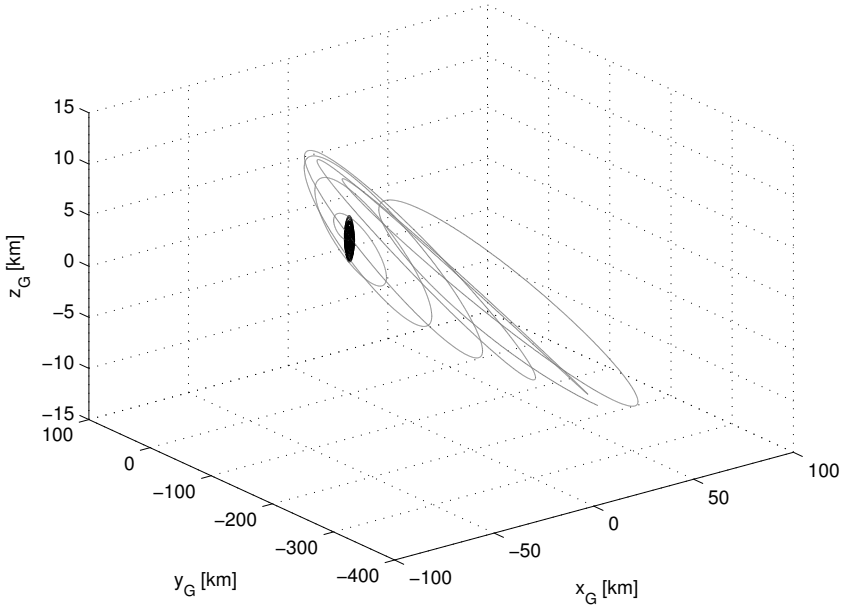

Figure 5.22: *Spacecraft state vector components (black) obtained over four weeks with the LQ state feedback controller above found and those ones (gray) obtained over one week without any control action (x_G vs y_G vs z_G).*

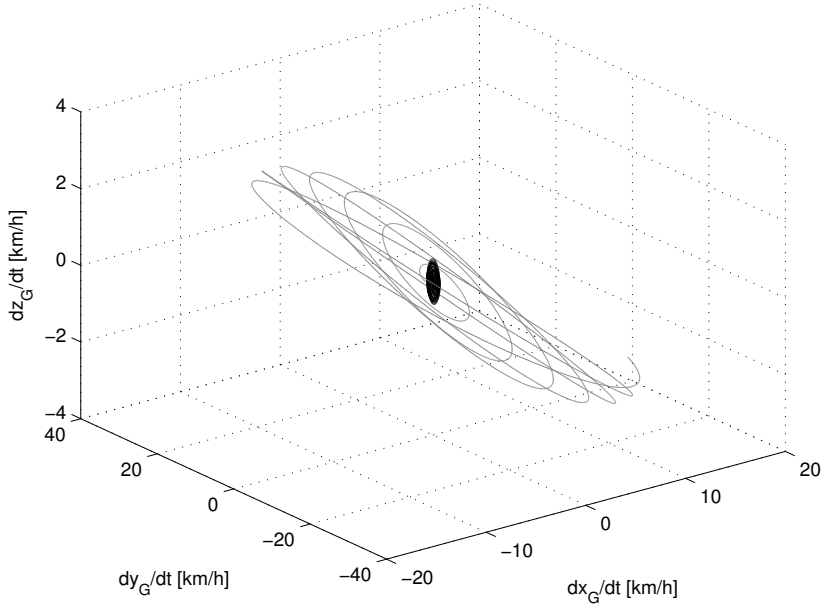

Figure 5.23: *Spacecraft state vector components (black) obtained over four weeks with the LQ state feedback controller above found and those ones (gray) obtained over one week without any control action ($\dot{x}_G$ vs $\dot{y}_G$ vs $\dot{z}_G$).*

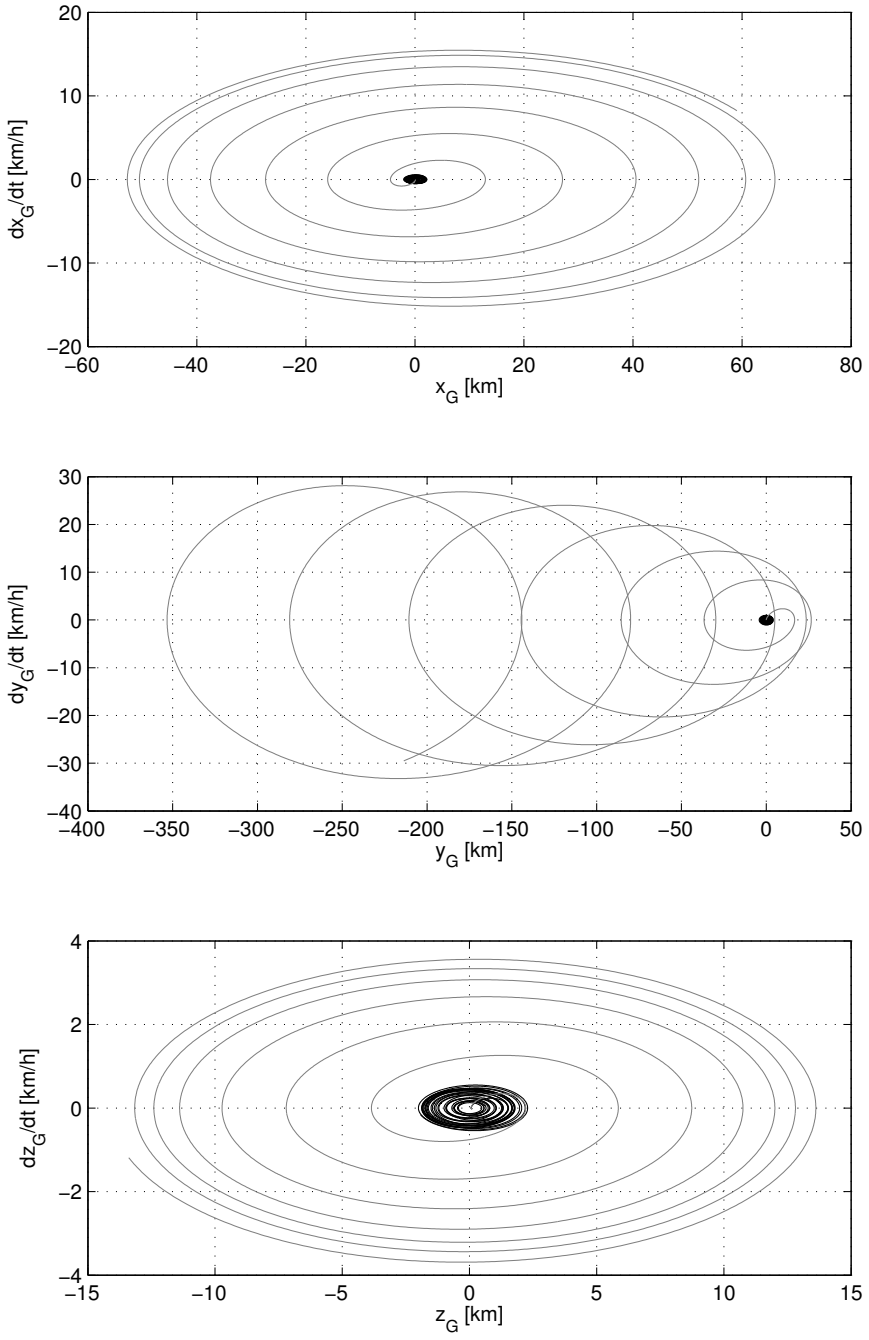

Figure 5.24: *Spacecraft state vector components (black) obtained over four weeks with the LQ state feedback controller above found and those ones (gray) obtained over one week without any control action ($\dot{x}_G$ vs x_G, $\dot{y}_G$ vs y_G, $\dot{z}_G$ vs z_G).*

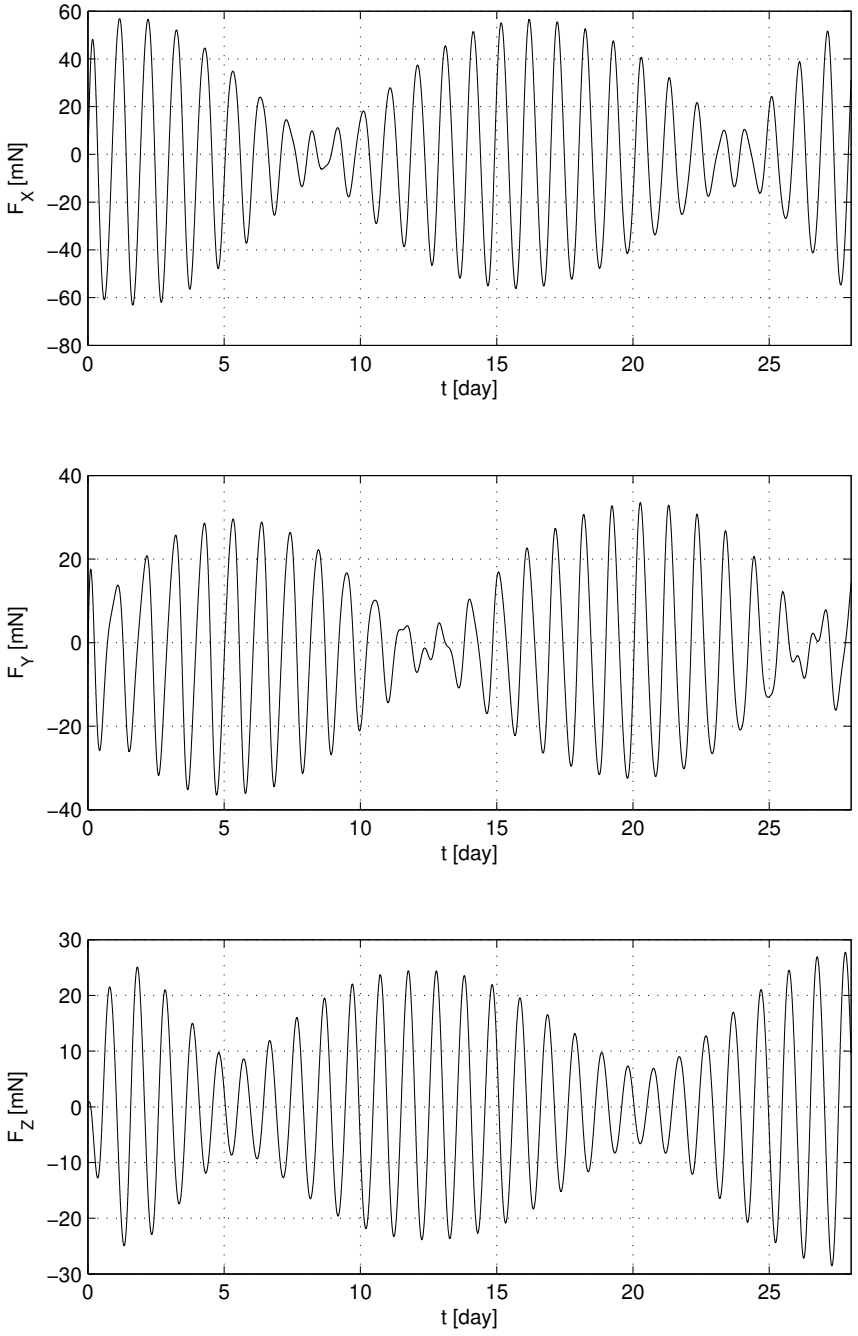

Figure 5.25: *Components along the X_G, Y_G and Z_G axes of the control force vector ($\boldsymbol{F}_t = m\boldsymbol{a}_t = -m\boldsymbol{K}_\infty\boldsymbol{\xi}$) in milli Newton.*

Chapter 6

Fixed and Receding Horizon Optimal SK Maneuver Planning

In this chapter we deal with the station keeping maneuver planning problem solving a sequence of optimal control problems over finite time horizons with constraints on the state variables and on the control variables. The first set of constraints is given by the mathematical translation of the mission orbital requirements. Once the spacecraft propulsion system has been chosen, the second set is given by the mathematical translation of the propulsion system technological requirements.

For a GEO spacecraft with given dry mass, orbital requirements and some possible structural requirements, we study and collate different solution results of the respective station keeping maneuver planning problems. The results depend on the propulsion system technological specifications, which introduce further requirements that have to be met in the station keeping problem. However, this last set of constraints is not taken into account in the beginning of this chapter. We consider them after having obtained an admissible comparison path only. In this context an admissible comparison path is an optimal spacecraft trajectory obtained minimizing a fuel consumption performance index, enforcing the constraints on the state variables, but not on the control variables (except when structural requirements have to be met, e.g., when it is not possible to exert a thrust in a given direction). Particular care has to be taken in building this admissible comparison path, which will be considered as very close to the global optimal one. Therefore, the introduction of the constraints on the control variables must be such that the new spacecraft trajectory moves away from the admissible comparison path as little as possible.

The method used to obtain an admissible comparison path is based on the conversion of a sequence of finite time optimal control problems (OCPs) into a sequence of parameter optimization problems (POPs). The POPs are then solved using existing optimization codes. This way of dealing with constrained optimal control problems is standard and well documented in the literature (see, e.g., [Hull, 1997], [Hull, 2003], [Goodwin et al., 2004]). This conversion approach together with the receding horizon optimization (RHO) principle is also the basis of the predictive control methods, which originated in the late seventies and have had great impact on the industrial world (see, e.g.,

[Camacho and Bordons, 1999], [Maciejowski, 2002], [Goodwin et al., 2004]). It is well known that, dealing with constrained optimal control problems formulated by means of time invariant linear models, the use of the RHO principle with respect to the fixed horizon has the advantage of allowing one to obtain time invariant control laws based always on the current value of the state variable. Unfortunately, even if formulated by means of linear versions of the spacecraft dynamical model, the SK maneuver planning problem depends always on time varying environmental perturbing forces. Consequently, the optimal control law will be always time varying. Nevertheless, the RHO principle can be used in the SK maneuver planning problem (globally formulated over a very long time horizon but solved in sequence over short sub horizons) as interesting and powerful means to find smooth optimal trajectories and control variable time histories over long time horizons. With the classical fixed horizon optimization (FHO) approach instead of the receding horizon one, the time derivative of the trajectories (i.e., the velocity) and the control variable time histories could show jumps at the beginning of each fixed time horizon. In general, as we will present in this chapter via simulation results, these jumps increase the total performance index value, i.e., the total fuel consumption over a long time horizon. The RHO approach, even if more onerous from a computing viewpoint with respect to the FHO approach, allows one to approximate the global optimal solution better.

The chapter is organized as follows.

In Section 6.1 we formulate in mathematical terms the SK maneuver planning problem under virtual technological conditions: the propulsion system is composed of six thrusters with infinite specific impulsion, orthogonally mounted along the three axes of the RTN reference frame and, at every instant, able to produce an acceleration vector with unbounded magnitude in any direction. We propose a solution based on direct transcription of the problem in terms of parameter optimization problems. In order to implement the solution with linear programming codes, we will refer to the first order Taylor's development of the nonlinear Gauss' VOP equations about the nominal station keeping trajectory; however, to validate the solution the nonlinear model will be used. This section contains also a brief state of the art about solution methods of trajectory optimization problems.

In Section 6.2 we present and discuss some simulation results of the above simplified problem, obtained with the fixed horizon optimization approach and with the receding horizon one.

In Section 6.3 we take gradually into account technological specifications relevant to the propulsion system and we perform feasibility studies in presence of new constraints on the control variables. We deal with two idealized models to describe the electrical thrusters (see also [Geffroy, 1997]). In the first model, we fix the maximum values of specific impulse and of thrust for each thruster (Limited jet Power — LP model). In the second model, we fix constant values of specific impulse and of thrust for each thruster (Constant effective Exhaust Velocity — CEV model). The first case corresponds to thrusters which are able to give thrusts that can be modulated. The latter case corresponds to thrusters which are able to work only in on off conditions. In Section 6.3 we relax the hypothesis of having six thrusters working independently, mounted orthogonally on the spacecraft

body. We try to answer the following question: do privileged thrust directions in the RTN frame exist, such that for thrusters mounted along them the number of thrusters can be reduced thanks to the fact of synchronizing the maneuvers in the three directions of the RTN reference frame?

6.1 Problem Formulation with State Constraints Only

We consider the mathematical formulation of the SK maneuver planning problem given in Section 5.3 at page 159 under some simplifying hypotheses.

➢ The state vector of the system (5.16) of nonlinear differential equations describing the translational dynamics of a GEO satellite subject to the effect of the environmental and thrust perturbing accelerations is the spacecraft state vector expressed in terms of equinoctial orbital elements

$$\boldsymbol{x} = \begin{bmatrix} a & P_1 & P_2 & Q_1 & Q_2 & l_\Theta \end{bmatrix}^T . \tag{6.1}$$

➢ The dynamics of the spacecraft state vector $\boldsymbol{x}$ is described by the nonlinear Gauss' VOP equations of motion

$$\frac{d\boldsymbol{x}}{dt} = \boldsymbol{K}(\boldsymbol{x}) - \boldsymbol{\omega}_\oplus + \boldsymbol{G}(\boldsymbol{x},t)\boldsymbol{a}_e(\boldsymbol{x},t) + \boldsymbol{G}(\boldsymbol{x},t)\boldsymbol{a}_t(t) \tag{6.2}$$

(see Section 4.2.1 at page 119). Here we prefer a model with explicit time dependence instead of a model expressing time dependence in an implicit way via the Greenwich sidereal time Θ and the number of centuries T with dynamics given by the equations (5.18) and (5.19).

➢ The acceleration vector $\boldsymbol{a}_t$ induced by the propulsion system is assumed to be generated by six ideal thrusters with infinite specific impulse and whatever thrust value mounted along the axes of the RTN reference frame. Such a system is able to produce an acceleration vector $\boldsymbol{a}_t$ with whatever modulus and direction

$$\boldsymbol{a}_t(t) = \begin{bmatrix} a_{tR}(t) \\ a_{tT}(t) \\ a_{tN}(t) \end{bmatrix} = \frac{1}{m} \begin{bmatrix} +1 & 0 & 0 & -1 & 0 & 0 \\ 0 & +1 & 0 & 0 & -1 & 0 \\ 0 & 0 & +1 & 0 & 0 & -1 \end{bmatrix} \begin{bmatrix} F_{+Z_B}(t) \\ F_{-X_B}(t) \\ F_{+Y_B}(t) \\ F_{-Z_B}(t) \\ F_{+X_B}(t) \\ F_{-Y_B}(t) \end{bmatrix} . \tag{6.3}$$

Since the specific impulses have been assumed infinite and the thrusts finite, there is no propellant mass consumption and the loaded spacecraft mass m remains constant.

Vector $\boldsymbol{a}_t$ will be considered as control variable of the following optimal control problem over a finite time horizon:

to find the control variable time history $\boldsymbol{a}_t = \boldsymbol{a}_t(t)$ over the time horizon $T_M = t_f - t_i$ minimizing the performance index

$$J = \int_{t_i}^{t_f} \boldsymbol{a}_t^T(t)\boldsymbol{a}_t(t)dt = \int_{t_i}^{t_f} \left[a_{tR}^2(t) + a_{tT}^2(t) + a_{tN}^2(t)\right] dt, \tag{6.4}$$

subject to the differential constraints

$$\frac{d\boldsymbol{x}}{dt} = \boldsymbol{K}(\boldsymbol{x}) - \boldsymbol{\omega}_\oplus + \boldsymbol{G}(\boldsymbol{x},t)\boldsymbol{a}_e(\boldsymbol{x},t) + \boldsymbol{G}(\boldsymbol{x},t)\boldsymbol{a}_t(t), \quad \boldsymbol{x}(t_i) = \boldsymbol{x}_i \tag{6.5}$$

and to the state inequality constraints

$$\begin{cases} \lambda(\boldsymbol{x},t) - \lambda_{max} \leq 0 \\ \lambda(\boldsymbol{x},t) + \lambda_{max} \geq 0 \end{cases} \tag{6.6}$$

$$\begin{cases} \varphi(\boldsymbol{x},t) - \varphi_{max} \leq 0 \\ \varphi(\boldsymbol{x},t) + \varphi_{max} \geq 0 \end{cases} \tag{6.7}$$

where

$$\lambda(\boldsymbol{x},t) = -2\cos(l_\Theta + \Theta)P_1 + 2\sin(l_\Theta + \Theta)P_2 + l_\Theta \tag{6.8}$$

$$\varphi(\boldsymbol{x},t) = -2\cos(l_\Theta + \Theta)Q_1 + 2\sin(l_\Theta + \Theta)Q_2 \tag{6.9}$$

and

$$\Theta = \omega_\oplus t + (\Theta_r - \omega_\oplus t_r)\,. \tag{6.10}$$

If it is not possible to exert any thrust in a given direction because of particular structural requirements, further inequality constraints on some control variable components have to be met. For example, if no thrusters can be mounted on the nadir face (the face towards the Earth), the radial control variable component is subject to the inequality constraint

$$a_{tR}(t) \leq 0. \tag{6.11}$$

The first idea would be that of converting this nonlinear optimal control problem into a parameter optimization problem and solving it using existing nonlinear programming codes. However, since the task consists in keeping the spacecraft position in a narrow box of the (λ, φ) plane, before converting the nonlinear differential constraints (6.5) and inequality constraints (6.6)–(6.7), we compare the solutions of their numerical integration with those of a numerical integration of a corresponding linearized version. If the difference between them is small with respect to the deadband box dimensions, it will be reasonable to formulate the parameter optimization problem as a linear POP and to solve it by means of linear optimization tools, which offer very good speed and convergence properties. In Section 6.1.1 we give a brief state of the art of the direct methods of solution of trajectory optimization problems. In Section 6.1.2 we present a linear model of the GEO spacecraft dynamics, which is obtained developing in Taylor's series up to the first order the nonlinear dynamics around the nominal station keeping trajectory. Finally, in Section 6.1.3 we formulate the station keeping problem as linear parameter optimization problem.

6.1.1 Direct Methods to Find Optimal Trajectories: State of the Art

Essentially, two approaches have emerged over the past forty years to solve optimal trajectory problems. In the first (also called indirect solution methods) the necessary conditions for optimality are derived using calculus of variations techniques. The resulting two point boundary value problem is solved numerically, where some sort of discretization is introduced. In the second (also called direct solution methods) the necessary conditions for the optimality are not explicitly employed. They approximate the continuous optimal control problem with a parameter optimization problem requiring mathematical programming for solution. These last methods have been discussed in the literature, developed over a long period of time and by different researchers: [Hargraves and Paris, 1987], [Enright and Conway, 1991], [von Stryk, 1993], [Seywald, 1994], [Scheel and Conway, 1994], [Tang and Conway, 1995], [Kumar and Seywald, 1996], [Conway and Larson, 1998], [Petit et al., 2001], [Murray et al., 2001], [Petit et al., 2002], [Neckel et al., 2003]. In this section we take up the synthetic explanation given by [Hull, 2003], who presents direct methods from a single viewpoint.

Direct methods to determine optimal trajectories are based on the conversion of an optimal control problem in a parameter optimization problem. The baseline optimal control problem is to find the design parameter vector $\boldsymbol{p}$ and the control time history $\boldsymbol{u}(t)$ that minimize the scalar performance index

$$J = J(\boldsymbol{x}_f, \boldsymbol{p}) \tag{6.12}$$

subject to the differential constraints

$$\frac{d\boldsymbol{x}}{dt} = \boldsymbol{f}(\boldsymbol{x}, \boldsymbol{u}, \boldsymbol{p}, t), \tag{6.13}$$

the prescribed initial conditions $\boldsymbol{x}(t_i) = \boldsymbol{x}_i$ and the prescribed final conditions at a fixed final time t_f

$$\boldsymbol{x}(t_f) = \boldsymbol{x}_f, \quad \boldsymbol{\psi}_E(\boldsymbol{x}_f, \boldsymbol{p}) = \boldsymbol{0}, \quad \boldsymbol{\psi}_I(\boldsymbol{x}_f, \boldsymbol{p}) \geq \boldsymbol{0}. \tag{6.14}$$

A problem with free final time can be transformed into this format by normalizing the time, considering $t_f = 1$ and the actual final time as one of the components of the design parameter vector $\boldsymbol{p}$.

The conversion of this optimal control problem into a parameter optimization problem begins with the definition of N fixed time instants

$$t_i = t_0 < t_1 < \cdots < t_k < \cdots < t_{N-1} < t_N = t_f \tag{6.15}$$

called nodes, which may or may not be equally spaced depending on the problem characteristics. Then, the functions of time $\boldsymbol{u}(t)$ and $\boldsymbol{x}(t)$ are replaced by their values at the nodes $\boldsymbol{u}_k = \boldsymbol{u}(t_k)$ and $\boldsymbol{x}_k = \boldsymbol{x}(t_k)$. The unknowns of the parameter optimization problem are the design parameter vector $\boldsymbol{p}$ and some combination of the control parameters $\boldsymbol{u}_k$ and/or the state parameters $\boldsymbol{x}_k$. Denoting

by $\boldsymbol{\mathcal{P}}$ the vector of the unknown parameters, the corresponding parameter optimization problem is to find the value of $\boldsymbol{\mathcal{P}}$ that minimizes the scalar performance index

$$J = J\left(\boldsymbol{\mathcal{P}}\right), \tag{6.16}$$

subject to the equality constraints

$$\boldsymbol{\Psi}_E\left(\boldsymbol{\mathcal{P}}\right) = \mathbf{0}, \tag{6.17}$$

and to the inequality constraints

$$\boldsymbol{\psi}_I\left(\boldsymbol{\mathcal{P}}\right) \geq \mathbf{0}. \tag{6.18}$$

The function $\boldsymbol{\Psi}_E$ contains $\boldsymbol{\psi}_E$, but it may also contain equality constraints imposed by the numerical integration of the differential equality constraints (6.13). In general the solution process is to guess values for the unknown parameters and to use a nonlinear programming code in order to find the values of the parameters that minimize the performance index and satisfy the constraints.

The optimal control problem can be made more complicated by including a free initial point with equality and inequality constraints, internal points with equality and inequality constraints, integral constraints, path equality constraints and path inequality constraints (see, e.g., the inequality constraints (6.6)–(6.7) on the longitude and latitude in the SK optimal control problem formulation). In all cases, the conversion into a parameter optimization problem is always possible. Path constraints can be imposed at each node. However, if a path constraint is in effect at several consecutive nodes, it is not, in general, satisfied between the nodes. Satisfaction can be improved by adding more nodes in this area.

[Hull, 1997] categorizes the existing methods for converting optimal control problems into parameter optimization problems by the unknown parameter type, the numerical integration technique, and the order of integration technique. He specifies four general classes of methods. The unknowns in each class are 1) the control parameters $\boldsymbol{u}_k$, 2) the control parameters $\boldsymbol{u}_k$ and some state parameters $\boldsymbol{x}_k$, 3) the control parameters and the state parameters $\boldsymbol{x}_k$, 4) the state parameters $\boldsymbol{x}_k$ only. In methods of class 1) and 2), the state differential equations (6.5) are integrated by explicit numerical integration. In methods of class 3) and 4), implicit numerical integration is used. In the explicit methods, at each time where the function $\boldsymbol{f}$ is evaluated, the value of $\boldsymbol{x}$ is known. In the implicit methods the value of $\boldsymbol{x}$ needed for evaluating $\boldsymbol{f}$ is not known and in order to perform one integration step, a predictor corrector approach must be used. All orders of numerical integration can be used in each method.

6.1.2 Linear Translational Dynamics of GEO Spacecraft

The goal of this section is twofold. First, we deduce from the nonlinear Gauss' VOP equations a continuous time linear model describing the translational dynamics of a GEO satellite which has to be kept confined in a latitude and longitude station keeping box. Second, we obtain a discrete time version of this linear model. We will use this discrete time linear model to solve the SK maneuver

planning problem via parameter optimization problem solutions. This discrete time linear model is validated evaluating the linearization and discretization errors. The length of the discretization time interval will be chosen depending on the latitude and longitude deadbands.

We denote the thrust acceleration vector $\boldsymbol{a}_t$ (which is the control variable of the SK optimal control problem) as $\boldsymbol{u}$. We develop the right-hand side of the nonlinear Gauss' VOP equations (6.5) up to the first order around the Keplerian nominal station keeping state vector

$$\boldsymbol{x}_{Ksk} = \begin{bmatrix} a_k & 0 & 0 & 0 & 0 & \lambda_s \end{bmatrix}^T \tag{6.19}$$

and around the control vector with all the components equal to zero

$$\boldsymbol{u}_{sk} = \begin{bmatrix} a_{tRsk} & a_{tTsk} & a_{tNsk} \end{bmatrix}^T = \boldsymbol{0}_{3\times 1}. \tag{6.20}$$

We obtain a first order approximated translational dynamics described by the time varying linear model

$$\frac{d\boldsymbol{x}}{dt} = \boldsymbol{A}(t)\left(\boldsymbol{x} - \boldsymbol{x}_{Ksk}\right) + \boldsymbol{B}(t)\boldsymbol{a}_{e_{sk}}(t) + \boldsymbol{B}(t)\boldsymbol{u}(t), \quad \boldsymbol{x}(t_i) = \boldsymbol{x}_i \tag{6.21}$$

where matrices $\boldsymbol{A}(t)$ and $\boldsymbol{B}(t)$ and vector $\boldsymbol{a}_{e_{sk}}(t)$ are defined as follows.

➢ Matrix $\boldsymbol{A}(t)$ is the Jacobian of the right-hand side of the nonlinear model (6.5) with respect to the state vector $\boldsymbol{x}$ and evaluated in $(\boldsymbol{x}, \boldsymbol{u}) = (\boldsymbol{x}_{Ksk}, \boldsymbol{u}_{sk})$:

$$\boldsymbol{A}(t) = \boldsymbol{A}_K + \boldsymbol{A}_e(t), \tag{6.22}$$

where

$$\boldsymbol{A}_K = \left[\boldsymbol{\nabla}_{EOE}\left[\boldsymbol{K}(\boldsymbol{x})\right]\right]_{\boldsymbol{x}=\boldsymbol{x}_{Ksk}} = \begin{bmatrix} \boldsymbol{0}_{5\times 1} & \boldsymbol{0}_{5\times 5} \\ -\frac{3}{2}\frac{n_k}{a_k} & \boldsymbol{0}_{1\times 5} \end{bmatrix} \tag{6.23}$$

with the nominal station keeping mean motion given by $n_k = \omega_\oplus$, and

$$\boldsymbol{A}_e(t) = \left[\boldsymbol{\nabla}_{EOE}\left[\boldsymbol{G}(\boldsymbol{x}, t)\boldsymbol{a}_e(\boldsymbol{x}, t)\right]\right]_{\boldsymbol{x}=\boldsymbol{x}_{Ksk}}. \tag{6.24}$$

➢ Matrix $\boldsymbol{B}(t)$ is the Jacobian of the right-hand side of the nonlinear model (6.5) with respect to the control vector $\boldsymbol{u}$ and evaluated in $(\boldsymbol{x}, \boldsymbol{u}) = (\boldsymbol{x}_{Ksk}, \boldsymbol{u}_{sk})$:

$$\boldsymbol{B}(t) = \boldsymbol{G}(\boldsymbol{x}_{Ksk}, t) = \frac{1}{v_{sk}} \begin{bmatrix} 0 & 2a_k & 0 \\ -\cos K_{sk} & 2\sin K_{sk} & 0 \\ \sin K_{sk} & 2\cos K_{sk} & 0 \\ 0 & 0 & \frac{1}{2}\sin K_{sk} \\ 0 & 0 & \frac{1}{2}\cos K_{sk} \\ -2 & 0 & 0 \end{bmatrix} \tag{6.25}$$

where v_{sk} is the nominal station keeping velocity of a GEO satellite

$$v_{sk} = \omega_\oplus a_k \approx 3.075 \quad \text{km/s}, \tag{6.26}$$

and K_{sk} is the nominal station keeping eccentric longitude, obtained replacing in the Kepler's equation (4.66) the nominal station keeping values of mean longitude ($l_\Theta = \lambda_s$) and eccentricity components ($P_1 = 0$, $P_2 = 0$)

$$K_{sk}(t) = \lambda_s + \Theta(t) \tag{6.27}$$

with

$$\Theta = \omega_\oplus t + (\Theta_r - \omega_\oplus t_r)\,. \tag{6.28}$$

➢ Vector $\boldsymbol{a}_{e_{sk}}(t)$ is the nominal environmental acceleration vector, i.e., the total environmental perturbing acceleration vector

$$\boldsymbol{a}_e(\boldsymbol{x}, t) = \boldsymbol{a}_g(\boldsymbol{x}, t) + \boldsymbol{a}_a(\boldsymbol{x}, t) + \boldsymbol{a}_p(\boldsymbol{x}, t) \tag{6.29}$$

evaluated in $\boldsymbol{x} = \boldsymbol{x}_{Ksk}$

$$\boldsymbol{a}_{e_{sk}}(t) = \boldsymbol{a}_e(\boldsymbol{x}_{Ksk}, t). \tag{6.30}$$

The nominal station keeping acceleration vector $\boldsymbol{a}_{e_{sk}}$ is the sum of the three following nominal acceleration contributions

$$\boldsymbol{a}_{g_{sk}} = \boldsymbol{\mathcal{R}}_{ZXZ_{sk}} \begin{bmatrix} a_{gX_{sk}} & a_{gY_{sk}} & a_{gZ_{sk}} \end{bmatrix}^T, \tag{6.31}$$

$$\boldsymbol{a}_{a_{sk}} = \boldsymbol{\mathcal{R}}_{ZXZ_{sk}} \begin{bmatrix} a_{aX_{sk}} & a_{aY_{sk}} & a_{aZ_{sk}} \end{bmatrix}^T, \tag{6.32}$$

$$\boldsymbol{a}_{p_{sk}} = \boldsymbol{\mathcal{R}}_{ZXZ_{sk}} \begin{bmatrix} a_{pX_{sk}} & a_{pY_{sk}} & a_{pZ_{sk}} \end{bmatrix}^T. \tag{6.33}$$

Matrix $\boldsymbol{\mathcal{R}}_{ZXZ_{sk}}$ is the rotation matrix in nominal station keeping conditions

$$\boldsymbol{\mathcal{R}}_{ZXZsk} = \begin{bmatrix} \cos K_{sk} & \sin K_{sk} & 0 \\ -\sin K_{sk} & \cos K_{sk} & 0 \\ 0 & 0 & 1 \end{bmatrix} \tag{6.34}$$

(see Section 2.3.4). The acceleration components with indexes X_{sk}, Y_{sk}, Z_{sk}, are those ones in the ECI reference frame and they are deduced from the formulas (3.26)–(3.28), (3.65)–(3.67), (3.91)–(3.93), with the expressions given in Tables 3.2, 3.3, 3.4 evaluated in the nominal station keeping inertial Cartesian coordinates

$$x_{sk}(t) = a_k \cos K_{sk}(t), \quad y_{sk}(t) = a_k \sin K_{sk}(t), \quad z_{sk} = 0. \tag{6.35}$$

Analytical expressions of the radial, tangent and normal components of the nominal accelerations are given in Table 6.1 for the Earth's gravity attraction, in Table 6.2 for the Sun's and Moon's gravity attraction, in Table 6.3 for the solar radiation pressure.

In the RTN reference frame, the components of the nominal acceleration vector induced by the Earth's gravity attraction are constant over time. Their constant values depend on the station longitude value λ_s. In Fig. 6.1 each component is plotted in function of λ_s.

Fig.s (6.2)–(6.4) show the time histories of the RTN components of the $\boldsymbol{a}_{e_{sk}}$ vector over time intervals equal respectively to one week, one month and one year.

a_{gRsk}	$GM_{\oplus}\left(R_{\oplus}^{2}a_{gRsk20}+R_{\oplus}^{2}a_{gRsk22}+R_{\oplus}^{3}a_{gRsk30}+R_{\oplus}^{3}a_{gRsk31}+R_{\oplus}^{3}a_{gRsk32}+R_{\oplus}^{3}a_{gRsk33}\right)$
a_{gTsk}	$GM_{\oplus}\left(R_{\oplus}^{2}a_{gRsk20}+R_{\oplus}^{2}a_{gTsk22}+R_{\oplus}^{3}a_{gTsk30}+R_{\oplus}^{3}a_{gTsk31}+R_{\oplus}^{3}a_{gTsk32}+R_{\oplus}^{3}a_{gTsk33}\right)$
a_{gNsk}	$GM_{\oplus}\left(R_{\oplus}^{2}a_{gNsk20}+R_{\oplus}^{2}a_{gNsk22}+R_{\oplus}^{3}a_{gNsk30}+R_{\oplus}^{3}a_{gNsk31}+R_{\oplus}^{3}a_{gNsk32}+R_{\oplus}^{3}a_{gNsk33}\right)$
a_{gRsk20}	$\frac{3C_{20}}{2a_k^4}$
a_{gTsk20}	0
a_{gNsk20}	0
a_{gRsk22}	$\frac{-9C_{22}\cos(2\lambda_s)-9S_{22}\sin(2\lambda_s)}{a_k^4}$
a_{gTsk22}	$\frac{-6C_{22}\sin(2\lambda_s)+6S_{22}\cos(2\lambda_s)}{a_k^4}$
a_{gNsk22}	0
a_{gRsk30}	0
a_{gTsk30}	0
a_{gNsk30}	$-\frac{3C_{30}}{2a_k^5}$
a_{gRsk31}	$\frac{6C_{31}\cos\lambda_s+6S_{31}\sin\lambda_s}{a_k^5}$
a_{gTsk31}	$\frac{3C_{31}\sin\lambda_s-3S_{31}\cos\lambda_s}{2a_k^5}$
a_{gNsk31}	0
a_{gRsk32}	0
a_{gTsk32}	0
a_{gNsk32}	$\frac{15C_{32}\cos(2\lambda_s)+15S_{32}\sin(2\lambda_s)}{a_k^5}$
a_{gRsk33}	$\frac{-60C_{33}\cos(3\lambda_s)-60S_{33}\sin(3\lambda_s)}{a_k^5}$
a_{gTsk33}	$\frac{-45C_{33}\sin(3\lambda_s)+45S_{33}\cos(3\lambda_s)}{a_k^5}$
a_{gNsk33}	0

Table 6.1: *Analytical expressions of radial, tangent and normal components of the nominal acceleration induced by the Earth's gravity attraction.*

a_{aRsk}	$GM_{\odot}a_{aRsk\odot} + GM_{\circledcirc}a_{aRsk\circledcirc}$
a_{aTsk}	$GM_{\odot}a_{aTsk\odot} + GM_{\circledcirc}a_{aTsk\circledcirc}$
a_{aNsk}	$GM_{\odot}a_{aNsk\odot} + GM_{\circledcirc}a_{aNsk\circledcirc}$
$a_{aRsk\odot}$	$\frac{x_S\cos K_{sk}+y_S\sin K_{sk}-a_k}{\sqrt{\left[(x_S-a_k\cos K_{sk})^2+(y_S-a_k\sin K_{sk})^2+z_S^2\right]^3}} - \frac{x_S\cos K_{sk}+y_S\sin K_{sk}}{\sqrt{(x_S^2+y_S^2+z_S^2)^3}}$
$a_{aRsk\circledcirc}$	$\frac{x_M\cos K_{sk}+y_M\sin K_{sk}-a_k}{\sqrt{\left[(x_M-a_k\cos K_{sk})^2+(y_M-a_k\sin K_{sk})^2+z_M^2\right]^3}} - \frac{x_M\cos K_{sk}+y_M\sin K_{sk}}{\sqrt{(x_M^2+y_M^2+z_M^2)^3}}$
$a_{aTsk\odot}$	$\frac{y_S\cos K_{sk}-x_S\sin K_{sk}}{\sqrt{\left[(x_S-a_k\cos K_{sk})^2+(y_S-a_k\sin K_{sk})^2+z_S^2\right]^3}} - \frac{y_S\cos K_{sk}-x_S\sin K_{sk}}{\sqrt{(x_S^2+y_S^2+z_S^2)^3}}$
$a_{aTsk\circledcirc}$	$\frac{y_M\cos K_{sk}-x_M\sin K_{sk}}{\sqrt{\left[(x_M-a_k\cos K_{sk})^2+(y_M-a_k\sin K_{sk})^2+z_M^2\right]^3}} - \frac{y_M\cos K_{sk}-x_M\sin K_{sk}}{\sqrt{(x_M^2+y_M^2+z_M^2)^3}}$
$a_{aNsk\odot}$	$\frac{z_S}{\sqrt{\left[(x_S-a_k\cos K_{sk})^2+(y_S-a_k\sin K_{sk})^2+z_S^2\right]^3}} - \frac{z_S}{\sqrt{(x_S^2+y_S^2+z_S^2)^3}}$
$a_{aNsk\circledcirc}$	$\frac{z_M}{\sqrt{\left[(x_M-a_k\cos K_{sk})^2+(y_M-a_k\sin K_{sk})^2+z_M^2\right]^3}} - \frac{z_M}{\sqrt{(x_M^2+y_M^2+z_M^2)^3}}$

Table 6.2: *Analytical expressions of the radial, tangent and normal components of the nominal acceleration induced by the Sun's and Moon's gravity attraction.*

a_{pRsk}	$-C_RP_{\odot}\frac{S}{m}\frac{x_S\cos K_{sk}+y_S\sin K_{sk}-a_k}{\sqrt{(x_S-a_k\cos K_{sk})^2+(y_S-a_k\sin K_{sk})^2+z_S^2}}$
a_{pTsk}	$-C_RP_{\odot}\frac{S}{m}\frac{y_S\cos K_{sk}-x_S\sin K_{sk}}{\sqrt{(x_S-a_k\cos K_{sk})^2+(y_S-a_k\sin K_{sk})^2+z_S^2}}$
a_{pNsk}	$-C_RP_{\odot}\frac{S}{m}\frac{z_S}{\sqrt{(x_S-a_k\cos K_{sk})^2+(y_S-a_k\sin K_{sk})^2+z_S^2}}$

Table 6.3: *Analytical expressions of the radial, tangent and normal components of the nominal acceleration induced by the solar radiation pressure.*

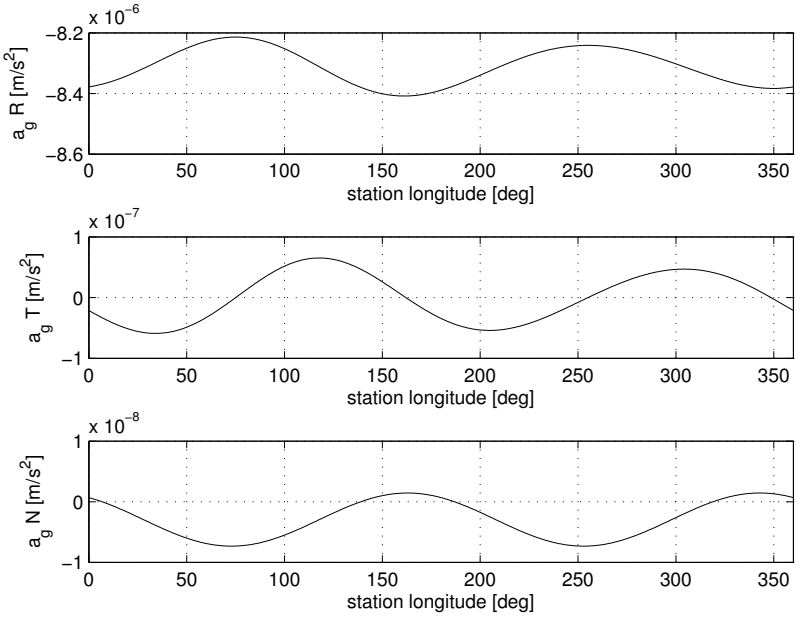

Figure 6.1: *Components (in the RTN reference frame) of the Earth's gravity attraction acceleration vector in function of the station longitude.*

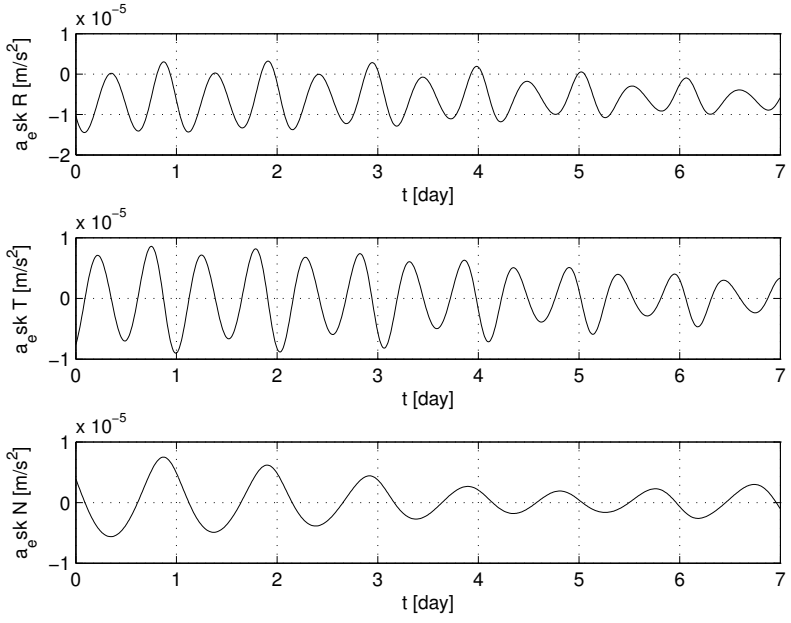

Figure 6.2: *Time histories over one week of the RTN components of the environmental perturbing acceleration vector in nominal station keeping conditions.*

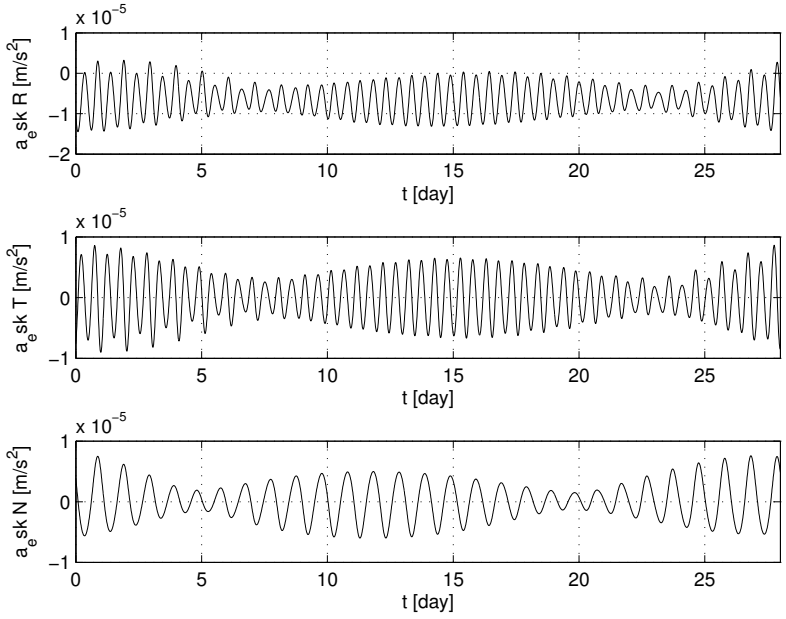

Figure 6.3: *Time histories over one month of the RTN components of the environmental perturbing acceleration vector in nominal station keeping conditions.*

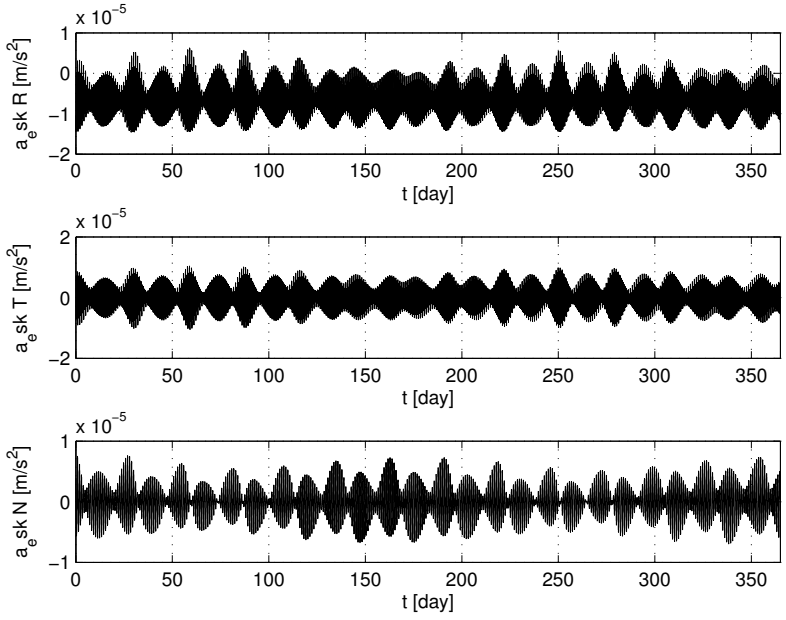

Figure 6.4: *Time histories over one year of the RTN components of the environmental perturbing acceleration vector in nominal station keeping conditions.*

We also linearize around the nominal station keeping state $\boldsymbol{x}_{Ksk}$ the spacecraft position vector expressed in geographical spherical coordinates

$$\boldsymbol{p} = \begin{bmatrix} r & \lambda & \varphi \end{bmatrix}^T, \tag{6.36}$$

which has been described in Section 4.3 as a nonlinear vectorial function of the equinoctial orbital elements and as explicitly dependent on time

$$\boldsymbol{p} = \boldsymbol{p}(\boldsymbol{x}, t) \tag{6.37}$$

with

$$\boldsymbol{x} = \begin{bmatrix} a & P_1 & P_2 & Q_1 & Q_2 & l_\Theta \end{bmatrix}^T, \tag{6.38}$$

$$\boldsymbol{p}(\boldsymbol{x}, t) = \begin{bmatrix} 1 & -a\sin(l_\Theta + \Theta) & -a\cos(l_\Theta + \Theta) & 0 & 0 & 0 \\ 0 & -2\cos(l_\Theta + \Theta) & 2\sin(l_\Theta + \Theta) & 0 & 0 & 1 \\ 0 & 0 & 0 & -2\cos(l_\Theta + \Theta) & 2\sin(l_\Theta + \Theta) & 0 \end{bmatrix} \boldsymbol{x}, \tag{6.39}$$

and

$$\Theta = \omega_\oplus t + (\Theta_r - \omega_\oplus t_r)\,. \tag{6.40}$$

We denote by $\boldsymbol{y}$ the spacecraft position vector $\boldsymbol{p}$, which can be considered as the output variable of the nonlinear model (6.5)

$$\boldsymbol{y} = \boldsymbol{p}(\boldsymbol{x}, t). \tag{6.41}$$

Taylor's development of the output variable $\boldsymbol{p}$ up to the first order around $\boldsymbol{x} = \boldsymbol{x}_{Ksk}$ can be written as

$$\boldsymbol{y} - \boldsymbol{y}_{sk} = \boldsymbol{C}(t)\,(\boldsymbol{x} - \boldsymbol{x}_{Ksk}) \tag{6.42}$$

where

$$\boldsymbol{y} - \boldsymbol{y}_{sk} = \boldsymbol{y} - \boldsymbol{p}(\boldsymbol{x}_{Ksk}, t) = \begin{bmatrix} r - a_k & \lambda - \lambda_s & \varphi \end{bmatrix}^T, \tag{6.43}$$

$$\begin{aligned} \boldsymbol{C}(t) &= \left[\boldsymbol{\nabla}_{EOE}\left[\boldsymbol{p}(\boldsymbol{x}, t)\right]\right]_{\boldsymbol{x}=\boldsymbol{x}_{Ksk}} = \\ &= \begin{bmatrix} 1 & -a_k \sin K_{sk} & -a_k \cos K_{sk} & 0 & 0 & 0 \\ 0 & -2\cos K_{sk} & 2\sin K_{sk} & 0 & 0 & 1 \\ 0 & 0 & 0 & -2\cos K_{sk} & 2\sin K_{sk} & 0 \end{bmatrix}, \end{aligned} \tag{6.44}$$

$$\boldsymbol{x} - \boldsymbol{x}_{Ksk} = \begin{bmatrix} a - a_k & P_1 & P_2 & Q_1 & Q_2 & l_\Theta - \lambda_s \end{bmatrix}^T. \tag{6.45}$$

Simplifying the first order Taylor expansion (6.42), the linear equation giving the output $\boldsymbol{y}$ in function of $\boldsymbol{x}$ becomes

$$\boldsymbol{y} = \boldsymbol{C}(t)\boldsymbol{x}. \tag{6.46}$$

Fig. 6.5 shows the differences over ten days between the state variables obtained integrating the nonlinear model (6.5) (with $\boldsymbol{a}_t = \mathbf{0}_{3\times1}$) by an explicit Runge-Kutta integration method[1] and the state variables obtained integrating the linear model (6.21) (with $\boldsymbol{u} = \mathbf{0}_{3\times1}$) by the same solver and initial conditions being equal. These errors are model errors.

Fig. 6.6 shows the above model errors in terms of output variables, i.e., the differences between the output variables obtained with the nonlinear function (6.41) and the output variables obtained with the linear function (6.46).

Fig.s 6.7 and 6.8 show the model errors for the state and output variables respectively, with

$$\boldsymbol{a}_t(t) = \boldsymbol{u}(t) = \begin{cases} (F/m)\mathbf{1}_{3\times1} & \text{for } 5 \le t \le 5.25 \\ \mathbf{0}_{3\times1} & \text{otherwise} \end{cases}, \tag{6.47}$$

$F = 100$ mN and $m = 4500$ kg.

Denoting by $\boldsymbol{\zeta}$ the deviation of the state variable $\boldsymbol{x}$ from its nominal station keeping value $\boldsymbol{x}_{Ksk}$

$$\boldsymbol{\zeta} = \boldsymbol{x} - \boldsymbol{x}_{Ksk}, \tag{6.48}$$

the linear time varying system (6.21) and the linear output variable (6.42) can be respectively written as

$$\frac{d\boldsymbol{\zeta}}{dt} = \boldsymbol{A}(t)\boldsymbol{\zeta} + \boldsymbol{B}(t)\boldsymbol{a}_{e_{sk}}(t) + \boldsymbol{B}(t)\boldsymbol{u}(t), \quad \boldsymbol{\zeta}(t_i) = \boldsymbol{\zeta}_i, \tag{6.49}$$

and

$$\boldsymbol{y} = \boldsymbol{C}(t)\boldsymbol{\zeta} + \boldsymbol{y}_{sk}. \tag{6.50}$$

The numerical integration rule used to formulate the station keeping optimal control problem in terms of parameter optimization problem will be the following

$$\boldsymbol{\zeta}(t_{k+1}) = \boldsymbol{\zeta}(t_k) + h\left[\boldsymbol{A}(\bar{t}_{k+1})\boldsymbol{\zeta}(\bar{t}_{k+1}) + \boldsymbol{B}(\bar{t}_{k+1})\boldsymbol{a}_{e_{sk}}(\bar{t}_{k+1}) + \boldsymbol{B}(\bar{t}_{k+1})\boldsymbol{u}(\bar{t}_{k+1})\right], \tag{6.51}$$

over a time interval $T = t_f - t_i$ discretized in N intervals with constant length h each, with nodes at the instants

$$t_k = t_i + kh, \qquad \text{for} \qquad k = 0, 1, \ldots, N, \tag{6.52}$$

and with interval centers at the instants

$$\bar{t}_{k+1} = t_k + \frac{h}{2} \qquad \text{for} \qquad k = 0, 1, \ldots, N-1. \tag{6.53}$$

Approximating the $\boldsymbol{\zeta}$ values at the center $\bar{t}_{k+1}$ of each kth interval by linear interpolation of $\boldsymbol{\zeta}(t_k)$ and $\boldsymbol{\zeta}(t_{k+1})$ values

$$\boldsymbol{\zeta}(\bar{t}_{k+1}) = \frac{\boldsymbol{\zeta}(t_k) + \boldsymbol{\zeta}(t_{k+1})}{2}, \tag{6.54}$$

the numerical integration rule (6.51) leads to the following discrete linear system

$$\boldsymbol{\zeta}(k+1) = \boldsymbol{A}_d(k)\boldsymbol{\zeta}(k) + \boldsymbol{B}_d(k)\boldsymbol{a}_{e_{sk}}(k) + \boldsymbol{B}_d(k)\boldsymbol{u}(k), \quad \boldsymbol{\zeta}(0) = \boldsymbol{\zeta}_i. \tag{6.55}$$

[1]The *ode45* Matlab solver based on the explicit Runge-Kutta (4,5) formula (the Dormand-Prince pair) has been used with a relative and absolute tolerance equal to 10^{-12}.

The discrete state variables, perturbing accelerations and control variables are defined at the nodes and at the center of each interval as follows

$$\boldsymbol{\zeta}(k+1) = \boldsymbol{\zeta}(t_{k+1}), \qquad \boldsymbol{\zeta}(k) = \boldsymbol{\zeta}(t_k), \qquad \boldsymbol{a}_{e_{sk}}(k) = \boldsymbol{a}_{e_{sk}}(\bar{t}_{k+1}), \qquad \boldsymbol{u}(k) = \boldsymbol{u}(\bar{t}_{k+1}). \tag{6.56}$$

Matrices $\boldsymbol{A}_d$ and $\boldsymbol{B}_d$ are defined as follows

$$\boldsymbol{A}_d(k) = \boldsymbol{A}_d(\bar{t}_{k+1}) = \left[\boldsymbol{I}_{6\times 6} - \frac{h}{2}\boldsymbol{A}(\bar{t}_{k+1})\right]^{-1}\left[\boldsymbol{I}_{6\times 6} + \frac{h}{2}\boldsymbol{A}(\bar{t}_{k+1})\right], \tag{6.57}$$

$$\boldsymbol{B}_d(k) = \boldsymbol{B}_d(\bar{t}_{k+1}) = \left[\boldsymbol{I}_{6\times 6} - \frac{h}{2}\boldsymbol{A}(\bar{t}_{k+1})\right]^{-1} h\boldsymbol{B}(\bar{t}_{k+1}). \tag{6.58}$$

In the station keeping parameter optimization problem, the output variable $\boldsymbol{y}$ will be evaluated at the nodes

$$t_k = t_i + kh, \qquad \text{for} \qquad k = 0, 1, \ldots, N, \tag{6.59}$$

as follows

$$\boldsymbol{y}(k) = \boldsymbol{C}_d(k)\boldsymbol{\zeta}(k) + \boldsymbol{y}_{sk}, \tag{6.60}$$

where

$$\boldsymbol{y}(k) = \boldsymbol{y}(t_k), \qquad \boldsymbol{C}_d(k) = \boldsymbol{C}(t_k), \qquad \boldsymbol{\zeta}(k) = \boldsymbol{\zeta}(t_k). \tag{6.61}$$

Fig. 6.9 shows the differences over ten days between the state variables obtained integrating the nonlinear model (6.5) (with $\boldsymbol{a}_t = \boldsymbol{0}_{3\times 1}$) by an explicit Runge-Kutta integration method and the state variables obtained integrating the linear model (6.21) (with $\boldsymbol{u} = \boldsymbol{0}_{3\times 1}$) by the integration rule (6.51) with $h = 0.01$ days ($h \approx 15$ minutes) and initial conditions being equal. These errors are the model errors plus the numerical integration errors.

Fig. 6.10 shows the above model plus numerical integration errors in terms of output variables, i.e., the differences between the output variables obtained with the nonlinear function (6.41) and by a Runge-Kutta solver and the output variables obtained with the linear function (6.46) and by the integration rule (6.51).

Comparing Fig.s 6.5 and 6.6 with Fig.s 6.9 and 6.10, we can deduce that with $h = 0.01$ day the linearization errors prevail over the discretization ones. For this value of h, the true longitude errors represent 2.5% of a longitude deadband equal to 0.01 deg. The latitude errors are 0.5% of a latitude deadband equal to 0.01 deg.

Fig. 6.11 shows the differences over ten days between the state variables obtained integrating the nonlinear model with the Runge-Kutta solver, and those ones obtained integrating the linear model by the integration rule (6.51) with respectively $h = 0.01$, $h = 0.02$, $h = 0.04$, $h = 0.08$ days (i.e., $h \approx 15$ minutes, $h \approx 30$ minutes, $h \approx 1$ hour, $h \approx 2$ hours).

Fig. 6.12 shows the differences over ten days between the output variables obtained integrating the nonlinear model with the Runge-Kutta solver, and those ones obtained integrating the linear model by the integration rule (6.51) with respectively $h = 0.01$, $h = 0.02$, $h = 0.04$, $h = 0.08$ days (i.e., $h \approx 15$ minutes, $h \approx 30$ minutes, $h \approx 1$ hour, $h \approx 2$ hours).

From Fig.s 6.11 and 6.12 we can deduce that the increase in the discretization time interval length is critical for the use of the discrete time linear model in the longitude controller design in narrow station keeping boxes. A value of $h = 0.08$ day is impracticable over five days when the longitude station keeping deadband is equal to 0.001 deg.

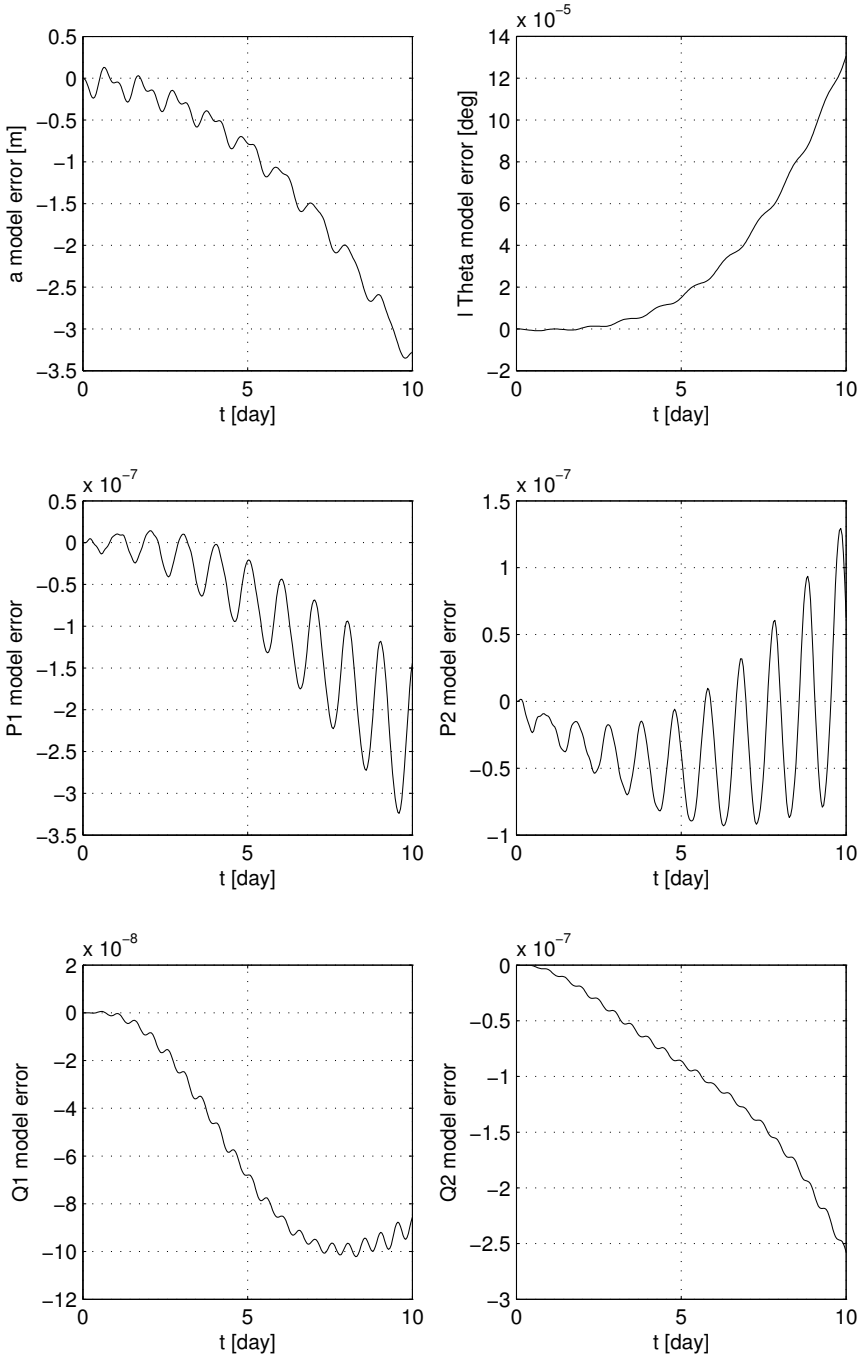

Figure 6.5: *Time histories over ten days of the differences between the state variables obtained integrating the nonlinear model (6.5) by a Runge-Kutta solver, and the state variables obtained integrating the linear model (6.21) by the same solver and initial conditions being equal.*

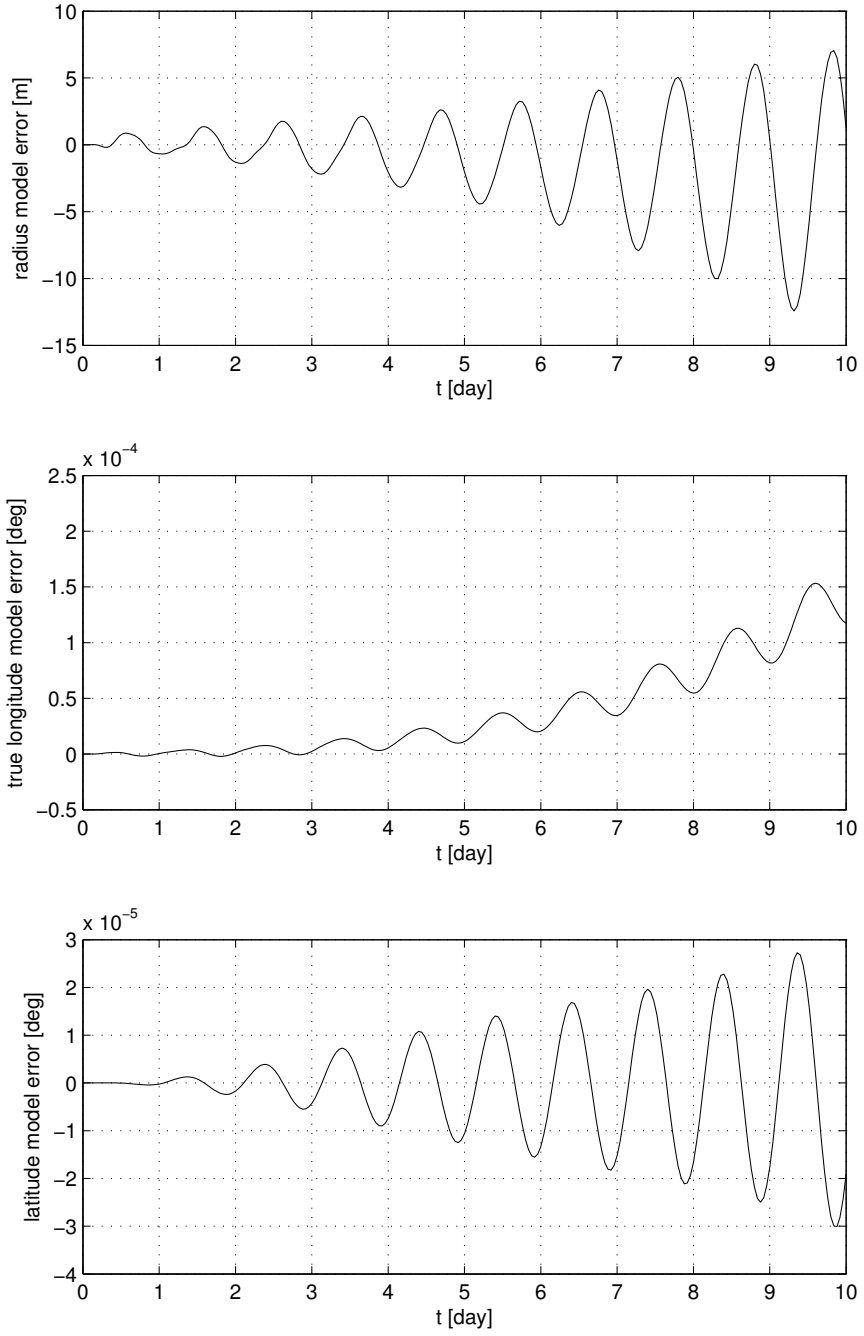

Figure 6.6: *Time histories over ten days of the differences between the output variables (6.41) (nonlinear functions of the state variables obtained integrating the nonlinear model (6.5) by a Runge-Kutta solver) and the output variables (6.46) (linear functions of the state variables obtained integrating the linear model (6.21) by the same Runge-Kutta solver and initial conditions being equal).*

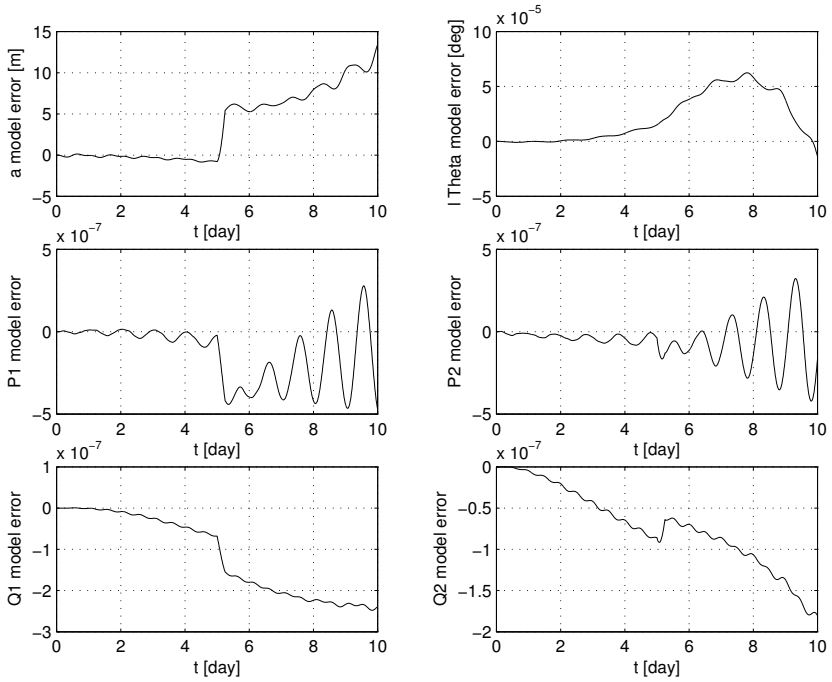

Figure 6.7: *Time histories over ten days of the differences between the state variables obtained integrating the nonlinear model (6.5) by a Runge-Kutta solver, and the state variables obtained integrating the linear model (6.21) by the same solver and initial conditions being equal (pulse input acceleration case).*

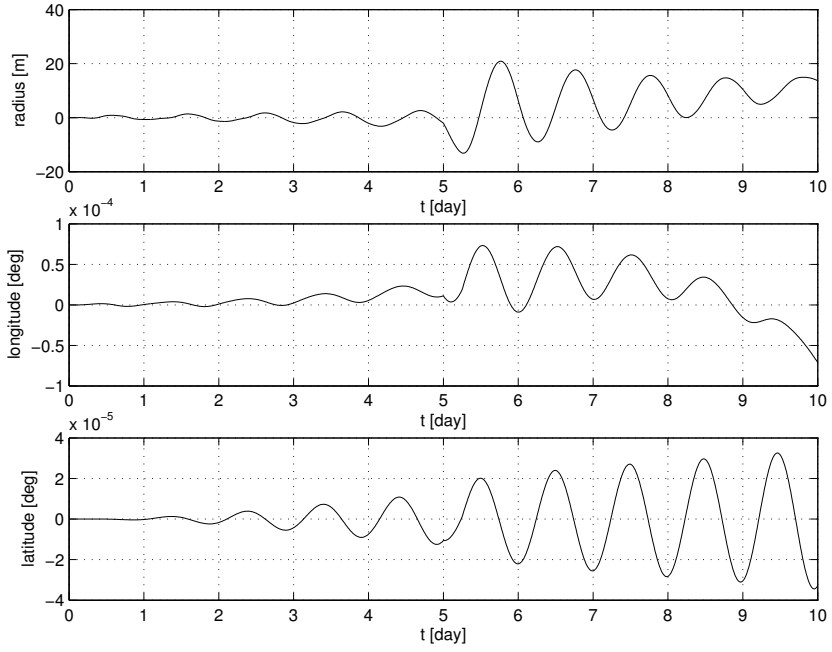

Figure 6.8: *Pulse input acceleration case: time histories over ten days of the differences between the output variables (6.41) (nonlinear functions of the state variables obtained integrating the nonlinear model (6.5) by a Runge-Kutta solver) and the output variables (6.46) (linear functions of the state variables obtained integrating the linear model (6.21) by the same Runge-Kutta solver and initial conditions being equal).*

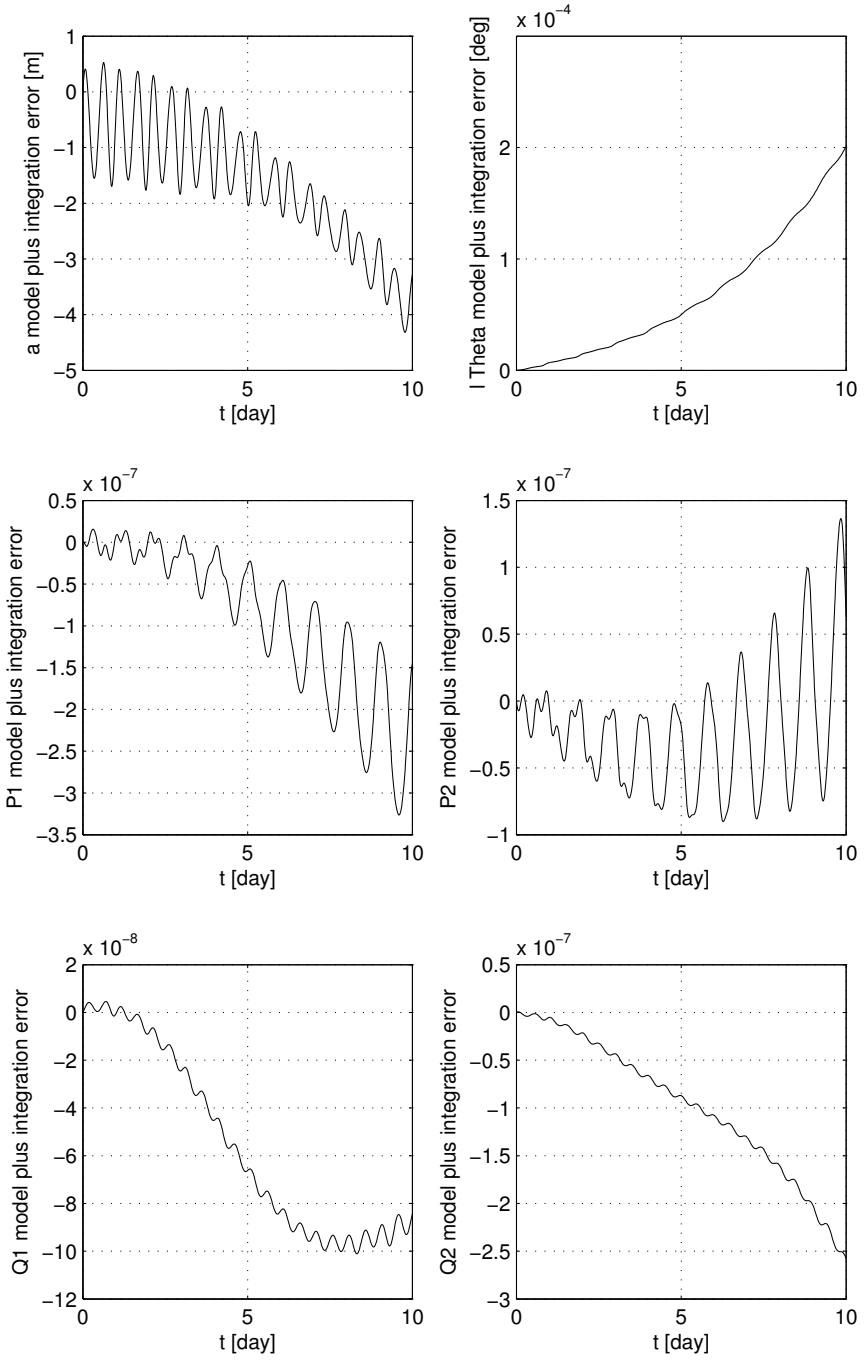

Figure 6.9: *Time histories over ten days of the differences between the state variables obtained integrating the nonlinear model (6.5) by a Runge-Kutta solver, and the state variables obtained integrating the linear model (6.21) by the integration rule (6.51) with* $h = 0.01$ *days* ($h \approx 15$ *minutes).*

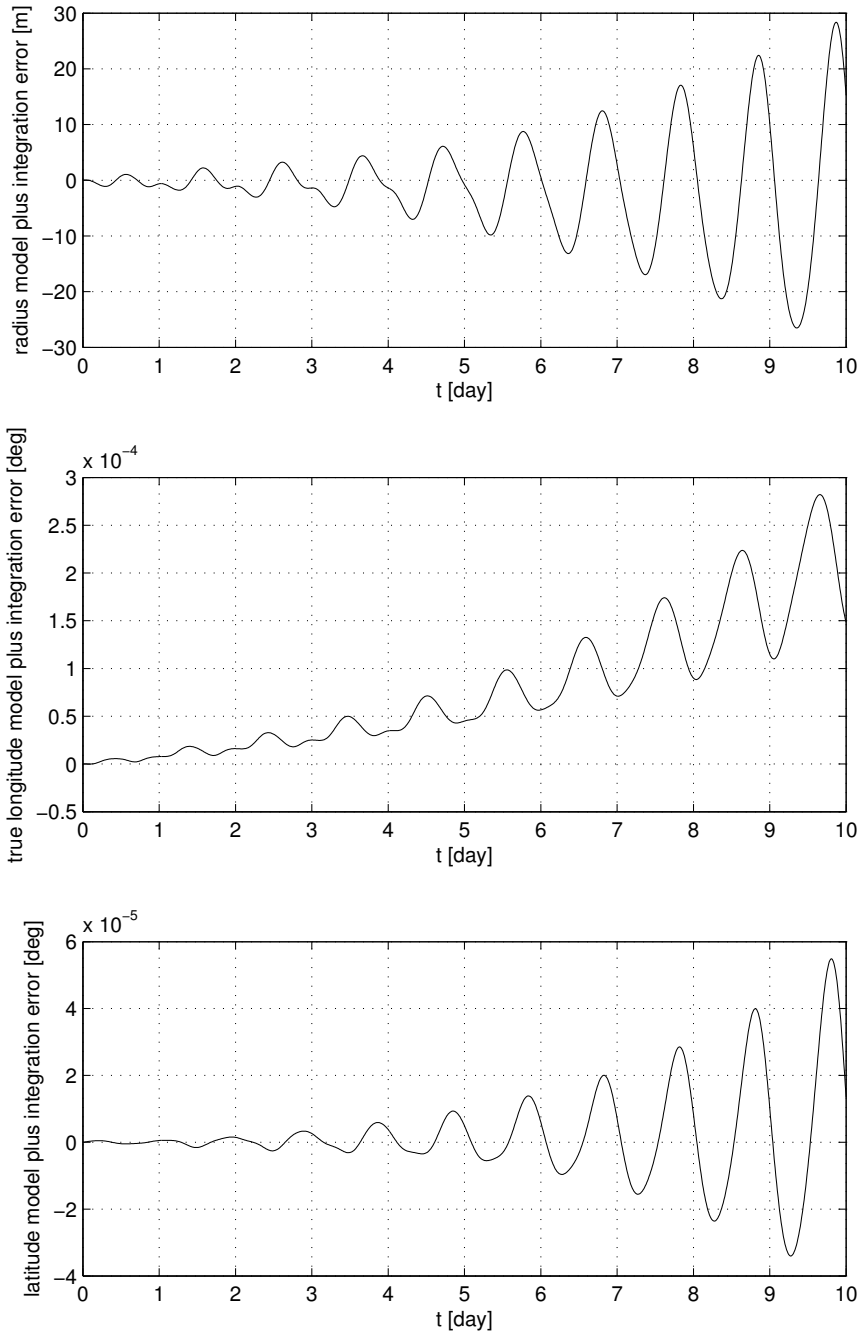

Figure 6.10: *Time histories over ten days of the differences between the output variables (6.41) (nonlinear functions of the state variables obtained integrating the nonlinear model (6.5) by a Runge-Kutta solver) and the output variables (6.46) (linear functions of the state variables obtained integrating the linear model (6.21) by the integration rule (6.51) with* $h = 0.01$ *days (*$h \approx 15$ *minutes).*

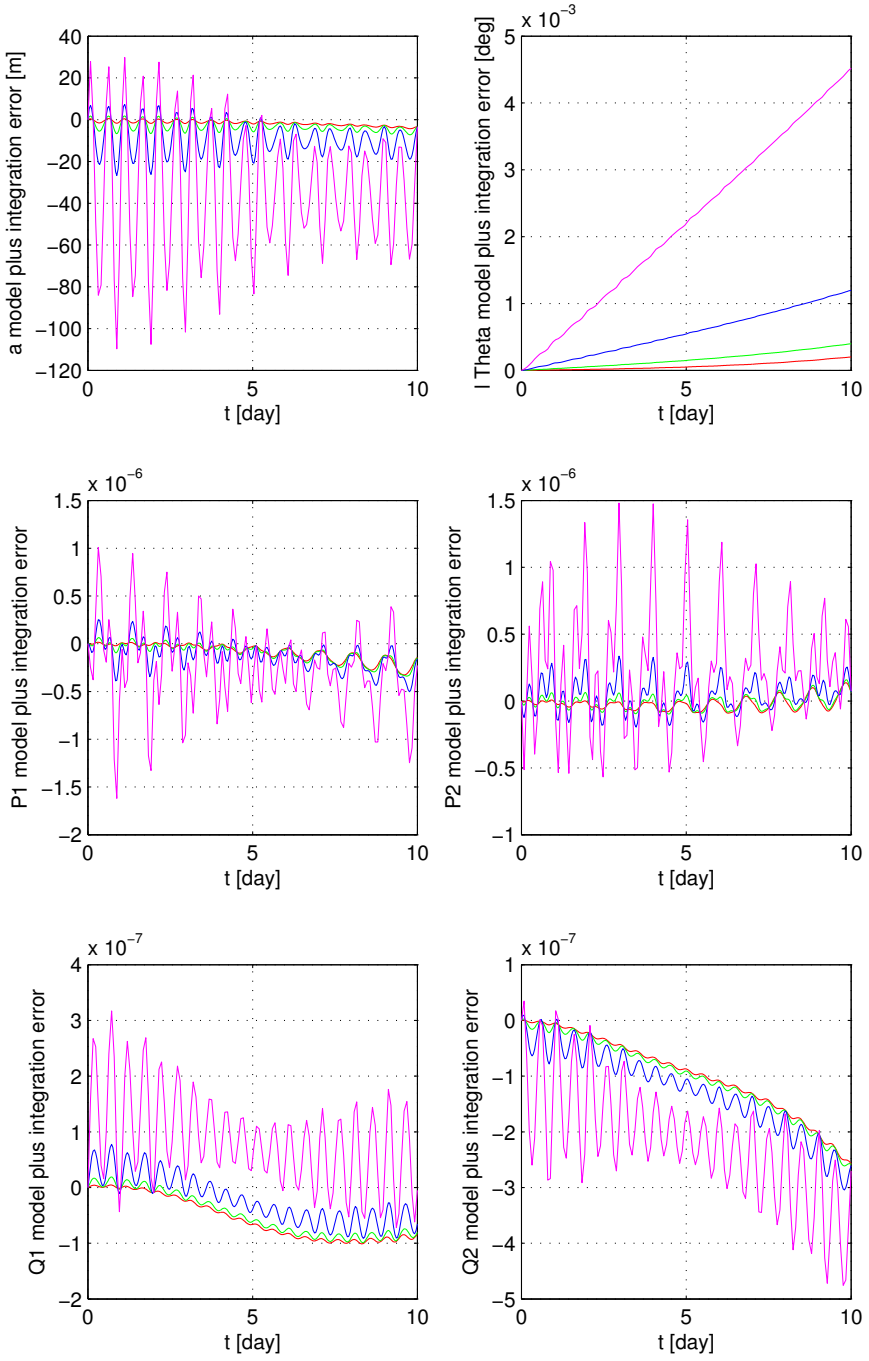

Figure 6.11: *Differences over ten days between the state variables obtained integrating the nonlinear model by the Runge-Kutta solver and those ones obtained integrating the linear model by the integration rule (6.51) with respectively* $h = 0.01$ *(red line),* $h = 0.02$ *(green line),* $h = 0.04$ *days (blue line),* $h = 0.08$ *days (magenta line).*

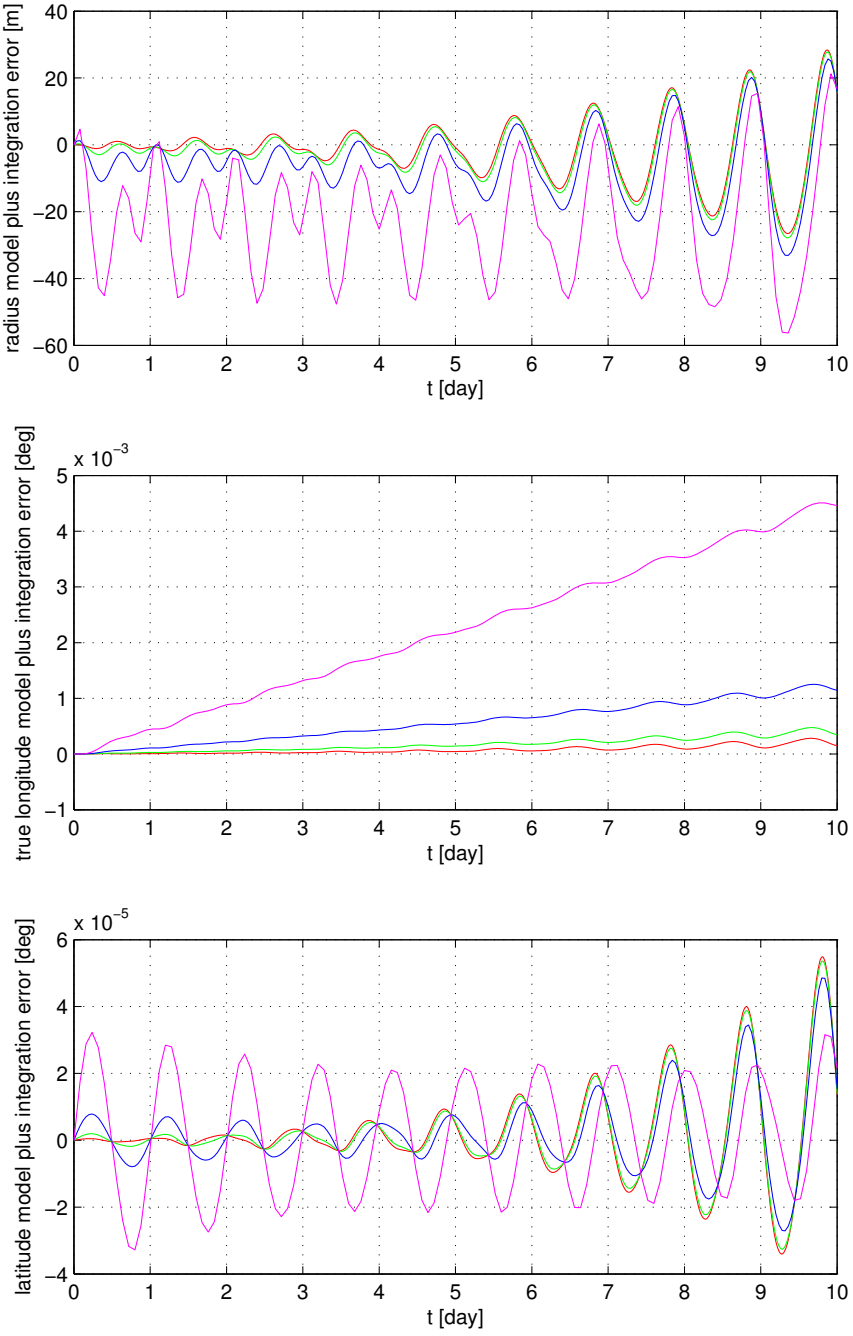

Figure 6.12: *Differences over ten days between the output variables obtained integrating the nonlinear model by the Runge-Kutta solver and those ones obtained integrating the linear model by the integration rule (6.51) with respectively* $h = 0.01$ *(red line),* $h = 0.02$ *(green line),* $h = 0.04$ *days (blue line),* $h = 0.08$ *days (magenta line).*

6.1.3 GEO Station Keeping Parameter Optimization Problem

We state the GEO station keeping parameter optimization problem over a generic time interval $T = t_f - t_i$ discretized in N intervals with constant length h each, with nodes at the instants

$$t_k = t_i + kh, \qquad \text{for} \qquad k = 0, 1, \ldots, N, \tag{6.62}$$

and with interval centers at the instants

$$\bar{t}_{k+1} = t_k + \frac{h}{2} \qquad \text{for} \qquad k = 0, 1, \ldots, N-1. \tag{6.63}$$

The vector of the unknown parameters is the control variable sample vector

$$\boldsymbol{\mathcal{U}} = \begin{bmatrix} \boldsymbol{u}^T(\bar{t}_1) & \cdots & \boldsymbol{u}^T(\bar{t}_{k+1}) & \cdots & \boldsymbol{u}^T(\bar{t}_N) \end{bmatrix}^T. \tag{6.64}$$

The scalar performance index that has to be minimized is

$$J = \boldsymbol{\mathcal{U}}^T \boldsymbol{\mathcal{U}}, \tag{6.65}$$

subject to the following path inequality constraints imposed at each node

$$\begin{bmatrix} \boldsymbol{I}_{(N+1)\times(N+1)} \\ -\boldsymbol{I}_{(N+1)\times(N+1)} \end{bmatrix} \boldsymbol{\Lambda} \leq \boldsymbol{\Lambda}_{max}, \tag{6.66}$$

$$\begin{bmatrix} \boldsymbol{I}_{(N+1)\times(N+1)} \\ -\boldsymbol{I}_{(N+1)\times(N+1)} \end{bmatrix} \boldsymbol{\Phi} \leq \boldsymbol{\Phi}_{max}, \tag{6.67}$$

where

$$\boldsymbol{\Lambda}_{max} = \lambda_{max} \mathbf{1}_{2(N+1)\times 1}, \tag{6.68}$$

$$\boldsymbol{\Phi}_{max} = \varphi_{max} \mathbf{1}_{2(N+1)\times 1}, \tag{6.69}$$

and

$$\boldsymbol{\Lambda} = \begin{bmatrix} \lambda(t_0) & \lambda(t_1) & \cdots & \lambda(t_k) & \cdots & \lambda(t_N) \end{bmatrix}^T - \lambda_s \mathbf{1}_{(N+1)\times 1}, \tag{6.70}$$

$$\boldsymbol{\Phi} = \begin{bmatrix} \varphi(t_0) & \varphi(t_1) & \cdots & \varphi(t_k) & \cdots & \varphi(t_N) \end{bmatrix}^T. \tag{6.71}$$

The vectors $\boldsymbol{\Lambda}$ and $\boldsymbol{\Phi}$ are linear functions of parameter vector $\boldsymbol{\mathcal{U}}$. In fact, vectors $\boldsymbol{\Lambda}$ and $\boldsymbol{\Phi}$ of the longitude and latitude deviations from the nominal station keeping values $\lambda = \lambda_s$ and $\varphi = 0$ respectively, can be written as

$$\boldsymbol{\Lambda} = \boldsymbol{\mathcal{S}}_\lambda \boldsymbol{\mathcal{Y}} \qquad \text{and} \qquad \boldsymbol{\Phi} = \boldsymbol{\mathcal{S}}_\varphi \boldsymbol{\mathcal{Y}} \tag{6.72}$$

where

$$\boldsymbol{\mathcal{S}}_\lambda = \begin{bmatrix} \boldsymbol{S}_\lambda & \mathbf{0}_{1\times 3} & \cdots & \mathbf{0}_{1\times 3} & \cdots & \mathbf{0}_{1\times 3} \\ \mathbf{0}_{1\times 3} & \boldsymbol{S}_\lambda & \cdots & \mathbf{0}_{1\times 3} & \cdots & \mathbf{0}_{1\times 3} \\ \vdots & \vdots & \ddots & \vdots & & \vdots \\ \mathbf{0}_{1\times 3} & \mathbf{0}_{1\times 3} & \cdots & \boldsymbol{S}_\lambda & \cdots & \mathbf{0}_{1\times 3} \\ \vdots & \vdots & & \vdots & \ddots & \vdots \\ \mathbf{0}_{1\times 3} & \mathbf{0}_{1\times 3} & \cdots & \mathbf{0}_{1\times 3} & \cdots & \boldsymbol{S}_\lambda \end{bmatrix} \qquad \text{with} \qquad \boldsymbol{S}_\lambda = \begin{bmatrix} 0 & 1 & 0 \end{bmatrix} \tag{6.73}$$

and

$$\boldsymbol{\mathcal{S}}_\varphi = \begin{bmatrix} \boldsymbol{S}_\varphi & \mathbf{0}_{1\times3} & \cdots & \mathbf{0}_{1\times3} & \cdots & \mathbf{0}_{1\times3} \\ \mathbf{0}_{1\times3} & \boldsymbol{S}_\varphi & \cdots & \mathbf{0}_{1\times3} & \cdots & \mathbf{0}_{1\times3} \\ \vdots & \vdots & \ddots & \vdots & & \vdots \\ \mathbf{0}_{1\times3} & \mathbf{0}_{1\times3} & \cdots & \boldsymbol{S}_\varphi & \cdots & \mathbf{0}_{1\times3} \\ \vdots & \vdots & & \vdots & \ddots & \vdots \\ \mathbf{0}_{1\times3} & \mathbf{0}_{1\times3} & \cdots & \mathbf{0}_{1\times3} & \cdots & \boldsymbol{S}_\varphi \end{bmatrix} \quad \text{with} \quad \boldsymbol{S}_\varphi = \begin{bmatrix} 0 & 0 & 1 \end{bmatrix}. \tag{6.74}$$

Vector $\boldsymbol{\mathcal{Y}}$ is the vector of the output variable deviations at the nodes

$$\boldsymbol{\mathcal{Y}} = \begin{bmatrix} \boldsymbol{y}^T(t_0) & \boldsymbol{y}^T(t_1) & \cdots & \boldsymbol{y}^T(t_k) & \cdots & \boldsymbol{y}^T(t_N) \end{bmatrix}^T - \begin{bmatrix} \boldsymbol{y}_{sk}^T & \boldsymbol{y}_{sk}^T & \cdots & \boldsymbol{y}_{sk}^T & \cdots & \boldsymbol{y}_{sk}^T \end{bmatrix}^T. \tag{6.75}$$

Thanks to Eq. (6.60), vector $\boldsymbol{\mathcal{Y}}$ can be written as

$$\boldsymbol{\mathcal{Y}} = \boldsymbol{\mathcal{C}}\boldsymbol{\mathcal{Z}} \tag{6.76}$$

where

$$\boldsymbol{\mathcal{C}} = \begin{bmatrix} \boldsymbol{C}_d(t_0) & \mathbf{0}_{3\times6} & \cdots & \mathbf{0}_{3\times6} & \cdots & \mathbf{0}_{3\times6} \\ \mathbf{0}_{3\times6} & \boldsymbol{C}_d(t_1) & \cdots & \mathbf{0}_{3\times6} & \cdots & \mathbf{0}_{3\times6} \\ \vdots & \vdots & \ddots & \vdots & & \vdots \\ \mathbf{0}_{3\times6} & \mathbf{0}_{3\times6} & \cdots & \boldsymbol{C}_d(t_k) & \cdots & \mathbf{0}_{3\times6} \\ \vdots & \vdots & & \vdots & \ddots & \vdots \\ \mathbf{0}_{3\times6} & \mathbf{0}_{3\times6} & \cdots & \mathbf{0}_{3\times6} & \cdots & \boldsymbol{C}_d(t_N) \end{bmatrix}, \tag{6.77}$$

and $\boldsymbol{\mathcal{Z}}$ is the vector of the state variable deviation at the nodes

$$\boldsymbol{\mathcal{Z}} = \begin{bmatrix} \boldsymbol{\zeta}^T(t_0) & \boldsymbol{\zeta}^T(t_1) & \cdots & \boldsymbol{\zeta}^T(t_k) & \cdots & \boldsymbol{\zeta}^T(t_N) \end{bmatrix}^T. \tag{6.78}$$

Finally, because of integration rule (6.51), vector $\boldsymbol{\mathcal{Z}}$ can be written as function of the initial state deviation $\boldsymbol{\zeta}(t_0)$ and the unknown parameter vector $\boldsymbol{\mathcal{U}}$ as follows

$$\boldsymbol{\mathcal{Z}} = \boldsymbol{\mathcal{Z}}_0 + \boldsymbol{\mathcal{B}}\boldsymbol{\mathcal{A}} + \boldsymbol{\mathcal{B}}\boldsymbol{\mathcal{U}} \tag{6.79}$$

where

$$\boldsymbol{\mathcal{Z}}_0 = \begin{bmatrix} \boldsymbol{I}_{6\times6} \\ \boldsymbol{A}_d(\bar{t}_1) \\ \vdots \\ \left[\prod_{j=1}^{k} \boldsymbol{A}_d^T(\bar{t}_j)\right]^T \\ \vdots \\ \left[\prod_{j=1}^{N} \boldsymbol{A}_d^T(\bar{t}_j)\right]^T \end{bmatrix} \boldsymbol{\zeta}(t_0), \tag{6.80}$$

$$\boldsymbol{\mathcal{B}} = \begin{bmatrix} \mathbf{0}_{6\times3} & \cdots & \mathbf{0}_{6\times3} & \cdots & \mathbf{0}_{6\times3} \\ \boldsymbol{B}_d(\bar{t}_1) & \cdots & \mathbf{0}_{6\times3} & \cdots & \mathbf{0}_{6\times3} \\ \vdots & \ddots & \vdots & & \vdots \\ \left[\boldsymbol{B}_d^T(\bar{t}_1)\prod_{j=2}^{k+1}\boldsymbol{A}_d^T(\bar{t}_j)\right]^T & \cdots & \boldsymbol{B}_d(\bar{t}_{k+1}) & \cdots & \mathbf{0}_{6\times3} \\ \vdots & & \vdots & \ddots & \vdots \\ \left[\boldsymbol{B}_d^T(\bar{t}_1)\prod_{j=2}^{N}\boldsymbol{A}_d^T(\bar{t}_j)\right]^T & \cdots & \left[\boldsymbol{B}_d^T(\bar{t}_{k+1})\prod_{j=k+2}^{N}\boldsymbol{A}_d^T(\bar{t}_j)\right]^T & \cdots & \boldsymbol{B}_d(\bar{t}_N) \end{bmatrix}, \tag{6.81}$$

$$\boldsymbol{\mathcal{A}} = \begin{bmatrix} \boldsymbol{a}_{e_{sk}}^T(\bar{t}_1) & \cdots & \boldsymbol{a}_{e_{sk}}^T(\bar{t}_{k+1}) & \cdots & \boldsymbol{a}_{e_{sk}}^T(\bar{t}_N) \end{bmatrix}^T. \tag{6.82}$$

Path constraints given by matrix Eq.s (6.66) and (6.67) in function of $\boldsymbol{\mathcal{U}}$ become

$$\begin{bmatrix} \boldsymbol{I}_{(N+1)\times(N+1)} \\ -\boldsymbol{I}_{(N+1)\times(N+1)} \end{bmatrix} \boldsymbol{\mathcal{S}}_\lambda \boldsymbol{\mathcal{C}}\boldsymbol{\mathcal{B}}\boldsymbol{\mathcal{U}} \leq \boldsymbol{\Lambda}_{max} - \begin{bmatrix} \boldsymbol{I}_{(N+1)\times(N+1)} \\ -\boldsymbol{I}_{(N+1)\times(N+1)} \end{bmatrix} \boldsymbol{\mathcal{S}}_\lambda \boldsymbol{\mathcal{C}} \left(\boldsymbol{\mathcal{Z}}_0 + \boldsymbol{\mathcal{B}}\boldsymbol{\mathcal{A}}\right), \tag{6.83}$$

$$\begin{bmatrix} \boldsymbol{I}_{(N+1)\times(N+1)} \\ -\boldsymbol{I}_{(N+1)\times(N+1)} \end{bmatrix} \boldsymbol{\mathcal{S}}_\varphi \boldsymbol{\mathcal{C}}\boldsymbol{\mathcal{B}}\boldsymbol{\mathcal{U}} \leq \boldsymbol{\Phi}_{max} - \begin{bmatrix} \boldsymbol{I}_{(N+1)\times(N+1)} \\ -\boldsymbol{I}_{(N+1)\times(N+1)} \end{bmatrix} \boldsymbol{\mathcal{S}}_\varphi \boldsymbol{\mathcal{C}} \left(\boldsymbol{\mathcal{Z}}_0 + \boldsymbol{\mathcal{B}}\boldsymbol{\mathcal{A}}\right). \tag{6.84}$$

These last conditions are the translation in parametric terms of inequalities (6.6) and (6.7). Any further condition on the control variable components can be translated in a similar form. For example, constraint (6.11) becomes

$$\boldsymbol{\mathcal{S}}_a \boldsymbol{\mathcal{U}} \leq \mathbf{0}_{N\times1} \tag{6.85}$$

where the selection matrix $\boldsymbol{\mathcal{S}}_a$ is

$$\boldsymbol{\mathcal{S}}_a = \begin{bmatrix} \boldsymbol{S}_a & \cdots & \mathbf{0}_{1\times3} & \cdots & \mathbf{0}_{1\times3} \\ \vdots & \ddots & \vdots & & \vdots \\ \mathbf{0}_{1\times3} & \cdots & \boldsymbol{S}_a & \cdots & \mathbf{0}_{1\times3} \\ \vdots & & \vdots & \ddots & \vdots \\ \mathbf{0}_{1\times3} & \cdots & \mathbf{0}_{1\times3} & \cdots & \boldsymbol{S}_a \end{bmatrix} \quad \text{with} \quad \boldsymbol{S}_a = \begin{bmatrix} 1 & 0 & 0 \end{bmatrix}. \tag{6.86}$$

6.2 Fixed and Receding Horizon Optimization Approaches

In the following we will denote

- by $T_{SKj} = t_{fSKj} - t_{iSKj}$ the jth station keeping maneuver planning interval, i.e., the interval over which a SK parameter optimization problem is solved to obtain the optimal SK maneuver time histories between t_{iSKj} and t_{fSKj};
- by $T_{Cj} = t_{fCj} - t_{iCj}$ the jth station keeping correction interval, i.e., the interval over which a share of optimal SK maneuver time histories is actually used to obtain the optimal path between t_{iCj} and t_{fCj}.

We will assume all the SK maneuver planning and correction intervals with constant durations equal respectively to T_{SK} and T_C, such that

$$T_{SK} = hN \geq hM = T_C \tag{6.87}$$

where h is the sampling interval of the discrete dynamics and N and M are two positive integer numbers.

Over the T_{SKj} intervals we will work in the discrete time domain with the discrete linear system (6.55) and output (6.60), to obtain an optimal control vector made up of N optimal control vectors

$$\boldsymbol{\mathcal{U}_j}^* = \left[\boldsymbol{u}_j^*(\bar{t}_1) \quad \cdots \quad \boldsymbol{u}_j^*(\bar{t}_{k+1}) \quad \cdots \quad \boldsymbol{u}_j^*(\bar{t}_N)\right]^T. \tag{6.88}$$

Over the T_{Cj} intervals we will work in the continuous time domain with the continuous nonlinear system (6.5) and output (6.41), to validate the spacecraft dynamical behavior between t_{iCj} and t_{fCj} with the following constant piecewise control vector time history

$$\boldsymbol{u}_j(t) = \begin{cases} \boldsymbol{u}_j^*(\bar{t}_{k+1}) & \text{if} \quad t_k \leq t < t_{k+1} \quad \text{for} \quad k = 0, 1, \ldots, M-1 \\ \boldsymbol{u}_j^*(\bar{t}_M) & \text{if} \quad t = t_M \end{cases}. \tag{6.89}$$

In Fig. (6.13) the time history of one control component deduced from its respective optimal sequence is depicted.

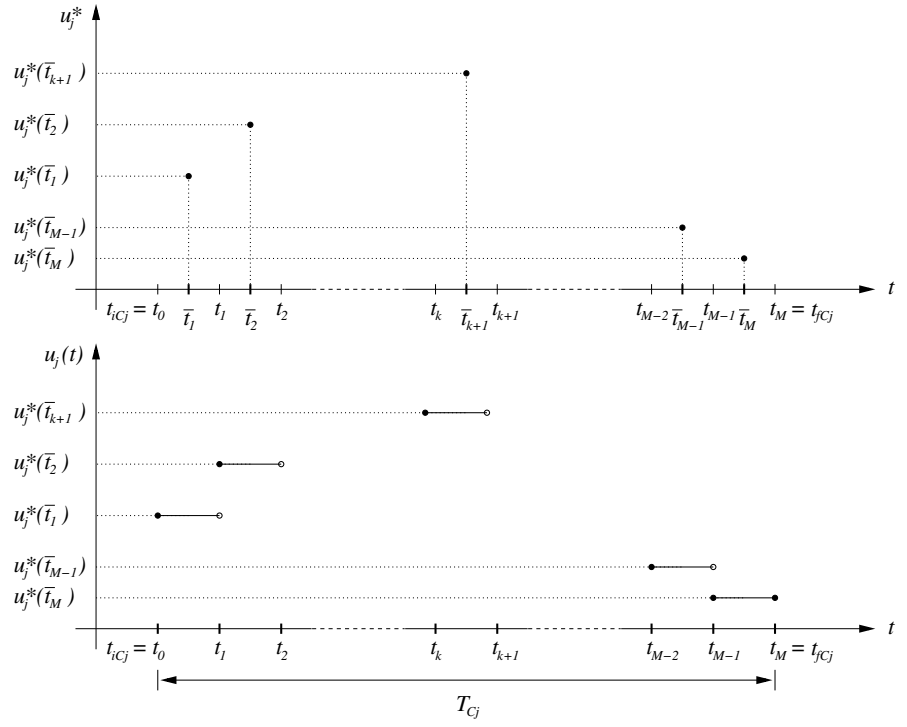

Figure 6.13: *Time history over a correction time interval T_{Cj} of a constant piecewise control component $u_j(t)$ deduced from the respective optimal sequence $u_j^*(\bar{t}_k)$ for $k = 1, 2, \ldots, M$.*

6.2.1 Fixed Horizon Optimization (FHO) Approach

In the fixed horizon optimization approach, the SK maneuver planning interval length is equal to the correction one

$$T_{SK} = hN = hM = T_C. \tag{6.90}$$

The SK maneuver planning over T_{SKj} is performed via a fixed horizon optimization. This approach leads to an optimal control vector sequence (6.88) which begins at the current time t_{iSKj}, ends at the future time t_{fSKj}, takes into account the current state

$$\boldsymbol{\zeta}(t_{iSKj}) = \boldsymbol{\zeta}(t_0) \tag{6.91}$$

and the future inequality constraints (6.83) and (6.84). These inequality constraints depend on the current state (see $\boldsymbol{\mathcal{Z}}_0$ term), on the matrices $\boldsymbol{\mathcal{C}}$ and $\boldsymbol{\mathcal{B}}$ and on the perturbing acceleration vector $\boldsymbol{\mathcal{A}}$, which are time varying over T_{SKj}. Once the optimal control vector sequence $\boldsymbol{\mathcal{U}}_j^*$ obtained, the maneuvers are executed over the correction interval T_{Cj} via the constant piecewise control time history (6.89). Over T_{Cj} an optimal spacecraft trajectory is obtained, characterized by a final state vector value $\boldsymbol{\zeta}(t_{fCj})$. This last state vector will become the current state of the next SK maneuver plan at fixed horizon.

Since the plan and the execution of the SK maneuvers are performed over the same time horizons, the GEO spacecraft model does not give any useful prediction information. The final state vector $\boldsymbol{x}_{fCj}$ is optimal over T_{SKj}, but, as initial state vector of the next SK maneuver plan, it could not be the optimal current state over the next maneuver planning interval.

6.2.2 Receding Horizon Optimization (RHO) Approach

In the receding horizon optimization approach, the SK maneuver planning interval length is longer than the correction one

$$T_{SK} = hN > hM = T_C. \tag{6.92}$$

This approach leads to the SK plan and execution of maneuvers in the following order.

1. At time t_{iSKj} and for the current state

$$\boldsymbol{\zeta}(t_{iSKj}) = \boldsymbol{\zeta}(t_0), \tag{6.93}$$

   an optimal control problem is solved over a fixed future interval T_{SKj}, taking into account the current state and the future inequality constraints (6.83) and (6.84).

2. Once the optimal sequence $\boldsymbol{\mathcal{U}}_j^*$ of N control vectors obtained, only the first M vectors are used to execute manuevers over the correction interval T_{Cj} via the constant piecewise control time history (6.89).

3. Over T_{Cj} an optimal spacecraft trajectory is obtained, characterized by a final state vector value $\boldsymbol{\zeta}(t_{fCj})$.

4. This last value becomes the current state of the next SK maneuver plan. Step 1. is taken up again. A parameter optimization problem is solved again over an optimization horizon $T_{SK(j+1)}$, which is the T_{SKj} horizon slid ahead of T_{Cj}

$$T_{SK(j+1)} = t_{fSK(j+1)} - t_{fCj}. \tag{6.94}$$

Unlike the fixed horizon approach, here the idea is to select only a first share of the optimal control vector sequence over a time interval of length T_C. This sequence share promises the best predicted behavior over a time interval of length $T_{SK} > T_C$. Only this first share is applied to the system. The remaining one serves to judge the impact of the applied control on the future decisions and to be sure that the applied control is optimal even over the remaining time interval $t_{fSKj} - t_{fCj}$ of length $T_{SK} - T_C$.

6.2.3 Some Remarks About the Receding Horizon Approach

From a barely control theory viewpoint, the time interval T_{SKj} is usually called *prediction horizon* and the time interval T_{Cj} is called *control horizon*. The receding horizon concept corresponds to the usual behavior of the Earth's horizon: as one moves towards it, it recedes, remaining a constant distance away.

This last concept is the basic idea in the methodology of all the controllers belonging to the MPC (Model Predictive Control) family (see, e.g., [Camacho and Bordons, 1999], [Maciejowski, 2002], [Goodwin et al., 2004]). In the MPC methodology, the future outputs of a process are predicted over a prediction horizon using the discrete version of a process model. These outputs depend on the past input and output signals and on the future control signals, which have to be calculated and to be sent to the plant. The set of future control signals is calculated by optimizing a determined criterion under constraints over a prediction horizon, but only the first optimal control sample is actually applied to the plant, i.e., $M = 1$ and $T_C = h$. Then the receding horizon concept is applied: the prediction horizon is slid ahead of a sampling interval. A new first optimal control simple is calculated as the first sample of an optimal sequence over the slid prediction horizon and it is applied to the plant. The prediction horizon is slid again of a sampling interval and so on. In this context, the control horizon duration is equal to that of the discretization interval of the model. Consequently, the control signals at each instant are functions of the current state at that instant.

The receding horizon optimization principle as just explained overcomes some drawbacks of the fixed horizon solution. In this last solution, the future control signals are calculated over a prediction horizon in function of an initial state (that one at the beginning of the prediction horizon). These signals are applied to the plant over the same horizon, unaware of what could happen to the plant at some time over the optimization interval. Moreover, in the fixed horizon solution, the impact of the control signal application on the future decisions is not taken into account in the controller design phase.

In the section above the receding horizon concept is applied in a "macroscopic" sense, in the context of the geostationary trajectory optimization. The prediction horizon T_{SKj} is slid ahead of a control horizon T_{Cj} one day long (that is an amount greater than the sampling interval) in order to update the spacecraft state vector target conditions at the end of each day. This update is made in anticipation of what could happen over the surplus $T_{SKj} - T_{Cj}$ of the prediction horizon.

6.2.4 FHO Simulation Results

We have carried out some simulations with the fixed horizon optimization approach explained in Section 6.2.1 without any constraint on the control variables, with the following values of fixed horizon duration and sampling interval

- $T_{SKj} = T_{Cj} = 1$ day, $\forall j = 1, 2, \ldots, 365$,
- $h = 0.01 \quad \Rightarrow \quad N = M = 100$,

and for three values of longitude and latitude deadbands

- $2\lambda_{max} = 2\varphi_{max} = 0.1$ deg;
- $2\lambda_{max} = 2\varphi_{max} = 0.01$ deg;
- $2\lambda_{max} = 2\varphi_{max} = 0.001$ deg.

To face up to the model and numerical integration errors gathered for the output variables over the fixed horizon of optimization, instead of considering constant lower and upper bounds for the longitude and latitude

$$\mathbf{\Lambda}_{max} = \lambda_{max}\mathbf{1}_{2(N+1)\times 1}, \tag{6.95}$$

$$\mathbf{\Phi}_{max} = \varphi_{max}\mathbf{1}_{2(N+1)\times 1}, \tag{6.96}$$

we have considered the raising and degrading bounds depicted in Fig. (6.14).

Table 6.4 summarizes the ideal velocity increment budgets over one year of mission (from 2010 January 1.0 to 2011 January 1.0) for a satellite with the following structural parameters: a mass $m = 4500$ km; a mean surface absorbing the solar radiation $S = 300$ m^2; a mean reflectivity coefficient $\epsilon = 0.3$, which entails a radiation pressure coefficient $C_R = 1.3$. The initial dynamical condition is that of nominal station keeping with $\lambda_s = 60$ deg.

Fig.s (6.15)–(6.17) show the state variable, output variable and control law time histories respectively, obtained over the first 30 days of the simulations explained above (longitude and latitude deadbands equal to 0.01 deg).

Fig.s (6.18)–(6.20) show the state variable, output variable and control law time histories respectively, obtained over the first 30 days of the simulations explained above (longitude and latitude deadbands equal to 0.001 deg).

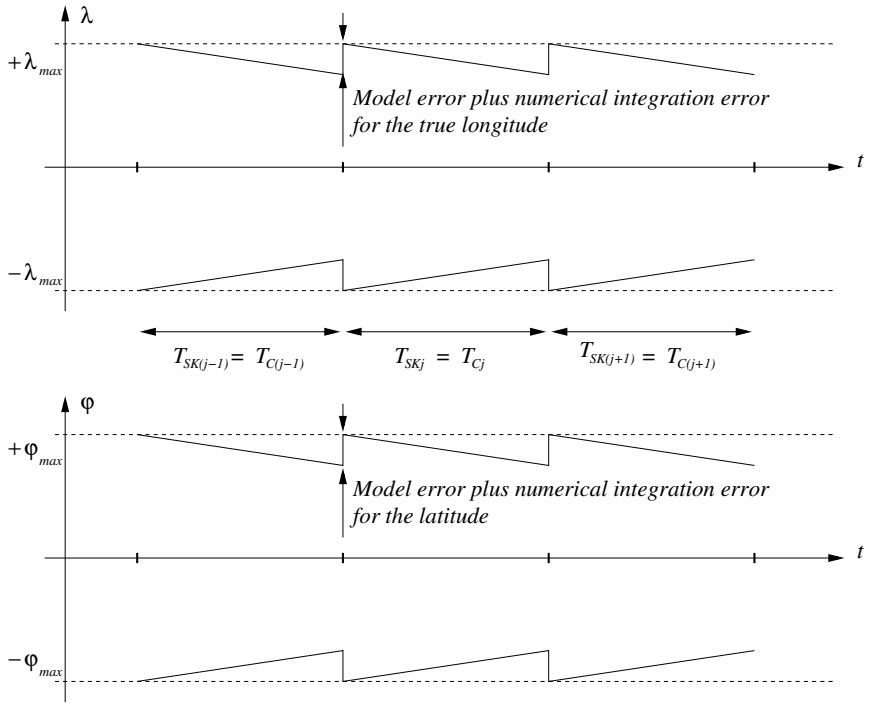

Figure 6.14: *Raising and degrading bounds over the fixed optimization horizons for the longitude and the latitude.*

DEADBANDS [deg]	**VELOCITY INCREMENT BUDGETS [m/s]**						
$2\lambda_{max} = 2\varphi_{max}$	Δv_{tR}^{+}	Δv_{tR}^{-}	Δv_{tT}^{+}	Δv_{tT}^{-}	Δv_{tN}^{+}	Δv_{tN}^{-}	$\Delta V = \sum \Delta v_t$
0.1	32.64	15.28	33.25	32.18	30.18	36.92	180.48
0.01	120.57	58.41	109.22	108.14	32.44	43.18	471.99
0.001	88.27	93.66	91.58	90.82	34.70	39.57	438.89

Table 6.4: *Ideal velocity increment budgets over one year of mission (from 2010 January 1.0 to 2011 January 1.0) obtained with the FHO approach.*

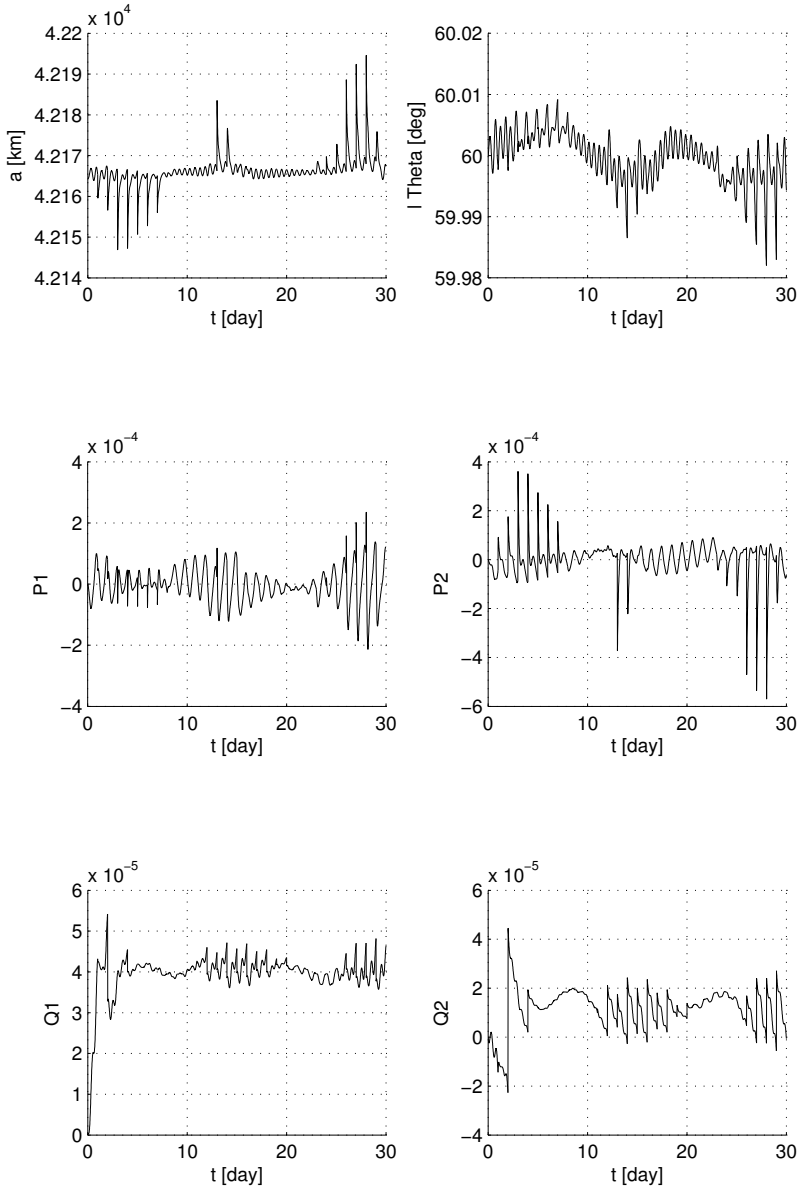

Figure 6.15: *Longitude and latitude deadbands equal to 0.01 deg; state variable time histories over 30 days obtained with control laws designed with the FHO approach.*

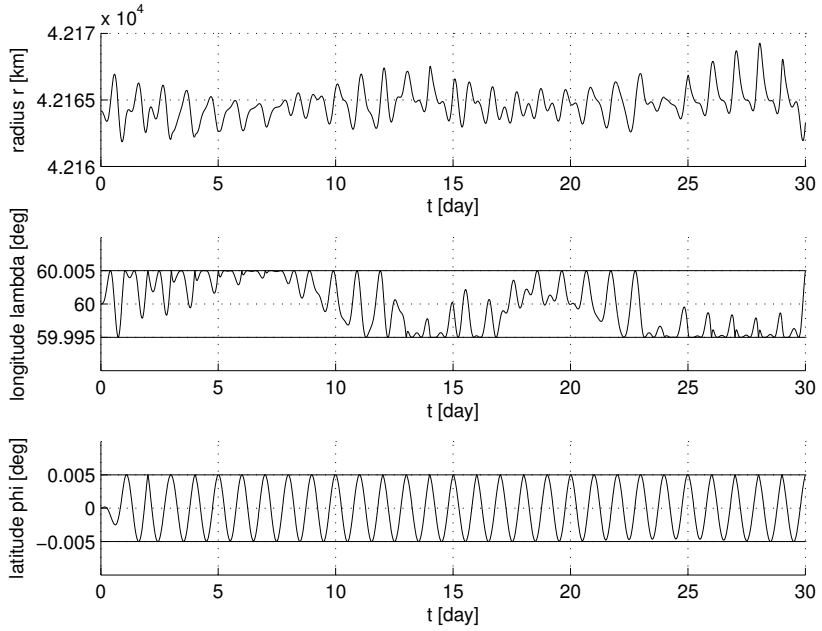

Figure 6.16: *Longitude and latitude deadbands equal to 0.01 deg; output variable time histories over 30 days obtained with control laws designed with the FHO approach.*

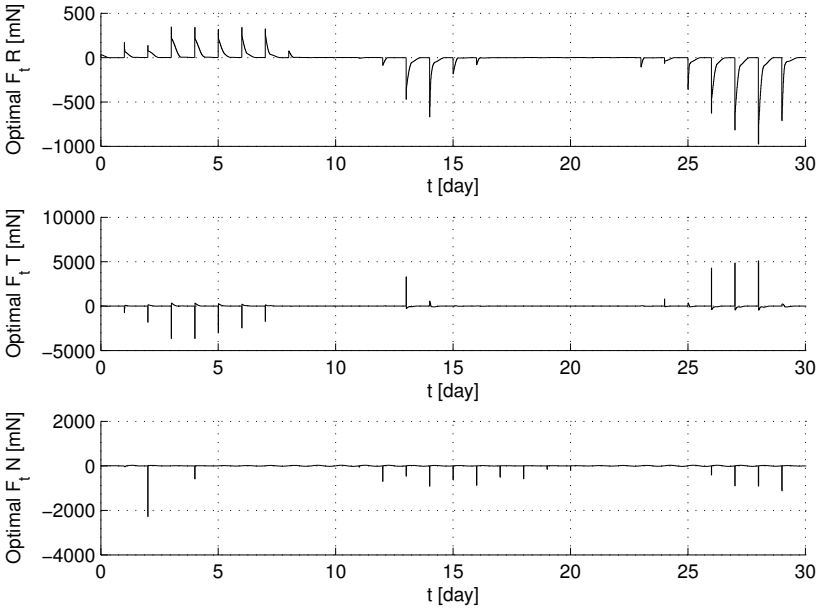

Figure 6.17: *Longitude and latitude deadbands equal to 0.01 deg; control laws (in terms of force) designed with the FHO approach.*

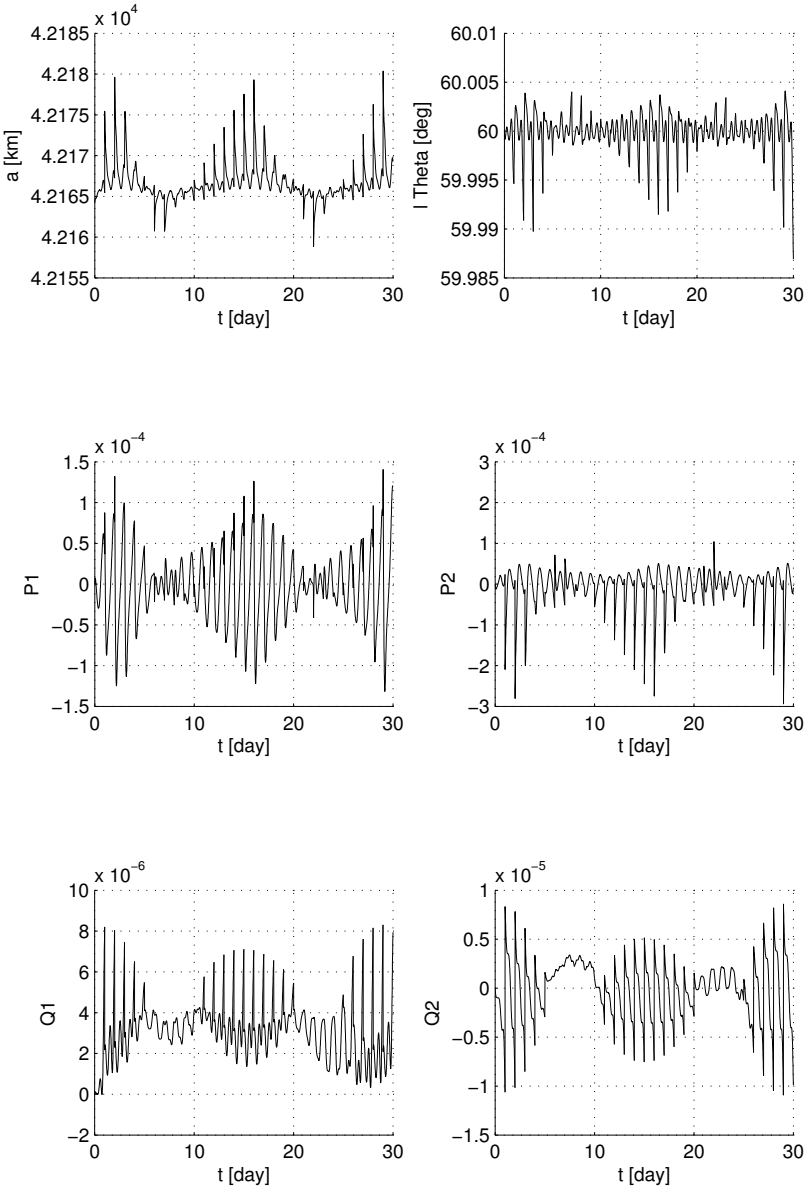

Figure 6.18: *Longitude and latitude deadbands equal to 0.001 deg; state variable time histories over 30 days obtained with control laws designed with the FHO approach.*

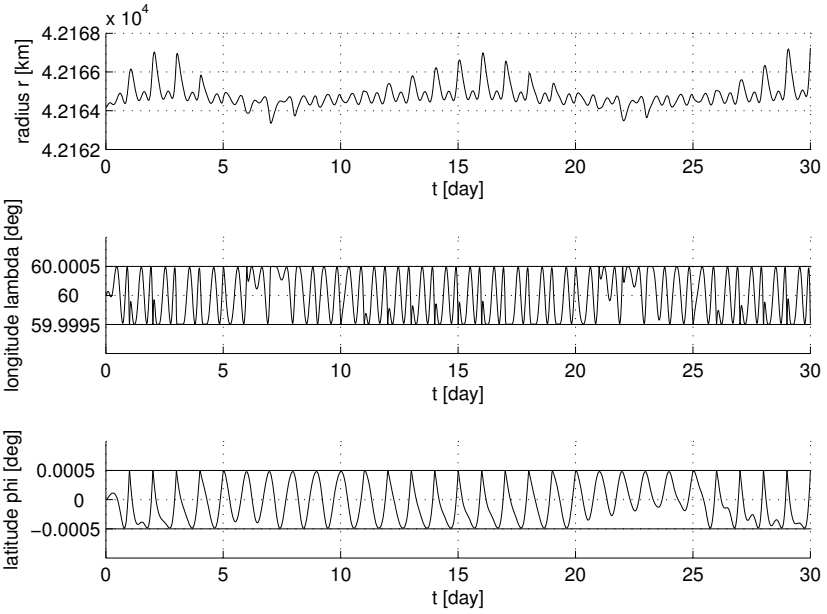

Figure 6.19: *Longitude and latitude deadbands equal to 0.001 deg; output variable time histories over 30 days obtained with control laws designed with the FHO approach.*

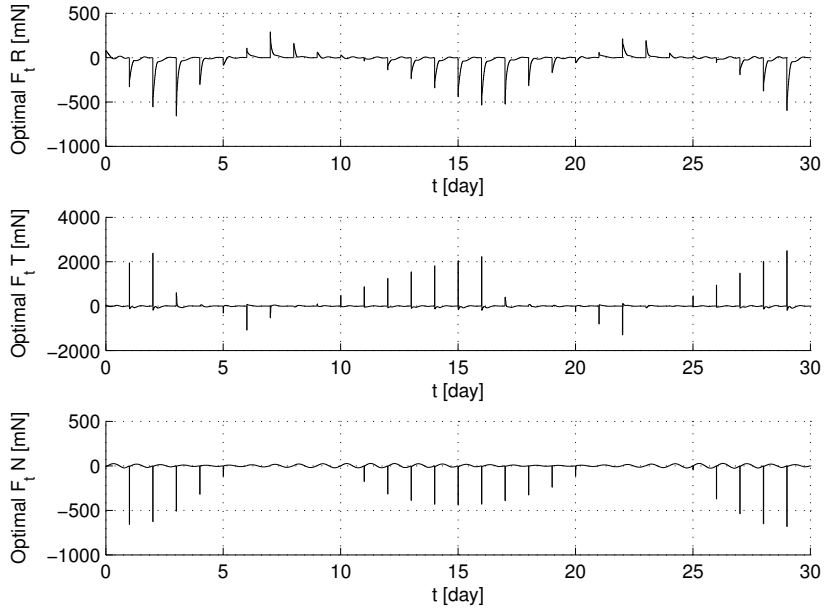

Figure 6.20: *Longitude and latitude deadbands equal to 0.001 deg; control laws (in terms of force) designed with the FHO approach.*

6.2.5 RHO Simulation Results

We have carried out some simulations with the receding horizon optimization approach explained in Section 6.2.2, without any constraint on the control variables, with the following values of receding horizon durations and sampling interval

- ➢ $T_{SKj} = 5$ days and $T_{Cj} = 1$ day, $\forall j = 1, 2, \ldots, 365$
- ➢ $h = 0.02 \quad \Rightarrow \quad N = 250$ and $M = 50$,

and for three values of longitude and latitude deadbands

- ➢ $2\lambda_{max} = 2\varphi_{max} = 0.1$ deg;
- ➢ $2\lambda_{max} = 2\varphi_{max} = 0.01$ deg;
- ➢ $2\lambda_{max} = 2\varphi_{max} = 0.001$ deg.

To face up to the model and numerical integration errors gathered for the output variables over the control horizon, instead of considering constant lower and upper bounds for the longitude and latitude

$$\mathbf{\Lambda}_{max} = \lambda_{max}\mathbf{1}_{2(N+1)\times 1}, \tag{6.97}$$

$$\mathbf{\Phi}_{max} = \varphi_{max}\mathbf{1}_{2(N+1)\times 1}, \tag{6.98}$$

over the prediction horizon we have considered the bounds depicted in Fig. (6.21).

Table 6.5 summarizes the ideal velocity increment budgets over one year of mission (from 2010 January 1.0 to 2011 January 1.0) for a satellite with the following structural parameters: a mass $m = 4500$ km; a mean surface absorbing the solar radiation $S = 300$ m^2; a mean reflectivity coefficient $\epsilon = 0.3$, which entails a radiation pressure coefficient $C_R = 1.3$. The initial dynamical condition is that of nominal station keeping with $\lambda_s = 60$ deg.

Fig.s (6.22)–(6.24) show the state variable, output variable and control law time histories respectively, obtained over the first 30 days of the simulations explained above (longitude and latitude deadbands equal to 0.01 deg).

Fig.s (6.25)–(6.27) show the state variable, output variable and control law time histories respectively, obtained over the first 30 days of the simulations explained above (longitude and latitude deadbands equal to 0.001 deg).

In Fig.s (6.28) and (6.29) we have drawn the time histories of the components of the environmental perturbing accelerations in nominal station keeping conditions (gray) on the plots of the control acceleration components (black) designed with the RHO approach for the deadbands equal to 0.01 deg and 0.001 deg respectively. We observe that in both cases the normal control components have the same one day periodic trend of the environmental perturbing acceleration normal component, but scaled in amplitude and shifted in phase of half a day. When the deadband is equal to 0.01 deg,

the radial and tangent control components also are one day periodic, even if the radial and tangent environmental acceleration components are half a day periodic. But, when the deadband is equal to 0.001 deg, besides the normal component, the radial and the tangent control components also are opposed in amplitude and phase to the radial and tangent environmental acceleration components. Consequently, they are half a day periodic.

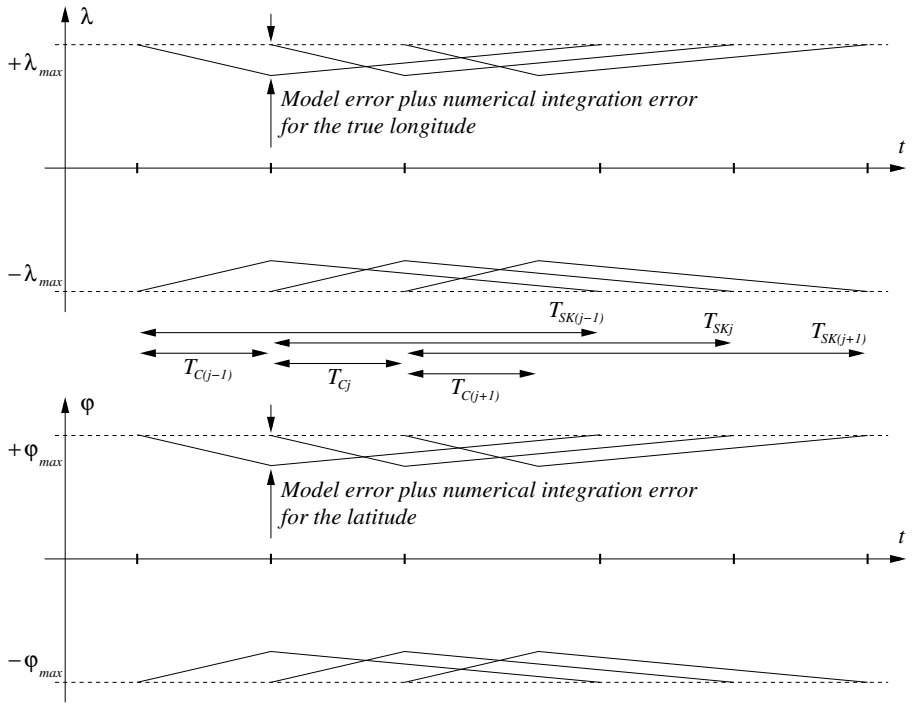

Figure 6.21: *Bounds over the prediction receding optimization horizons for the longitude and the latitude.*

DEADBANDS [deg]	**VELOCITY INCREMENT BUDGETS [m/s]**						
$2\lambda_{max} = 2\varphi_{max}$	Δv_{tR}^{+}	Δv_{tR}^{-}	Δv_{tT}^{+}	Δv_{tT}^{-}	Δv_{tN}^{+}	Δv_{tN}^{-}	$\Delta V = \sum \Delta v_t$
0.1	1.80	1.80	4.23	3.16	29.36	29.18	69.56
0.01	2.39	2.29	5.17	4.10	32.13	31.29	77.40
0.001	25.42	25.65	43.11	42.01	34.75	34.73	205.70

Table 6.5: *Ideal velocity increment budgets over one year of mission (from 2010 January 1.0 to 2011 January 1.0) obtained with the RHO approach.*

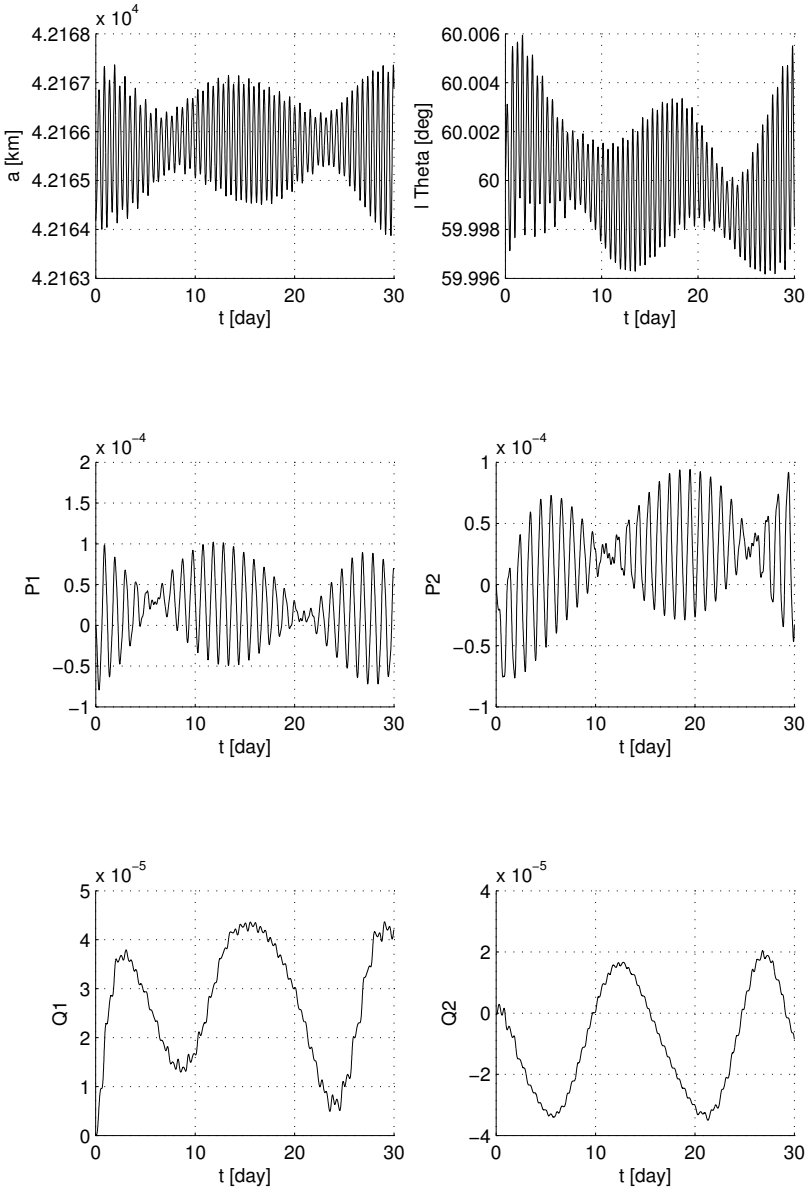

Figure 6.22: *Longitude and latitude deadbands equal to 0.01 deg; state variable time histories over 30 days obtained with control laws designed with the RHO approach.*

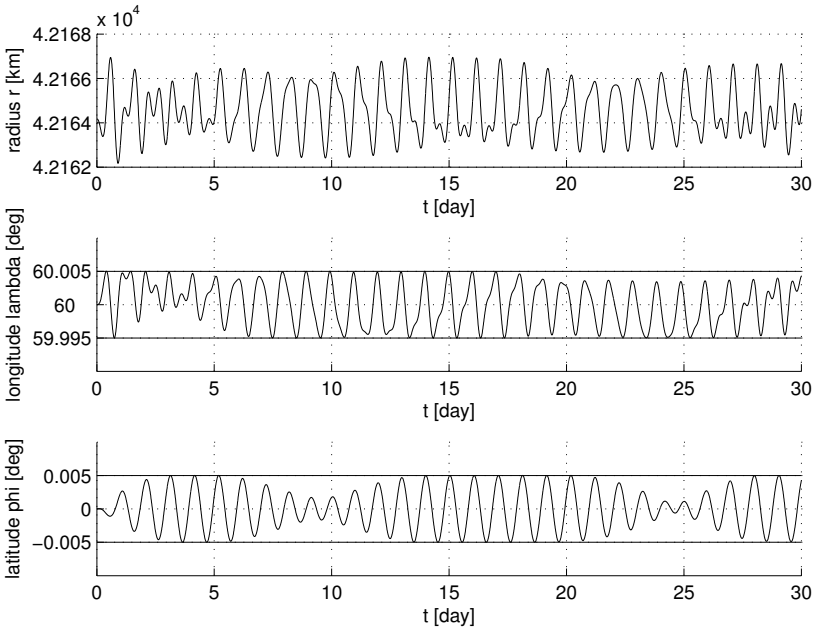

Figure 6.23: *Longitude and latitude deadbands equal to 0.01 deg; output variable time histories over 30 days obtained with control laws designed with the RHO approach.*

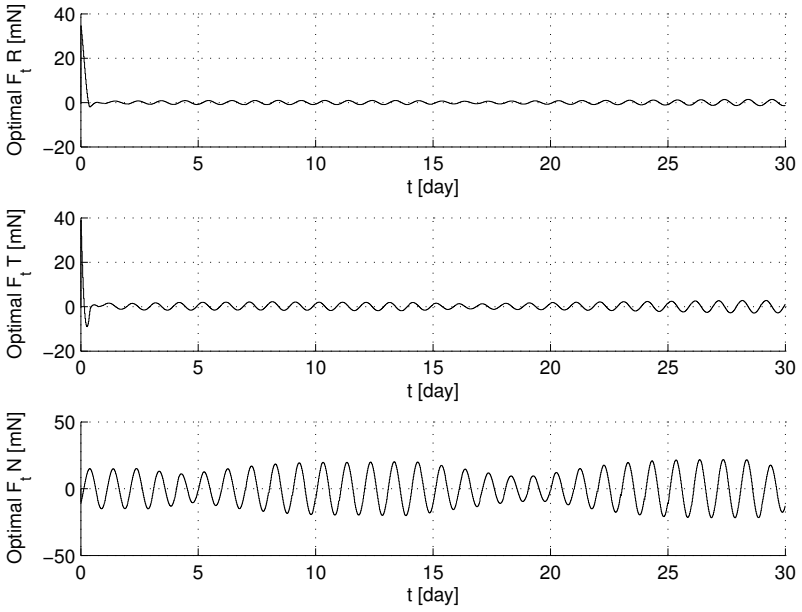

Figure 6.24: *Longitude and latitude deadbands equal to 0.01 deg; control laws (in terms of force) designed with the RHO approach.*

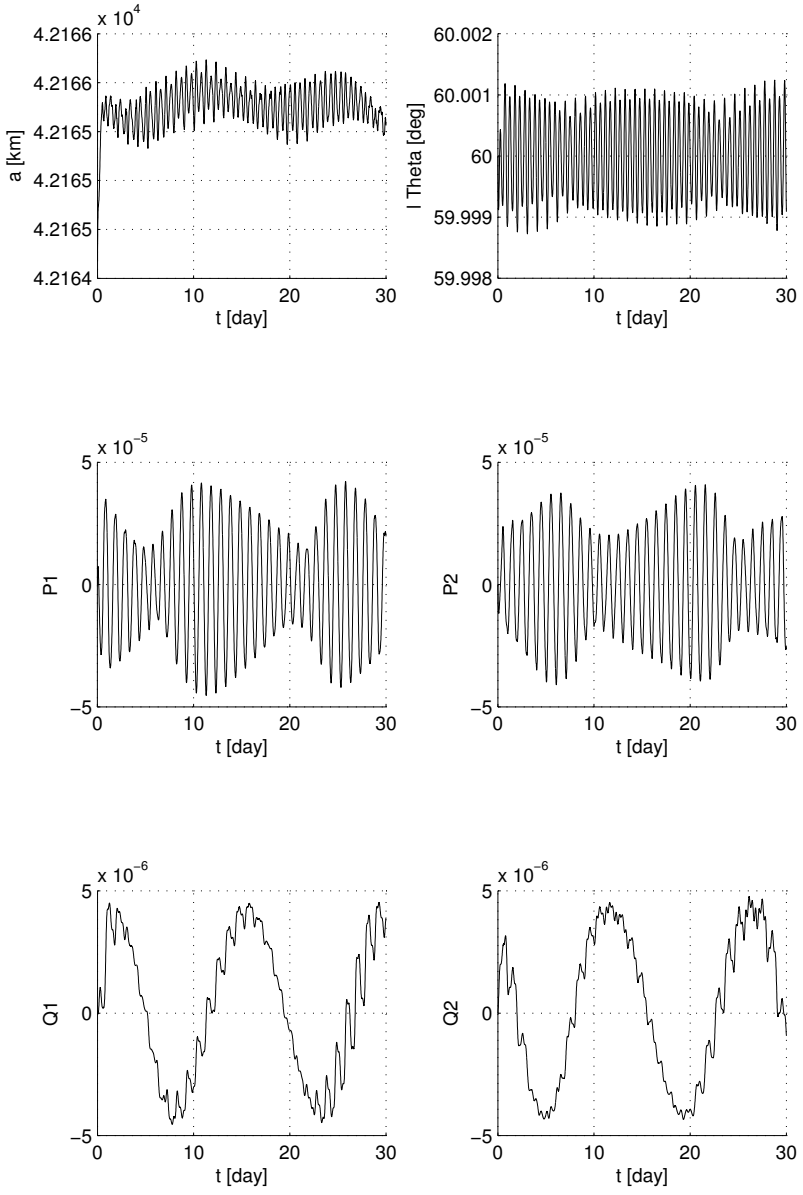

Figure 6.25: *Longitude and latitude deadbands equal to 0.001 deg; state variable time histories over 30 days obtained with control laws designed with the RHO approach.*

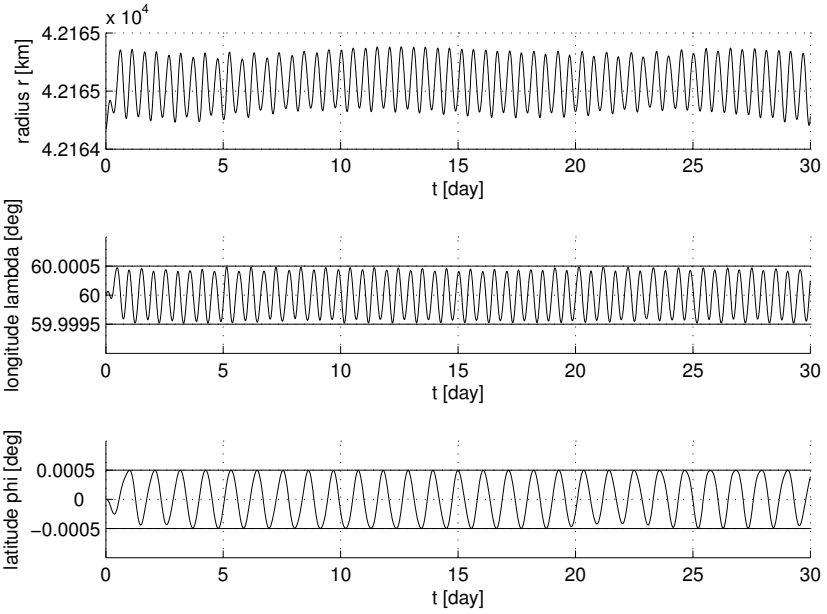

Figure 6.26: *Longitude and latitude deadbands equal to 0.001 deg; output variable time histories over 30 days obtained with control laws designed with the RHO approach.*

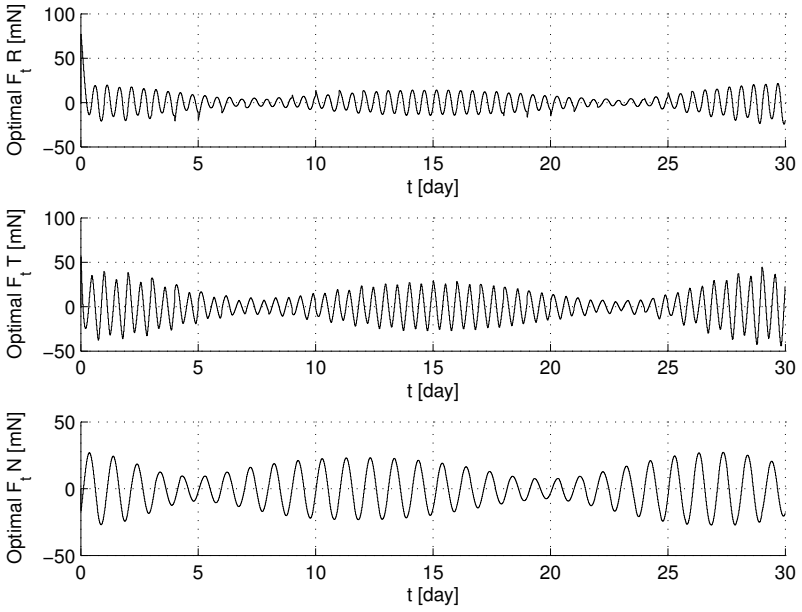

Figure 6.27: *Longitude and latitude deadbands equal to 0.001 deg; control laws (in terms of force) designed with the RHO approach.*

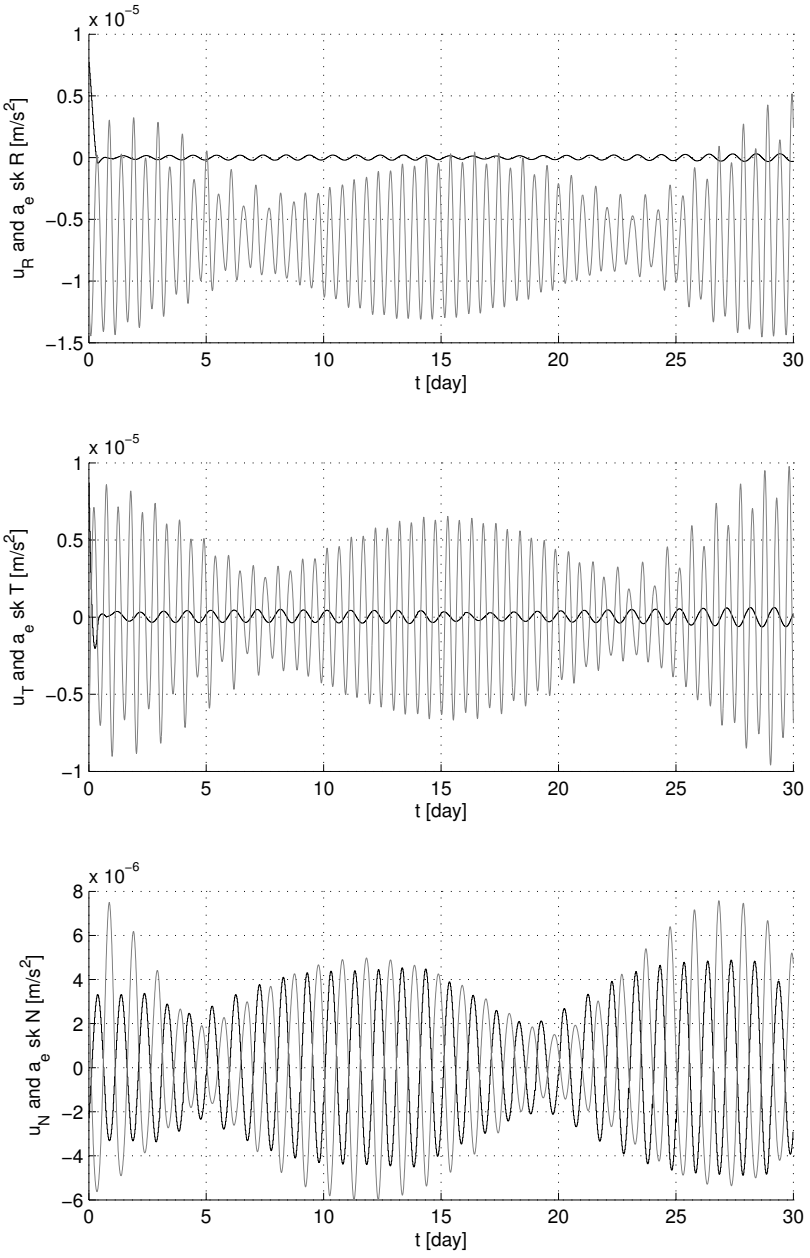

Figure 6.28: *Longitude and latitude deadbands equal to 0.01 deg; control acceleration components designed with the RHO approach (black) and environmental perturbing acceleration components (gray).*

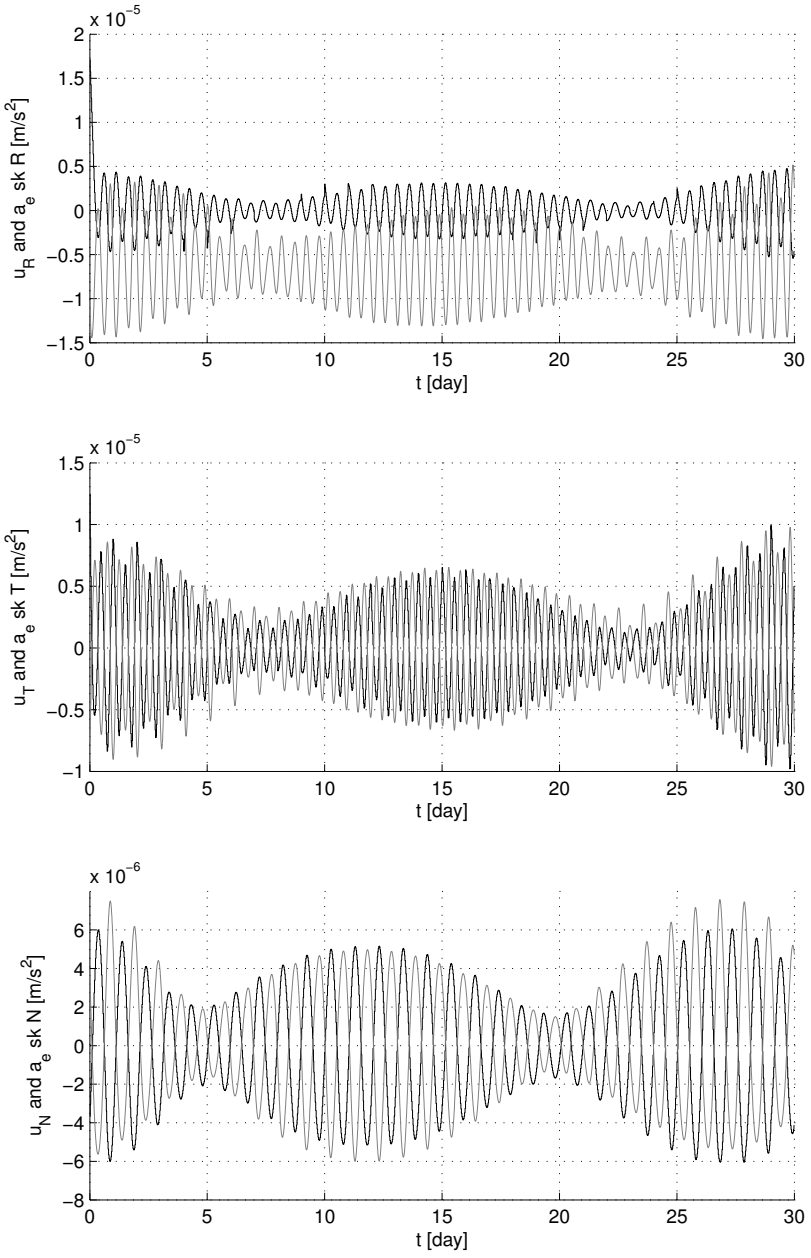

Figure 6.29: *Longitude and latitude deadbands equal to 0.001 deg; control acceleration components designed with the RHO approach (black) and environmental perturbing acceleration components (gray).*

In Fig.s (6.30) and (6.31) we have drawn in the (l_Θ, a) plane the semi-major axis vs the true longitude over one year, with the control applied, for deadband equal to 0.01 deg and 0.001 deg respectively. We have calculated the average value of the semi-major axis with the control applied over one year. In both cases (deadband equal to 0.01 deg and 0.001 deg) and for $\lambda_s = 60$ deg, this mean value is nearly equal to 42165.73 km, which is 1.56 km greater than the Keplerian semi-major axis (i.e., the semi-major axis initial value). In a first approximation we can interpret this mean semi-major axis as the synchronous semi-major axis (see, e.g., [Kamel et al., 1973], [Legendre, 1980a], [Legendre, 1983], [Campan et al., 1995b]).

In Fig.s (6.32) and (6.33) we have drawn in the (P_2, P_1) plane the P_1 vs the P_2 eccentricity vector component over one year, with the control applied, for deadband equal to 0.01 deg and 0.001 deg respectively.

In Fig.s (6.34) and (6.35) we have drawn in the (Q_2, Q_1) plane the Q_1 vs the Q_2 inclination vector component over one year, with the control applied, for deadband equal to 0.01 deg and 0.001 deg respectively. In red we have depicted the inclination tolerance circle.

The values at the end of each day of the state variables with the control applied will be the target values to determine the actual control laws taking into account the technological specifications. In other words, the above plots give an idea of the target time histories of the six orbital parameters, which have to be tracked with a real low thrust propulsion system.

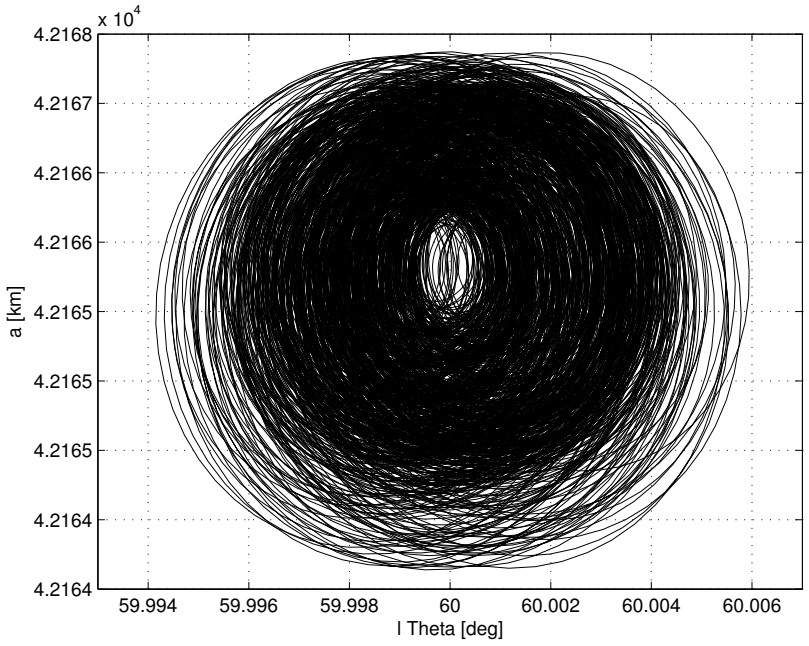

Figure 6.30: *Semi-major axis vs the true longitude over one year, with the control applied, for deadband equal to 0.01 deg.*

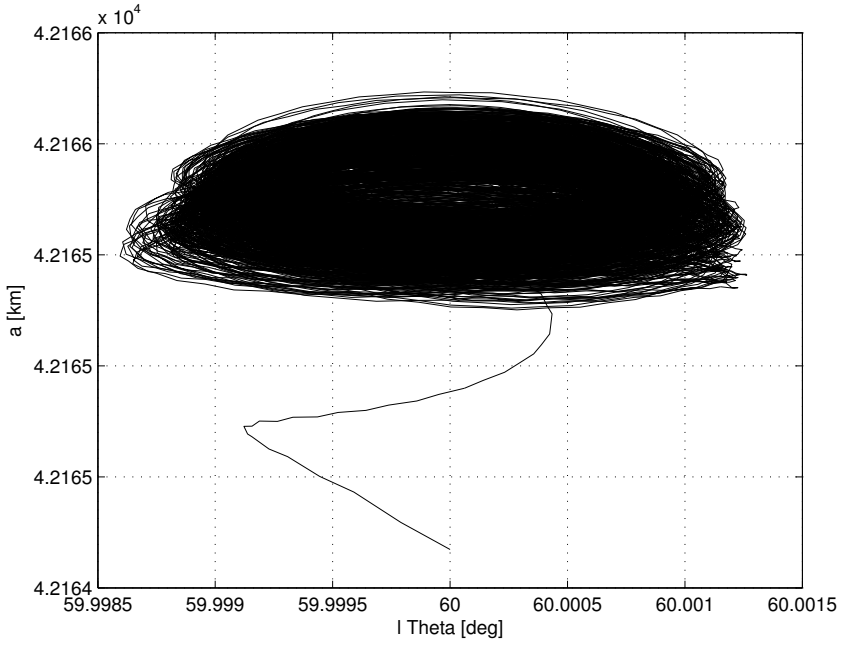

Figure 6.31: *Semi-major axis vs the true longitude over one year, with the control applied, for deadband equal to 0.001 deg.*

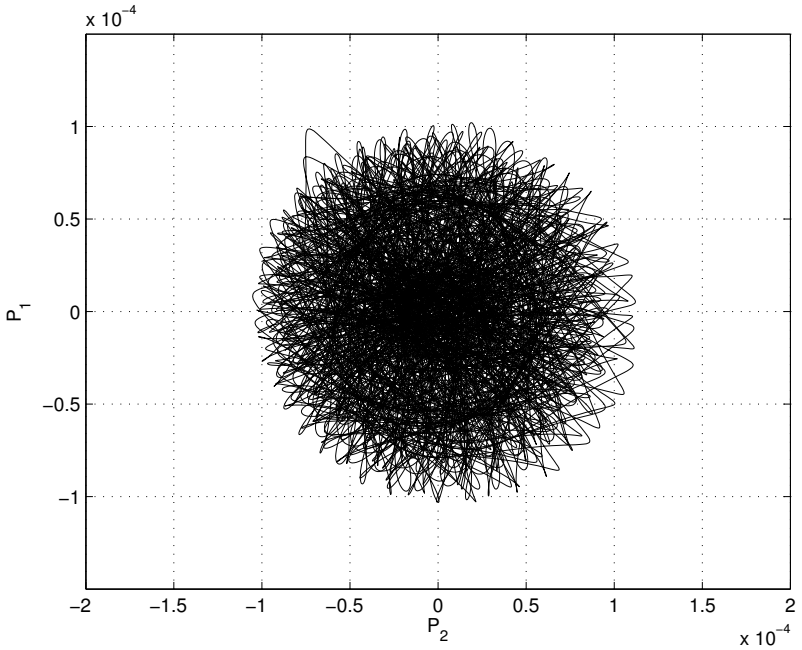

Figure 6.32: P_1 *vs the* P_2 *eccentricity vector component over one year, with the control applied, for deadband equal to 0.01 deg.*

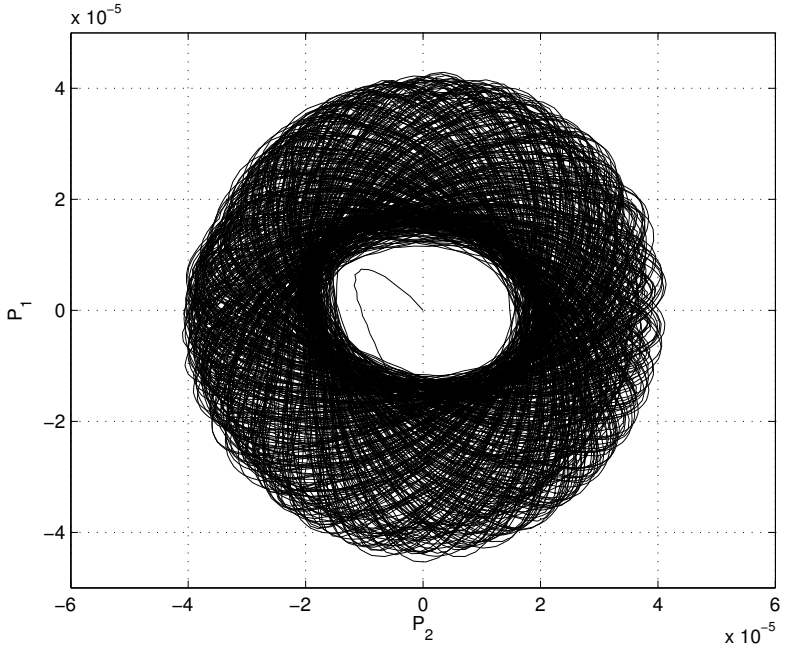

Figure 6.33: P_1 *vs the* P_2 *eccentricity vector component over one year, with the control applied, for deadband equal to 0.001 deg.*

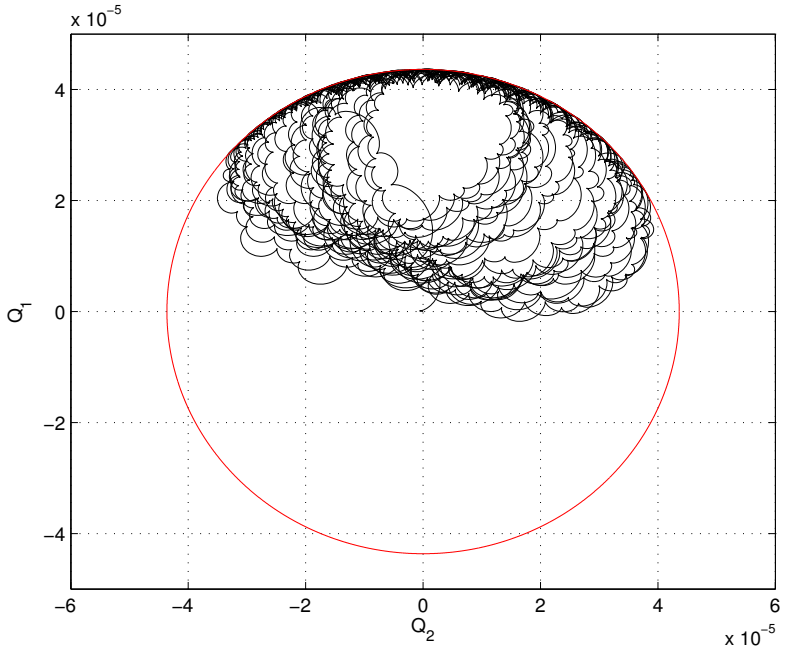

Figure 6.34: Q_1 *vs the* Q_2 *eccentricity vector component over one year, with the control applied, for deadband equal to 0.01 deg. In red the inclination tolerance circle.*

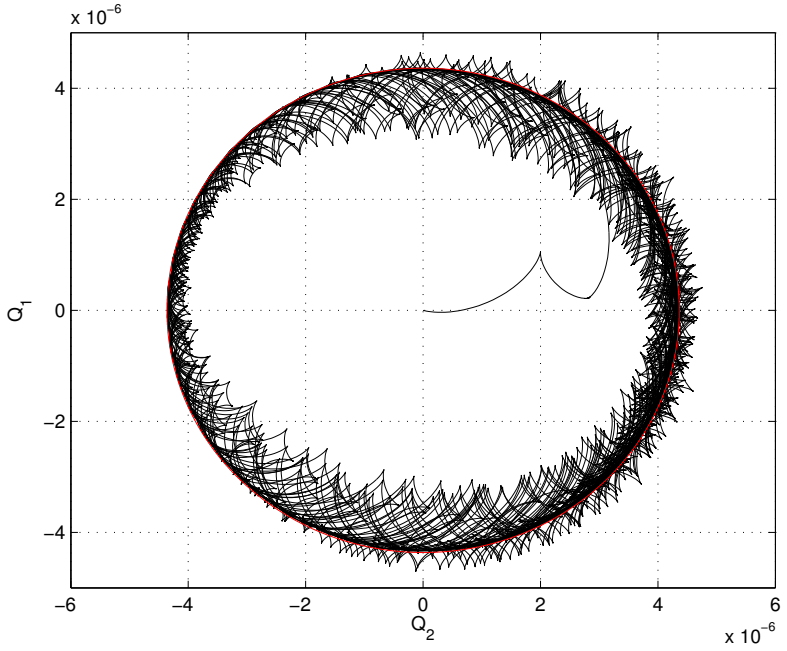

Figure 6.35: Q_1 *vs the* Q_2 *eccentricity vector component over one year, with the control applied, for deadband equal to 0.001 deg. In red the inclination tolerance circle.*

6.3 Technological Specifications

The time histories of the control components obtained in the previous section and drawn in Fig.s (6.24) and (6.27) are not practically realizable because they would imply a propulsion system always on and providing thrusts that can be modulated. In practice the electrical thrusters employed for GEO station keeping purposes are able to work only in on off conditions and they can not work more than few hours a day.

To derive on off control laws from the modulated ones, we have first tried to apply the classical method of concentrating a control action spread over a long time interval in a shorter time interval centered in the barycenter of the long time interval. Once the constant value of the thrust fixed, this operation is performed in a such a way that the integral of the modulated control action over the long time interval remains equal to the integral of the on off control action over the short time interval.

We have applied the above idea to the case with longitude and latitude deadbands equal to 0.01 deg. First we have estimated the daily mean velocity increments produced over one year by each of the six thrusters mounted along the axes of the RTN reference frame as follows

$$\Delta v_R^+ = \frac{\int_T u_R^+(t)dt}{365}, \qquad \Delta v_R^- = \frac{\int_T u_R^-(t)dt}{365} \tag{6.99}$$

$$\Delta v_T^+ = \frac{\int_T u_T^+(t)dt}{365}, \qquad \Delta v_T^- = \frac{\int_T u_R^-(t)dt}{365} \tag{6.100}$$

$$\Delta v_N^+ = \frac{\int_T u_N^+(t)dt}{365}, \qquad \Delta v_N^- = \frac{\int_T u_R^-(t)dt}{365} \tag{6.101}$$

where $T = 1$ year and

$$u_R^+(t) = \begin{cases} u_R(t) & \text{for } t \text{ s.t. } u_R(t) \geq 0 \\ 0 & \text{for } t \text{ s.t. } u_R(t) < 0 \end{cases}, \qquad u_R^-(t) = \begin{cases} 0 & \text{for } t \text{ s.t. } u_R(t) \geq 0 \\ u_R(t) & \text{for } t \text{ s.t. } u_R(t) < 0 \end{cases},$$

$$u_T^+(t) = \begin{cases} u_T(t) & \text{for } t \text{ s.t. } u_T(t) \geq 0 \\ 0 & \text{for } t \text{ s.t. } u_T(t) < 0 \end{cases}, \qquad u_T^-(t) = \begin{cases} 0 & \text{for } t \text{ s.t. } u_T(t) \geq 0 \\ u_T(t) & \text{for } t \text{ s.t. } u_T(t) < 0 \end{cases},$$

$$u_N^+(t) = \begin{cases} u_N(t) & \text{for } t \text{ s.t. } u_N(t) \geq 0 \\ 0 & \text{for } t \text{ s.t. } u_N(t) < 0 \end{cases}, \qquad u_N^-(t) = \begin{cases} 0 & \text{for } t \text{ s.t. } u_N(t) \geq 0 \\ u_N(t) & \text{for } t \text{ s.t. } u_N(t) < 0 \end{cases}.$$

Once the maximum daily switching on time interval T_{mMAX} known, thanks to the daily mean velocity increment values (6.99)–(6.101) we can fix the thrust level of each thruster as follows

$$F_R^+ = m\frac{\Delta v_R^+}{T_{mMAX}}, \qquad F_R^- = m\frac{\Delta v_R^-}{T_{mMAX}} \tag{6.102}$$

$$F_T^+ = m\frac{\Delta v_T^+}{T_{mMAX}}, \qquad F_T^- = m\frac{\Delta v_T^-}{T_{mMAX}} \tag{6.103}$$

$$F_N^+ = m\frac{\Delta v_N^+}{T_{mMAX}}, \qquad F_N^- = m\frac{\Delta v_N^-}{T_{mMAX}}, \tag{6.104}$$

where m is the spacecraft mass. Once the thrust levels of each thruster and the actual velocity increments needed in the jth day known, the short switching on time intervals can be calculated as follows

$$T_{R_j^+} = m\frac{\Delta v_{Rj}^+}{F_R^+}, \qquad T_{R_j^-} = m\frac{\Delta v_{Rj}^-}{F_R^-} \tag{6.105}$$

$$T_{T_j^+} = m\frac{\Delta v_{Tj}^+}{F_T^+}, \qquad T_{T_j^-} = m\frac{\Delta v_{Tj}^-}{F_T^-} \tag{6.106}$$

$$T_{N_j^+} = m\frac{\Delta v_{Nj}^+}{F_N^+}, \qquad T_{N_j^-} = m\frac{\Delta v_{Nj}^-}{F_N^-}, \tag{6.107}$$

where

$$\Delta v_j = \int_{j\text{th day}} u(t)dt. \tag{6.108}$$

The instants of each maneuvers on the jth day are the barycenters of the long time intervals (i.e., the average of the control acceleration components weighted on the time)

$$t_{mR_j^+} = \frac{\int_{j\text{th day}} tu_R^+(t)dt}{\int_{j\text{th day}} u_R^+(t)dt}, \qquad t_{mR_j^-} = \frac{\int_{j\text{th day}} tu_R^-(t)dt}{\int_{j\text{th day}} u_R^-(t)dt}, \tag{6.109}$$

$$t_{mT_j^+} = \frac{\int_{j\text{th day}} tu_T^+(t)dt}{\int_{j\text{th day}} u_T^+(t)dt}, \qquad t_{mT_j^-} = \frac{\int_{j\text{th day}} tu_T^-(t)dt}{\int_{j\text{th day}} u_T^-(t)dt}, \tag{6.110}$$

$$t_{mN_j^+} = \frac{\int_{j\text{th day}} tu_N^+(t)dt}{\int_{j\text{th day}} u_N^+(t)dt}, \qquad t_{mN_j^-} = \frac{\int_{j\text{th day}} tu_N^-(t)dt}{\int_{j\text{th day}} u_N^-(t)dt}. \tag{6.111}$$

Since the control components are piecewise constant, the integrals in formulas (6.99)–(6.101), (6.105)–(6.107) and (6.109)–(6.111) can be replaced with the discrete expressions in function of the optimal samples of control

$$\Delta v = \frac{\int_T u(t)dt}{365} \quad \longrightarrow \quad \Delta v = \frac{\sum_{k=1}^{365M}[u^*(\bar{t}_k)h]}{365}, \tag{6.112}$$

$$\Delta v_j = \int_{j\text{th day}} u(t)dt \quad \longrightarrow \quad \Delta v_j = \sum_{k=1}^{M}\left[u_j^*(\bar{t}_k)h\right] \tag{6.113}$$

and

$$t_{mj} = \frac{\int_{j\text{th day}} tu(t)dt}{\int_{j\text{th day}} u(t)dt} \quad \longrightarrow \quad t_{mj} = \frac{\sum_{k=1}^{M}\left[\bar{t}_k u_j^*(\bar{t}_k)h\right]}{\sum_{k=1}^{M}\left[u_j^*(\bar{t}_k)h\right]}. \tag{6.114}$$

As regards the deadbands equal to 0.01 deg, Fig.s 6.36 and 6.37 show the on off control laws obtained over eight days with the procedure just described with $T_{mMAX} = 1.5$ hours. In Fig.s 6.38 and 6.39 we have drawn the state and output variables obtained applying modulated control laws (dashed lines) and those ones obtained applying the on off control laws (solid lines).

Fig.s 6.40–6.43 have been obtained with $T_{mMAX} = 3$ hours.

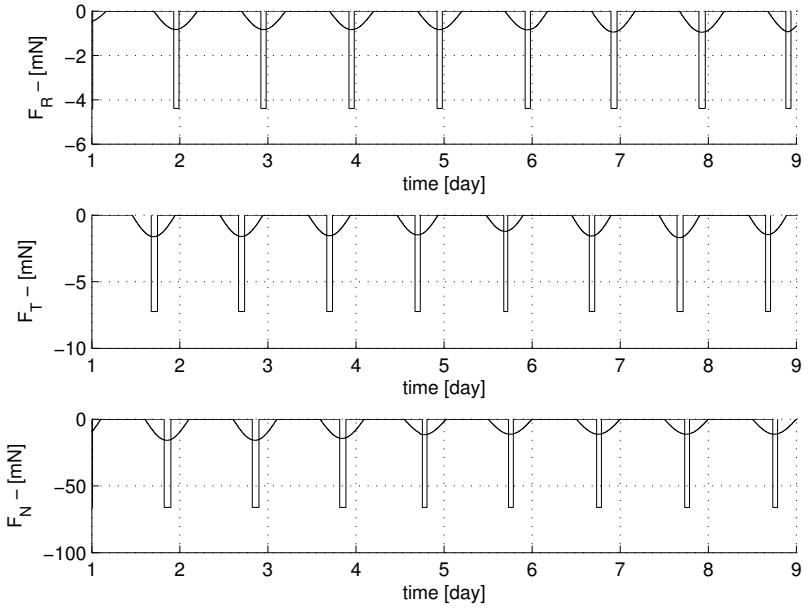

Figure 6.36: *Modulated and on off negative control vector components in terms of force ($T_{mMAX} = 1.5$ hours).*

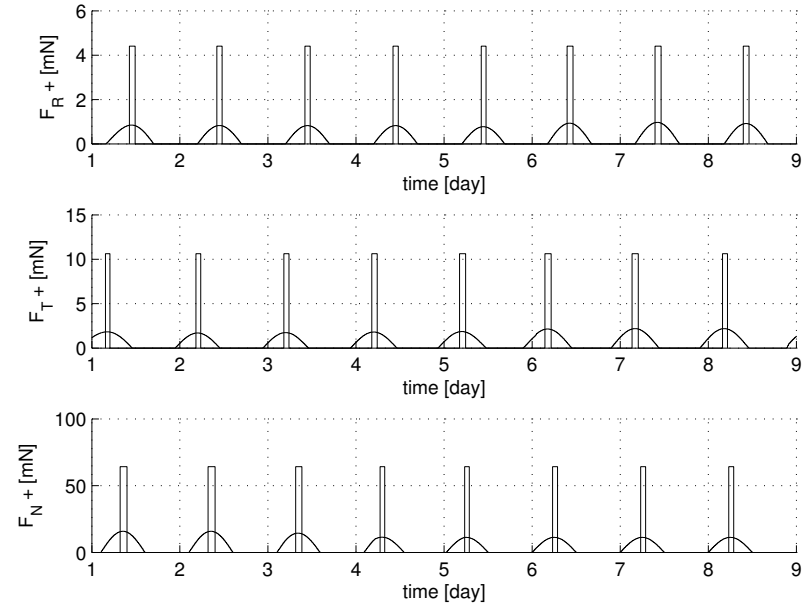

Figure 6.37: *Modulated and on off positive control vector components in terms of force ($T_{mMAX} = 1.5$ hours).*

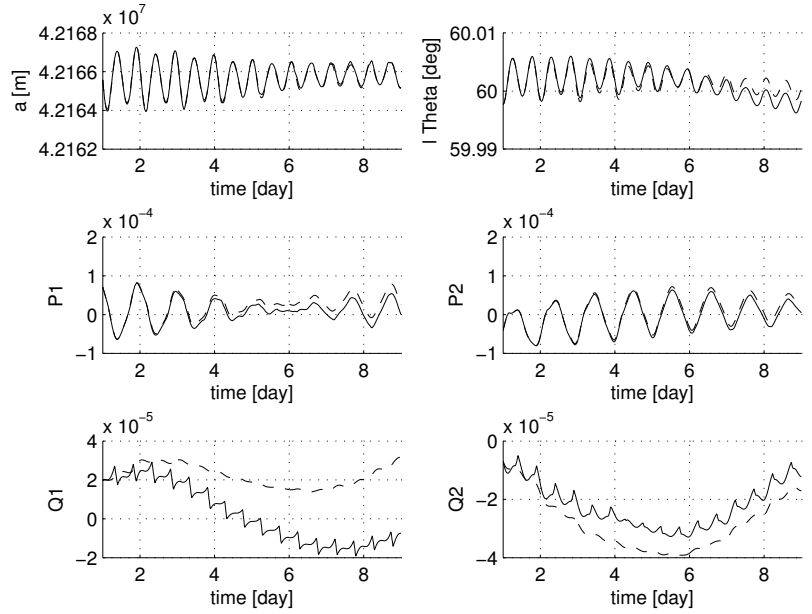

Figure 6.38: *State variables obtained applying modulated control laws (dashed lines) and the on off control laws (solid lines) ($T_{mMAX} = 1.5$ hours).*

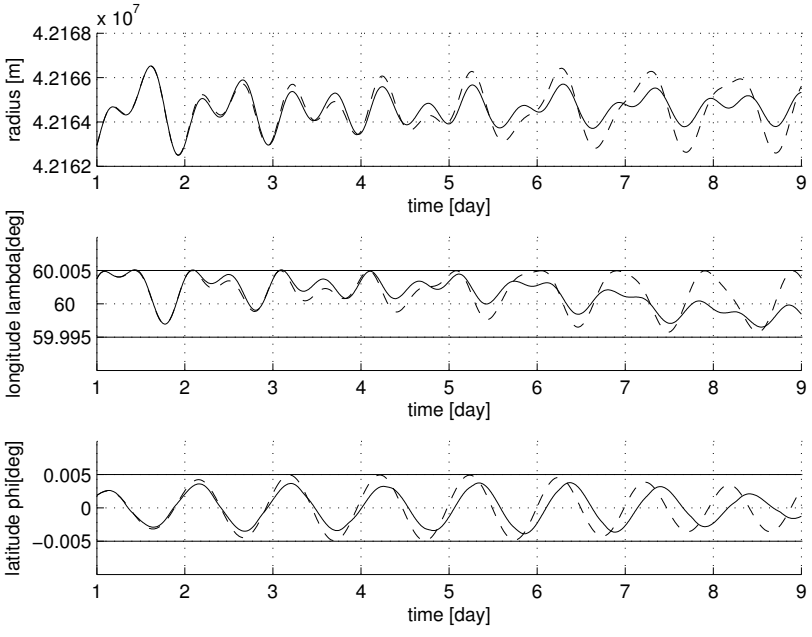

Figure 6.39: *Output variables obtained applying modulated control laws (dashed lines) and the on off control laws (solid lines) ($T_{mMAX} = 1.5$ hours).*

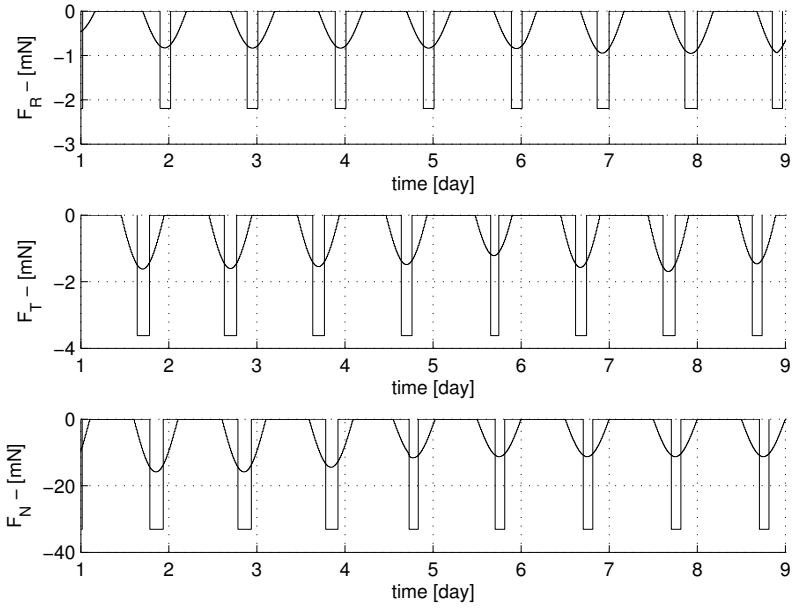

Figure 6.40: *Modulated and on off negative control vector components in terms of force ($T_{mMAX} = 3$ hours).*

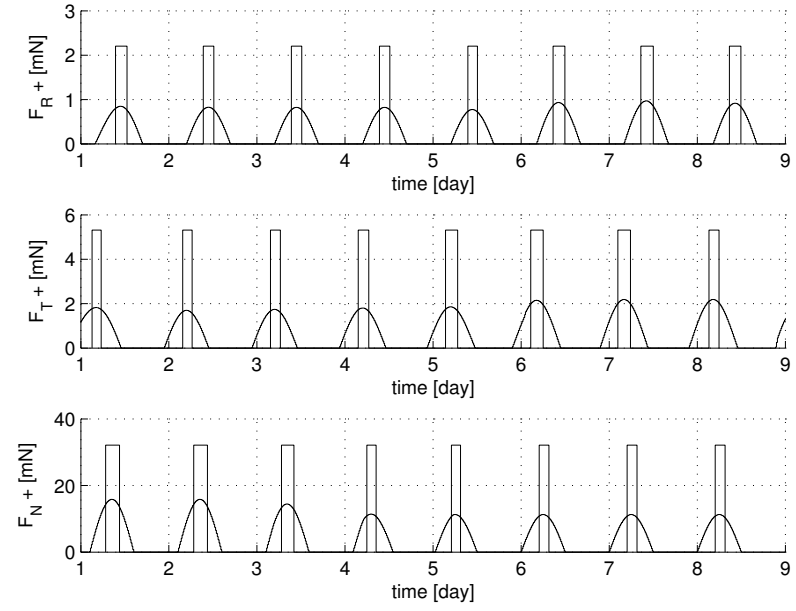

Figure 6.41: *Modulated and on off positive control vector components in terms of force ($T_{mMAX} = 3$ hours).*

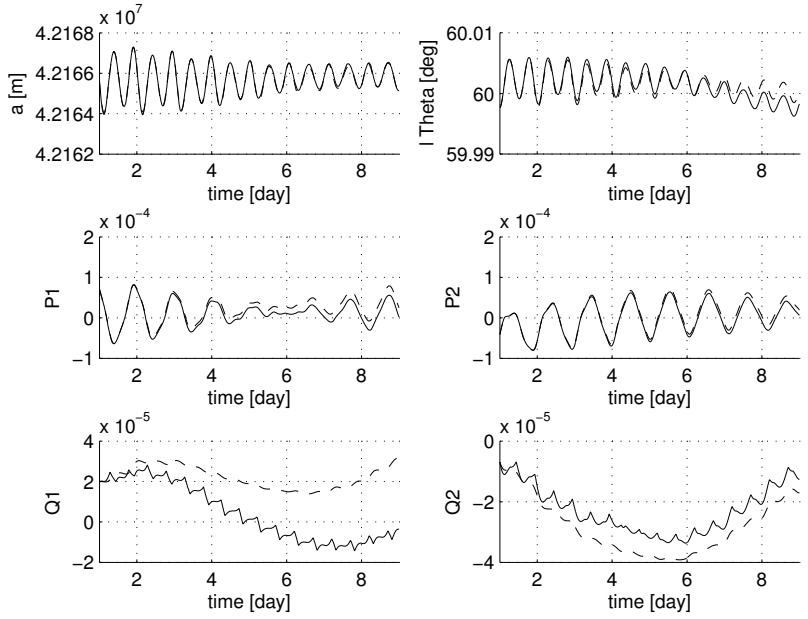

Figure 6.42: *State variables obtained applying modulated control laws (dashed lines) and the on off control laws (solid lines) ($T_{mMAX} = 3$ hours).*

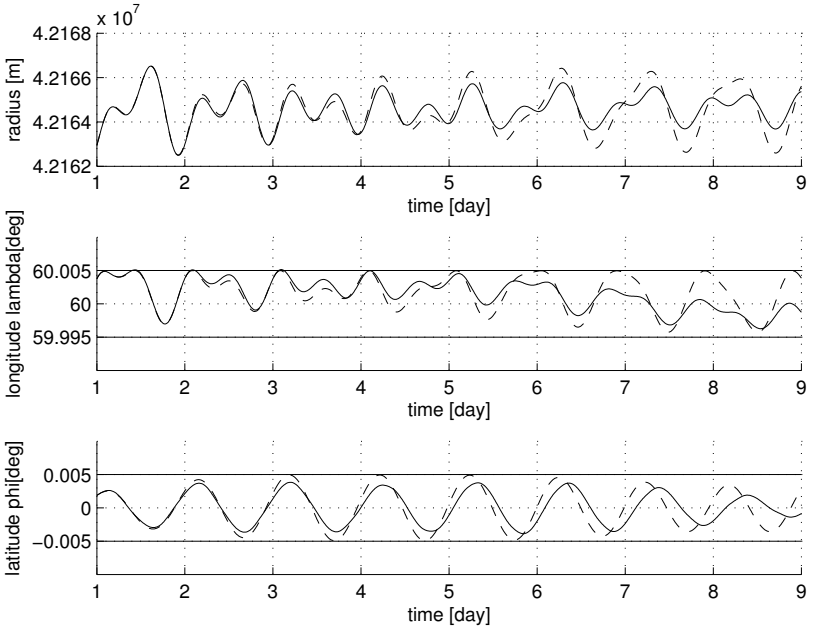

Figure 6.43: *Output variables obtained applying modulated control laws (dashed lines) and the on off control laws (solid lines) ($T_{mMAX} = 3$ hours).*

To determine the switching on and switching off instants of the propulsion system thrusters in a less "empirical" and more systematic way, a nonlinear optimization problem has to be solved over each day imposing that the target conditions found with the RHO approach are reached at the end of each day with on off thrusts. In the following sections we evaluate the thrust acceleration effects by means of a thrust effect linear model.

6.3.1 Thrust Acceleration Effects

Using a thrust effect model and the optimal modulated time histories of the control variables found in the previous sections, the exact maneuver durations

$$T_m = t_m^{off} - t_m^{on} \tag{6.115}$$

and maneuver epochs located in the middle of the corresponding maneuver intervals

$$t_m = \frac{t_m^{on} + t_m^{off}}{2} = t_m^{on} + \frac{T_m}{2} = t_m^{off} - \frac{T_m}{2} \tag{6.116}$$

can be obtained forcing to reach target conditions at the end of each correction cycle T_j one day long. To this purpose, the first task is to evaluate analytically the effect of the following six thrust acceleration time histories over the jth correction time interval

$$u_{Rj}^{+}(t) = \begin{cases} \bar{u}_R^{+} & \text{if} \quad t_{R_j^+}^{on} \le t \le t_{R_j^+}^{off} \\ 0 & \text{otherwise} \end{cases}, \qquad u_{Rj}^{-}(t) = \begin{cases} -\bar{u}_R^{-} & \text{if} \quad t_{R_j^-}^{on} \le t \le t_{R_j^-}^{off} \\ 0 & \text{otherwise} \end{cases}, \tag{6.117}$$

$$u_{Tj}^{+}(t) = \begin{cases} \bar{u}_T^{+} & \text{if} \quad t_{T_j^+}^{on} \le t \le t_{T_j^+}^{off} \\ 0 & \text{otherwise} \end{cases}, \qquad u_{Tj}^{-}(t) = \begin{cases} -\bar{u}_T^{-} & \text{if} \quad t_{T_j^-}^{on} \le t \le t_{T_j^-}^{off} \\ 0 & \text{otherwise} \end{cases}, \tag{6.118}$$

$$u_{Nj}^{+}(t) = \begin{cases} \bar{u}_N^{+} & \text{if} \quad t_{N_j^+}^{on} \le t \le t_{N_j^+}^{off} \\ 0 & \text{otherwise} \end{cases}, \qquad u_{Nj}^{-}(t) = \begin{cases} -\bar{u}_N^{-} & \text{if} \quad t_{N_j^-}^{on} \le t \le t_{N_j^-}^{off} \\ 0 & \text{otherwise} \end{cases}, \tag{6.119}$$

where the constant acceleration values $\bar{u}$ are the thrust levels (6.102)–(6.104) divided by the mass m. The thrust acceleration effect is evaluated in terms of total changes of the equinoctial orbital element deviations

$$\boldsymbol{\zeta}_t = \begin{bmatrix} \zeta_{t1} & \zeta_{t2} & \zeta_{t3} & \zeta_{t4} & \zeta_{t5} & \zeta_{t6} \end{bmatrix}^T = \begin{bmatrix} a_t - a_k & P_{1t} & P_{2t} & Q_{1t} & Q_{2t} & l_{\Theta t} - \lambda_s \end{bmatrix}^T \tag{6.120}$$

induced by the thrust accelerations (6.117)–(6.119) only. The total changes will be indicated by the notation $\tilde{\Delta}$ used also in Section 5.5.2:

$$\tilde{\Delta}_j \boldsymbol{\zeta}_t = \boldsymbol{\zeta}_t(t_{fCj}) - \boldsymbol{\zeta}_t(t_{iCj}) \tag{6.121}$$

with

$$\boldsymbol{\zeta}_t(t_{iCj}) = \mathbf{0}_{6\times 1} \tag{6.122}$$

for every j. Condition (6.122) is a reset condition of the thrust effects. This means that, to calculate on off control laws over consecutive finite time horizons, the spacecraft state deviation $\boldsymbol{\zeta} = \boldsymbol{\zeta}_e + \boldsymbol{\zeta}_t$ with

$$\frac{d\boldsymbol{\zeta}_e}{dt} = \boldsymbol{A}(t)\boldsymbol{\zeta}_e + \boldsymbol{B}(t)\boldsymbol{a}_{e_{sk}}(t), \quad \boldsymbol{\zeta}_e(t_{iCj}) = \boldsymbol{\zeta}_{iCj}, \tag{6.123}$$

and

$$\frac{d\boldsymbol{\zeta}_t}{dt} = \boldsymbol{A}(t)\boldsymbol{\zeta}_t + \boldsymbol{B}(t)\boldsymbol{u}(t), \quad \boldsymbol{\zeta}_t(t_{iCj}) = \boldsymbol{0}_{6\times 1}, \tag{6.124}$$

is considered at the beginning of each horizon as ascribable to the environmental perturbing accelerations only. In the following we will indicate with $\tilde{\Delta}_j^+$ and with $\tilde{\Delta}_j^-$ the total changes induced by positive and negative thrust accelerations respectively. Since $u_j(t) = u_j^+(t) + u_j^-(t)$, for the superposition property the following relation holds

$$\tilde{\Delta}_j \boldsymbol{\zeta}_t = \tilde{\Delta}_j^+ \boldsymbol{\zeta}_t + \tilde{\Delta}_j^- \boldsymbol{\zeta}_t. \tag{6.125}$$

Total changes $\tilde{\Delta}_j^+ \boldsymbol{\zeta}_t$, $\tilde{\Delta}_j^+ \boldsymbol{\zeta}_t$ will be evaluated as follows

$$\tilde{\Delta}_j^+ \boldsymbol{\zeta}_t = \boldsymbol{\zeta}^+(t_{fCj}) - \boldsymbol{\zeta}_e(t_{fCj}), \tag{6.126}$$

$$\tilde{\Delta}_j^- \boldsymbol{\zeta}_t = \boldsymbol{\zeta}^-(t_{fCj}) - \boldsymbol{\zeta}_e(t_{fCj}), \tag{6.127}$$

where $\boldsymbol{\zeta}^+$ and $\boldsymbol{\zeta}^-$ are the state vector deviations affected by the environmental perturbing accelerations and by the positive and negative thrust accelerations respectively, $\boldsymbol{\zeta}_e$ is the state vector deviation affected by the environmental perturbing accelerations only.

In the following sections, the matrix $\boldsymbol{A}(t)$ will be approximated with the time invariant matrix

$$\boldsymbol{A}_c = \begin{bmatrix} 0 & 0 & 0 & 0 & 0 & A_{al_\Theta} \\ 0 & 0 & 0 & 0 & 0 & 0 \\ 0 & 0 & 0 & 0 & 0 & 0 \\ 0 & 0 & 0 & 0 & 0 & 0 \\ 0 & 0 & 0 & 0 & 0 & 0 \\ A_K & 0 & 0 & 0 & 0 & 0 \end{bmatrix}. \tag{6.128}$$

This approximation leads to an analytical simpler form of the transition matrix. It will be justified and described in detail in the next chapter.

6.3.1.1 Semi-Major Axis and Longitude Total Changes

The analytical expressions of the total changes induced by the radial and tangent thrust accelerations on the semi-major and the mean longitude deviations ζ_{t1} and ζ_{t6} are the solution of the differential system

$$\frac{d}{dt}\begin{bmatrix} \zeta_{t1} \\ \zeta_{t6} \end{bmatrix} = \begin{bmatrix} 0 & A_{al_\Theta} \\ A_K & 0 \end{bmatrix}\begin{bmatrix} \zeta_{t1} \\ \zeta_{t6} \end{bmatrix} + \frac{1}{v_{sk}}\begin{bmatrix} 0 & 2a_k \\ -2 & 0 \end{bmatrix}\begin{bmatrix} u_R(t) \\ u_T(t) \end{bmatrix}, \tag{6.129}$$

with the following acceleration components

$$u_R(t) = u_{Rj}^+(t) + u_{Rj}^-(t), \tag{6.130}$$

$$u_T(t) = u_{Tj}^+(t) + u_{Tj}^-(t). \tag{6.131}$$

Thanks to the approximation (7.31) of the transition matrix, the total changes over the jth day are the following

$$\begin{bmatrix} \tilde{\Delta}_j \zeta_{t1} \\ \tilde{\Delta}_j \zeta_{t6} \end{bmatrix} = \int_{t_{iCj}}^{t_{fCj}} \begin{bmatrix} 1 & A_{al_\Theta}(t_{fCj} - \tau) \\ A_K(t_{fCj} - \tau) & 1 \end{bmatrix} \frac{1}{v_{sk}} \begin{bmatrix} 0 & 2a_k \\ -2 & 0 \end{bmatrix} \begin{bmatrix} u_R(\tau) \\ u_T(\tau) \end{bmatrix} d\tau. \tag{6.132}$$

Since the time histories u_{Rj}^+, u_{Rj}^-, u_{Tj}^+ and u_{Tj}^- are different from zero only over the time interval $T_{mR_j^+}$, $T_{mR_j^-}$, $T_{mT_j^+}$ and $T_{mT_j^-}$ respectively, the total changes of the semi-major axis and the mean longitude induced by the positive and negative thrust accelerations over the jth day become

$$\begin{bmatrix} \tilde{\Delta}_j^+ \zeta_{t1} \\ \tilde{\Delta}_j^+ \zeta_{t6} \end{bmatrix} = \frac{1}{v_{sk}} \begin{bmatrix} -A_{al_\Theta} T_{mR_j^+}^2 & 2a_k T_{mT_j^+} \\ -2T_{mR_j^+} & A_K a_k T_{mT_j^+}^2 \end{bmatrix} \begin{bmatrix} \bar{u}_R^+ \\ \bar{u}_T^+ \end{bmatrix} \tag{6.133}$$

and

$$\begin{bmatrix} \tilde{\Delta}_j^- \zeta_{t1} \\ \tilde{\Delta}_j^- \zeta_{t6} \end{bmatrix} = -\frac{1}{v_{sk}} \begin{bmatrix} -A_{al_\Theta} T_{mR_j^-}^2 & 2a_k T_{mT_j^-} \\ -2T_{mR_j^-} & A_K a_k T_{mT_j^-}^2 \end{bmatrix} \begin{bmatrix} \bar{u}_R^- \\ \bar{u}_T^- \end{bmatrix}. \tag{6.134}$$

6.3.1.2 Eccentricity Components Total Changes

The analytical expressions of the total changes induced by the radial and tangent thrust accelerations on the eccentricity component deviations ζ_{t2} and ζ_{t3} are the solution of the differential system

$$\frac{d}{dt} \begin{bmatrix} \zeta_{t2} \\ \zeta_{t3} \end{bmatrix} = \frac{1}{v_{sk}} \begin{bmatrix} -\cos K_{sk}(t) & 2\sin K_{sk}(t) \\ \sin K_{sk}(t) & 2\cos K_{sk}(t) \end{bmatrix} \begin{bmatrix} u_R(t) \\ u_T(t) \end{bmatrix}, \tag{6.135}$$

with the following acceleration components

$$u_R(t) = u_{Rj}^+(t) + u_{Rj}^-(t), \tag{6.136}$$

$$u_T(t) = u_{Tj}^+(t) + u_{Tj}^-(t). \tag{6.137}$$

Thanks to the approximation (7.31) of the transition matrix, the total changes over the jth day are the following

$$\begin{bmatrix} \tilde{\Delta}_j \zeta_{t2} \\ \tilde{\Delta}_j \zeta_{t3} \end{bmatrix} = \int_{t_{iCj}}^{t_{fCj}} \frac{1}{v_{sk}} \begin{bmatrix} -\cos K_{sk}(\tau) & 2\sin K_{sk}(\tau) \\ \sin K_{sk}(\tau) & 2\cos K_{sk}(\tau) \end{bmatrix} \begin{bmatrix} u_R(\tau) \\ u_T(\tau) \end{bmatrix} d\tau. \tag{6.138}$$

For the superposition property and the trigonometric identities

$$\sin a - \sin b = 2\cos\frac{a+b}{2}\sin\frac{a-b}{2}, \qquad \cos a - \cos b = -2\sin\frac{a+b}{2}\sin\frac{a-b}{2}, \tag{6.139}$$

the total changes of the eccentricity components induced by the positive and negative thrust accelerations over the jth day become

$$\begin{bmatrix}\tilde{\Delta}_j^+\zeta_{t2}\\ \tilde{\Delta}_j^+\zeta_{t3}\end{bmatrix} = \frac{2}{\omega_\oplus v_{sk}}\begin{bmatrix}-\cos K_{sk}(t_{mR_j^+}) & 2\sin K_{sk}(t_{mT_j^+})\\ \sin K_{sk}(t_{mR_j^+}) & 2\cos K_{sk}(t_{mT_j^+})\end{bmatrix}\begin{bmatrix}\bar{u}_R^+\sin\left(\omega_\oplus T_{mR_j^+}/2\right)\\ \bar{u}_T^+\sin\left(\omega_\oplus T_{mT_j^+}/2\right)\end{bmatrix} \tag{6.140}$$

and

$$\begin{bmatrix}\tilde{\Delta}_j^-\zeta_{t2}\\ \tilde{\Delta}_j^-\zeta_{t3}\end{bmatrix} = -\frac{2}{\omega_\oplus v_{sk}}\begin{bmatrix}-\cos K_{sk}(t_{mR_j^-}) & 2\sin K_{sk}(t_{mT_j^-})\\ \sin K_{sk}(t_{mR_j^-}) & 2\cos K_{sk}(t_{mT_j^-})\end{bmatrix}\begin{bmatrix}\bar{u}_R^-\sin\left(\omega_\oplus T_{mR_j^-}/2\right)\\ \bar{u}_T^-\sin\left(\omega_\oplus T_{mT_j^-}/2\right)\end{bmatrix}. \tag{6.141}$$

6.3.1.3 Inclination Components Total Changes

The analytical expressions of the total changes induced by the radial and tangent thrust accelerations on the eccentricity component deviations ζ_{t4} and ζ_{t5} are the solution of the differential system

$$\frac{d}{dt}\begin{bmatrix}\zeta_{t4}\\ \zeta_{t5}\end{bmatrix} = \frac{1}{v_{sk}}\begin{bmatrix}\frac{1}{2}\sin K_{sk}(t)\\ \frac{1}{2}\cos K_{sk}(t)\end{bmatrix}u_N(t), \tag{6.142}$$

with the following normal acceleration component

$$u_N(t) = u_{Nj}^+(t) + u_{Nj}^-(t). \tag{6.143}$$

Thanks to the approximation (7.31) of the transition matrix, the total changes over the jth day are the following

$$\begin{bmatrix}\tilde{\Delta}_j\zeta_{t4}\\ \tilde{\Delta}_j\zeta_{t5}\end{bmatrix} = \int_{t_{iCj}}^{t_{fCj}}\frac{1}{v_{sk}}\begin{bmatrix}\frac{1}{2}\sin K_{sk}(\tau)\\ \frac{1}{2}\cos K_{sk}(\tau)\end{bmatrix}u_N(\tau)d\tau. \tag{6.144}$$

The total changes of the inclination components induced by the positive and negative thrust accelerations over the jth day become

$$\begin{bmatrix}\tilde{\Delta}_j^+\zeta_{t4}\\ \tilde{\Delta}_j^+\zeta_{t5}\end{bmatrix} = \frac{1}{\omega_\oplus v_{sk}}\begin{bmatrix}\sin K_{sk}(t_{mN_j^+})\\ \cos K_{sk}(t_{mN_j^+})\end{bmatrix}\bar{u}_N^+\sin\left(\omega_\oplus T_{mN_j^+}/2\right) \tag{6.145}$$

and

$$\begin{bmatrix}\tilde{\Delta}_j^-\zeta_{t4}\\ \tilde{\Delta}_j^-\zeta_{t5}\end{bmatrix} = -\frac{1}{\omega_\oplus v_{sk}}\begin{bmatrix}\sin K_{sk}(t_{mN_j^-})\\ \cos K_{sk}(t_{mN_j^-})\end{bmatrix}\bar{u}_N^-\sin\left(\omega_\oplus T_{mN_j^-}/2\right). \tag{6.146}$$

6.3.2 On Off Maneuvers as Solutions of a Nonlinear POP

Once the total changes $\tilde{\Delta}_j^+$ and $\tilde{\Delta}_j^-$ are known over a correction time horizon, the nonlinear system of the equations (6.133), (6.134), (6.140), (6.141), (6.145) and (6.146) can be used as nonlinear equality constraints of a nonlinear optimization problem formulated over a time interval one

day long and it can be solved with the Matlab function *fmincon*. The maneuver intervals (6.105)–(6.107) and the maneuver epochs (6.109)–(6.111) deduced from the modulated thrust accelerations time histories are used as starting guess of the solution.

However, the more recently proposed low thrust propulsion system (see [Anzel, 1995] patent and Chapter 3 at page 109) are able to give radial tangent and normal thrust acceleration components simultaneously. For example, the thrust configuration of the [Anzel, 1995] patent is able to produce only a thrust vector which is the sum of four vectors with modulus equal to either zero or a maximum value F_{max}. In Fig. 6.44 we have plotted the tip trace of the thrust vector found over one year with the RHO approach and with longitude and latitude deadbands equal to 0.01 deg (see Section 6.2.5). We can recognize that there are really two planes to which the thrust belong (see Fig.s 6.45–6.47). But, when the station keeping box is with deadbands equal to 0.001 deg, we can not individuate such planes (see Fig.s 6.48–6.51). From this fact we can deduce that, with very small station keeping box, a propulsion system with six thrusters mounted respectively in the RTN directions and working independently is more suitable.

Fig.s 6.52–6.55 show some simulation results over a time interval of ten days obtained performing an additional step of optimization between each determination of the target conditions over correction horizon and the following determination of the continuous optimal control laws over a prediction horizon. With this additional optimization the following nonlinear parameter optimization problem is solved

to find the maneuver time intervals T_{m_i} with $i = 1, 2, 3, 4$ and the maneuver epochs t_{m_i} (located in the middle of the corresponding maneuver intervals), minimizing the total velocity increment budget

$$\Delta_j V = \frac{\sum_{i=1}^{4} F_i T_{m_i}}{m_j} \tag{6.147}$$

over the jth day and subject to the following equality constraints

$$\tilde{\Delta}_j \zeta_{t1} = \frac{1}{v_{sk}} \sum_{i=1}^{4} \begin{bmatrix} -A_{al\Theta} T_{m_i}^2 & 2 a_k T_{m_i} \end{bmatrix} \begin{bmatrix} u_{R_i} \\ u_{T_i} \end{bmatrix}, \tag{6.148}$$

$$\tilde{\Delta}_j \zeta_{t6} = \frac{1}{v_{sk}} \sum_{i=1}^{4} \begin{bmatrix} -2 T_{m_i} & A_K a_k T_{m_i}^2 \end{bmatrix} \begin{bmatrix} u_{R_i} \\ u_{T_i} \end{bmatrix} \tag{6.149}$$

$$\tilde{\Delta}_j \zeta_{t2} = \frac{2}{\omega_{\oplus} v_{sk}} \sum_{i=1}^{4} \begin{bmatrix} -\cos K_{sk}(t_{m_i}) & 2 \sin K_{sk}(t_{m_i}) \end{bmatrix} \begin{bmatrix} \sin\left(\omega_{\oplus} T_{m_i}/2\right) u_{R_i}, \\ \sin\left(\omega_{\oplus} T_{m_i}/2\right) u_{T_i} \end{bmatrix} \tag{6.150}$$

$$\tilde{\Delta}_j \zeta_{t3} = \frac{2}{\omega_{\oplus} v_{sk}} \sum_{i=1}^{4} \begin{bmatrix} \sin K_{sk}(t_{m_i}) & 2 \cos K_{sk}(t_{m_i}) \end{bmatrix} \begin{bmatrix} \sin\left(\omega_{\oplus} T_{m_i}/2\right) u_{R_i}, \\ \sin\left(\omega_{\oplus} T_{m_i}/2\right) u_{T_i} \end{bmatrix} \tag{6.151}$$

$$\tilde{\Delta}_j \zeta_{t4} = \frac{1}{\omega_\oplus v_{sk}} \sum_{i=1}^{4} \sin K_{sk}(t_{m_i}) \sin\left(\omega_\oplus T_{m_i}/2\right) u_{N_i}, \tag{6.152}$$

$$\tilde{\Delta}_j \zeta_{t5} = \frac{1}{\omega_\oplus v_{sk}} \sum_{i=1}^{4} \cos K_{sk}(t_{m_i}) \sin\left(\omega_\oplus T_{m_i}/2\right) u_{N_i}, \tag{6.153}$$

where

$$\begin{bmatrix} u_{R_i} \\ u_{T_i} \\ u_{N_i} \end{bmatrix} = \frac{1}{m_j} \mathbf{\Gamma}_i F_i, \tag{6.154}$$

The configuration vectors $\mathbf{\Gamma}_i$ are those of the [Anzel, 1995] configuration

$$\begin{bmatrix} \mathbf{\Gamma}_1 & \mathbf{\Gamma}_2 & \mathbf{\Gamma}_3 & \mathbf{\Gamma}_4 \end{bmatrix} = \begin{bmatrix} -\sin\gamma\cos\sigma & -\sin\gamma\cos\sigma & -\sin\gamma\cos\sigma & -\sin\gamma\cos\sigma \\ +\sin\gamma\sin\sigma & -\sin\gamma\sin\sigma & -\sin\gamma\sin\sigma & +\sin\gamma\sin\sigma \\ -\cos\gamma & -\cos\gamma & +\cos\gamma & +\cos\gamma \end{bmatrix} \tag{6.155}$$

with $\gamma = 50$ deg and $\sigma = 15$ deg. The thrust levels

$$F_1 = F_{NW}, \quad F_2 = F_{NE}, \quad F_3 = F_{SE}, \quad F_4 = F_{SW}, \tag{6.156}$$

are all equal to 170 mN

$$F_i = F_{max} = 170 \text{ mN} \qquad \forall i. \tag{6.157}$$

The spacecraft mass m_j is constant over the jth day and it is the spacecraft mass of the previous day reduced by the amount

$$\Delta_j m = \frac{F_{max} \sum_{i=1}^{4} T_{m_i}}{g I_{sp}}, \tag{6.158}$$

with a specific impulse I_{sp} of each thruster equal to 3800 seconds.

Actually, the steps of nonlinear optimization problems can include further operational constraints. For example, the simulations results shown in Fig. 6.52–6.55 have been obtained adding to the nonlinear optimization problems the following inequality constraints on the distance between the switching off and switching on time of the same thruster

$$\left[t_{m_i} + \frac{T_{m_i}}{2}\right]_{(j+1)\text{th day}} - \left[t_{m_i} - \frac{T_{m_i}}{2}\right]_{j\text{th day}} \geq 15 \text{ minutes} \qquad \forall i. \tag{6.159}$$

The same simulation has been performed over also one year. The main results are the following:

- total fuel mass consumption equal to 13 kg;
- average switching on time per thruster equal to 200 hours;
- total impulsion per thruster equal to $1.22 \cdot 10^6$ Ns.

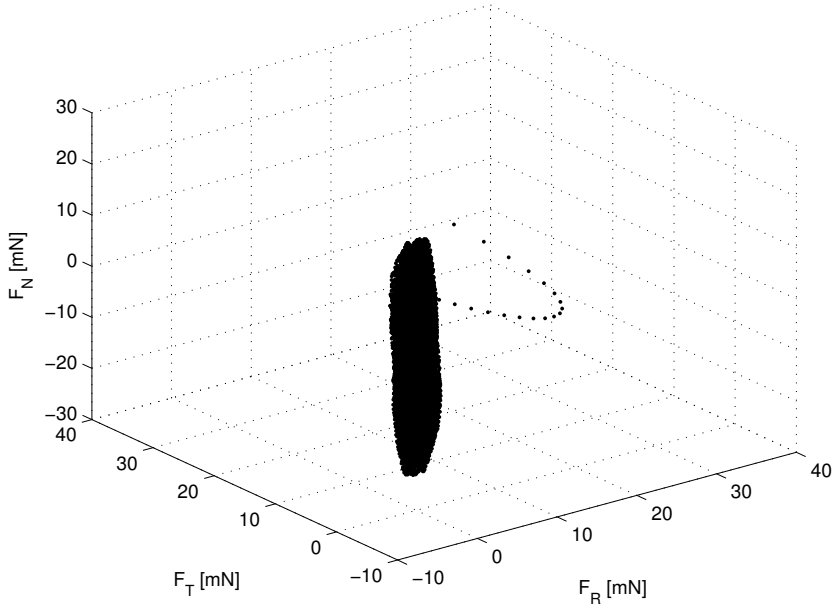

Figure 6.44: *Tip trace of the optimal control force vector obtained with the RHO approach (longitude and latitude deadbands equal to 0.01 deg).*

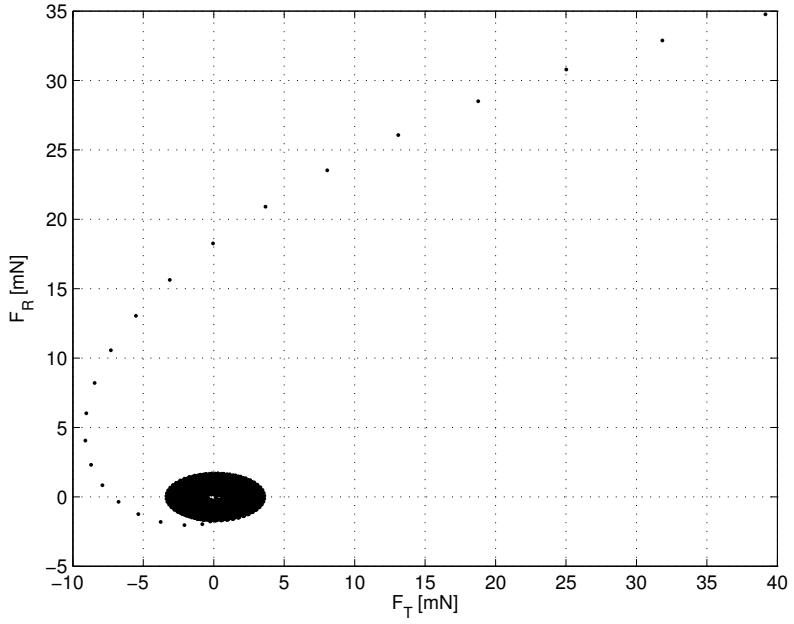

Figure 6.45: *Projection in the (R, T) plane of the tip trace of the optimal control force vector obtained with the RHO approach (longitude and latitude deadbands equal to 0.01 deg).*

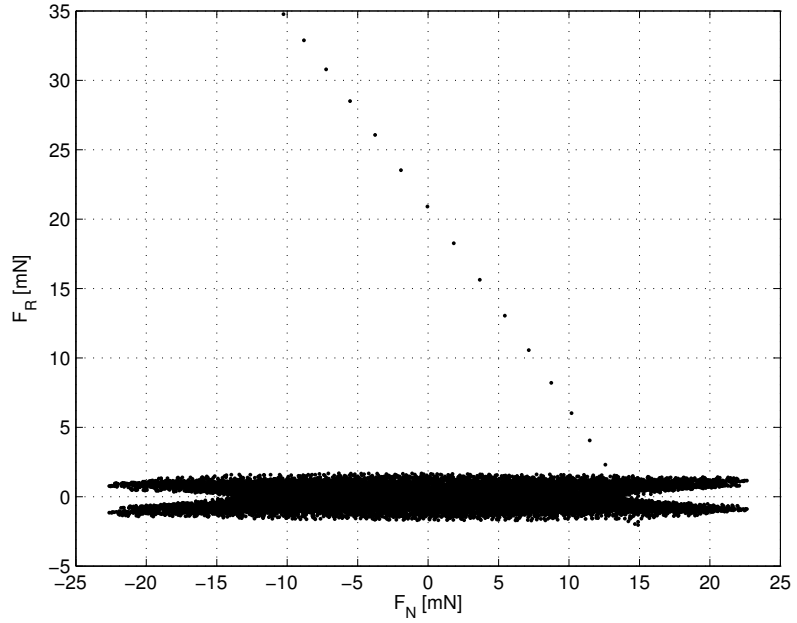

Figure 6.46: *Projection in the* (R, N) *plane of the tip trace of the optimal control force vector obtained with the RHO approach (longitude and latitude deadbands equal to 0.01 deg).*

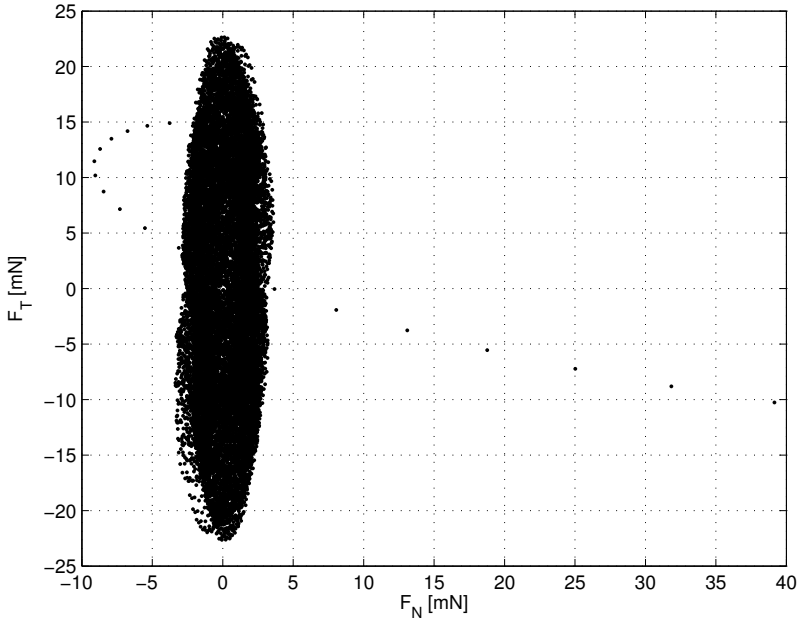

Figure 6.47: *Projection in the* (T, N) *plane of the tip trace of the optimal control force vector obtained with the RHO approach (longitude and latitude deadbands equal to 0.01 deg).*

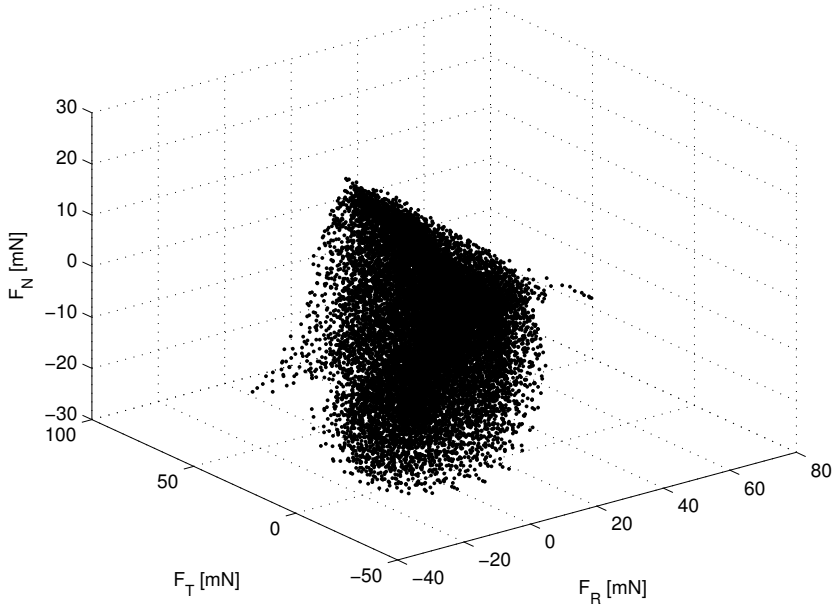

Figure 6.48: *Tip trace of the optimal control force vector obtained with the RHO approach (longitude and latitude deadbands equal to 0.001 deg).*

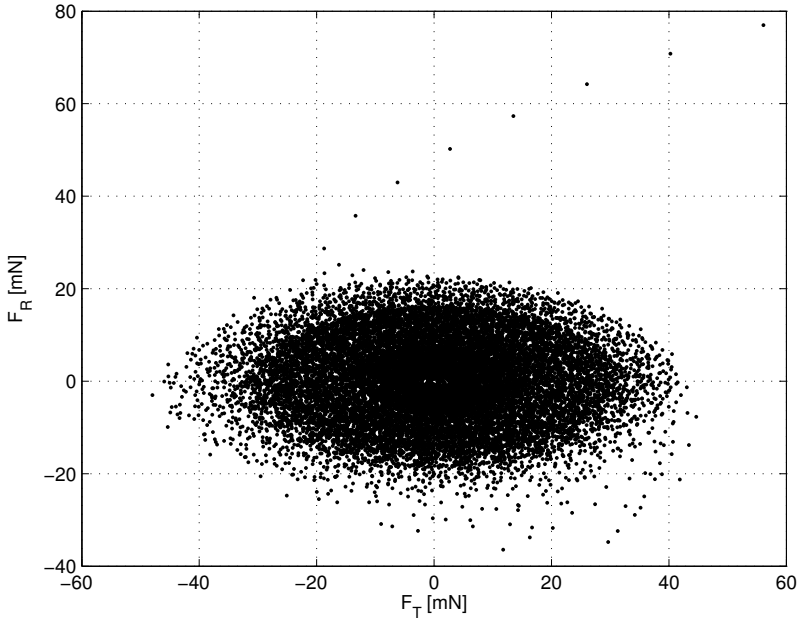

Figure 6.49: *Projection in the (R, T) plane of the tip trace of the optimal control force vector obtained with the RHO approach (longitude and latitude deadbands equal to 0.001 deg).*

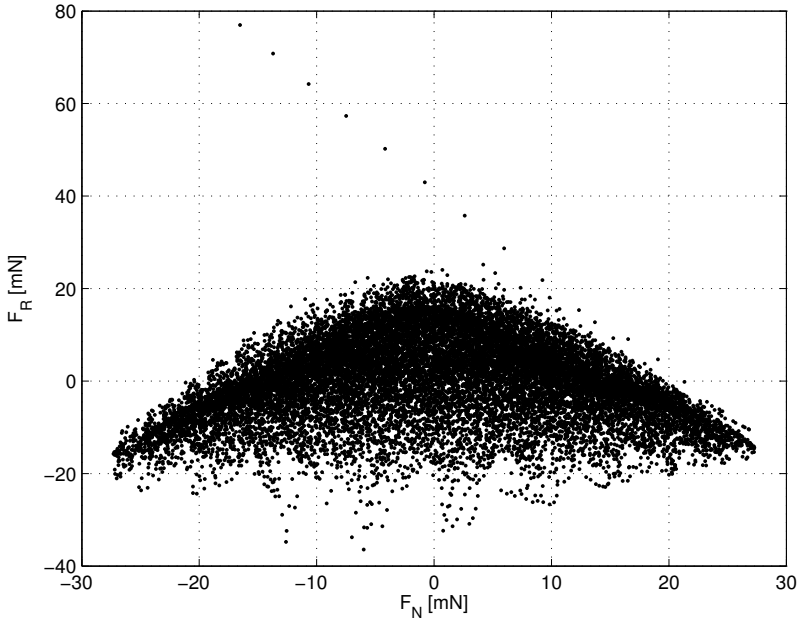

Figure 6.50: *Projection in the* (R, N) *plane of the tip trace of the optimal control force vector obtained with the RHO approach (longitude and latitude deadbands equal to 0.001 deg).*

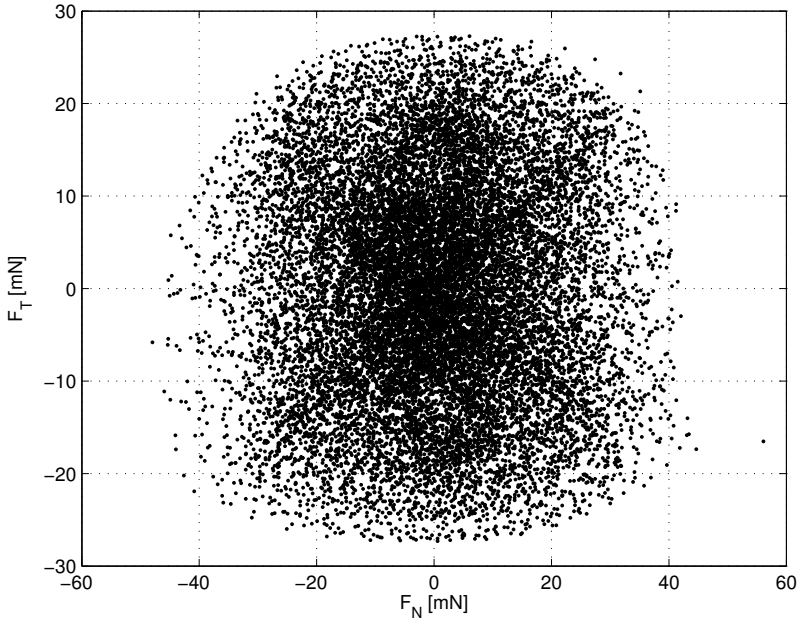

Figure 6.51: *Projection in the* (T, N) *plane of the tip trace of the optimal control force vector obtained with the RHO approach (longitude and latitude deadbands equal to 0.001 deg).*

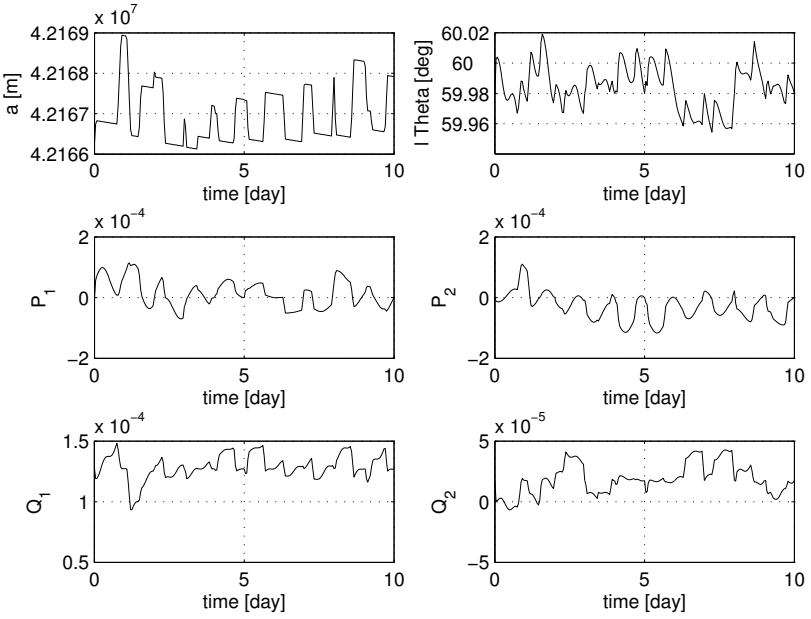

Figure 6.52: *State variable time histories obtained with the thrusts on off.*

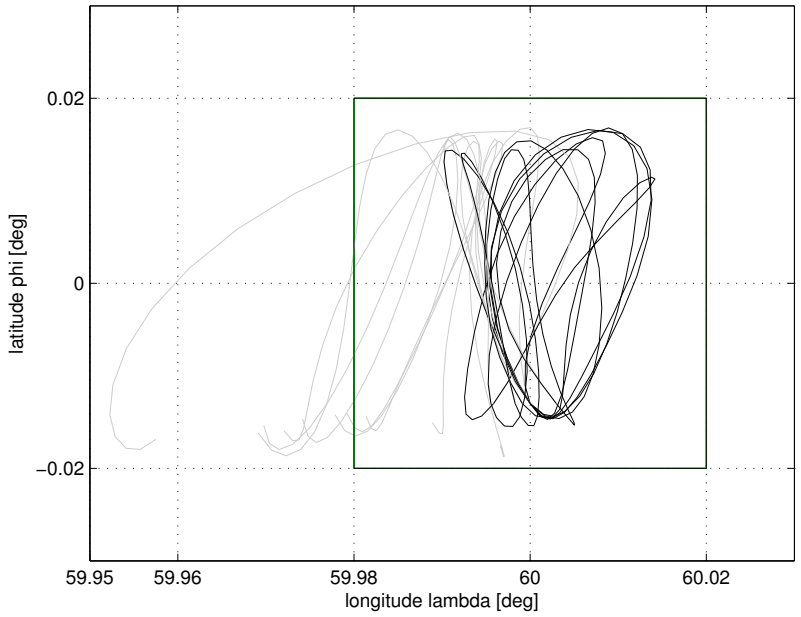

Figure 6.53: *Latitude vs longitude uncontrolled (gray line) and controlled with thrusts on off (black line).*

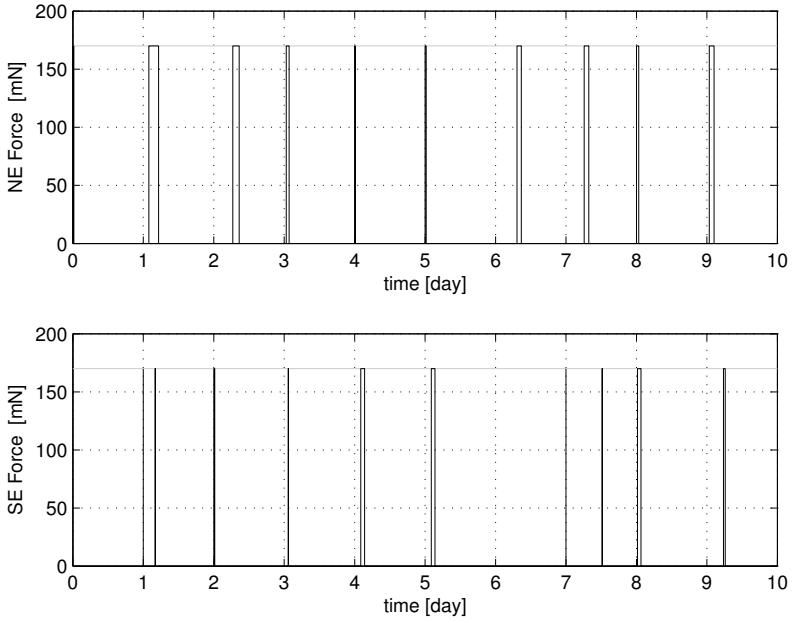

Figure 6.54: *Time histories of the East thrusts on off.*

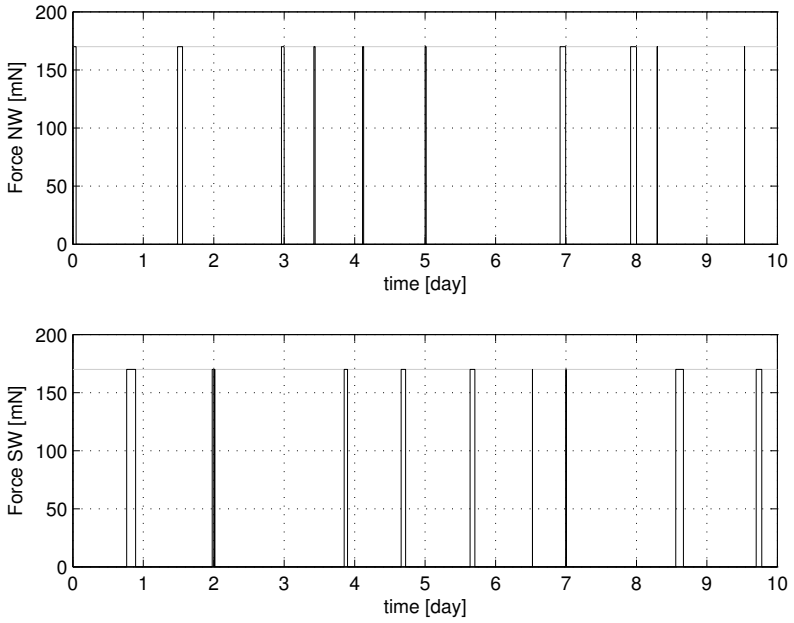

Figure 6.55: *Time histories of the West thrusts on off.*

Chapter 7

Differential Flatness in the GEO Satellite SK Problem

In this chapter, we explain the way to transform the linear system (6.49)–(6.50) with time varying coefficients in a linear system with time invariant coefficients without modifying its stability properties. This transformation leads to recognize differential flatness in the GEO satellite dynamics.

7.1 Differential Flatness

We use the notation $\boldsymbol{u}^{(\boldsymbol{k})}$ and $\boldsymbol{\varsigma}^{(\boldsymbol{k})}$ to indicate the kth order derivatives of the vectors $\boldsymbol{u}$ and $\boldsymbol{\varsigma}$. A system is said to be differentially flat (see, e.g., [Fliess et al., 1995], [Fliess et al., 1999]) if it exists a set of independent variables referred to as "flat outputs" such that every other system variable (including the input variables) is a function of the flat outputs and a finite number of its successive time derivatives. More precisely, the system

$$\frac{d\boldsymbol{\zeta}}{dt} = \boldsymbol{f}\left(\boldsymbol{\zeta}, \boldsymbol{u}\right), \qquad \boldsymbol{\zeta} \in \mathbb{R}^n, \qquad \boldsymbol{u} \in \mathbb{R}^m, \tag{7.1}$$

is differentially flat if it is possible to find a set of variables (flat outputs)

$$\boldsymbol{\varsigma} = \boldsymbol{h}\left(\boldsymbol{\zeta}, \boldsymbol{u}, \dot{\boldsymbol{u}}, \ddot{\boldsymbol{u}}, \ldots, \boldsymbol{u}^{(\boldsymbol{p})}\right), \qquad \boldsymbol{\varsigma} \in \mathbb{R}^m \tag{7.2}$$

with p a finite $m$tuple of integers, such that

$$\boldsymbol{\zeta} = \boldsymbol{\alpha}\left(\boldsymbol{\varsigma}, \dot{\boldsymbol{\varsigma}}, \ddot{\boldsymbol{\varsigma}}, \ldots, \boldsymbol{\varsigma}^{(\boldsymbol{q})}\right), \qquad \boldsymbol{u} = \boldsymbol{\beta}\left(\boldsymbol{\varsigma}, \dot{\boldsymbol{\varsigma}}, \ddot{\boldsymbol{\varsigma}}, \ldots, \boldsymbol{\varsigma}^{(\boldsymbol{q})}\right) \tag{7.3}$$

with q a finite $m$tuple of integers, and such that the equations

$$\frac{d\boldsymbol{\alpha}}{dt}\left(\boldsymbol{\varsigma}, \dot{\boldsymbol{\varsigma}}, \ddot{\boldsymbol{\varsigma}}, \ldots, \boldsymbol{\varsigma}^{(\boldsymbol{q})}\right) = \boldsymbol{f}\left(\boldsymbol{\alpha}\left(\boldsymbol{\varsigma}, \dot{\boldsymbol{\varsigma}}, \ddot{\boldsymbol{\varsigma}}, \ldots, \boldsymbol{\varsigma}^{(\boldsymbol{q})}\right), \boldsymbol{\beta}\left(\boldsymbol{\varsigma}, \dot{\boldsymbol{\varsigma}}, \ddot{\boldsymbol{\varsigma}}, \ldots, \boldsymbol{\varsigma}^{(\boldsymbol{q})}\right)\right) \tag{7.4}$$

are identically satisfied. For an $m$tuple of integers $p = (p_1, \ldots, p_m)$ and an m dimensional vector $\boldsymbol{u}$, the notation $\boldsymbol{u^{(p)}}$ stands for the vector $\begin{bmatrix} u_1^{(p_1)} & \ldots & u_m^{(p_m)} \end{bmatrix}^T$.

In the following of this section we deduce a set of flat outputs for the system describing the GEO satellite dynamics.

7.2 Lyapunov Transformation in the EOE Deviation Space

We consider the input-state equations (6.21) and the state-output equations (6.42) describing the translational dynamics of a GEO satellite linearized around the Keplerian nominal station keeping trajectory $\boldsymbol{x} = \boldsymbol{x}_{Ksk}$

$$\frac{d\boldsymbol{\zeta}}{dt} = \boldsymbol{A}(t)\boldsymbol{\zeta} + \boldsymbol{B}(t)\boldsymbol{a}_{e_{sk}}(t) + \boldsymbol{B}(t)\boldsymbol{u}(t), \qquad \boldsymbol{\zeta}(t_i) = \boldsymbol{\zeta}_i, \tag{7.5}$$

$$\boldsymbol{\varsigma} = \boldsymbol{C}(t)\boldsymbol{\zeta}, \tag{7.6}$$

where

- the vector $\boldsymbol{\zeta}$ is the deviation of the state variable $\boldsymbol{x}$ from its nominal station keeping value $\boldsymbol{x}_{Ksk}$

$$\boldsymbol{\zeta} = \boldsymbol{x} - \boldsymbol{x}_{Ksk} = \begin{bmatrix} a - a_k & P_1 & P_2 & Q_1 & Q_2 & l_\Theta - \lambda_s \end{bmatrix}^T; \tag{7.7}$$

- the vector $\boldsymbol{\varsigma}$ is the deviation of the output variable $\boldsymbol{y}$ from its nominal station keeping value $\boldsymbol{y}_{sk}$

$$\boldsymbol{\varsigma} = \boldsymbol{y} - \boldsymbol{y}_{sk} = \begin{bmatrix} r - a_k & \lambda - \lambda_s & \varphi \end{bmatrix}^T; \tag{7.8}$$

- the matrices $\boldsymbol{B}(t)$ and $\boldsymbol{C}(t)$ are one sidereal day periodic function

$$\boldsymbol{B}(t) = \frac{1}{v_{sk}} \begin{bmatrix} 0 & 2a_k & 0 \\ -\cos K_{sk} & 2\sin K_{sk} & 0 \\ \sin K_{sk} & 2\cos K_{sk} & 0 \\ 0 & 0 & \frac{1}{2}\sin K_{sk} \\ 0 & 0 & \frac{1}{2}\cos K_{sk} \\ -2 & 0 & 0 \end{bmatrix}, \tag{7.9}$$

$$\boldsymbol{C}(t) = \begin{bmatrix} 1 & -a_k \sin K_{sk} & -a_k \cos K_{sk} & 0 & 0 & 0 \\ 0 & -2\cos K_{sk} & 2\sin K_{sk} & 0 & 0 & 1 \\ 0 & 0 & 0 & -2\cos K_{sk} & 2\sin K_{sk} & 0 \end{bmatrix}, \tag{7.10}$$

with K_{sk} dependent on time as follows

$$K_{sk}(t) = \omega_\oplus t + (\Theta_r - \omega_\oplus t_r) + \lambda_s. \tag{7.11}$$

➢ The matrix $\boldsymbol{A}(t)$ should be taken equal to the time varying matrix given by Eq. (6.22). However, we have performed some numerical simulations of the homogeneous system

$$\frac{d\boldsymbol{\Phi}(t,t_i)}{dt} = \boldsymbol{A}(t)\boldsymbol{\Phi}(t,t_i), \qquad \boldsymbol{\Phi}(t_i,t_i) = \boldsymbol{I}_{6\times 6}. \tag{7.12}$$

We have obtained the time histories of the elements of the impulsive response matrix

$$\boldsymbol{C}(t)\boldsymbol{\Phi}(t,\tau)\boldsymbol{B}(\tau) \tag{7.13}$$

of the output

$$\boldsymbol{\varsigma}(t) = \boldsymbol{C}(t)\boldsymbol{\Phi}(t,t_i)\boldsymbol{\zeta}_i + \int_{t_i}^{t} \boldsymbol{C}(t)\boldsymbol{\Phi}(t,\tau)\boldsymbol{B}(\tau)\boldsymbol{a}_{e_{sk}}(\tau)d\tau. \tag{7.14}$$

We have observed that the simulation results obtained with the complete time varying matrix $\boldsymbol{A}(t)$ are not appreciably different from those obtained with the constant matrix

$$\boldsymbol{A}_c = \begin{bmatrix} 0 & 0 & 0 & 0 & 0 & A_{al_\Theta} \\ 0 & 0 & 0 & 0 & 0 & 0 \\ 0 & 0 & 0 & 0 & 0 & 0 \\ 0 & 0 & 0 & 0 & 0 & 0 \\ 0 & 0 & 0 & 0 & 0 & 0 \\ A_K & 0 & 0 & 0 & 0 & 0 \end{bmatrix}, \tag{7.15}$$

where

– the constant element A_K is the nominal partial derivative with respect to a of the variational contribution coming from the Keplerian gravity attraction

$$A_K = \left[\frac{\partial}{\partial a}\left[\sqrt{\frac{GM_\oplus}{a^3}} - \omega_\oplus\right]\right]_{a=a_k} = -\frac{3}{2}\frac{n_k}{a_k} \approx -2.6\times 10^{-12} \quad \mathrm{m^{-1}s^{-1}}; \tag{7.16}$$

– the constant element A_{al_Θ} is the nominal partial derivative with respect to l_Θ of the variational contribution coming from the non uniform and oblate Earth gravity attraction

$$A_{al_\Theta} = \left[\frac{\partial}{\partial l_\Theta}\left[\frac{2}{na}\frac{\partial \mathcal{E}_g(\boldsymbol{x},t)}{\partial l_\Theta}\right]\right]_{\boldsymbol{x}=\boldsymbol{x}_{Ksk}} = 2\sqrt{\frac{a_k}{GM_\oplus}}\left[\frac{\partial^2 \mathcal{E}_g(r,\lambda,\varphi)}{\partial \lambda^2}\right]_{r=a_k,\lambda=\lambda_s,\varphi=0}. \tag{7.17}$$

The constant element A_{al_Θ} has the dimension of a velocity and it varies in function of the station longitude λ_s as depicted in Fig. 7.1. In fact, from the equation (3.12) we obtain

$$\begin{aligned} A_{al_\Theta}(\lambda_s) = &-24\sqrt{\frac{GM_\oplus}{a_k}}\left(\frac{R_\oplus}{a_k}\right)^2 [C_{22}\cos(2\lambda_s) + S_{22}\sin(2\lambda_s)] + \\ &+3\sqrt{\frac{GM_\oplus}{a_k}}\left(\frac{R_\oplus}{a_k}\right)^3 [C_{31}\cos(\lambda_s) + S_{31}\sin(\lambda_s)] + \\ &-270\sqrt{\frac{GM_\oplus}{a_k}}\left(\frac{R_\oplus}{a_k}\right)^3 [C_{33}\cos(3\lambda_s) + S_{33}\sin(3\lambda_s)]\,. \end{aligned} \tag{7.18}$$

This function of λ_s is positive for

$$34^\circ \lesssim \lambda_s \lesssim 117^\circ, \qquad 205^\circ \lesssim \lambda_s \lesssim 304^\circ,$$

and negative for

$$0^\circ \lesssim \lambda_s \lesssim 34^\circ, \qquad 117^\circ \lesssim \lambda_s \lesssim 205^\circ, \qquad 304^\circ \lesssim \lambda_s \lesssim 360^\circ.$$

The sign of the element A_{al_Θ} decides on the stability of the motion for the deviations

$$\zeta_1 = a - a_k \qquad \text{and} \qquad \zeta_6 = l_\Theta - \lambda_s \tag{7.19}$$

as solutions of the homogeneous system

$$\frac{d}{dt}\begin{bmatrix}\zeta_1\\ \zeta_6\end{bmatrix} = \begin{bmatrix}0 & A_{al_\Theta}\\ A_K & 0\end{bmatrix}\begin{bmatrix}\zeta_1\\ \zeta_6\end{bmatrix}. \tag{7.20}$$

If $A_{al_\Theta} > 0$, then there is a conjugate pair of purely imaginary eigenvalues equal to $\pm j\sqrt{|A_{al_\Theta} A_K|}$. If $A_{al_\Theta} < 0$, then there is a pair of purely real eigenvalues equal to $\pm\sqrt{|A_{al_\Theta} A_K|}$, symmetric with respect to the origin in the complex plane. Denoting

$$\bar{A}_c = \sqrt{|A_{al_\Theta} A_K|}, \tag{7.21}$$

the transition matrix $\boldsymbol{\Phi}_c$, solution of the matrix differential equation

$$\frac{d\boldsymbol{\Phi}_c(t,t_i)}{dt} = \boldsymbol{A}_c\boldsymbol{\Phi}_c(t,t_i), \qquad \boldsymbol{\Phi}_c(t_i,t_i) = \boldsymbol{I}_{6\times 6}, \tag{7.22}$$

comes out as follows

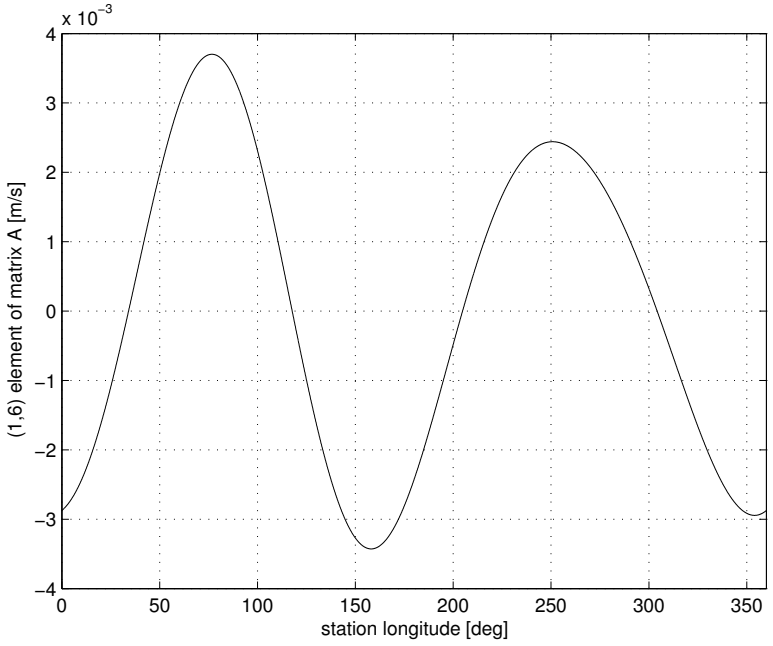

Figure 7.1: *(1,6) element of matrix $\boldsymbol{A}_c$ in function of the station longitude λ_s*

- if $A_{al_\Theta} > 0$

$$\mathbf{\Phi}_c(t,t_i) = \begin{bmatrix} \cos\left[\bar{A}_c(t-t_i)\right] & 0 & 0 & 0 & 0 & (A_{al_\Theta}/\bar{A}_c)\sin\left[\bar{A}_c(t-t_i)\right] \\ 0 & 1 & 0 & 0 & 0 & 0 \\ 0 & 0 & 1 & 0 & 0 & 0 \\ 0 & 0 & 0 & 1 & 0 & 0 \\ 0 & 0 & 0 & 0 & 1 & 0 \\ (A_K/\bar{A}_c)\sin\left[\bar{A}_c(t-t_i)\right] & 0 & 0 & 0 & 0 & \cos\left[\bar{A}_c(t-t_i)\right] \end{bmatrix}; \tag{7.23}$$

- if $A_{al_\Theta} < 0$

$$\mathbf{\Phi}_c(t,t_i) = \begin{bmatrix} \cosh\left[\bar{A}_c(t-t_i)\right] & 0 & 0 & 0 & 0 & (A_{al_\Theta}/\bar{A}_c)\sinh\left[\bar{A}_c(t-t_i)\right] \\ 0 & 1 & 0 & 0 & 0 & 0 \\ 0 & 0 & 1 & 0 & 0 & 0 \\ 0 & 0 & 0 & 1 & 0 & 0 \\ 0 & 0 & 0 & 0 & 1 & 0 \\ (A_K/\bar{A}_c)\sinh\left[\bar{A}_c(t-t_i)\right] & 0 & 0 & 0 & 0 & \cosh\left[\bar{A}_c(t-t_i)\right] \end{bmatrix}. \tag{7.24}$$

However, from the constant value of $A_K \approx -2.6 \times 10^{-12}$ $\mathrm{m^{-1}s^{-1}}$ and the values of A_{al_Θ} plotted in Fig. 7.1, we deduce that the magnitude of $\bar{A}_c$ will assume one value of the following interval

$$0 \leq \bar{A}_c \leq \sqrt{(2.6 \times 10^{-12})(3.75 \times 10^{-3})} \approx 10^{-7} \quad \mathrm{s^{-1}}. \tag{7.25}$$

Since the linear GEO satellite dynamics is used to plan the station keeping maneuvers in order to maintain the longitude near to its station keeping value, A_{al_Θ} will remain nearly constant. Moreover, in low thrust station keeping the control will be designed over successive time intervals one day long. Over each of such intervals, the arguments of the trigonometric functions in $\mathbf{\Phi}_c$ will assume one value of the following interval

$$0^\circ \leq \bar{A}_c(t-t_i) \lesssim 0.5^\circ. \tag{7.26}$$

Consequently, over $(t-t_i) = 1$ day we can approximate the trigonometric functions in $\mathbf{\Phi}_c$ with their first order Taylor series expansion

$$\sin[\bar{A}_c(t-t_i)] = \bar{A}_c(t-t_i), \tag{7.27}$$

$$\sinh[\bar{A}_c(t-t_i)] = \bar{A}_c(t-t_i), \tag{7.28}$$

$$\cos[\bar{A}_c(t-t_i)] = 1, \tag{7.29}$$

$$\cosh[\bar{A}_c(t-t_i)] = 1. \tag{7.30}$$

Transition matrix formulas (7.23) and (7.24) come out to be equal to the unique expression

$$\boldsymbol{\Phi}_c(t,t_i) = \begin{bmatrix} 1 & 0 & 0 & 0 & 0 & A_{al_\Theta}(t-t_i) \\ 0 & 1 & 0 & 0 & 0 & 0 \\ 0 & 0 & 1 & 0 & 0 & 0 \\ 0 & 0 & 0 & 1 & 0 & 0 \\ 0 & 0 & 0 & 0 & 1 & 0 \\ A_K(t-t_i) & 0 & 0 & 0 & 0 & 1 \end{bmatrix}. \tag{7.31}$$

We look for a transformation of the EOE deviation space such that the transformed GEO satellite dynamics linear model would result time invariant and maintain the same internal stability property of the original realization of the system (7.5)–(7.6). In particular this transformation should be non singular and differentiable for every t, it should make time invariant the matrix multiplying the control and forcing vectors in the input-state system (7.5) and the one multiplying the state vector in the state-output system (7.6). Transformations obeying to the above conditions are known as Lyapunov transformations (see, e.g., [Kailath, 1980]). Such a transformation could be performed on the system (7.5)–(7.6), for example, by means of the periodic matrix

$$\boldsymbol{W}(t) = 2v_{sk} \begin{bmatrix} 0 & \cos K_{sk} & -\sin K_{sk} & 0 & 0 & -\frac{1}{2} \\ 0 & \cos K_{sk} & -\sin K_{sk} & 0 & 0 & -\frac{3}{4} \\ -\frac{3}{4a_k} & \sin K_{sk} & \cos K_{sk} & 0 & 0 & 0 \\ 0 & 0 & 0 & \cos K_{sk} & -\sin K_{sk} & 0 \\ 0 & 0 & 0 & \sin K_{sk} & \cos K_{sk} & 0 \\ -\frac{1}{a_k} & \sin K_{sk} & \cos K_{sk} & 0 & 0 & 0 \end{bmatrix}, \tag{7.32}$$

which has a time derivative defined and bounded for every t

$$\dot{\boldsymbol{W}}(t) = 2v_{sk}\omega_\oplus \begin{bmatrix} 0 & -\sin K_{sk} & -\cos K_{sk} & 0 & 0 & 0 \\ 0 & -\sin K_{sk} & -\cos K_{sk} & 0 & 0 & 0 \\ 0 & \cos K_{sk} & -\sin K_{sk} & 0 & 0 & 0 \\ 0 & 0 & 0 & -\sin K_{sk} & -\cos K_{sk} & 0 \\ 0 & 0 & 0 & \cos K_{sk} & -\sin K_{sk} & 0 \\ 0 & \cos K_{sk} & -\sin K_{sk} & 0 & 0 & 0 \end{bmatrix}, \tag{7.33}$$

it is non singular for every t with a constant determinant

$$\det\left[\boldsymbol{W}(t)\right] = 4\frac{v_{sk}^6}{a_k}, \tag{7.34}$$

and

$$\boldsymbol{W}^{-1}(t) = \frac{1}{2v_{sk}} \begin{bmatrix} 0 & 0 & 4a_k & 0 & 0 & -4a_k \\ 3\cos K_{sk} & -2\cos K_{sk} & 4\sin K_{sk} & 0 & 0 & -3\sin K_{sk} \\ -3\sin K_{sk} & 2\sin K_{sk} & 4\cos K_{sk} & 0 & 0 & -3\cos K_{sk} \\ 0 & 0 & 0 & \cos K_{sk} & \sin K_{sk} & 0 \\ 0 & 0 & 0 & -\sin K_{sk} & \cos K_{sk} & 0 \\ 4 & -4 & 0 & 0 & 0 & 0 \end{bmatrix}. \quad (7.35)$$

Writing the input-output linear system given by Eq.s (7.5) and (7.6) in function of the transformed state vector

$$\tilde{\boldsymbol{\zeta}} = \boldsymbol{W}(t)\boldsymbol{\zeta}, \quad (7.36)$$

(i.e., replacing $\boldsymbol{\zeta}$ with $\boldsymbol{W}^{-1}\tilde{\boldsymbol{\zeta}}$ and $\dot{\boldsymbol{\zeta}}$ with $\boldsymbol{W}^{-1}\dot{\tilde{\boldsymbol{\zeta}}} - \boldsymbol{W}^{-1}\dot{\boldsymbol{W}}\boldsymbol{W}^{-1}\tilde{\boldsymbol{\zeta}}$), we obtain the following linear system

$$\frac{d\tilde{\boldsymbol{\zeta}}}{dt} = \tilde{\boldsymbol{A}}\tilde{\boldsymbol{\zeta}} + \tilde{\boldsymbol{B}}\boldsymbol{a}_{e_{sk}}(t) + \tilde{\boldsymbol{B}}\boldsymbol{u}(t), \qquad \tilde{\boldsymbol{\zeta}}(t_i) = \tilde{\boldsymbol{\zeta}}_i = \boldsymbol{W}(t_i)\boldsymbol{\zeta}_i, \quad (7.37)$$

$$\boldsymbol{\varsigma} = \tilde{\boldsymbol{C}}\tilde{\boldsymbol{\zeta}}, \quad (7.38)$$

with constant coefficients

$$\tilde{\boldsymbol{A}} = \dot{\boldsymbol{W}}(t)\boldsymbol{W}^{-1}(t) + \boldsymbol{W}(t)\boldsymbol{A}_c\boldsymbol{W}^{-1}(t) =$$

$$= \omega_{\oplus} \begin{bmatrix} 0 & 0 & -4 & 0 & 0 & 3 \\ 0 & 0 & -4 & 0 & 0 & 3 \\ 3 & -2 & 0 & 0 & 0 & 0 \\ 0 & 0 & 0 & 0 & -1 & 0 \\ 0 & 0 & 0 & 1 & 0 & 0 \\ 3 & -2 & 0 & 0 & 0 & 0 \end{bmatrix} + \begin{bmatrix} 0 & 0 & -2A_K a_k & 0 & 0 & 2A_K a_k \\ 0 & 0 & -3A_K a_k & 0 & 0 & 3A_K a_k \\ -3A_{al_\Theta}/a_k & 3A_{al_\Theta}/a_k & 0 & 0 & 0 & 0 \\ 0 & 0 & 0 & 0 & 0 & 0 \\ 0 & 0 & 0 & 0 & 0 & 0 \\ -4A_{al_\Theta}/a_k & 4A_{al_\Theta}/a_k & 0 & 0 & 0 & 0 \end{bmatrix}, \quad (7.39)$$

$$\tilde{\boldsymbol{B}} = \boldsymbol{W}(t)\boldsymbol{B}(t) = \begin{bmatrix} 0 & 0 & 0 \\ 1 & 0 & 0 \\ 0 & 1 & 0 \\ 0 & 0 & 0 \\ 0 & 0 & 1 \\ 0 & 0 & 0 \end{bmatrix}, \quad (7.40)$$

$$\tilde{\boldsymbol{C}} = \boldsymbol{C}(t)\boldsymbol{W}^{-1}(t) = -\frac{1}{v_{sk}} \begin{bmatrix} 0 & 0 & 0 & 0 & 0 & a_k/2 \\ 1 & 0 & 0 & 0 & 0 & 0 \\ 0 & 0 & 0 & 1 & 0 & 0 \end{bmatrix}. \quad (7.41)$$

Since the state controllability matrix

$$\boldsymbol{Q}_c = \begin{bmatrix} \tilde{\boldsymbol{B}} & -\tilde{\boldsymbol{A}}\tilde{\boldsymbol{B}} & \tilde{\boldsymbol{A}}^2\tilde{\boldsymbol{B}} & -\tilde{\boldsymbol{A}}^3\tilde{\boldsymbol{B}} & \tilde{\boldsymbol{A}}^4\tilde{\boldsymbol{B}} & -\tilde{\boldsymbol{A}}^5\tilde{\boldsymbol{B}} \end{bmatrix} \quad (7.42)$$

has maximum rank equal to 6 (state vector dimension), the linear system (7.37)–(7.38) is totally state-controllable, i.e., on every finite interval $[t_i, t_f]$, each initial state $\boldsymbol{\zeta}(t_i)$ can be transferred to any final state $\boldsymbol{\zeta}(t_f)$ using some bounded control $\boldsymbol{u}(t)$ over the closed interval $[t_i, t_f]$ (see Chapter 4 of [D'Angelo, 1970]).

Since the output controllability matrix

$$\boldsymbol{S}_c = \tilde{\boldsymbol{C}} \begin{bmatrix} \tilde{\boldsymbol{B}} & -\tilde{\boldsymbol{A}}\tilde{\boldsymbol{B}} & \tilde{\boldsymbol{A}}^2\tilde{\boldsymbol{B}} & -\tilde{\boldsymbol{A}}^3\tilde{\boldsymbol{B}} & \tilde{\boldsymbol{A}}^4\tilde{\boldsymbol{B}} & -\tilde{\boldsymbol{A}}^5\tilde{\boldsymbol{B}} \end{bmatrix} \tag{7.43}$$

has maximum rank equal to 3 (output vector dimension), the linear system (7.37)–(7.38) is totally output-controllable, i.e., on every finite interval $[t_i, t_f]$, each initial output $\boldsymbol{\varsigma}(t_i)$ can be transferred to any final output $\boldsymbol{\varsigma}(t_f)$ using some bounded control $\boldsymbol{u}(t)$ over the closed interval $[t_i, t_f]$ (see Chapter 4 of [D'Angelo, 1970]).

7.3 A New Set of Orbital Parameters

Let be $\tilde{\zeta}_i$ with $i = 1, \ldots, 6$, the components of the transformed state vector $\tilde{\boldsymbol{\zeta}} = \boldsymbol{W}(t)\boldsymbol{\zeta}$

$$\tilde{\boldsymbol{\zeta}} = \begin{bmatrix} \tilde{\zeta}_1 & \tilde{\zeta}_2 & \tilde{\zeta}_3 & \tilde{\zeta}_4 & \tilde{\zeta}_5 & \tilde{\zeta}_6 \end{bmatrix}^T. \tag{7.44}$$

Their time varying expressions in terms of the equinoctial orbital element deviations $(a - a_k)$, P_1, P_2, Q_1, Q_2 and $(l_\Theta - \lambda_s)$ are the following

$$\tilde{\zeta}_1 = 2v_{sk}\tilde{P}_1 - v_{sk}(l_\Theta - \lambda_s) \tag{7.45}$$
$$\tilde{\zeta}_2 = 2v_{sk}\tilde{P}_1 - 3/2v_{sk}(l_\Theta - \lambda_s) \tag{7.46}$$
$$\tilde{\zeta}_3 = 2v_{sk}\tilde{P}_2 - 3/2\omega_\oplus(a - a_k) \tag{7.47}$$
$$\tilde{\zeta}_4 = 2v_{sk}\tilde{Q}_1 \tag{7.48}$$
$$\tilde{\zeta}_5 = 2v_{sk}\tilde{Q}_2 \tag{7.49}$$
$$\tilde{\zeta}_6 = 2v_{sk}\tilde{P}_2 - 2\omega_\oplus(a - a_k) \tag{7.50}$$

with

$$\tilde{P}_1 = P_1 \cos K_{sk} - P_2 \sin K_{sk}, \tag{7.51}$$
$$\tilde{P}_2 = P_1 \sin K_{sk} + P_2 \cos K_{sk}, \tag{7.52}$$
$$\tilde{Q}_1 = Q_1 \cos K_{sk} - Q_2 \sin K_{sk}, \tag{7.53}$$
$$\tilde{Q}_2 = Q_1 \sin K_{sk} + Q_2 \cos K_{sk}. \tag{7.54}$$

To understand the geometrical and physical meaning of the orbital parameters $\tilde{P}_1$, $\tilde{P}_2$, $\tilde{Q}_1$ and $\tilde{Q}_2$, we expand the right-hand sides of the equations (7.51)–(7.54) replacing in them the definitions of the equinoctial orbital parameters $P_1 = e\sin(\omega + \Omega)$, $P_1 = e\cos(\omega + \Omega)$, $Q_1 = \tan(i/2)\sin\Omega$ and

$Q_2 = \tan(i/2)\cos\Omega$ and using trigonometric identities. We obtain

$$\tilde{P}_1 = e\sin(\omega + \Omega - K_{sk}), \tag{7.55}$$
$$\tilde{P}_2 = e\cos(\omega + \Omega - K_{sk}), \tag{7.56}$$
$$\tilde{Q}_1 = \tan(i/2)\sin(\Omega - K_{sk}), \tag{7.57}$$
$$\tilde{Q}_2 = \tan(i/2)\cos(\Omega - K_{sk}), \tag{7.58}$$

which are depicted in Fig. 7.2. In this drawing the nominal station keeping situation is represented in the orbital plane by the station keeping line $\mathbf{L_{SK}}$ and by the station keeping point $\mathbf{P_{SK}}$. Line $\mathbf{L_{SK}}$ forms an angle K_{sk} with the principal axis of the equinoctial orbital reference frame with orthonormal basis $\boldsymbol{EQW}$ (see also Fig. 2.8 at page 63). Point $\mathbf{P_{SK}}$ is not the spacecraft position but a geometrical point belonging to the station keeping line (i.e., to the orbital plane) and with a distance equal to the Keplerian semi-major axis a_k from the center of the Earth. The transformed elements $\tilde{P}_1$ and $\tilde{P}_2$ are the components of the eccentricity vector $\boldsymbol{e}$ (belonging to the line of nodes) in the $\boldsymbol{EQW}$ reference frame rotated of an angle K_{sk} around the $\boldsymbol{W}$ axis. The transformed elements $\tilde{Q}_1$ and $\tilde{Q}_2$ are the components of the inclination vector $\boldsymbol{i} = \tan i/2\boldsymbol{n}$ (belonging to the line of apsis) in the same rotated reference frame.

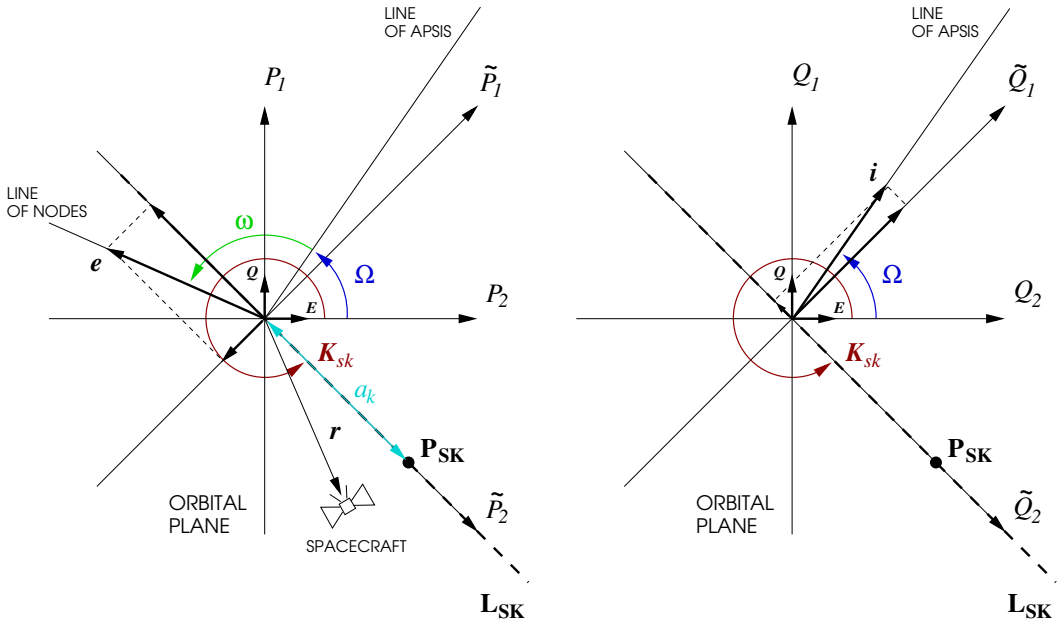

Figure 7.2: *Eccentricity and inclination vector components perpendicular and parallel to the station keeping line.*

7.4 Flat Outputs of the GEO Satellite Dynamics

Expanding the right-hand side of the input-state linear system (7.37), we obtain the following linear differential equations of the GEO satellite dynamics in the transformed state space

$$\frac{d\tilde{\zeta}_1}{dt} = -\omega_{\oplus}(4\tilde{\zeta}_3 - 3\tilde{\zeta}_6) - 2A_K a_k(\tilde{\zeta}_3 - \tilde{\zeta}_6), \tag{7.59}$$

$$\frac{d\tilde{\zeta}_2}{dt} = -\omega_{\oplus}(4\tilde{\zeta}_3 - 3\tilde{\zeta}_6) - 3A_K a_k(\tilde{\zeta}_3 - \tilde{\zeta}_6) + a_{eR_{sk}}(t) + u_R(t), \tag{7.60}$$

$$\frac{d\tilde{\zeta}_3}{dt} = \omega_{\oplus}(3\tilde{\zeta}_1 - 2\tilde{\zeta}_2) - 3\frac{A_{al_\Theta}}{a_k}(\tilde{\zeta}_1 - \tilde{\zeta}_2) + a_{eT_{sk}}(t) + u_T(t), \tag{7.61}$$

$$\frac{d\tilde{\zeta}_4}{dt} = -\omega_{\oplus}\tilde{\zeta}_5, \tag{7.62}$$

$$\frac{d\tilde{\zeta}_5}{dt} = \omega_{\oplus}\tilde{\zeta}_4 + a_{eN_{sk}}(t) + u_N(t), \tag{7.63}$$

$$\frac{d\tilde{\zeta}_6}{dt} = \omega_{\oplus}(3\tilde{\zeta}_1 - 2\tilde{\zeta}_2) - 4\frac{A_{al_\Theta}}{a_k}(\tilde{\zeta}_1 - \tilde{\zeta}_2), \tag{7.64}$$

where the linear combinations of the transformed elements between parentheses at the right-hand side are proportional to the semi-major axis and mean longitude deviations $(a - a_k)$ and $(l_\Theta - \lambda_s)$ and to the eccentricity components $\tilde{P}_1$ and $\tilde{P}_2$ along and perpendicular to the station keeping line

$$(4\tilde{\zeta}_3 - 3\tilde{\zeta}_6) = 2v_{sk}\tilde{P}_2, \tag{7.65}$$

$$(\tilde{\zeta}_3 - \tilde{\zeta}_6) = \omega_{\oplus}(a - a_k)/2, \tag{7.66}$$

$$(3\tilde{\zeta}_1 - 2\tilde{\zeta}_2) = 2v_{sk}\tilde{P}_1, \tag{7.67}$$

$$(\tilde{\zeta}_1 - \tilde{\zeta}_2) = v_{sk}(l_\Theta - \lambda_s)/2, \tag{7.68}$$

(see the definitions of $\tilde{\zeta}_1$-$\tilde{\zeta}_6$ given by Eq.s (7.45)–(7.50)).

Let be ς_1, ς_2, ς_3 the components of the output vector $\boldsymbol{\varsigma} = \tilde{\boldsymbol{C}}\tilde{\boldsymbol{\zeta}}$

$$\boldsymbol{\varsigma} = \begin{bmatrix} \varsigma_1 & \varsigma_2 & \varsigma_3 \end{bmatrix}^T = \begin{bmatrix} r - a_k & \lambda - \lambda_s & \varphi \end{bmatrix}^T. \tag{7.69}$$

These components come out to be proportional to the transformed state vector components $\tilde{\zeta}_6$, $\tilde{\zeta}_1$ and $\tilde{\zeta}_4$ respectively

$$\varsigma_1 = -\tilde{\zeta}_6/(2\omega_{\oplus}), \tag{7.70}$$

$$\varsigma_2 = -\tilde{\zeta}_1/v_{sk}, \tag{7.71}$$

$$\varsigma_3 = -\tilde{\zeta}_4/v_{sk}, \tag{7.72}$$

(see the structure of the matrix $\tilde{\boldsymbol{C}}$ in the state-output equation (7.38)).

We recognize the outputs ς_1, ς_2, ς_3 as flat outputs of the GEO satellite dynamics. They are the deviation of the geographical inertial coordinates from their nominal station keeping values and they are equal to the transformed state variables $\tilde{\zeta}_6$, $\tilde{\zeta}_1$ and $\tilde{\zeta}_4$ up to a scaling factor. Each

transformed state variable vector and control variable vector component can be parametrized by means of these flat outputs and their derivatives as follows

$$\tilde{\zeta}_1 = -v_{sk}\varsigma_2, \tag{7.73}$$

$$\tilde{\zeta}_2 = \frac{2\omega_\oplus\dot{\varsigma}_1 - v_{sk}(3\omega_\oplus - 4A_{al_\Theta}/a_k)\varsigma_2}{2\left(\omega_\oplus - 2A_{al_\Theta}/a_k\right)}, \tag{7.74}$$

$$\tilde{\zeta}_3 = \frac{v_{sk}\dot{\varsigma}_2 - 2\omega_\oplus(3\omega_\oplus + 2A_K a_k)\varsigma_1}{2\left(2\omega_\oplus + A_K a_k\right)}, \tag{7.75}$$

$$\tilde{\zeta}_4 = -v_{sk}\varsigma_3, \tag{7.76}$$

$$\tilde{\zeta}_5 = a_k\dot{\varsigma}_3, \tag{7.77}$$

$$\tilde{\zeta}_6 = -2\omega_\oplus\varsigma_1, \tag{7.78}$$

and

$$u_R(t) = \frac{\omega_\oplus\left(2\omega_\oplus + A_K a_k\right)\ddot{\varsigma}_1 - v_{sk}\left(\omega_\oplus^2 + A_K A_{al_\Theta}\right)\dot{\varsigma}_2 + \omega_\oplus^2 A_K a_k\left(\omega_\oplus - 2A_{al_\Theta}/a_k\right)\varsigma_1}{\left(\omega_\oplus - 2A_{al_\Theta}/a_k\right)\left(2\omega_\oplus + A_K a_k\right)} - a_{eR_{sk}}(t), \tag{7.79}$$

$$u_T(t) = \frac{v_{sk}\left(\omega_\oplus - 2A_{al_\Theta}/a_k\right)\ddot{\varsigma}_2 + 2\omega_\oplus\left(\omega_\oplus^2 + A_K A_{al_\Theta}\right)\dot{\varsigma}_1 - \omega_\oplus^2 A_{al_\Theta}\left(2\omega_\oplus + A_K a_k\right)\varsigma_2}{2\left(\omega_\oplus - 2A_{al_\Theta}/a_k\right)\left(2\omega_\oplus + A_K a_k\right)} - a_{eT_{sk}}(t), \tag{7.80}$$

$$u_N(t) = a_k\ddot{\varsigma}_3 + a_k\omega_\oplus^2\varsigma_3 - a_{eN_{sk}}(t). \tag{7.81}$$

7.5 Summary

In this chapter, we have explained the way to transform the linear system with time varying coefficients given by Eq.s (6.49) and (6.50) in a linear system with time invariant coefficients without modifying its stability properties. This transformation leads to recognize some differential flatness characteristics in the GEO satellite dynamics. Over time horizons one day long, the nominal station keeping environmental accelerations can be approximated with their Fourier expansion up to the second order. Once the target conditions known at the end of each day, the SK maneuver planning problem over the correction time intervals can be solved using flatness algorithms, i.e., parameterizing the highest order derivatives of the flat outputs with a suitable set of basis functions (see, e.g., [Fliess et al., 1995], [Fliess et al., 1999], [Fliess and Marquez, 2000], [Varigonda et al., 2001], [Varigonda et al., 2004]). These algorithms eliminate the need for the numerical integration of differential equations.

The ideas explained in this chapter are subject of a paper whose writing is in progress.

Chapter 8

Conclusion

8.1 Thesis Contributions

This thesis presents a detailed model of the GEO satellite translational dynamics in terms of osculating equinoctial orbital parameters and a control design method for station keeping purposes based on parameter optimization programs.

We explain in detail the nonlinear dynamical model used to design the station keeping controller and the analytical approximations done to implement this model. We present validation simulation results, which have been obtained implementing Gauss' VOP equations instead of Langange's ones traditionally used to plan high thrust station keeping maneuvers. Even if Lagrange's traditional equations have been utilized at the beginning of this PhD thesis work (see, e.g., [Losa et al., 2005a], [Losa et al., 2005b], [Losa et al., 2006]), in the sequel of the work we have preferred to use Gauss' equations, which lend themselves to formulate the station keeping problem in terms of osculating parameters with less approximations. We choose to use a model in terms of osculating parameters instead of averaged ones in view of a finer control of the spacecraft position, i.e., in view of very narrow station keeping windows. In this last case the use of low thrusts performed with electrical propulsion systems is essential and the SK maneuver planning method has to be considered as a continuous process to be optimized. We have presented a survey of the works of the last three decades related with the GEO satellite SK maneuver planning. We have payed particular attention to the understanding of the maneuver planning method traditionally used with high thrust maneuvers and with quite large (greater than 0.01 deg) longitude and latitude deadbands of the station keeping box. Almost none of the bibliographic references we surveyed deals with the station keeping maneuver planning problem in a unified way both for the North-South and the East-West maneuvers, except some works which handle the problem as a formation keeping maneuver planning problem (i.e., as a regulation problem), and the works of Anzel with reference to the patent of an electrical propulsion system able to control simultaneously longitude and latitude ([Anzel, 1995], [Anzel, 1998]). Moreover, the works about the low thrust maneuver planning are deficient in terms of control techniques taking into account technical specifications. These specifications are consid-

ered only a posteriori, after having planned the maneuvers with very simplified dynamical models. The main reason of this lack is the attempt to adapt the standard SK control strategies used for a long time with the high thrust propulsion system to the low thrust case. Hence, our intent has been to try to cover this deficiency and, from a control viewpoint, we have performed the SK maneuver planning following two planning phases.

- ➢ In a first phase the SK maneuver planning is performed with a linearized version of Gauss' VOP equations by means of a direct method of trajectory optimization based on a receding horizon approach. In this phase only the orbital requirements (i.e., the constraints on the state variables) are taken into account to determine the target conditions in terms of optimal trajectory. A sequence of linear parameter optimization problems is solved. Performing this first phase of the maneuver planning over a time interval of one year allows one to choose the thrust level of the thrusters of the propulsion system.
- ➢ In a second phase the technological specifications are taken into account and a nonlinear programming problem is solved over a time interval of one day in order to find the switching on and switching off optimal instants of the thrusters such that the target conditions are reached at the end of each day.

An advantage of this method of maneuver planning that we proposed and which is based on an optimization chain, is that further operational constraints can be easily introduced in the control design, e.g., the impossibility of switching the thrusters on over some time intervals.

8.2 Areas of Future Works

An aspect which has been completely omitted in this work is the attitude control and its interaction with the geostationary orbit control system. The rotational dynamics part could be added to the translational one. Alternatively, this aspect should be taken into account modeling directly the secondary and undesired effects of attitude maneuvers as disturbances affecting the spacecraft position.

It would be interesting to study the SK maneuver planning for geosynchronous satellites not necessary geostationary, i.e., for satellites with mean motion n equal to the angular rotation of the Earth $\omega_\oplus$ but not necessarily with inclination and eccentricity equal to zero. In these cases the nominal station keeping trajectory is clearly different from the Keplerian one. The linearization point changes and the time varying matrices $\boldsymbol{A}$, $\boldsymbol{B}$ and $\boldsymbol{C}$ of the linear model used to plan the maneuvers will be different from those ones presented in this work. Consequently, the Lyapunov transformation used to point out the differential flatness of the linear GEO dynamics will be different and the equations utilized to plan the on off maneuvers will change.

This last neglected aspect would be the first aspect to tackle in order to study the station keeping of geosynchronous spacecraft constellations. In the case of LEO (Low Earth Orbit) con-

stellations, the nonlinear model has to be modified adding to the environmental perturbing forces the atmospheric drag.

Another area of future work is to solve the SK maneuver planning problem with flatness based algorithms (see, e.g., [Fliess et al., 1995], [Fliess et al., 1999], [Fliess and Marquez, 2000], [Varigonda et al., 2001], [Varigonda et al., 2004]). We have begun to consider this approach from a modeling viewpoint. In Chapter 7, we have explained the way to transform the linear system with time varying coefficients given by Eq.s (6.49) and (6.50) in a linear system with time invariant coefficients without modifying its stability properties. This transformation leads to recognize differential flatness in the GEO satellite dynamics. Over time horizons one day long, the nominal station keeping environmental accelerations can be approximated with their Fourier expansion up to the second order. Once the target conditions known at the end of each day, the SK maneuver planning problem over the correction time intervals can be solved using flatness algorithms, i.e., parameterizing the highest order derivatives of the flat outputs with a suitable set of basis functions. These algorithms eliminate the need for the numerical integration of differential equations.

8.3 Final Comments

The method proposed in this thesis could be used either in a ground based or in an autonomous SK control loop. The use of a model based on osculating elements (like the orbit determination and models) makes the proposed maneuver planning method particularly suitable for being embedded in autonomous control of geostationary Earth orbits. However, to conclude, we think it is interesting to quote some remarks by [Soop, 1994] and [Wertz and Larson, 1999] about the feasibility and the convenience in opting for an autonomous GEO control instead for a ground based one.

> *In the past, there was no realistic alternative to orbit control from the ground. Now, autonomous navigation systems have made autonomous orbit maintenance possible, economical and safe. Autonomous orbit control reduces the cost and risk of missions by having a major part of the day-to-day operations on board the spacecraft.*
>
> *The general trend of development in space operations is to perform more and more functions on-board in automatic mode, including orbit determination and maneuver planning. There is, however, less incentive to perform functions on board a geostationary spacecraft, which has uninterrupted ground contact, than for other types of missions with only short and infrequent passes over ground stations. When the purpose of the automation is to reduce the manual workload for operations, one can equally well implement the automatic system on ground for a geostationary mission. A further reason is that the tracking measurements are produced on ground, although there exist proposals by which the Earth would be tracked by a system on the spacecraft instead of vice versa (see Section 8.2 of [Soop, 1994]).*

In geosynchronous station keeping, the main reason for autonomous orbit maintenance is to reduce operation cost and risk, rather than a specific technical requirement. A technical requirement for autonomous orbit control can arise in geosynchronous station keeping when additional satellites should be placed in a narrow orbit slot. In this case it would impractical to send frequent commanding from the ground when the size of the orbit control deadband is very small. For a constellation of satellites at any altitude, the overall process of orbit determination and control represents a major operational cost. It also represents a significant risk element in which any operational error or failure of the ground system could damage or destroy the constellation. The orbit maintenance operation is necessarily carried out on board the spacecraft by firing thrusters. Performing the control computations on board the spacecraft can reduce both cost and risk. First, it eliminates the potential of operator error in a very repetitive function. Second, it reduces communication errors of failures frequently associated with operational activities.

The principal reason for no undertaking autonomous orbit maintenance and control for future missions is tradition. It has not been done that way in the past, and there is a very strong desire in expensive space missions to maintain those procedures that have worked previously. A mechanism for overcoming this potential risk is a supervised autonomy solution, in which orbit maintenance maneuvers are computed on board the spacecraft and verification from the ground is required before they are executed. This allows mission personnel to gain confidence in the on board computations before permitting fully autonomous operation.

A second alternative is to implement autonomous orbit control from the ground. In this case, the computations would be done autonomously, but would be done at the ground station and then sent to the spacecraft for execution. This has the advantage of maintaining some characteristics of traditional orbit maintenance and also minimizes the amount of hardware on board the spacecraft. Unfortunately, this approach can add significant complexity and risk to the mission. If the navigation data is obtained on board the spacecraft, it would need to be communicated to the ground for processing. Then the results and commands would go to the spacecraft and be verified for latter execution. This makes the process much more complex and increases the potential for communications errors and transmitting the wrong data to the wrong spacecraft. Most likely, these disadvantages would outweigh any advantage of doing the small amount of command processing on the ground. If the spacecraft has enough computing power on board, a reasonable alternative might be to compute the orbit control on-board the spacecraft and send it to the ground for verification and approval before actually executing the command. This allows full ground override. It also allows the system to use an on orbit process with less cost and higher reliability, whenever operators are confident that the system is working smoothly.

Conclusion (*en français*)

Contributions

Ce travail de thèse présente un modèle détaillé de la dynamique de translation d'un satellite géostationnaire en termes de paramètres osculateurs équinoxiaux et une méthode de conception du contrôle pour le maintient à poste basée sur des programmes d'optimisation paramétrique.

Nous avons expliqué dans le détails le modèle dynamique non linéaire utilisé pour concevoir le contrôleur de maintient à poste et les approximations analytiques qui ont été utilisées pour implémenter ce modèle. Nous avons présenté des résultats des simulations de validation obtenus en implémentant les équations des variations des paramètres de Gauss à la place de celles de Lagrange, normalement utilisées pour la planification des manoeuvres de maintient à poste à poussée forte. Même si les équations traditionnelles de Lagrange ont été utilisées dans la première partie du travail de thèse (voir par exemple [Losa et al., 2005a], [Losa et al., 2005b], [Losa et al., 2006]), nous avons préféré dans la suite utiliser les équations de Gauss, qui permettent de formuler le problème de maintient à poste en termes de paramètres osculateurs avec un degré de précision accru. Nous avons choisi d'utiliser un modèle qui se base sur les paramètres osculateurs au lieu des paramètres moyens pour permettre un contrôle plus fin de la position du satellite, ou en d'autres termes, d'une fenêtre de maintient à poste très étroite. Dans ce dernier cas, il est essentiel d'utiliser des poussées faibles effectuées avec des systèmes de propulsion électrique, et le problème de planification du maintient à poste doit être vu comme un processus continu à optimiser.

Nous avons présenté un état de l'art des travaux des dernières trois décennies qui concernent la planification du maintient à poste pour les satellites géostationnaires. Nous avons prêté une attention particulière à la compréhension des méthodes de planification traditionnellement utilisées pour les manoeuvres à poussée forte avec amplitudes de la fenêtre de maintient à poste (en longitude comme en latitude) assez larges (supérieures à 0.01 deg). Parmi les références bibliographiques que nous avons étudiées, presque aucune ne traite le problème de planification de maintient à poste en unifiant à la fois les manoeuvres Nord-Sud et celles Est-Ouest. Les seules exceptions sont représentées par quelques travaux qui traitent le problème comme un problème de régulation, et les travaux de Anzel qui concernent son brevet d'un système de propulsion électrique capable de contrôler simultanément la latitude et la longitude ([Anzel, 1995], [Anzel, 1998]). De plus, les travaux qui concernent la planification de manoeuvres à poussée faible n'utilisent aucune technique

de contrôle en mesure de prendre en compte les spécifications techniques. Ces dernières sont considérées seulement a posteriori, après avoir planifié les manoeuvres avec un modèle dynamique très simple. La raison principale de cette lacune provient de l'effort d'adapter aux systèmes à poussée faible les stratégies standards de contrôle qui sont utilisées depuis longtemps pour les systèmes à poussée forte. Notre intention a donc été d'essayer de combler cette lacune et, du point de vue du contrôle, nous avons exécuté la planification des manoeuvres de maintient à poste en suivant ces deux phases :

- ➢ Dans une première phase, la planification des manoeuvres de maintient à poste est exécutée avec une version linéarisée des équations de Gauss des variations des paramètres orbitaux, en utilisant une méthode directe d'optimisation de trajectoire basée sur l'approche à horizon glissant. Pendant cette phase, pour déterminer la condition visée en terme de trajectoire optimale, on ne prend en compte que les contraintes orbitales (c'est à dire les contraintes sur les variables d'état). On résout alors une séquence de problèmes d'optimisation linéaire de paramètres. Le fait d'effectuer cette première phase de la planification de manoeuvres sur un intervalle de temps d'un an permet de choisir le niveau de poussé des tuyères du système de propulsion.
- ➢ Dans une seconde phase, les spécifications techniques sont prises en compte et un problème de programmation non linéaire est résolu sur un intervalle de temps d'un jour, pour trouver les instants optimaux d'allumage et coupure tels que les conditions visées soient atteintes à la fin de chaque jour.

Un avantage de cette méthode de planification des manoeuvres que nous avons proposée et qui se base sur une chaîne d'optimisation est que des contraintes opérationnelles additionnelles (par exemple l'impossibilité d'allumer les tuyères sur certains intervalles de temps) peuvent être facilement introduites dans la phase de conception du contrôle.

Ouvertures et perspectives

Un aspect qui a été complètement ignoré dans ce travail est le contrôle d'attitude et son interaction avec le système de contrôle d'orbite géostationnaire. La partie de dynamique de rotation devrait être ajoutée à celle de dynamique de translation. Comme alternative, cet aspect pourrait être considéré en modélisant directement les effets secondaires non désirés des manoeuvres d'attitude comme des perturbations affectant la position du satellite.

Il serait intéressant d'étudier la planification de maintient à poste pour les satellites géosynchrones et non nécessairement géostationnaires, c'est à dire les satellites avec mouvement moyen n égal à la rotation angulaire de la terre $\omega_\oplus$ mais avec inclination et excentricité non nécessairement nulles. Dans ces cas, la trajectoire de maintient à poste nominale est clairement différente de la képlérienne. Le point de linéarisation change et les matrices $\boldsymbol{A}$, $\boldsymbol{B}$ et $\boldsymbol{C}$ qui dépendent du temps

du modèle linéaire utilisé pour planifier les manoeuvres sont différentes de celles présentées dans ce travail. Par conséquent, la transformation de Lyapunov utilisée pour souligner la platitude différentielle de la dynamique linéaire du satellite est différente et les équations utilisées pour planifier les manoeuvres d'allumage et de coupure changent également.

Ce dernier aspect que nous avons négligé serait le premier à être pris en compte si on voulait étudier le maintient à poste de constellations de satellites géosynchrones. Dans le cas des constellations LEO le modèle non linéaire doit être modifié en rajoutant aux perturbations environnementales le frottement atmosphérique.

Une autre direction possible pour des travaux futurs serait de résoudre le problème de planification des manoeuvres de maintient à poste avec des algorithmes basés sur la platitude (voir par exemple [Fliess et al., 1995], [Fliess et al., 1999], [Fliess and Marquez, 2000], [Varigonda et al., 2001], [Varigonda et al., 2004]). Nous avons commencé à considérer cette approche pour la modélisation. Dans le chapitre 7, nous avons expliqué comment transformer le système linéaire avec coefficients dépendants du temps (Eq.s (6.49) et (6.50)) en un système linéaire avec coefficients indépendants du temps, et ce sans en modifier les propriétés de stabilité. Cette transformation conduit à reconnaître la présence de platitude différentielle dans la dynamique des satellites géostationnaires. Sur des horizons temporels d'une journée, l'accélération environnementale nominale du maintient à poste peut être approximée avec son développement en série de Fourier du deuxième ordre. Une fois que les conditions visées sont connues à la fin de chaque jour, le problème de planification de maintient à poste sur les intervalles de correction peut être résolu avec des algorithmes de platitude, c'est à dire avec une paramétrisation des dérivées d'ordre le plus élevé des sorties plates par un ensemble de fonctions de base adéquates. Ces algorithmes éliminent le besoin d'intégrer numériquement des équations différentielles.

Commentaires finals

La méthode proposée dans cette thèse peut être utilisée à la fois pour une boucle de contrôle de maintient à poste autonome et pour une boucle basée au sol. L'utilisation d'un modèle basé sur les éléments osculateurs (comme la détermination d'orbite et les modèles) rend la méthode de planification des manoeuvres que nous avons proposée particulièrement adaptée pour être embarquée dans les systèmes de contrôle autonome des orbites géostationnaires. Cependant, pour conclure, nous pensons intéressant de citer dans la suite les considérations faites par [Soop, 1994] et [Wertz and Larson, 1999] à propos de la faisabilité et de l'intérêt (ou du manque d'intérêt) de choisir, pour les satellites géostationnaires, un contrôle autonome plutôt qu'un contrôle basé au sol.

> *Dans le passé, il n'y avait pas réellement d'alternatives au contrôle d'orbite effectué du sol. Aujourd'hui, les systèmes de navigation autonomes ont rendu le maintient d'orbite autonome possible, économique et sûr. Les contrôles d'orbite autonomes réduisent le coût et les risques des missions puisque la plupart des opérations quotidiennes sont*

effectuées à bord du satellite.

La tendance générale du développement dans le domaine des opérations spatiales est d'effectuer de plus en plus de fonctions automatiquement à bord, y compris la détermination d'orbite et la planification des manoeuvres. Cependant, il y a une moindre volonté d'exécuter ces opérations à bord d'un satellite géostationnaire, qui est en contact permanent avec la terre, par rapport à d'autres types de missions où les passages du satellite sur des stations au sol sont courts et rares. Si le but de l'automation est de réduire l'intervention humaine nécessaire pour effectuer ces opérations, pour une mission géostationnaire, on peut, avec le même résultat, implémenter le système automatique au sol. Une raison ultérieure vient du fait que les mesures de suivi de trajectoire sont effectuées au sol, même si des propositions existent pour effectuer le suivi de la terre par un système sur le satellite au lieu du contraire (voir la section 8.2 de [Soop, 1994]).

Pour le maintient à poste géosynchrone, la raison principale d'effectuer le maintient de l'orbite de façon autonome ne vient pas d'une contrainte technique spécifique mais de l'effort de réduire les coûts et les risques de cette opération. Une contrainte technique qui pousserait vers le contrôle d'orbite autonome peut apparaître pour le maintient à poste des satellites géosynchrones quand plusieurs satellites doivent être placés dans des fenêtres orbitales étroites. Dans ce cas où l'amplitude de la fenêtre de maintient à poste est très réduite, il ne serait pas pratique d'envoyer fréquemment des commandes du sol. Pour une constellation de satellites à une altitude quelconque, la tâche globale de détermination d'orbite et de contrôle représente un coût opérationnel majeur. Cette tâche représente aussi un risque significatif car toute erreur ou défaillance du système au sol peut endommager ou détruire la constellation. L'opération de maintient d'orbite est nécessairement effectuée à bord du satellite en allumant les tuyères. Le fait d'effectuer les calculs de contrôle à bord du satellite peut réduire à la fois les coûts et les risques. En premier lieu, on réduit ainsi l'occurrence d'une erreur humaine due à des manipulations très répétitives. Deuxièmement, on réduit les erreurs de communication et les défaillances qui sont fréquemment associées avec les activités opérationnelles.

La raison principale pour ne pas faire recours au maintient d'orbite et au contrôle autonome pour les missions futures est essentiellement une question de tradition. Cela n'a jamais été fait auparavant, et il y a une motivation forte, dans le cadre de missions spatiales coûteuses, de réutiliser les procédures qui ont bien fonctionnées dans le passé. Un mécanisme pour pallier ce risque potentiel est représenté par des solutions autonomes mais supervisées, dans lesquelles les manoeuvres de maintient d'orbite sont calculées à bord du satellite mais une vérification faite au sol est nécessaire avant leur exécution. Ceci permet au personnel en charge de la mission de gagner confiance dans le calcul à bord avant de permettre l'exécution d'opérations complètement autonomes.

Une deuxième alternative est d'implémenter le contrôle d'orbite autonome au sol. Les calculs seraient ainsi effectués de façon autonome mais par la station au sol, et ensuite envoyés au satellite pour être exécutés. Ceci présente l'avantage de maintenir certaines caractéristiques du maintient d'orbite traditionnel et aussi de minimiser le matériel embarqué dans le satellite. Malheureusement cette approche peut rajouter une complexité et des risques significatifs à la mission. Si les données de navigation sont obtenues à bord du satellite, il est alors nécessaire de les envoyer au sol pour les élaborer. Ensuite les résultats de l'élaboration et les commandes doivent être envoyées au satellite et vérifiées avant leur exécution. Ce processus rend la tâche beaucoup trop compliquée et augmente la probabilité d'une erreur de communication ou d'envoyer les mauvaises données au mauvais satellite. Très probablement ces inconvénients dépassent l'intérêt d'effectuer l'élaboration au sol. Si le satellite possède suffisamment de puissance de calcul dans son électronique embarquée, une alternative raisonnable pourrait être de calculer le contrôle d'orbite à bord du satellite et de l'envoyer à terre pour vérification et approbation avant d'exécuter les commandes. Ceci permet toute modification des commandes au sol. Ceci permet aussi au système d'utiliser un processus exécuté totalement à bord, avec des coûts réduits et une fiabilité accrue, une fois que les opérateurs ont gagné confiance en la fiabilité du système.

Bibliography

[Anzel, 1988] Anzel, B. M. (1988). Controlling a stationary orbit using electric propulsion. In *DGLR/AIAA/JSASS 20th International Electric propulsion Conference*, Garmisch-Partenkirchen, Germany.

[Anzel, 1995] Anzel, B. M. (1995). Method and apparatus for a satellite stationkeeping. Patent 5443231, Hughes Aircraft Company, Los Angeles, CA.

[Anzel, 1998] Anzel, B. M. (1998). Stationkeeping the Hughes HS 702 satellite with a xenon ion propulsion system. In *49th International Astronautical Congress*, Melbourne, Australia.

[Battin, 1999] Battin, R. H. (1999). *An Introduction to the Mathematics and Methods of Astrodynamics, Revised Edition*. Education. AIAA.

[Camacho and Bordons, 1999] Camacho, E. F. and Bordons, C. (1999). *Model Predictive Control*. Advanced Textbooks in Control and Signal Processing. Springer-Verlag London Limited.

[Campan et al., 1995a] Campan, G., Agrotis, L., Alby, F., Dufor, F., Duhamel, T., Frémeaux, C., Gautier, H., Moury, M., and Perdu, M. (1995a). La réalisation de maintien à poste de satellites géostationnaires. In CNES, editor, *Mécanique spatiale, Tome II*, chapter 22, pages 1497–1557. Cépaduès-Éditions, Toulouse, France.

[Campan et al., 1995b] Campan, G., Alby, F., and Gautier, H. (1995b). Les techniques de maintien à poste de satellites géostationnaires. In CNES, editor, *Mécanique spatiale, Tome II*, chapter 15, pages 983–1085. Cépaduès-Éditions, Toulouse, France.

[Chao, 1984] Chao, C. C. (1984). Semiautonomous stationkeeping of geosynchronous satellites. *Journal of Guidance, Control, and Dynamics*, 7(1):57–61.

[Chao and Bernstein, 1994] Chao, C. C. and Bernstein, H. (1994). Onboard stationkeeping of geosynchronous satellites using a global positioning system receiver. *Journal of Guidance, Control, and Dynamics*, 17(4):778–786.

[CNES, 1995a] CNES, editor (1995a). *Mécanique spatiale, Tome I*. Cépaduès-Éditions, Toulouse, France.

[CNES, 1995b] CNES, editor (1995b). *Mécanique spatiale, Tome II.* Cépaduès-Éditions, Toulouse, France.

[Conway and Larson, 1998] Conway, B. A. and Larson, K. M. (1998). Collocation versus differential inclusion in direct optimization. *Journal of Guidance, Control, and Dynamics*, 21(5):780–785.

[Cot, 1984] Cot, D. (1984). *Etude analytique de l'évolution de l'orbite d'un satellite géostationnaire.* PhD thesis, Centre Spatial de Toulouse. CNES report no. 99148.

[D'Angelo, 1970] D'Angelo, H. (1970). *Linear Time-Varying Systems: Analysis and Synthesis.* Allyn and Bacon, Inc.

[Eckstein, 1980] Eckstein, M. C. (1980). Optimal station keeping by electric propulsion with thrust operation constraints. *Celestial Mechanics*, 21:129–147.

[Eckstein and Hechler, 1981] Eckstein, M. C. and Hechler, F. (1981). Station acquisition and station keeping with low-thrust systems. In *International Symposium Spacecraft Flight Dynamics*, Darmstadt, Germany.

[Eckstein et al., 1981] Eckstein, M. C., Leibord, A., and Hechler, F. (1981). Optimal autonomous station keeping of geostationary satellites. In *AAS/AIAA Astrodynamics Specialist Conference*, Lake Tahoe, Nevada.

[Emma and Pernicka, 2003] Emma, B. P. and Pernicka, H. J. (2003). Algorithm for autonomous longitude and eccentricity control for geostationary spacecraft. *Journal of Guidance, Control, and Dynamics*, 26(3):483–490.

[Enright and Conway, 1991] Enright, P. J. and Conway, B. A. (1991). Optimal finite-thrust spacecraft trajectories using collocation and nonlinear programming. *Journal of Guidance, Control, and Dynamics*, 14(5):981–985.

[Fliess et al., 1995] Fliess, M., Lï£¡ine, J., Martin, P., and Rouchon, P. (1995). Flatness and defect of nonlinear systems: introductory theory and applications. *International Journal of Control*, 61:1327–1361.

[Fliess et al., 1999] Fliess, M., Lï£¡ine, J., Martin, P., and Rouchon, P. (1999). A Lie-Bäcklund approach to equivalence and flatness of nonlinear systems. *IEEE Transaction on Automatic Control*, 44(5):922–937.

[Fliess and Marquez, 2000] Fliess, M. and Marquez, R. (2000). Continuous-time linear predictive control and flatness: a module-theoretic setting with examples. *International Journal of Control*, 73:606–623.

[Gartrell, 1981] Gartrell, C. F. (1981). Simultaneous eccentricity and drift rate control. *Journal of Guidance, Control, and Dynamics*, 4(3):310–315.

[Geffroy, 1997] Geffroy, S. (1997). *Généralisation des Techniques de Moyennation en Contrôle Optimal — Application aux Problèmes de transfert et Rendez-Vous Orbitaux à Poussée Faible*. PhD thesis, Institut National Polytechnique de Toulouse.

[Goebel et al., 2005] Goebel, D. M., Brophy, J. R., Polk, J. E., Katz, I., and Anderson, J. (2005). Variable specific impulse high power ion thruster. In *41st AIAA/ASME/SAE/ASEE Joint Propulsion Conference and Exhibit AIAA*, pages 10–13.

[Goodwin et al., 2004] Goodwin, G. C., Seon, M. M., and Doná, J. A. D. (2004). *Constrained Control and Estimation — An Optimisation Approach*. Communications and Control Engineering. Springer.

[Gopinath and Srinivasamuthy, 2003] Gopinath, N. S. and Srinivasamuthy, K. N. (2003). Optimal low thrust orbit transfer from gto to geosynchronous orbit and stationkeeping using electric propulsion system. In *54th International Astronautical Congress of the International Astronautical Federation, the International Academy of Astronautics, and the International Institute of Space Law*, Bremen, Germany.

[Hargraves and Paris, 1987] Hargraves, C. R. and Paris, S. W. (1987). Direct trajectory optimization using nonlinear programming and collocation. *Journal of Guidance, Control, and Dynamics*, 10(4):338–342.

[Hull, 1997] Hull, D. G. (1997). Conversion of optimal control problems into parameter optimization problems. *Journal of Guidance, Control, and Dynamics*, 20(1):57–60.

[Hull, 2003] Hull, D. G. (2003). *Optimal Control Theory for Applications*. Mechanical Engineering. Springer-Verlag.

[Jehn et al., 2005] Jehn, R., Agapov, V., and Hernández, C. (2005). The situation in the geostationary ring. *Advances in Space Research*, 35:1318–1327.

[Kailath, 1980] Kailath, T. (1980). *Linear Systems*. Prentice-Hall.

[Kamel, 1975] Kamel, A. A. (1975). East-west stationkeeping requirements of 24-h satellites due to earth's triaxiality and luni-solar effects. *Celestial Mechanics*, 12:425–438.

[Kamel et al., 1973] Kamel, A. A., Ekman, D., and Tibbitts, R. (1973). East-west stationkeeping requirements of nearly synchronous satellites due to earth's triaxiality and luni-solar effects. *Celestial Mechanics*, 8:129–148.

[Kamel and Tibbitts, 1973] Kamel, A. A. and Tibbitts, R. (1973). Some useful results on initial node locations for near-equatorial circular satellite orbits. *Celestial Mechanics*, 8:45–73.

[Kamel and Wagner, 1981] Kamel, A. A. and Wagner, C. A. (1981). On the orbital eccentricity control of synchronous satellites. In *AAS/AIAA Astrodynamics Specialist Conference*, Lake Tahoe, Nevada.

[Kelly et al., 1994] Kelly, T. J., White, L. K., and Gamble, D. W. (1994). Stationkeeping of geostationary satellites with simultaneous eccentricity and longitude control. *Journal of Guidance, Control, and Dynamics*, 17(4):769–777.

[Kluever and Tanck, 1997] Kluever, C. A. and Tanck, G. S. (1997). A feedback control law for stationkeeping with on-off thrusters. *Advances in the Astronautical Sciences*, 97(1):387–399.

[Kumar and Seywald, 1996] Kumar, R. R. and Seywald, H. (1996). Should controls be eliminated while solving optimal control problems via direct methods? *Journal of Guidance, Control, and Dynamics*, 19(2):418–423.

[Legendre, 1980a] Legendre, P. (1980a). Le maintien à poste de satellites géostationnaires. évolution de l'orbite. In CNES, editor, *Cours de Technologie Spatiale*, pages 583–609. Cépaduès-Éditions, Toulouse, France.

[Legendre, 1980b] Legendre, P. (1980b). Le maintien à poste de satellites géostationnaires. Stratégies des corrections d'orbites. In CNES, editor, *Cours de Technologie Spatiale*, pages 611–625. Cépaduès-Éditions, Toulouse, France.

[Legendre, 1983] Legendre, P. (1983). Analytical model of the evolution of orbit parameters of a quasi geostationary satellite. In *34th IAF International Astronautical Congress*, Budapest, Hungary.

[Losa et al., 2005a] Losa, D., Lovera, M., and Drai, R. (2005a). Maintien à poste de satellites géostationnaires par propulsion électrique. In *JDMACS – JNMACS*, Lyon, France.

[Losa et al., 2005b] Losa, D., Lovera, M., Drai, R., Dargent, T., and Amalric, J. (2005b). Electric station keeping of geostationary satellites: a differential inclusion approach. In *44th IEEE Conference on Decision and Control*, Sevilla, Spain.

[Losa et al., 2006] Losa, D., Lovera, M., Marmorat, J.-P., Dargent, T., and Amalric, J. (2006). Station keeping of geostationary satellites with on-off electric thrusters. In *IEEE International Conference on Control Applications*, Munich, German.

[Lyszyk and Garnero, 2004] Lyszyk, M. and Garnero, P. (2004). Electric propulsion system on @bus platform. In *ESA SP-555: 4th International Spacecraft Propulsion Conference*.

[Maciejowski, 2002] Maciejowski, J. M. (2002). *Predictive Control with Constraints*. Prentice Hall.

[Marcuccio et al., 1997] Marcuccio, S., Genovese, A., and Andreucci, M. (1997). FEEP microthruster technology status and potential applications. In *48th International Astronautical Federation Congress*, Torino, Italy.

[Martinez-Sanchez and Pollard, 1998] Martinez-Sanchez, M. and Pollard, J. (1998). Spacecraft electric propulsion — an overview. *Journal of Propulsion and Power*, 14(5):688–699.

[Meeus, 1998] Meeus, J. (1998). *Astronomical Algorithms*. Willmann-Bell.

[Montenbruck and Gill, 2000] Montenbruck, O. and Gill, E. (2000). *Satellite Orbits — Models, Methods, and Applications*. Springer-Verlag.

[Murray et al., 2001] Murray, R. M., Hauser, J., Jadbabaie, A., Milam, M. B., Petit, N., Dunbar, W. B., and Franz, R. (2001). Online control customization via optimization-based control. In Samad, T. and Balas, G., editors, *Software-Enabled Control: Information Technology for Dynamical Systems*. IEEE Press. (submitted).

[Neckel et al., 2003] Neckel, T., Talbot, C., and Petit, N. (2003). Collocation and inversion for a reentry optimal control problem. In *5th International Conference on Launcher Technology*.

[Park et al., 2005] Park, B.-K., Tahk, M.-J., Bang, H.-C., Park, C.-S., and Jin, J.-H. (2005). A new approach to on-board stationkeeping of geo-satellites. *Aerospace Science and Technology*, 9(8):722–731.

[Petit et al., 2001] Petit, N., Milam, M. B., and Murray, R. M. (2001). Inversion based trajectory optimization. In *IFAC Symposium on Nonlinear Control Systems Design*.

[Petit et al., 2002] Petit, N., Milam, M. B., and Murray, R. M. (2002). A new computational method for optimal control of a class of constrained systems governed by partial differential equations. In *IFAC World Congress*.

[Rauschenbakh et al., 2003] Rauschenbakh, B. V., Ovchinnikov, M. Y., and McKenna-Lawlor, S. (2003). *Essential Spaceflight Dynamics and Magnetospherics*. Microcosm Press and Kluwer Academic Publishers.

[Romero and Gambi, 2004] Romero, P. and Gambi, J. M. (2004). Optimal control in east/west station-keeping manoeuvres for geostationary satellites. *Aerospace Science and Technology*, 8:729–734.

[Saccoccia et al., 2000] Saccoccia, G., Gonzalez del Amo, J., and Estublier, D. (2000). Electric propulsion: A key technology for space missions in the new millennium. *ESA Bulletin*, 101.

[Scheel and Conway, 1994] Scheel, W. A. and Conway, B. A. (1994). Optimization of very-low-thrust, many-revolution spacecraft trajectories. *Journal of Guidance, Control, and Dynamics*, 17(6):1185–1192.

[Seywald, 1994] Seywald, H. (1994). Trajectorie optimization based on differential inclusion. *Journal of Guidance, Control, and Dynamics*, 17(3):480–487.

[Sidi, 1997] Sidi, M. (1997). *Spacecraft Dynamics and Control*. Cambridge University Press.

[Skipper et al., 2004] Skipper, J. K., Racicot, D., Li, S., Provencher, R., and Palimaka, J. (2004). Hybrid (ion and chemical) geo stationkeeping maneuver planning software. In *8th International Conference on Space Operations, SpaceOps 2004 — A Global Enterprise*, Montréal, Canada.

[Slavinskas et al., 1984] Slavinskas, D. D., Dabbaghi, H., and Benden, W. J. (1984). Efficient inclination control for geostationary satellites. *Journal of Guidance, Control, and Dynamics*, 11(6):584–589.

[Soop, 1985] Soop, E. M. (1985). Geostationary orbit inclination strategy. *ESA Journal*, 9:65–74.

[Soop, 1994] Soop, E. M. (1994). *Handbook of Geostationary Orbits*. Kluwer Academic Publishers Group.

[Tang and Conway, 1995] Tang, S. and Conway, B. A. (1995). Optimization of low-thrust interplanetary trajectories using collocation and nonlinear programming. *Journal of Guidance, Control, and Dynamics*, 18(3):599–604.

[Vallado, 2001] Vallado, D. A. (2001). *Fundamentals of Astrodynamics and Applications*. Microcosm Press and Kluwer Academic Publishers, second edition.

[Varigonda et al., 2001] Varigonda, S., Georgiou, T., and Daoutidis, P. (2001). A flatness based algorithm for optimal periodic control problems. In *American Control Conference*, pages 831–836, Arlington, VA, USA.

[Varigonda et al., 2004] Varigonda, S., Georgiou, T., and Daoutidis, P. (2004). Numerical solution of the optimal periodic control problem using differential flatness. *IEEE Transaction on Automatic Control*, 49(2):271–275.

[von Stryk, 1993] von Stryk, O. (1993). Numerical solution of optimal control problems by direct collocation. In Bulirsch, R., Miele, A., Stoer, J., and Well, K.-H., editors, *Optimal Control — Calculus of Variations, Optimal Control Thery and Numerical Methods*, volume 111 of *International Series of Numerical Mathematics*, pages 129–143. Basel, Birkhauser.

[Wertz and Larson, 1999] Wertz, J. R. and Larson, W. J., editors (1999). *Space Mission Analysis and Design*. Microcosm Press and Kluwer Academic Publishers, third edition.

[Zarrouati, 1987] Zarrouati, O. (1987). *Trajectoires spatiales*. Cépaduès-Éditions.